



University
of Glasgow

<https://theses.gla.ac.uk/>

Theses Digitisation:

<https://www.gla.ac.uk/myglasgow/research/enlighten/theses/digitisation/>

This is a digitised version of the original print thesis.

Copyright and moral rights for this work are retained by the author

A copy can be downloaded for personal non-commercial research or study,
without prior permission or charge

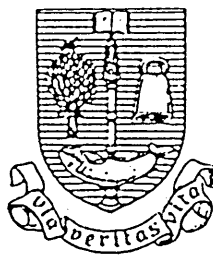
This work cannot be reproduced or quoted extensively from without first
obtaining permission in writing from the author

The content must not be changed in any way or sold commercially in any
format or medium without the formal permission of the author

When referring to this work, full bibliographic details including the author,
title, awarding institution and date of the thesis must be given

Enlighten: Theses

<https://theses.gla.ac.uk/>
research-enlighten@glasgow.ac.uk



ABSORPTION OF RADIATION
IN THE TRANSWALL

by

KONSTANTINOS GREVENIOTIS

M.Sc. Thesis

DEPARTMENT OF MECHANICAL ENGINEERING
UNIVERSITY OF GLASGOW

MAY 1986

ProQuest Number: 10907200

All rights reserved

INFORMATION TO ALL USERS

The quality of this reproduction is dependent upon the quality of the copy submitted.

In the unlikely event that the author did not send a complete manuscript and there are missing pages, these will be noted. Also, if material had to be removed, a note will indicate the deletion.



ProQuest 10907200

Published by ProQuest LLC (2018). Copyright of the Dissertation is held by the Author.

All rights reserved.

This work is protected against unauthorized copying under Title 17, United States Code
Microform Edition © ProQuest LLC.

ProQuest LLC.
789 East Eisenhower Parkway
P.O. Box 1346
Ann Arbor, MI 48106 – 1346

DEDICATED TO

My parents,

Ecaterini and Christos.

The author would like to express his thanks to Dr. S.K. Nisbet, who supervised the present work, for his esteemed guidance, advice and encouragement which makes this work a most worthwhile and interesting experience.

The author would also like to express his thanks to Prof. A. Roy of the Dept. of Astronomy, Dr. Peacock of the Dept. of Chemistry for their advice on certain aspects of this work.

Thanks also due to:

Prof. B.F. Scott and the Dept. of Mechanical Engineering, Glasgow University for making laboratory facilities available for the present work. Also Miss Ruth Kelly who typed this thesis with much care.

CONTENTS

	Page
SUMMARY	i
NOMENACLATURE	iii
INTRODUCTION	vi
CHAPTER 1	PASSIVE SOLAR HEATING
1.0	Introduction 1
1.1	Solar collection systems 1
1.2	Concepts of passive heating 2
1.3	Passive system types 3
1.3.1	Direct gain 3
1.3.2	Attached greenhouses/ Conservatories 4
1.3.3	Thermal storage walls 5
1.3.4	Water roof 8
1.4	Transwall - A review 9
1.5	The transwall system compared to other passive systems 14
1.6	Transwall module design 17
1.6.1	Description of the transwall module used 18
1.7	Economic considerations 19
CHAPTER 2	PROPOSED STANDARD RADIATION CURVES FOR THE WEST OF SCOTLAND
2.0	Introduction 22
2.1	The sun 22
2.2	The solar constant 23
2.3	A cloudless sky atmosphere and its optics 23
2.3.1	The earth's atmosphere 24
2.3.2	Clean dry air 24
2.3.3	Water vapour 25
2.3.4	Aerosols 25
2.4	Optical mass 27
2.4.1	Optical air mass 28
2.4.2	Optical ozone mass 28
2.4.3	Optical water vapour 29
2.5	Attenuation of (direct) solar radiation 29
2.5.1	Scattering of air molecules 30

2.5.2	Transmittance of uniformly mixed gases	30
2.5.3	Transmittance of water vapour	30
2.5.4	Transmittance of aerosols	31
2.5.5	Transmittance of ozone	32
2.5.6	Direct spectral irradiance on the ground	33
2.6	Origins of diffuse spectral radiation	33
2.6.1	Rayleigh scattered spectral diffuse irradiance	34
2.6.2	Aerosol scattered spectral diffuse irradiance	35
2.6.3	Atmospheric reflectance	35
2.6.4	Multi-reflected spectral diffuse irradiance	36
2.6.5	Diffuse spectral irradiance on the horizontal	37
2.6.6	Global radiation	37
2.7	Total and spectral solar irradiance at ground level	38
2.8	Glasgow standard atmosphere	38
2.9.	Results - Conclusions	38

CHAPTER 3 OPTICS

3.0	Introduction	49
3.1	Reflection of radiation	49
3.1.1	Index of refraction and extinction coefficient	49
3.1.2	Fresnel's law	51
3.1.3	Reflection at normal incidence	52
3.2	Absorption of radiation	53
3.2.1	Laws of attenuation	53
3.2.2	Optical density	54
3.3	Transmittance through an absorbing medium-Stokes' equations	55
3.4	Glass spectral transmission	57
3.4.1	Glass spectral reflection	57
3.4.2	Glass composition	57
3.4.3	Iron oxide	58

3.4.4	Iron oxide optical absorption in soda lime silica glass	58
3.5	Glass solar heat transmission	60
3.6	Optical constants of water	62
3.6.1	The choice of a heat transfer storage fluid for the transwall application	63
3.7	Absorption characteristics of various dyes	63
3.7.1	Beer's law check	65
3.7.2	Results -Conclusions	66
3.7.3	Dye selection for glass-house transwalls	67

CHAPTER 4 THE LUMPED SYSTEM APPROACH

4.0	Introduction	72
4.1	Treatment of the transwall	74
4.2	Thermal Capacity of the transwall module	76
4.3	One-dimensional absorption of radiation	78
4.3.1	1-D ray tracing technique with infinite internal reflections between the sub-systems	78
4.3.2	A closed formula example for the 1-D ray tracing technique	81
4.3.3	Comparison of the infinite reflections with the simple one reflection technique-Numerical example	85
4.4	Diffuse radiation from the sky	85
4.4.1	Isotropic model	86
4.4.2	Ground reflected diffuse radiation on an inclined surface	87
4.4.3	Ground reflectance	88
4.4.4	Transmission of diffuse radiation	90
4.5	Measurement of solar radiation	91
4.5.1	Solarimeter corrections	92
4.6	Description of the test cell	97
4.7	Temperature measurement	101
4.7.1	Temperature of water	102
4.7.2	Temperatures of transwall surfaces and test cell space	105

4.8	Computing program operation	107
4.9	Water temperature measurement	108
4.10	Lumped system results	111
CHAPTER 5	2-D ANALYSIS OF THE RADIATION ABSORBED IN A TRANSWALL MODULE	
5.0	Introduction	117
5.1	Treatment of absorption in a 2-D transwall	120
5.2	Refractive altitude and azimuth angles	122
5.3	Slab divisions	124
5.4	Factor affecting the absorption of a transwall	126
5.4.1	Reverberations of incident radiation between the transwall and the window	126
5.4.2	Number of reflections	128
5.4.3	Shadow factors	128
5.4.4	Acceptance factors	131
5.4.5	Reflection of radiation in bottom glass	132
5.5	Beam radiation absorbed by the transwall	134
5.5.1	Beam radiation absorbed in outer transwall glass	134
5.5.2	Beam radiation absorbed in inner transwall glass	135
5.5.3	Beam radiation absorbed in water slabs	136
5.6	Diffuse radiation absorbed by the transwall	137
5.6.1	Effective sky dome angle	138
5.6.2	Diffuse radiation absorbed in outer glass	141
5.6.3	Diffuse radiation absorbed in inner glass	141
5.6.4	Diffuse radiation absorbed in water slabs	142
5.7	Single waveband analysis	144
5.8	Treatment of backwards radiation from room	145
5.8.1	Room radiation measurement	145
5.9	Computer program validation	149

5.10	Model simulation results	150
CHAPTER 6	CONCLUSIONS AND FUTURE WORK	159
APPENDICES		
A	SOLAR GEOMETRY AND TIME	164
B	SOLAR RADIATION TABLES	168
C	OPTICAL CONSTANTS OF WATER, DYES AND GLASS	177
D	EXPERIMENTS IN DETERMINING THE SPECTRAL ABSORPTION COEFFICIENTS OF DYES	181
E	AVERAGE OPTICAL CONSTANTS FOR WATER AND GLASS	184
F	STRENGTH OF REFLECTED RAYS IN A TRANSWALL MODULE	187
G	MEASUREMENT OF HEAT TRASFER COEFFICIENT	188
H	NON-HOMOGENEOUS HALF SLAB METHOD	191
I	AIR MASS CONSIDERATION FOR THE LATITUDE OF GLASGOW - FRACTION OF ENERGY FOR DIFFUSE RADIATION IN BRITAIN	193
REFERENCES		197

SUMMARY

This thesis is concerned with the study of the absorption of solar radiation in a transwall module, an element of a passive solar system.

The transwall system is reviewed and its merits discussed. The design criteria of the transwall module and the costs associated with the various module design variations are given. It is concluded that the best design for building is a 10 mm thick glass tank 1.5 m long x 0.75 m high filled with a water/dye solution.

The calculation of the insolation absorbed by the transwall requires knowledge of the fractional energy in various wavebands and the absorption coefficients of the transwall materials. A standard atmosphere is defined for the Glasgow area, its parameters listed, and the fractional energy levels for beam and diffuse radiation (clear sky) are derived. Plots demonstrate how the extraterrestrial spectrum is modified by various atmospheric parameters. The absorption coefficients for the transwall dyes, Lissamine Red 3GX, Carbolan Rubine, Methyl Orange and Acid Green have been measured and their individual use described.

The performance of a transwall module has been analysed by assuming the module to have an infinite thermal conductivity (a lumped system) and predictions tested against measurement. It is shown that the predicted temperature rise is liable to be in error by 20% due mainly to elevated glass temperatures, and by 8% when cooling on the cessation of insolation. The effect of other parameters on the accuracy of this method is

examined, and the curious temperature profiles described.

After demonstrating that the lumped system approach has fundamental problems a case is made for a two-dimensional finite difference solution. As a first step in this work a computer program has been written to give the absorption of radiation in the various volumes of the transwall and it has been validated by measurement. The methodology of internal shade and acceptance factors for the volumetric slabs of the transwall is given. The program is used to quantify various factors, such as the sensitivity of slab numbers, the effects of dyes and solar absorbing glass, the effects of solar spectra and the number of wavebands, the effect of taking into account room reflected radiation.

This thesis concludes by suggesting directions for future work.

NOMENCLATURE

A	optical density, area
a	solar azimuth angle in degrees
a _r	solar azimuth angle of refracted ray
a _w	wall azimuth angle, East positive
AF	acceptance factor
AU	astronomical unit (1 AU = 1.496 x 10 ⁸ km)
c _p	constant pressure specific heat capacity
C	dye concentration (mol of dye/ kg of solvent)
CF	shade ring correction factor
d _n	day number of year
E ₀	eccentricity correction factor of earth (r ₀ /r) ²
E _t	equation of time (minutes)
F _λ	spectral fraction of solar radiation
F _c	ratio of energy scattered in the forward direction to the total energy scattered (dimensionless)
h	heat transfer coefficient
\overline{H}_e	extraterrestrial daily radiation on a horizontal surface (MJm ⁻² day ⁻¹)
\overline{H}	daily global radiation on a horizontal surface
I _{sc}	solar constant (Wm ⁻²)
I _{onλ}	extraterrestrial spectral irradiance at wavelength (Wm ⁻² μm ⁻¹)
I _{nλ}	direct normal spectral irradiance
I _{dλ}	diffuse spectral radiation on a horizontal surface
I _λ	global spectral irradiance on a horizontal surface
I _{daλ}	Aerosol scattered spectral diffuse radiation
I _{dmλ}	multi-reflected spectral diffuse radiation
I _{drλ}	Rayleigh-scattered spectral diffuse radiation
I _τ	intensity of transmitted light
I ₀	intensity of incident light
k _λ	monochromatic attenuation coefficient (dimensionless)
k(λ)	extinction coefficient (m ⁻¹)
k _{aλ}	coefficient of attenuation due to aerosols
k _{gλ}	coefficient of attenuation due to mixed gases
k _{oλ}	coefficient of attenuation due to ozone
k _{rλ}	coefficient of attenuation due to air molecules
k _{wλ}	coefficient of attenuation due to water vapour
k _τ	clearness index (dimensionless)
l	ozone layer thickness (cm(NTP))

L	path length (m)
L	local longitude (degrees)
L	standard longitude (degrees)
m	optical mass (dimensionless)
m_a	optical air mass (km)
m_w	optical mass for water vapour
m_o	optical mass for ozone.
n	refractive index
Nu	Nusselt number
p	atmospheric pressure (mbars)
$P_{0.1}$	percentage of solar constant
r	actual sun-earth distance (AU)
r_o	mean sun-earth distance
R	reflectance at normal incidence
SF	shade factor
t	time, thickness
T	temperature
T_s	solar time
V	volume
VF	view factor
w	precipitable water thickness (cm)
W	strength of solution (ppm)
x	distance, displacement
z_o	height of ozone layer concentration

Greek letters

α	solar altitude angle, Ångström wavelength exponent, absorptance
α_r	solar altitude of refracted ray
β	Ångström's turbidity parameter, absorptance per unit concentration
δ	declination
δ_c	declination on characteristic days
γ	inclination of surface from horizontal position
θ	angle of incidence
θ_r	angle of refraction
θ_z	zenith angle
λ	wavelength (μm)
μ	ratio of refractive indices
ξ	component of polarization
ρ	density, reflectance, reflectivity
ϕ	geographic latitude, north positive

ϕ_r	relative humidity in fractions of one
χ	effective sky dome angle
ψ	effective angle of incidence for diffuse radiation
w	hour angle, solar noon and morning positive
w_s	sunrise hour angle for a horizontal surface
w_a	ratio of energy scattered to total attenuation by the aerosols
α	absorptance
τ	transmittance
Γ	day angle, (radians)

Subscripts

a	air
b	beam, bottom
d	diffuse
g	glass
g_1	front glass
g_2	rear glass
gr	ground
gz	glazing
m	mean
n	normal
r	room, refractive
sc	solar constant
w	water
λ	spectral
$//$	parallel component of polarization
\perp	perpendicular component of polarization

INTRODUCTION

The ever growing concern for energy conservation has promoted a great deal of interest in the use of solar energy for the purpose of heating dwellings. As most heating requirements utilize low grade heat, considerable savings could be obtained by using thermally efficient structures in conjunction with renewable energy sources.

Passive solar heating systems incorporate the solar collection and, possibly, storage into the building structure and distribute the heat by natural means. A type of passive solar home heating system is the "Transwall".

The transwall system is a modular visually transparent thermal storage wall which is placed in building areas receiving direct solar radiation. The transwall is essentially a wall of water filled glass tanks in a metal support frame. It combines some characteristics of the direct gain and thermal storage wall system, see figure 1.

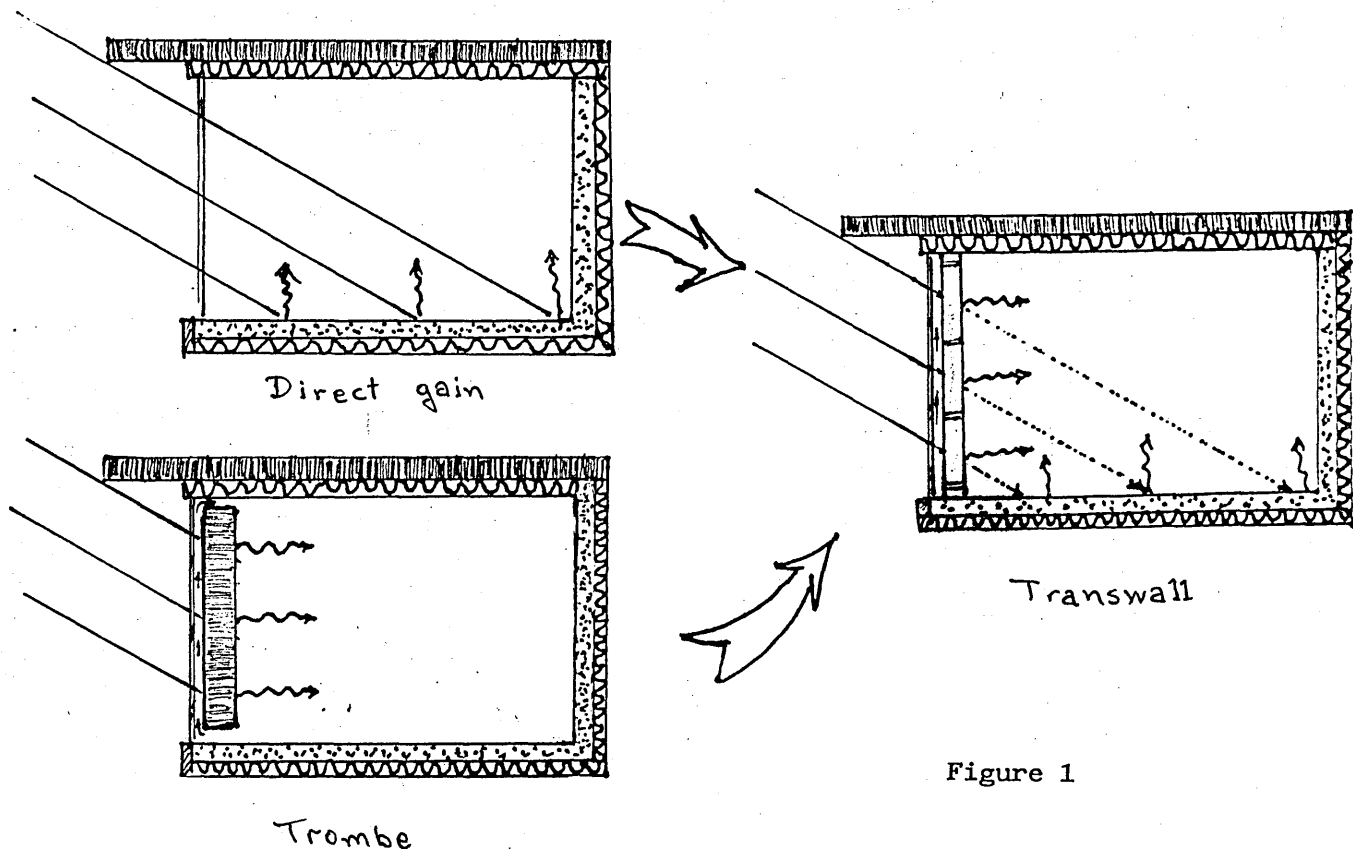


Figure 1

The solar energy absorbed in the transwall is thermalized, thus raising the temperature of the modules. Part of this thermal energy is then slowly transmitted by radiative, convective, and conductive processes to the interior space. The remaining stored thermal energy is lost to the exterior window. The room is also heated directly and illuminated by the transmitted fraction of the solar energy, as in a direct gain system. However, this fraction can be made small enough to avoid large fluctuations of the interior air temperature, glare, and photodegradation of interior furnishings, which are undesirable characteristics of conventional direct gain systems, while still allowing good visual transmission and daylighting.

The calculation of the solar radiation absorbed by the transwall requires knowledge of the fractional energy in the various wavebands. For this reason a 'Glasgow standard atmosphere' has been developed which, for the usual test conditions of clear skies, gives the fractional intensities for beam and diffuse radiation for varying air masses. The absorption of radiation within a transwall depends also on its dimensions and on its materials of construction and filling. A cost effective way to enhance absorption is by the addition of a suitable dye, and the optical characteristics of several such dyes were investigated by experimental means.

The aim of the present work was to provide analytical and experimental methods of studying aspects of the absorption of radiation and the temperature rise in a transwall. For the temperature prediction the lumped system approach was used, in which the transwall has

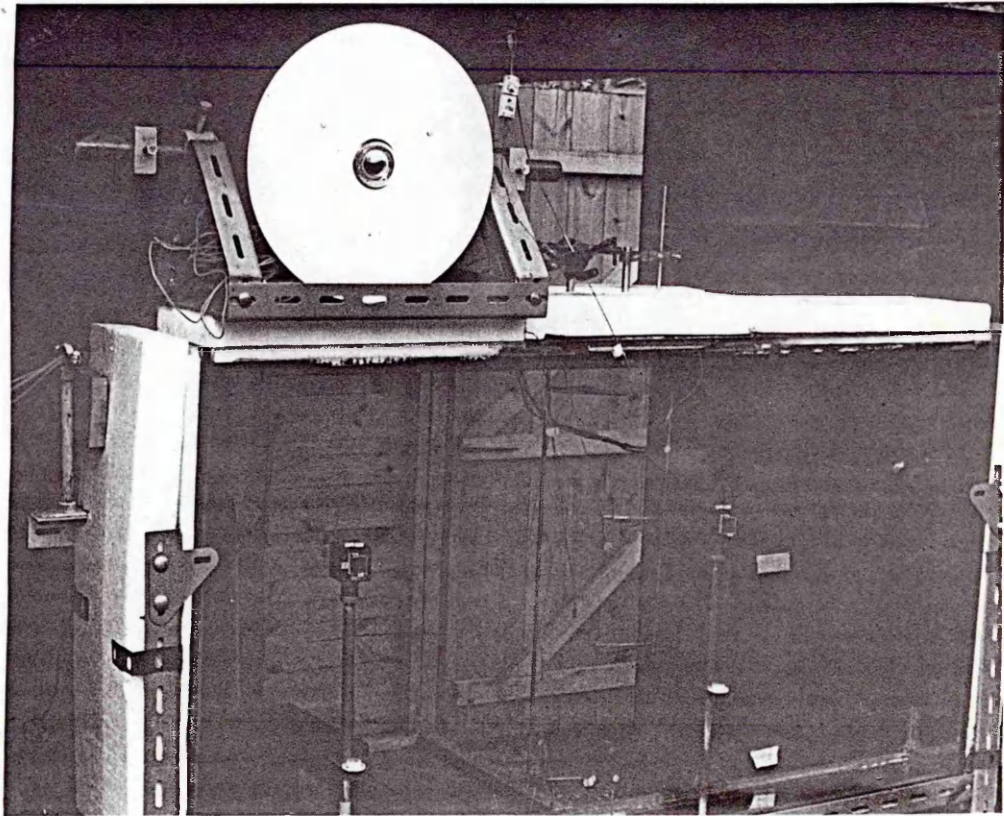
an infinite thermal conductivity, has the great advantage of simplicity but it has recognized disadvantages relative to more complicated approaches such as finite differences and effective conductivity. The above system was used to predict the temperature changes on heating and cooling and the ^{computed} results were then compared against measurements.

If solar insolation is absent then the lumped system approach can predict the temperature fall to within 8%. When the insolation is present the temperature prediction is limited to 18%, and so some other, more accurate method is required.

The vigorous circulation within the transwall module when first receiving insolation and the stratification cannot be predicted with the analyses developed here but these effects have been experimentally observed and quoted. The convective circulation patterns within the transwall will be possibly accounted for using finite differences and effective conductivity ~~methods~~ and the analysis in Chapter 5 was developed towards this objective. As a first step in this work a computing program has been written to give the absorption of radiation in the various volumetric slabs of the transwall accounting for their internal shade and acceptance factors. This is the first part of a programme to model the transwall phenomena using finite difference methods which incorporate the concept of effective conductivity. The above analyses were validated by experiment obtaining good agreement.

The actual measurements associated with the transwall's performance and validation of the two dimensional absorption computing program were performed in a test cell containing

a full size transwall module situated at the Mechanical Engineering Research Annexe (M.E.R.A.), Glasgow University. See photograph I.1 below.



Photograph I.1. A close-up photograph of the transwall module used, installed in the test cell 10 cm behind the glazing (see p. 98, 99).

CHAPTER 1

PASSIVE SOLAR HEATING

1.0 Introduction

This chapter sets the scene for the transwall. The distinction is made between active, passive and direct gain systems. The major passive storage systems are then considered, viz. Trombe wall, opaque water wall, water roof, and the transwall. A review is undertaken of transwall publications and their major conclusions quoted. The advantages and disadvantages of the transwall system are given in relation to other competing systems with consideration being given to such aspects as thermal and optical performance and architectural features. The practical design of transwall modules is commented upon with due regard to economic features.

1.1 SOLAR COLLECTION SYSTEMS

Thermal collection can be classified into active and passive systems.

a) Active Systems

An active system uses solar collecting panels, storage tanks or bins, an energy transfer mechanism and an energy distribution system. It always employs one or more working fluids which collect, transfer, store and distribute the collected solar energy. The working fluids are circulated by means of fans or pumps.

b) Passive Systems

Passive systems use natural elements to distribute the collected heat. Often a passive system becomes a "live in" solar collector with an impact on the architectural design of the structure and the life style of the occupants.

Since temperatures differences are used to distribute heat, most passive heating systems cannot, and do not attempt to, maintain a uniform indoor temperature. Many achieve a degree of control with adjustable drapes or louvers on glazed portions of the structure, or even use circulation fans.

1.2 CONCEPTS OF PASSIVE HEATING

Passive design seeks to reduce the house's energy budget by close attention to orientation, insulation, window placement and design, and to the subtleties of the energy transfer properties of building materials.

Since solar gains are present in every building, all buildings are passively solar heated to some extent. It is when the building has been designed to optimise the use of solar energy and when solar energy contributes substantially to the heating requirements of the building that it is termed a solar building.

Passive Systems Components

Passive systems contain five basic components:

1. Collector dark walls, windows, water ponds.
2. Storage walls, large interior thermal masses

irradiated by sunlight in winter, water ponds. Frequently these are integrated with the collector.

3. **Distribution System** radiation, free convection, simple circulation fans.
4. **Controls** moving insulation panels to control building or collector heat loss, vents and windows. These are frequently manual.
5. **Backup System** any nonsolar heating system.

1.3 PASSIVE SYSTEMS TYPES

The majority of passive systems for space conditioning (both heating and cooling) can be placed within one of the four generic system types:

- a) Direct gain
- b) Attached greenhouse / conservatory
- c) Thermal storage walls
- d) Water roofs.

1.3.1 Direct Gain

The direct gain of energy through windows can meet part of building heating loads. The window acts as a collector and the building itself provides some storage. The interior materials of the building are capable of absorbing large amounts of energy through radiation and convection.

Overhangs, wingwalls, or other architectural devices are used to shade the windows during times when heating is not wanted. It is also necessary, in cold climates, to insulate the windows during periods of low solar radiation to prevent excessive losses.

The system aperture is usually double pane glass, always located on the south face of a building.

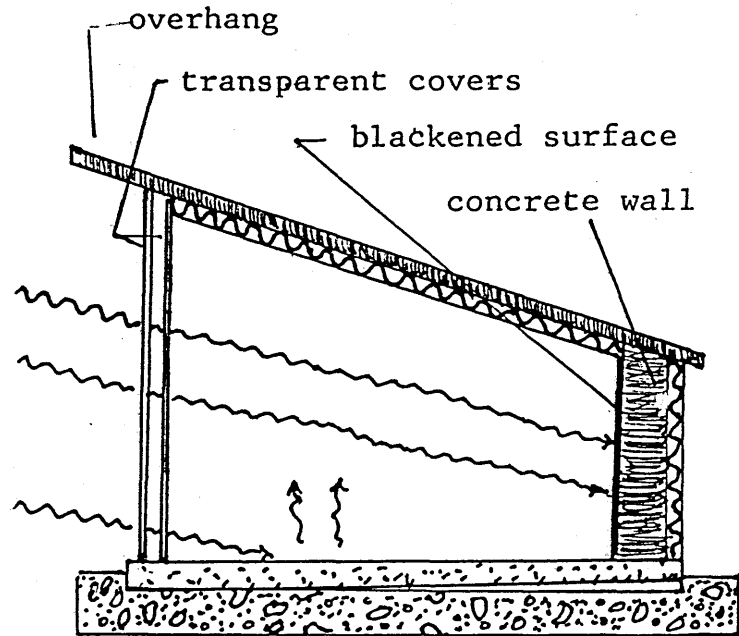


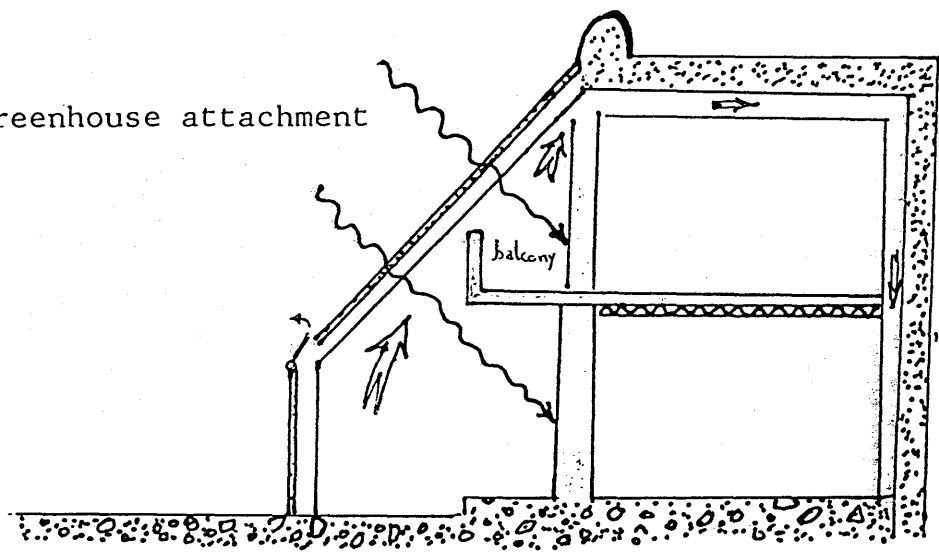
fig.1.3.1 Direct gain structure using massive rear wall for heat storage.

1.3.2 Attached Greenhouses/Conservatories

Attached greenhouses, or conservatories, are a mix between direct gain and thermal storage wall systems. Greenhouse attachments to buildings have been used as solar collectors, with pebble bed storage units and forced air circulation to the rooms added as options to improve storage and utilization of absorbed energy.

An important, but difficult to quantify, aspect of attached greenhouses is their esthetic and food functions.

fig.1.3.2 Greenhouse attachment



1.3.3 Thermal Storage Walls

(i) Trombe Wall

The essential solar feature of a typical Trombe Wall is the use of the south facing wall (Northern Hemisphere) as a solar collector, a storage facility and a heat transfer medium all in one, that is part of a building structure. The efficiency of the collector is enhanced by placing single or double glazing in front of the outer face of the concrete slab; the latter painted a suitable dark colour to absorb solar radiation. Heat is transferred from the storage wall into the internal environment by both conduction through the wall, and by natural convection currents in the air gap between the glass and the outer concrete face, fed by ventilation ports at the top and bottom of the wall, see fig. 1.3.3(i)

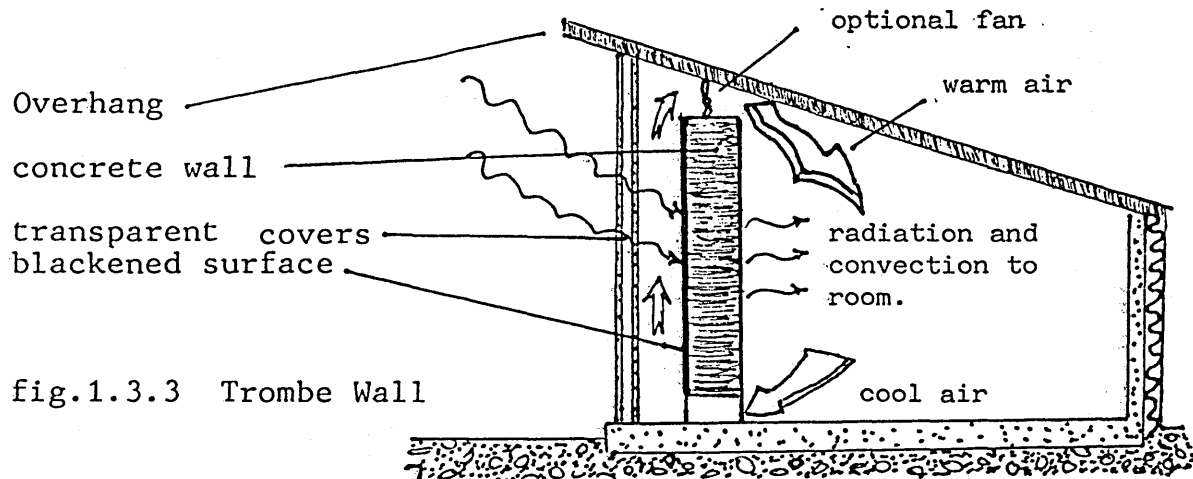


fig.1.3.3 Trombe Wall

Losses during non sunny periods can be an important factor in long term performance and movable insulation may have to be provided in any but mild climates.

The thermal storage wall principle may be used with other materials than concrete.

(ii) Water wall (Drum wall)

The water wall is similar in concept to the Trombe wall but uses contained water instead of masonry. Water heat storage is of great potential benefit because it distributes heat gains quickly by convection and thus it has the capability of providing passive solar energy storage with greatly reduced surface temperatures. Also the circulation within the tanks gives a high effective conductivity and the inner wall becomes warmer.

Water is cheap, easy to install in tanks or drums and compared with concrete has a high thermal capacity per unit volume (two times that of concrete).

(iii) Transwall

(a) In buildings, see 1.4

- solar radiation
- 1 exterior glazing
 - 2 Transwall modules
 - 3 air passage
 - 4 foundation insulation

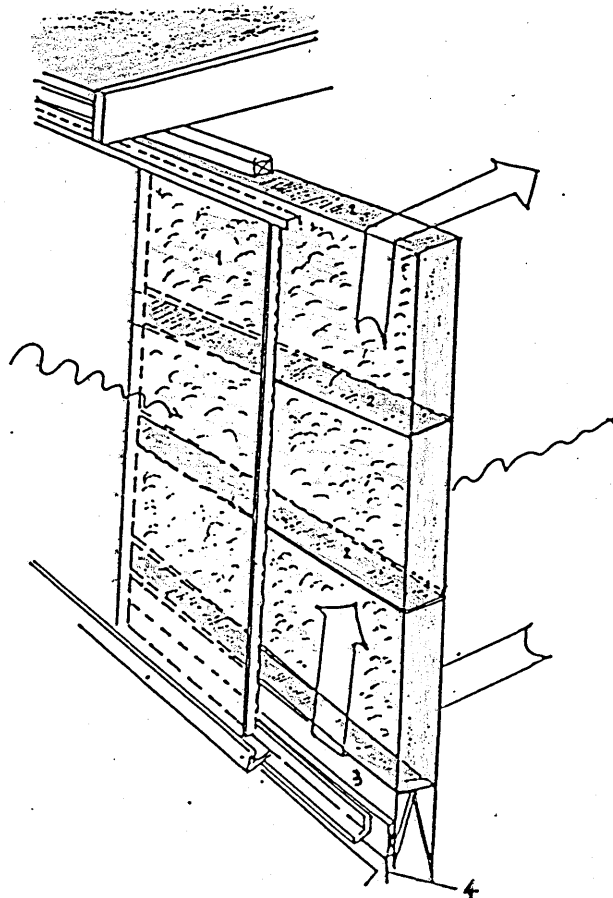


Figure 1.3.3(iii)a.

A transwall modular passive solar system

(b) In horticultural Glasshouses

Nisbet and Kwan (29), investigated by computer simulation the energy savings resulting from the installation of transwalls in horticultural glasshouses. They found that annual energy savings of 20% could be achieved for sites in the West of Scotland and South England giving payback periods in the range $2\frac{1}{2}$ to $5\frac{1}{2}$ and 4 to 8 years respectively. The lower figure for South England reflects the principle that the transwall is most economic where there is a combination of adequate solar radiation and low ambient temperatures. The computer simulation revealed that conventional transwalls of glass construction were unlikely to be cost effective and it became necessary to develop an alternative module which in its final form, fig. 1.3.3(iii)b, consists of a water filled plastic bag retained in a mesh cage. The cage is constructed from 3.5mm wire, 75mm mesh and its dimensions of 1.4m x 0.75m x 0.15m. It is reinforced by two twin angle iron strips to reduce its otherwise gravid appearance. The plastic bag is formed by a simple seam welder and is made from 0.15mm Fromoclear Z27 clear PVC sheet.

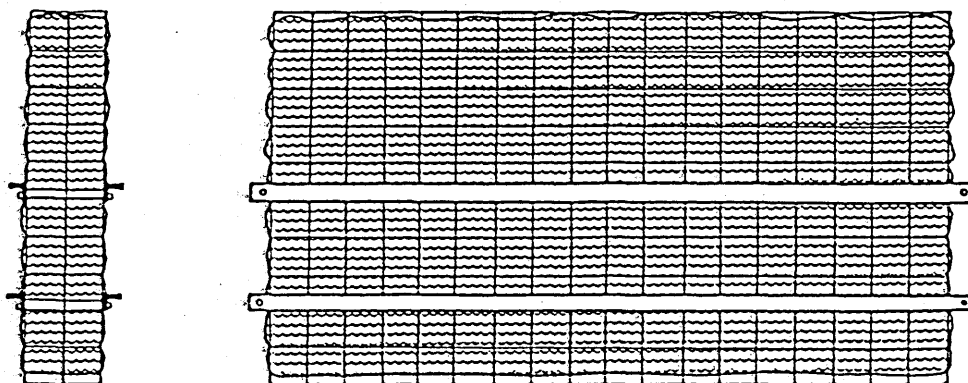


fig.1.3.3(iii)b Transwall, water bag in a mesh cage.

The absorption was enhanced by using Lissamine Red 3GX dye whose absorption spectrum transmits the wavelengths necessary for plant growth.

1.3.4 Water Roof

The principles are similar to a collector wall, but energy transport into the rooms is primarily by radiation from the storage ceiling. A roof carries a shallow, usually 0.15m^{deep}, water filled pond, either in tanks or in plastic bags in thermal contact with a strong, but highly conductive, flat roof and ceiling structure (5). Solar energy is stored in the water which in turn heats the ceiling. Some system of insulating the pond at night is required.

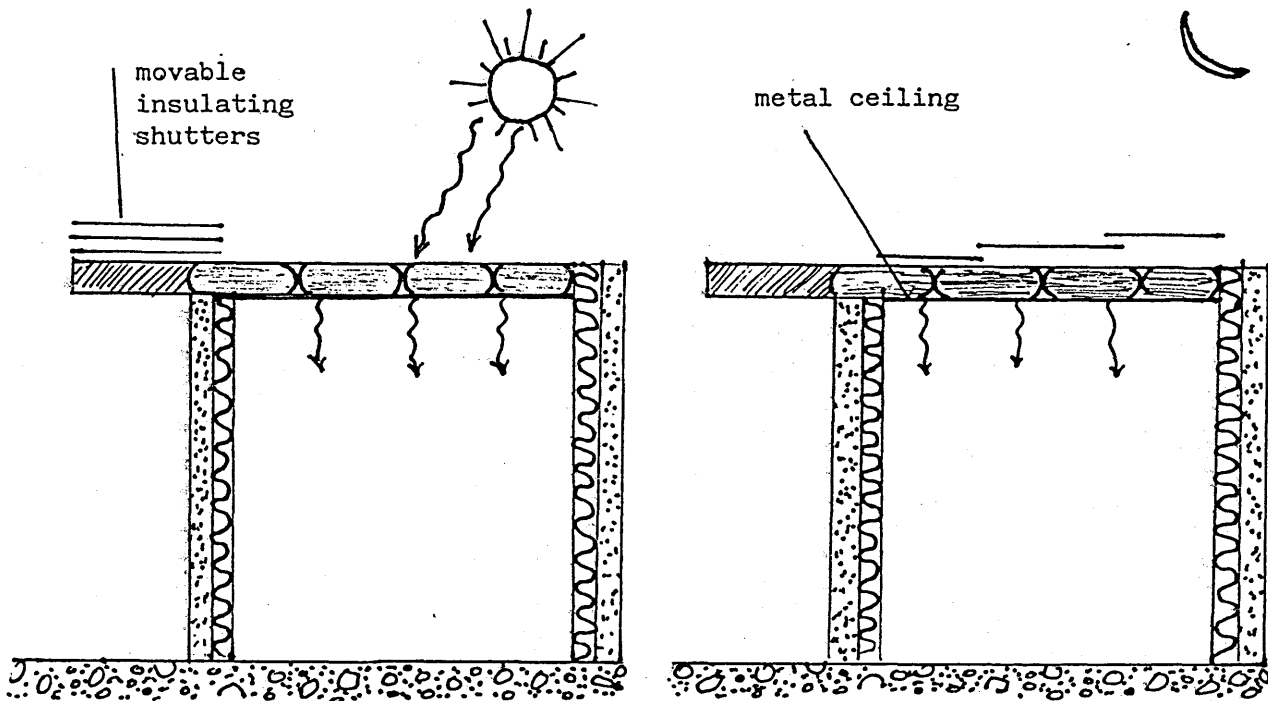


Figure 1.3.4a Winter heating

The system can also be used for cooling by exposing the pond surface at night and excluding solar radiation by day. In this case, the movable insulation covers the roof during the day and is opened at night. See fig. 1.3.4b.

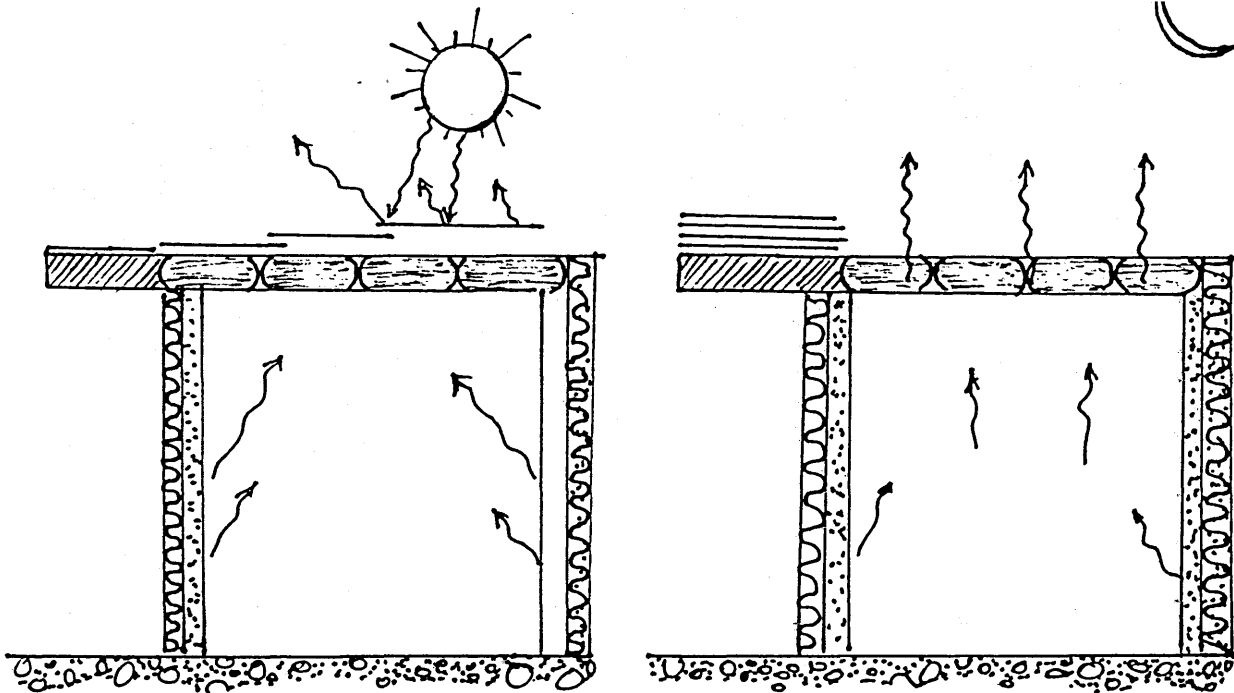


Figure 1.3.4b Summer cooling

The solar roof pond is the equivalent of the transwall for regions within the tropics, with their high altitude angles. Clearly the projected area of a vertical transwall normal to beam radiation will make the transwall of dubious use in the tropics.

1.4 TRANSWALL - A REVIEW

Most of the research concerning transwall systems has been undertaken by the A M E S. laboratory USDOE, at Iowa State University, U.S.A. The concept of transwall systems was first introduced in the 3rd National Passive Solar Conference in January 1979 (15). A paper was published in Solar Energy (12), in March 1979, and in the following year the work was reported in the Internat. Solar Energy Conf. in Phoenix, Arizona in June (13) and further work in the 5th Nat. Pass. Sol. Conf. in October at Amhrest, Masschusetts (11). In 1981 a report appeared in the Solar World Forum at Brighton, England (16) and another in the 6th Nat. Pass. Solar Conf. in September at Portland, Oregon (14). Then two reports followed from the A M E S. team (17,18).

In 1983 an extensive analysis of the system was presented in Paparsenos' PhD thesis (3), a work that started 4 years earlier at Glasgow University M.E.R.A.

and a paper in Applied Energy (19) by an Indian team of the Indian Institute of Technology, Hawz Khas, New Delhi. In (15),(12),(13),(11) the analytical results are based on 1 dimensional steady state thermal network models of the thermal performance of the passive systems.

Experimental evidence has been collected from measurements in test rooms, on the south facing side of which are various passive solar systems (13). Calculations using thermal network models and based on reasonable assumptions for relative comparisons have been used to compare thermal performances of transwall, Trombe wall and direct gain systems. Ref.(12,15) compared a convection quenched and a high conductance transwall against Trombe walls with and without vents and against a direct gain system. They found that the thermal performance of the quenched transwall can be superior to that of the other systems and that the high conductance transwall has a somewhat lower performance, but it is approximately as good as the best competing system, the concrete wall with air circulation. Paparsenos (3) examined the distribution of solar radiation of the direct and the transwall systems. He found that the radiation absorbed by the various internal surfaces of an enclosure with the direct system is much larger than that absorbed by the corresponding surfaces of the transwall systems. This difference can be 2 to 10% of the incident radiation for the side and north wall and about 9 to 15% for the floor. This fact reveals the tendency of direct solar systems to overheat under certain conditions.

Sodha et al. (19) argued that the temperature varies appreciably over a day and the wall stores large amounts of heat, so an appreciable error may result in the hourly evaluation of the thermal load from a steady state analysis. They developed an analysis which enables one to predict the time dependent thermal performance of the transwall.

The transwall modules suggested by A.M.E.S. are listed in table 1.4. The first transwall modules were made from acrylic plastic but they were abandoned because of reliability problems.

Enhancement of module solar radiation absorptance by using a central semi-transparent plate was suggested by (15,12,13,17,18,19). Design changes such as a) the effect on performance of moving the absorber plate from the centre to the inside tank wall, and b) the use of a transmitting selective coating (heat mirror) on the exterior facing transwall module walls to reduce radiative heat losses were investigated using a computer thermal network analysis (16,14). They found 1) for a double glazed room, without night insulation, the change in location of the absorber plate did not significantly effect the performance and 2) the addition of a heat mirror reduced the auxiliary energy required by 50% with double glazing but could not compensate for the replacement by single outside glazing for double glazing. It produced a higher predicted performance improvement than movable night insulation.

At present, the thermal performance of the transwall system with heat mirror coating modules is under test in A.M.E.S. (16).

TABLE 1.4

SUGGESTED TRANSWALL MODULES

Year	Reference	Tank material		Outer module dimensions		Enhancement of module:		heat transfer
		type	thickness (mm)	width (cm)	height (cm)	thickness (cm)	absorptance	
1979	(12, 15)	glass				15.2 gap	absorbing plate at the centre of transwall $\tau = 80\%$	baffles & gelling compound
1980	(11)	acrylic plastic	13	58	58	17.8		
1980	(13, 17)	acrylic plastic	9.5	132	59	17.8	absorbing plate, 9.5 mm thick neutral gray plexiglass, $\tau = 84\%$	
1981	(14, 16)	annealed glass	6.4	58	38	14.0	grey tinted glass 3.2 mm thick, $\tau = 31\%$. Investigated by computer: i) heat mirror coating at the outer plate, ii) absorbing plate placed as inner plate	
1983	(3)	annealed glass	6.0	113.2	63.5	16.2	Acid green dye	gelling compound
1983	(3)	annealed glass	10.0	114.0	63.0	17.0	Antisun grey glass, 4 mm thick, as central plate	
At present		annealed glass	10.0	114.0	63.0	17.0	Experimentally: acid green dye by computer: various dyes at different concentrations Antisun grey glass, 10 mm to form inner wall	

Paparsenos (3) suggest the use of a suitable dye diluted into the water as another enhancement of the absorptance of the module.

Hull et al.(11) also studied analytically the importance of various design parameters on the thermal performance of a transwall system throughout the heating season for three different climates. The design parameters varied are: collector area to building load ratio, transwall thickness, transmittance of the absorber plate, and the amount of internal thermal mass. Results indicate that an excellent thermal performance may be obtained while still allowing substantial design flexibility especially in respect to module thickness and the plate absorptivity. An increase in thickness beyond 10 cm gains little in SSF (Solar Savings Fraction⁺). The analyses are based though on a water Nusselt number (Nu) of 2.5 and this has proved uncertain (see later, p.14)

Preliminary analytical results by Fuchs et al. (15,12) suggest that enhanced performance can be achieved when the heat (and mass) transfer rate is reduced to that approaching conductive transfer by a combination of baffles and a gelling compound.

Paparsenos (3) considered the use of baffles to inhibit the water convection to be a rather difficult and uneconomical solution and that gelling agents provide a better solution. Two different types were tried in MERA, Courtaulds Courlose F1000G and Celanese Celacol HA7 150000S, the former being the better for clarity.

In fact dilute wallpaper paste can be used.

There are problems though arising with the use of gelling agents such as the above.

$$^+ \text{SSF} = 1 - (\text{AUX. HEAT REQUIRED} / \text{HEAT REQUIRED w/o SOLAR})$$

- 1) they enhance the growth of micro-organisms,
- 2) the long chain molecules contract over several weeks leaving the upper regions clear and the lower regions opaque. Solutions stronger than 0.5% (kg of agent/kg of water) avoid this problem but at the expense of visual clarity and add extra costs to the system.

Experiments by Hull et al. (11) suggest that horizontal convective heat transfer is suppressed somewhat because of vertical temperature stratification. They found Nu to be 2.5. The experimental results of Paparsenos(3) for a continuous radiation input of about $400 - 500 \text{ W/m}^2$ showed a high effective conductivity which is compatible with a Nu value of 20 and not that of Hull's 2.5.

Paparsenos (3) used elaborate analytical models for some of the elements of the passive solar system analysis. He found that a 1-D model cannot match the 3-D nature of the radiation field in the room behind the transwall module, and showed that the velocity and temperature fields, and therefore the heat transfer, in a transwall module are 3-D with complex circulation patterns.

The elaborate analyses were very demanding of computer time to the extent that the ratio of computer time to real time was in excess of 200 to 1.

1.5 THE TRANSWALL SYSTEM COMPARED TO OTHER PASSIVE SYSTEMS

The transwall has several favourable thermal, optical and architectural advantages relative to Trombe wall and direct gain systems.

a) Thermal

(i) Analytical and experimental results have shown that the thermal performance of the transwall system is equal to or better than that of the "direct gain" or the "thermal storage wall systems" (12,13,14,15)

(ii) The most important advantage, in terms of thermal performance between a transwall and a conventional thermal storage wall is that the solar input is deposited in the interior of the wall, rather than at the front surface facing the windows, as in the case for conventional systems. This results in a low heat loss to the window.

(iii) It reduces overheating.

(iv) It reduces the magnitude of the temperature swings in the living space which often occur in direct gain systems.

b) Optical

(i) Water is transparent in the visible part of the spectrum. In fact for a 10cm thick layer of water and for air mass 2 only 2.6% of the visible part is absorbed

The visible portion of the sunlight is partially absorbed at the transwall glass (and/or rear absorber plate) and partially transmitted into the interior of the building and provides illumination and some direct gain heating.

(ii) It reduces glare.

(iii) It reduces the risk of damage to the interior materials.

(iv) It has been found that the transwall gives better distribution of radiation within the room.

(c) Architectural

From an architectural view point, the transwall overcomes the disadvantages frequently experienced in both Trombe wall and direct gain systems, viz.

(i) The transwall is architecturally more attractive than the completely absorbing Trombe wall, since it admits light to the interior space and allows the occupants to see out through the window.

(ii) Water based thermal storage reduces weight and requires less space than its concrete counterpart by factors of approximately 4 and 2 respectively. Water has the highest heat capacity per kg of any ordinary material (e.g. rock, masonry, adobe). In a 15.2cm thick transwall the water provides a heat capacity per unit area of $660 \text{ kJ/m}^2\text{C}$ which is equivalent to a 33 cm concrete wall (15). Water also is very inexpensive and therefore is an attractive storage and heat transfer medium.

(iii) Other advantages when compared to conventional passive systems are that it does not need to form part of the structure of the building and the system is designed for on site assembly in new or retrofitted buildings.

a) Module dimensions

The absorption of radiation within a transwall depends on its dimensions and on its materials of construction and filling. Transwalls will be supported in a framework and in order to minimize visual obstruction each module should be as large as possible in the length and height dimensions. The total height of the transwall in a typical private house will be about 2.3m giving a transwall module height of about 75cm. This is greater than the current ones under test, 60cm, but stress considerations would suggest that this height is feasible. The current length of 1.2m should be capable of extension to 1.5m without too much difficulty provided the top is securely strapped.

b) Water quality control

A sealed system does not appear to be economically practical at this time. A simple lid can be used which reduces water evaporation and contamination. A permanent syphon tube would be located in one corner for emptying.

Water evaporation is not a significant short term problem in modules. The long term evaporation can be retarded by using a thin layer of low vapour pressure oil that floats on and seals the top water surface from the atmosphere. It has been suggested (14) ^{that} flourosilicone oil is the most suitable because it is not biologically active, it has a low ^{vapour} pressure and it is compatible with the silicone glass bonding adhesive.

There is a problem though using such oils. When the tank is emptied completely the oil covers all the interior walls and it is hard to clean it off.

Algae growth and suspended precipitates may be produced in a transwall module when tap water (without being boiled) is used. It has been suggested (14) that if water is treated with 100ppm CuSO_4 and 150ppm disodium ethylenediamine tetracetate (EDTA) such problems will disappear. CuSO_4 is a common algicide and EDTA a chelating compound often used to keep metal ions in solution. Care is required in the choice of an algicide if a dye system is used. Algicides based on chlorine might bleach the dye (37).

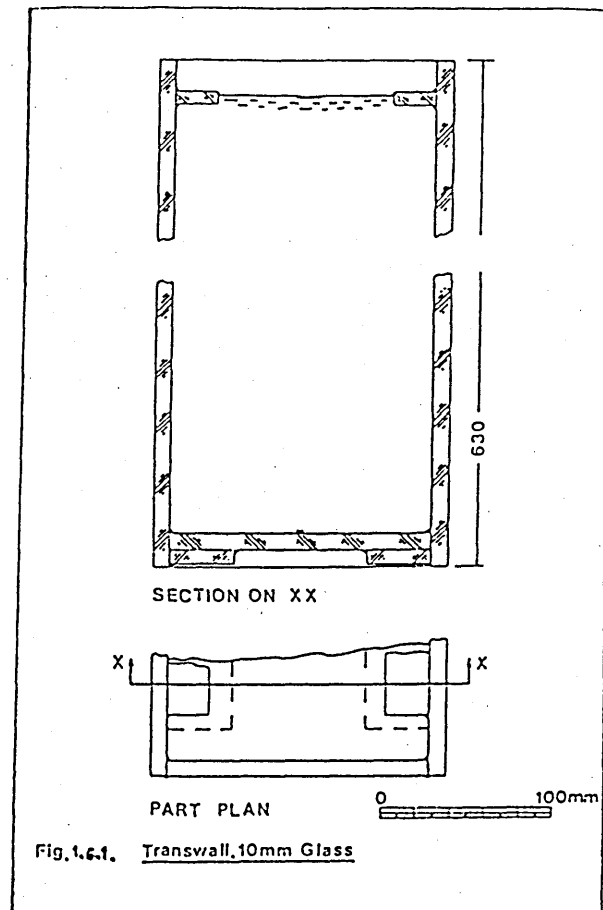
1.6.1 Description of The Transwall Module Used

A transwall test prototype system was designed/fabricated for the solar test cell studies. The transwall structure used in the passive solar test cell consists of a single vertical module supported in a metal frame.

The following module design was planned to serve as a test prototype for thermal and optical performance evaluation and is not considered as necessarily prototypical of a commercial product. The module is a simple rectangular container, fabricated from 10mm thick annealed glass (Pilkington Ltd.) using silicone adhesive sealant to bond butt and lap joints, see fig. 1.6.1.

This is a standard aquarium construction technique and has provided reliable leak free containment without additional structural reinforcement. The outer module dimensions are 1.14m long by 0.63m height and 0.17m thick. A module of similar dimensions was also constructed from 6mm glass but it was found that the module bowed alarmingly without the support of its

aluminium lid. It is felt that the extra strength and stiffness provided by 10mm glass is well worth the extra cost. The hydrostatic deflection of the face plates produces negligible visual distortion. In practice it is filled to a height of 0.6m. The volume of water in the module is 0.11 m³ which has a mass of approximately 110 kg.



1.7 ECONOMIC CONSIDERATIONS

The transwall system has broad significance for both the residential and commercial passive program because of its potential as a marketable primary-system product affording both heating and daylighting.

A comprehensive economic evaluation is beyond the

scope of this thesis. In order to obtain useful results it is not only necessary to have a validated computer model of the transwall behaviour but it is essential to have a realistic program which provides an interaction between the transwall and the building environment. Obviously these have to be treated as dynamic systems. Only programs such as the Environmental Systems Performance (ESP) (30) of the Abacus Unit of the University of Strathclyde are likely to prove adequate to this task.

A few important economic considerations have been identified.

Transwalls have to be cost effective and unfortunately costs on a few-off basis can differ by up to a factor of 3 from different suppliers. If glass is bought cut to size, then the cost per unit area can easily triple to £34/m². A glass tank manufacturer with stocks of 10mm glass can produce finished tanks 1.14m x 0.63m x 0.17m for £33 (retail).

The increase in the absorptance of the module by using an extra absorber plate, suggested by all AMES papers, is unlikely to be cost effective. This is the reason for the current examination of transwall modules in AMES (14,16), in which the absorber plate is transferred from the centre to form the long side inner module wall. Even this approach might increase the cost substantially. Bought in bulk Pilkington's Antisun grey 41/60, 10mm thick, costs 50% more than plain 10mm float glass and the £33 for the clear glass tank would rise to £40 plus if the Antisun glass were to form one wall. However, if bought cut to size the cost of the tank would double.

The use of dyes, diluted into the water seems to be a

more cost effective way of increasing the absorptance of the transwall module and provides much greater flexibility.

Both module and frame costs are very sensitive to the amount of labour involved. If there were a large demand for transwalls and they were produced in quantities upwards of 30000 units per year then the cost could reduce by moulding them in polycarbonate. This production volume would justify the mould charges in the region of £50000. This would reduce the retail cost to about £20 (£8 to manufacturer), but substantial internal ribbing of the 5 mm thick wall is likely to prove visually obstructive.

The author was unable to find worthwhile published work on the saving in energy costs resulting from the installation of a transwall in a purpose built house. Tentative estimates at M.E.R.A. suggest a figure of 25% with a payback period of about 5 years.

PROPOSED STANDARD RADIATION CURVES FOR THE WEST
OF SCOTLAND

2.0 Introduction

The absorption of energy in the transwall depends crucially on the wavelength of the radiation. Since it is impractical⁺ to deal in other than wavebands, in practice 8 to 12, it is important that the fraction of the total energy received in each waveband is known. This will depend not only on whether the radiation is beam or diffuse but also on the atmospheric attenuation. This in turn depends on the atmospheric parameters and thus on the locality. The sensitivity of the parameters to different localities is examined and standard radiation curves for the Glasgow area are calculated.

2.1 THE SUN

The sun is the star closest to the earth and its radiant energy is practically the only source of energy that influences atmospheric motions and our climate. The sun is a sphere of intensely hot gaseous matter, composed mainly of hydrogen, with a diameter of 1.39×10^5 km comprising many layers of gases which are progressively hotter and denser toward its centre. The outermost layer from which energy radiates into the solar system has an effective blackbody emitting temperature of about 5800K for the same energy output, and 6300K for the same wavelength of maximum radiation. ^{temperature at} The centre of the sun may be from 15×10^6 to 40×10^6 K. It is generally accepted

⁺ see p. 158

Chapter 2

that a hydrogen-to-helium thermonuclear reaction is the source of the sun's energy.

2.2 THE SOLAR CONSTANT

In a survey of solar radiation measurement a parameter that should be considered first is the irradiance received outside the earth's atmosphere, namely the solar constant. The solar constant is the total irradiance in the solar spectrum. This quantity, however, is not sufficient since most solar applications are strongly wavelength dependant. It is necessary then, to examine the distribution of irradiance within the spectrum, see also Appendix B.

2.3 A CLOUDLESS SKY ATMOSPHERE AND ITS OPTICS

Solar radiation emanating from the sun is attenuated, before reaching the ground, by the earth's atmosphere which can be classified into three broad types: a) clear, b) partly cloudy and c) cloudy. This analysis is concerned only with both direct and diffuse radiation during clear days. Böer (20) selected five typical clear weather days to represent typical seasonal conditions in respect to air mass, water vapour, ozone and turbidity. Solar energy availability is needed for all types of weather conditions but clear-day radiation is the most important because solar effects are large. In addition, a study of clear-day radiation is a logical start into the problem of ^{the} incidence of solar energy on partly cloudy and cloudy days.

A method is introduced here to calculate the fractional irradiance per waveband for the direct and diffuse components as a function of air mass for the Glasgow area.

2.3.1 The Earth's Atmosphere

The earth's atmosphere consists mainly of molecular nitrogen and molecular oxygen. In addition it contains water vapour and aerosols such as dust, soot, water drops and ice crystals. Consequently, in order to determine the transmittance of the atmosphere to solar radiation, the total atmosphere of the earth is usually divided into three groups: clean dry air molecules, water vapour and aerosols. Solar radiation entering the earth's atmosphere is attenuated by each of these groups.

2.3.2 Clean Dry Air

Clean dry air contains about 78% nitrogen, 21% oxygen, 1% argon and 0.33% carbon dioxide by volume. The actual composition and concentration of the constituents of clean dry air vary with geographic location, elevation and season. Air molecules, though, absorb solar radiation only at selective wavelengths. In the upper atmosphere, ozone is created mainly by UV solar radiation. On the ground, it is formed through decomposition of nitrogen oxide that enters the atmosphere from power plant pollutants and forest fires for example. Ozone is mainly concentrated between a 10 -35 km altitude, fig. B.1.

The amount of total ozone l , in a vertical column of air is given in cm (NTP). Table 2.3.2 gives the seasonal variation of ozone content for two different latitudes (10). The middle line is the interpolation values for Glasgow. For an annual average in Glasgow $l = 0.344$ (in cm (NTP)).

2.3.3 Water Vapour

The amount of water vapour present in the atmosphere can be defined as:

Precipitable water w is the total amount of water vapour in the zenith direction, between the surface of the earth and the top of the atmosphere.

The following formula by Leckner (21) will be used, which expresses precipitable water in terms of relative humidity.

$$w = \frac{0.493}{T} \cdot \phi_r \cdot \exp\left(26.23 - \frac{5416}{T}\right) \quad (2.3.3)$$

where ϕ_r is the fractional relative humidity, T is the ambient temperature (in kelvins)

Average values (over a 10 year period from 1956 to 1965) (22) of relative humidity and dry bulb temperature at 9h and 15h, GMT at Renfrew Airport Glasgow are given in tables 2.3.3a and 2.3.3b respectively.

Average yearly relative humidity $\phi_r = 0.78$

Average yearly ambient temperature = 9.85°C

= 283 K

Using (eq. 2.3.3), for Glasgow $w = 1.62 \text{ cm}$

2.3.4 Aerosols

An aerosol is a colloidal system of small solid or liquid particles that remain suspended in the air and follow the motion of the air. Aerosols are highly variable in size, distribution, composition and optical properties.

An atmosphere containing aerosols is also called turbid or hazy. The presence of aerosols in the atmosphere can be quantified by any one of the following:

Month	Jan	Feb	Mar	Apr	May	June	July	Aug	Sep	Oct	Nov	Dec	Year
-------	-----	-----	-----	-----	-----	------	------	-----	-----	-----	-----	-----	------

Table 2.3.2 SEASONAL VARIATION OF ATMOSPHERIC OZONE (in cm (NTP))

Latitude													
60.0°N	0.33	0.39	0.42	0.40	0.39	0.36	0.34	0.32	0.30	0.38	0.30	0.31	
55.9°N	0.33	0.38	0.40	0.39	0.38	0.36	0.34	0.32	0.30	0.34	0.30	0.31	
50.0°N	0.32	0.36	0.38	0.38	0.37	0.35	0.33	0.31	0.30	0.28	0.29	0.30	

Table 2.3.3a

RELATIVE HUMIDITY (%)

Time													
09 h GMT	89	86	84	78	75	75	79	82	85	87	89	89	83%
15 h GMT	82	76	71	65	63	64	68	70	72	77	81	84	73%

Table 2.3.3b

DRY BULB TEMPERATURE (in degrees C)

Time													
09 h GMT	2.3	2.8	4.9	7.9	10.9	13.7	14.4	14.0	12.4	9.8	5.5	3.6	8.5
15 h GMT	4.4	5.7	8.2	11.1	14.2	16.8	17.0	16.8	15.3	12.2	7.8	5.1	11.2

ATMOSPHERIC PROPERTIES - GLASGOW AREA

- 1) Number of dust particles per cubic centimeter
- 2) Atmospheric turbidity* and
- 3) Visibility*

Aerosols in the atmosphere can alter the solar radiation incident at the ground in two ways: by decreasing the ground level irradiance and by changing the relative amounts of direct and diffuse radiation.

2.4 OPTICAL MASS

Optical mass,[#] m , is the ratio of ^{the} actual path length of the sun's rays through the atmosphere, to the path length vertically above the surface in question. Air mass zero refers to the absence of atmospheric attenuation at 1 AU from the sun.

Ignoring the earth's curvature and assuming that the atmosphere is nonrefractive and completely homogeneous (fig. 2.4a), the optical mass applied to all the atmospheric constituents is:

$$m = \sec \theta_z \quad (2.4)$$

where θ_z is the zenith angle.

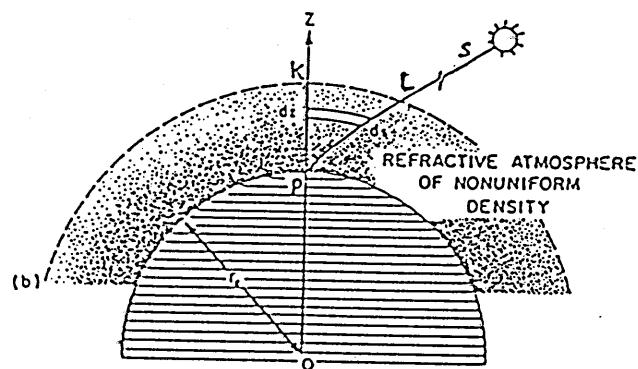
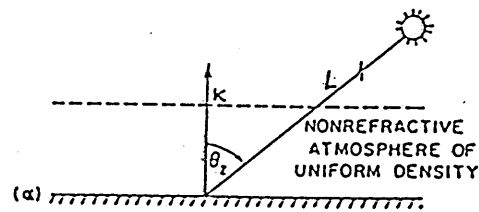


Figure (2.4) The trajectory of a solar ray through the earth's atmosphere.

- * scattering of solar radiation by other than dry air molecules (6)
- * meteorological range (6)
- # accurately this Relative Optical Air Mass but in place of this lengthy expression Optical Mass or simply Air Mass is used (6)

However, density is actually variable with height. Furthermore, because of the curvature of the earth and refraction through the atmosphere, the slant path of the beam radiation will follow the path PL, fig. 2.4b.

The optical mass is ^{therefore} a function of the distribution, with height, of atmospheric density and refractive index.

2.4.1 ^{Relative} Optical Air Mass m_a^+

Kasten (24) presented tables of the ^{relative} optical air mass and the following formula which approximates ^{to} his tables:

$$m_a = \left(\frac{p}{1013.25} \right) \left[\cos \theta_z + 0.15(93.885 - \theta_z)^{-1.253} \right]^{-1} \quad (2.4.1)$$

where p is the local pressure in mbars.

The above equation was also employed to compute the optical aerosol mass (6).

2.4.2 Optical Ozone Mass m_o

Fig. B.1 gives the concentration profile of ozone in the atmosphere. Assuming that all ozone is concentrated in a thin layer centred at height z_o , Robinson (10) through simple geometry, has shown:

$$m_o = \frac{1 + \frac{z_o}{r_e}}{\left[\cos^2 \theta_z + \left(\frac{z_o}{r_e} \right) \right]^{1/2}} \quad (2.4.2)$$

$z_o = 21.3$ km above sea level

r_e = mean radius of earth, 6370 km.

Götz et al. (25) has shown that the mean effective height z_o , is higher when the total amount of ozone is low. For $l = 0.34$ cm, z_o is 21.3 km.

⁺ see (6) p. 100

2.4.3 Optical Water Vapour Mass m_w

The vertical water vapour density profile is very different from that of dry air. Kasten (24) has developed the following formula:

$$m_w = \left[\cos \theta_z + 0.0548 \cdot (92.65 - \theta_z)^{-1.452} \right]^{-1} \quad (2.4.3)$$

2.5 ATTENUATION OF (DIRECT) SOLAR RADIATION

The solar spectrum is substantially modified in passing through the earth's atmosphere, and approximately 25-50% of its irradiance is lost by scattering and absorption. Scattering, results in attenuation of the beam radiation by air molecules, water vapour and dust.

Depending on the particles size scattering is determined by either Rayleigh's or Mie's theory. Rayleigh's theory is based on the assumption that the scattering particles are spherical, that ^{they} scatter independently of one another and that their ^{diameters} are less than one tenth the wavelength of light.

Mie's theory takes into the account the size, shape, dielectric constant, and absorptivity of the particles. It is applied for particle size diameters greater than $\frac{1}{10} \lambda$.

See fig. 2.5

Scattering by air molecules is Rayleigh scattering and of water vapour, ⁽⁶⁾ dust particles and aerosols it is Mie scattering.

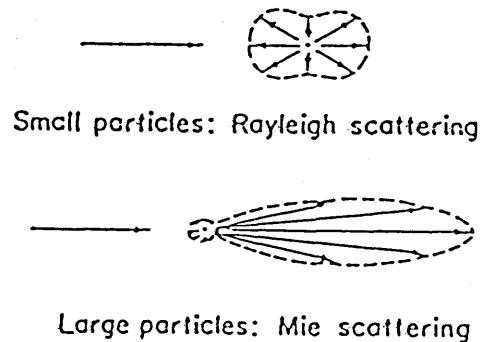


Fig. 2.5 Angular distribution in Rayleigh and Mie scattering.

Absorption of radiation in the atmosphere in the solar energy spectrum is due largely to ozone in the ultraviolet and water vapour in bands in the infrared.

Simple formulations are given describing attenuation of direct radiation by the various atmospheric constituents. For calculation purposes the extraterrestrial spectrum listed in Table B.1. shall be used.

2.5.1 Scattering of Air Molecules , $\tau_{r\lambda}$

Leckner (21) has presented the following approximate formula for the transmittance of dry air at standard conditions:

$$\tau_{r\lambda} = \exp \left(- 0.008735 \cdot \lambda^{-4.08} \cdot m_a \right) \quad (2.5.1)$$

2.5.2 Transmittance of Uniformly Mixed Gases , $\tau_{g\lambda}$

The spectral transmittance for molecular absorption due to CO_2 , O_2 etc., combined under a general denomination of uniformly mixed gases is given by the following:

$$\tau_{g\lambda} = \exp \left[- 1.41 \cdot K_{g\lambda} \cdot m_a / (1 + 118.93 K_{g\lambda} \cdot m_a)^{0.45} \right] \quad (2.5.2)$$

by Leckner (22), $K_{g\lambda}$ is taken from table B.2 and is the spectral absorption coefficient of uniformly mixed gases.

2.5.3 Transmittance of Water Vapour , $\tau_{wa\lambda}$

The special transmittance due to water vapour absorption

is:

$$\tau_{wa\lambda} = \exp \left[- 0.2385 \cdot K_{wa\lambda} \cdot W \cdot m_w / (1 + 20.07 K_{wa\lambda} \cdot W \cdot m_w)^{0.45} \right] \quad (2.5.3)$$

by Leckner (21), $K_{wa\lambda}$ from table B.3 is the absorption coefficient of water vapour.

2.5.4 Transmittance of Aerosols

The absorption of solar energy by a layer of aerosols increases the radiative heating of the atmosphere and decreases the amount of energy available at the surface.

The turbidity of the atmosphere measured at any site depends partly on local weather which determines the input of aerosols from domestic and industrial sources and mainly on the origin of the prevailing air mass which determines the input of aerosols from much distant sources.

The interaction between solar radiation and atmospheric pollution is reciprocal - solar radiation influences air pollutants and pollutants influence solar radiation. Peterson (23) et al. studied the interaction between air pollutants and solar radiation. Unsworth (26) et al. found that, from a long series of measurement of τ_a in Britain, τ_a depends on the air stream prevailing over the area and also that τ_a depends mostly on the amount of aerosol in the atmosphere.

Since attenuation effects of scattering and absorption by dust are difficult to separate, Ångström^{via} (6) suggests a single formula.

$$\tau_{a\lambda} = \exp(-\beta \cdot \lambda^{-\alpha} \cdot m_a) \quad (2.5.4)$$

A different procedure is that of Moon (27) in which separate coefficients for water and dust particles are used.

In equation (2.5.4), β is called Angstrom's turbidity coefficient and varies 0.0 to 0.5. α is an index representing the amount of aerosols present in the atmosphere in the vertical direction.

The wavelength exponent, α , is related to the size distribution of the aerosol particles and varies from 4 to 0. When the aerosol particles are very small α should approach 4 and it should approach 0 for very large particles. For Glasgow's atmospheric condition $\alpha = 0.66$, $\beta = 0.085$, I believe it to be typical. Kreith and Kreider (5) also propose similar values for their tables. Rearranging McClatchy and Selby's equation (6)[†] the above values will give a visibility of 134Km, a useful measure of atmospheric clarity.

Different researchers in the field suggest different approaches and also suggest various combinations of the parameters α , β , with various degrees of atmospheric cleanliness.

Atmosphere	β	α	Visibility (km)	
Clean	0.00	1.30	340	
Clear	0.10	1.30	28	
Turbid	0.20	1.30	11	Iqbal (6)
Very turbid	0.40	1.30	5	

Weather Type	α	β	
Very clear/cold, (-10°C), Winter day	1.5	0.03	
Clear/cool, (5°C), Spring day	1.3	0.06	
Clear/cool, (15°C), Summer day	1.1	0.09	Böer (20)
Hazy/hot, (35°C), Summer day	0.6	0.25	
Hazy, warm, (20°C), Autumn day	0.8	0.15	

2.5.5 Transmittance of Ozone, $\tau_{o\lambda}$

By Bouguer's-Lambert's-Beer's laws, see 3.2 for ozone

$$\tau_{o\lambda} = \exp(-k_o \cdot l \cdot m_o)$$

For 1 see 2.3.2 and the attenuation coefficients $k_{o\lambda}$ are given in table B.4.

[†] via Iqbal

2.5.6 Direct Spectral Irradiance On The Ground, $I_{n\lambda}$

Direct or beam radiation is the solar radiation intercepted by a surface with negligible direction change and scattering in the atmosphere, figure 2.6.

The monochromatic distribution of direct solar beam can now be computed as a function of a number of variables, including optical mass and a wide variety of atmospheric parameters. The total transmittance due to the molecular absorbers can be written as:

$$\tau_{ma\lambda} = \tau_{o\lambda} \cdot \tau_{g\lambda} \cdot \tau_{wa\lambda} \quad (2.5.6a)$$

and due to continuum attenuation as:

$$\tau_{c\lambda} = \tau_{r\lambda} \cdot \tau_{a\lambda} \quad (2.5.6b)$$

The monochromatic transmittance is:

$$\begin{aligned} \tau_{\lambda} &= \tau_{c\lambda} \cdot \tau_{ma\lambda} \\ &= \tau_{r\lambda} \cdot \tau_{a\lambda} \cdot \tau_{o\lambda} \cdot \tau_{g\lambda} \cdot \tau_{wa\lambda} \end{aligned} \quad (2.5.6c)$$

Direct spectral irradiance at any wavelength on a surface normal to the sun's rays and at mean sun-earth distance is:

$$I_{n\lambda} = I_{on\lambda} \cdot \tau_{\lambda} \quad (2.5.6d)$$

2.6 ORIGINS OF DIFFUSE SPECTRAL RADIATION

Diffuse radiation is generated by the scattering effects of air molecules and aerosols, figure 2.6.

It does not have a unique direction and shows a shift⁺ to shorter wavelength when compared with direct radiation, see figure 2.9.3.

⁺ in the peak monochromatic irradiance

It was found[†] that for Glasgow's typical clear sky atmosphere, this component of solar radiation is equivalent to 21% of the total radiation falling on a horizontal surface at air mass 2.

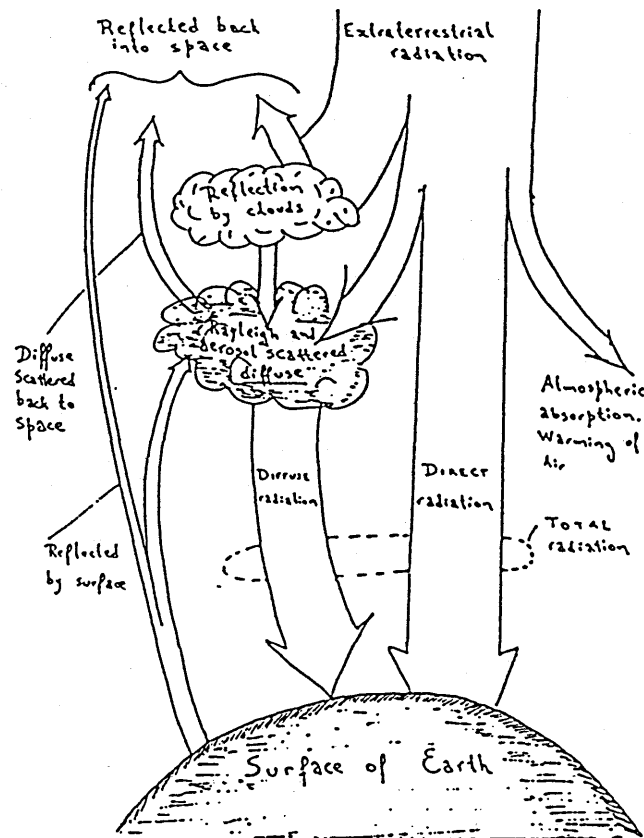


Figure 2.6. Direct, Diffuse and Total Solar Radiation.

2.6.1 Rayleigh - Scattered Spectral Diffuse Irradiance, $I_{dr\lambda}$

Irrespective of the angle of incidence, about half the diffuse radiation is directed toward the ground and the remainder goes back to space. Brine (28) et al. suggest the following equation for Rayleigh scattered diffuse radiation reaching the ground after the first pass through the atmosphere:

$$I_{dr\lambda} = I_{0\lambda} \cdot \cos\theta_z \cdot \tau_{m\lambda} \cdot [0.5 \cdot (1 - \tau_{r\lambda}) \cdot \tau_{a\lambda}] \quad (2.6.1)$$

[†] from theory

2.6.2 Aerosol Scattered Spectral Diffuse Irradiance, $I_{da\lambda}$

Brine (28) et al. suggest the following equation for diffuse radiation reaching the ground after the first pass through the atmosphere:

$$I_{da\lambda} = I_{0a\lambda} \cdot \cos \theta_z \cdot \tau_{ma\lambda} \cdot [F_c \cdot \omega_0 \cdot (1 - \tau_{a\lambda}) \tau_{a\lambda}] \quad (2.6.2)$$

where $F_c = \frac{\text{energy scattered in the forward direction}}{\text{total energy scattered}}$

For Britain, Robinson (10), provides us with the following table:

TABLE 2.6.2										
θ_z	0	10	20	30	40	50	60	70	80	85
F_c	0.92	0.92	0.90	0.90	0.90	0.85	0.78	0.68	0.60	0.50

and $\omega_0 = \frac{\text{energy scattered by aerosols}}{\text{total attenuation under the first impingement of direct energy}}$

$\omega_0 = 0.6$ was chosen for Glasgow, as it is appropriate for for urban industrial regions (6).

2.6.3 Atmospheric Reflectance, $\rho'_{a\lambda}$

Reflectance is defined as the ratio of the energy[†] reflected back to the incident energy[†]. Atmospheric reflectance is the diffuse component reflected back to space. Iqbal (6) assumes a single angle of incidence corresponding to air mass $m = 1.9$, and hence $\theta_z \approx 58$ and from table 2.6.2, $F'_c = 0.79$.

$$\rho'_{a\lambda} = \underbrace{\tau'_{ma\lambda} \cdot [0.5 \cdot (1 - \tau'_{a\lambda}) \cdot \tau'_{a\lambda}]}_{\text{reflectance of air molecules}} + \underbrace{(1 - F'_c) \cdot \omega_0 \cdot (1 - \tau'_{a\lambda}) \cdot \tau'_{a\lambda}}_{\text{reflectance of aerosols}} \quad (2.6.3)$$

* The dashed characters correspond to $m = 1.9$

† strictly irradiance

The atmospheric reflectance is greater at shorter wavelengths and increases with α and β .

2.6.4 Multi-reflected Spectral Diffuse Irradiance

Diffuse radiation arriving on the ground after the first pass through the atmosphere and direct radiation are in part reflected by the ground. This upward radiation is partly reflected back to the ground by the atmosphere. This process continues ad infinitum.

Consider diffuse radiation reaching the ground after the first pass, and beam radiation on a horizontal surface, and let

$$Q_{\lambda} = (I_{dr\lambda} + I_{da\lambda}) + I_{n\lambda} \cos \theta_z$$

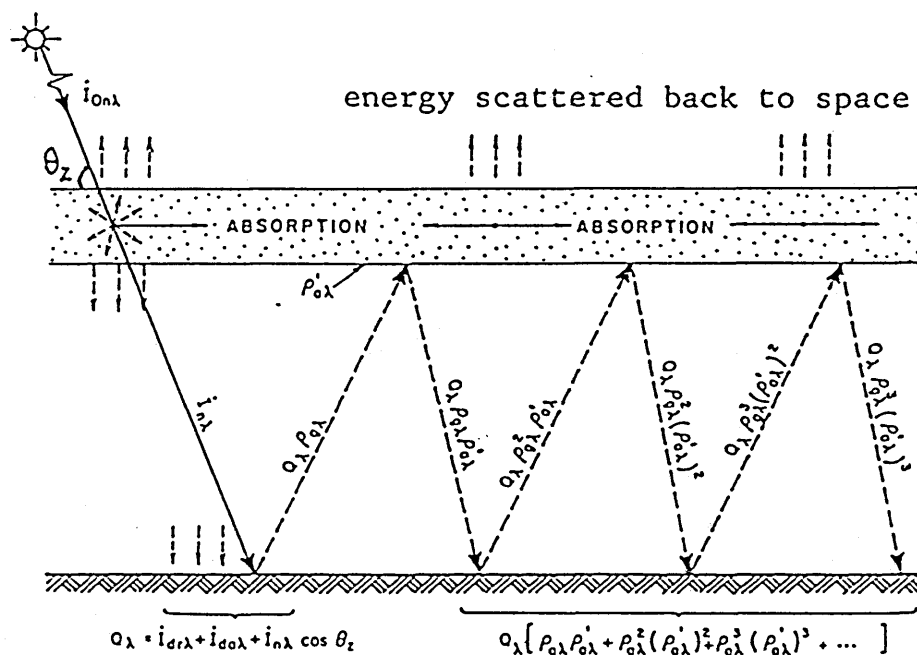


Fig. 2.6.4 The process of multiple reflection of radiation between the atmosphere and the ground.

From fig. 2.6.4, it can be seen that the total amount of multi-reflected radiation reaching the ground is:

$$I_{dm\lambda} = \frac{(I_{dr\lambda} + I_{da\lambda}) \cdot \rho_{dg\lambda} \cdot \rho'_{a\lambda}}{1 - \rho_{dg\lambda} \cdot \rho'_{a\lambda}} + \frac{I_{n\lambda} \cdot \cos \theta_z \cdot \rho_{bg\lambda} \cdot \rho'_{a\lambda}}{1 - \rho_{bg\lambda} \cdot \rho'_{a\lambda}} \quad (2.6.4)$$

where $\rho_{dg\lambda}$ is the ground reflectivity due to diffuse radiation and $\rho_{bg\lambda}$ is the ground reflectivity due to beam radiation.

2.6.5 Diffuse Spectral Irradiance on the Horizontal, $I_{d\lambda}$

The diffuse spectral irradiance on a horizontal surface, $I_{d\lambda}$ is composed of three parts: a) the diffuse spectral irradiance produced by Rayleigh scattering $I_{dr\lambda}$, b) by aerosols after the first pass through the atmosphere $I_{da\lambda}$ and c) by multiple reflections $I_{dm\lambda}$.

Consequently

$$I_{d\lambda} = I_{dr\lambda} + I_{da\lambda} + I_{dm\lambda} \quad (2.6.5)$$

A comparison between $I_{dr\lambda}$, $I_{da\lambda}$ and $I_{dm\lambda}$ was performed for the proposed Glasgow atmosphere. It was found that $I_{dr\lambda} = 64\%$, $I_{da\lambda} = 25\%$ and $I_{dm\lambda} = 11\%$ of the total diffuse radiation.

2.6.6 Global Radiation, I_{λ}

Global, or total irradiance, is all solar radiation incident on a surface, including scattered, reflected and direct, figure 2.6.

On a horizontal surface the global spectral irradiance is:

$$I_{\lambda} = I_{n\lambda} \cos \theta_z + I_{d\lambda} \quad (2.6.6)$$

It is shown clearly in table B.5 that at all wavelengths longer than $1 \mu\text{m}$, global radiation is almost entirely composed of the direct component.

* from the work of this chapter

2.7 TOTAL AND SPECTRAL SOLAR IRRADIANCE AT GROUND LEVEL

All the information and formulae listed in chapter 2 were used to construct a computing program. The program permits the atmospheric parameters such as ozone layer thickness, precipitable water vapour, turbidity, and ground reflectivity to be varied independently. The results which establish standard curves for direct, diffuse and global ^{radiation} at air mass 2 are listed in Appendix B, in tabular form, (table B.5).

2.8 GLASGOW STANDARD ATMOSPHERE

ozone layer thickness = 0.34 cm

precipitable water vapour = 1.62 cm

wavelength exponent, α , = 0.66

turbidity parameter, β , = 0.085

Extensive data in tabular form are given in table B.5 for the above parameters and for an air mass 2. Moon (27) suggests that air mass 2 should be used whenever a single, standard solar radiation curve is needed in engineering calculations for places near sea level.

2.9 RESULTS CONCLUSIONS

The total integrated direct solar irradiance value, found to be 734.7 Wm^{-2} , agrees with Thekaekara's (5) within -2% after linear interpolation, and with Moon's (27) within -4% under similar atmospheric conditions and for the same solar constant.

Energy in the infrared band ($0.77 \mu\text{m} - 10^3 \mu\text{m}$) accounts for 50% of the total direct irradiance.

The fraction in the visible spectrum ($0.39 - 0.77 \mu\text{m}$)

accounts for about 63% of the total diffuse radiation arriving on the ground.

After transmission through the atmosphere, very little UV energy reaches the earth.

The method used in this analysis was similar to the one proposed by Iqbal (6) and applied to Montreal (45.5°), Canada. Results for both beam and diffuse spectral irradiance showed an excellent agreement. Quantitatively diffuse radiation for Glasgow and Montreal were very similar and for direct the Montreal ^{irradiance} was somewhat less.

Böer (20) gives similar graphs for a latitude of 40°N in the U.S.A., but only for the direct component of solar radiation. His method is dependent on the type of weather according to a particular season, see 2.3.4, and ^{the} best agreement was for hazy/hot (35°C) Summer days when his results for beam radiation were compared with the ones provided in this thesis.

The amounts and spectra of beam and diffuse ^{radiation} for two different places in Britain were also investigated see Chapter 6.

For most solar engineering problems determining the amount of radiation over a certain bandwidth or over the complete spectrum is required. The fraction of direct and diffuse energy in different colours (6) and regions of the spectrum is shown in table 2.9.

As the zenith angle increases, the fraction in the infrared band increases.

For a fairly clean atmosphere maximum ^{monochromatic irradiance} k_λ is in the UV and violet bands.

$m = 11.5$ $\theta_2 = 85^\circ$

TOTAL RADIATION[†], I_r (Wm⁻²)

TABLE 2.9

Through a series of plots it is demonstrated how the extraterrestrial spectrum is modified by atmospheric parameters before it reaches the ground.

Firstly, it is instructive to look at the relative magnitudes of diffuse, direct* and extraterrestrial radiation for the conditions of the proposed typical Glasgow atmosphere, see figure 2.9.1. In figure 2.9.2 the amount of radiation attenuated by the atmosphere is shown as the shaded area. The lower curve represents the sum of the direct normal and diffuse irradiance. From figure 2.9.3 it is clearly seen that the spectra of direct and diffuse radiation are very different in the region of $0.25 - 0.55 \mu\text{m}$. For this reason it is necessary to perform calculations using two different spectra for beam and diffuse radiation. Also at wavelengths longer than $1.25 \mu\text{m}$ the total radiation is almost entirely composed of the direct component.

In figure 2.9.4 the various molecular absorption bands are identified. The first curve under the extraterrestrial line represents depletion of the direct beam by Rayleigh scattering only. The next curve below represents the actual amount of direct solar flux reaching the ground. The amount of energy absorbed by the various gases is shown by the darkened areas. The size of the shaded areas (except those for O_2 and CO_2) depends on the amount of O_3 and H_2O present in the atmosphere.

The effect of a variation in ozone only is shown in figure 2.9.5. Attenuation by ozone is confined to the UV and the visible spectrum. The absorption effects increase, however, with an increase in the zenith angle.

* The term direct in this Chapter means the direct irradiance normal to the sun's rays.

Varying the amount of water vapour in the atmosphere from 1.62 to 3.5 cm is demonstrated in fig. 2.9.6. Even a small amount of moisture in the atmosphere shuts off all radiation beyond approximately $2.5\mu\text{m}$.

Similar results were observed for the diffuse spectral irradiance, see fig. 2.9.7.

The effect of variation in the turbidity parameter, β , and of the wavelength exponent α , is shown in figs. 2.9.8 and 2.9.9, respectively. β has a strong influence on the spectral flux reaching the ground, α , however, has only a minor influence on the spectral irradiance. Furthermore, irradiance at $\lambda > 0.85\mu\text{m}$ remains unchanged by a change in α .

Fig. 2.9.10 shows the effect of a change in turbidity parameter β . Naturally, greater turbidity results in higher amounts of diffuse radiation.

The effect of a variation in α is demonstrated in fig. 2.9.11. A small average particle size represented by high values of α produces greater amounts of diffuse irradiance.

Finally the influence of ground reflectivity on spectral diffuse irradiance can be examined in fig. 2.9.12. An increase in ground reflectivity from 0.2 to 0.75 (the case of fresh snow cover) substantially increases diffuse irradiance.

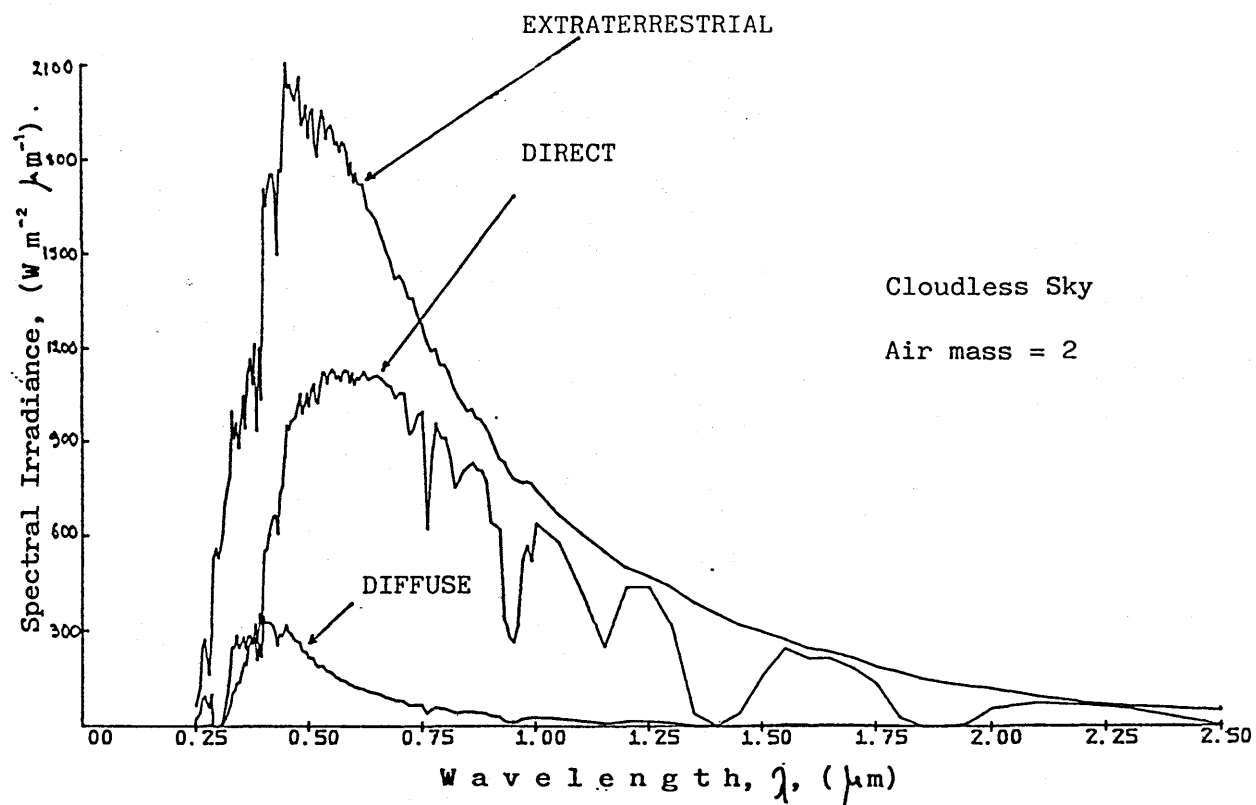


Figure 2.9.1 Magnitudes of extraterrestrial, direct, and diffuse radiation.

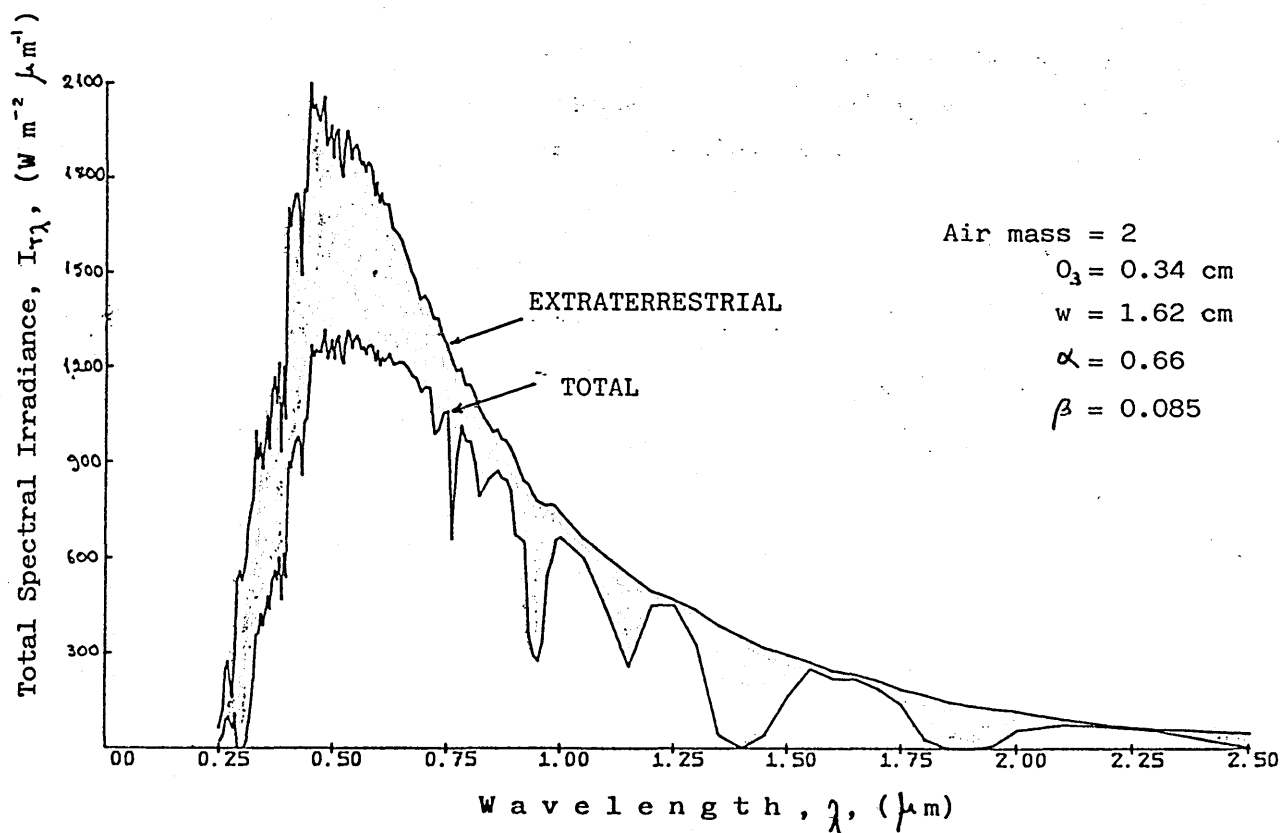


Figure 2.9.2 Amount of radiation attenuated by a proposed Standard Glasgow Atmosphere under cloudless skies.

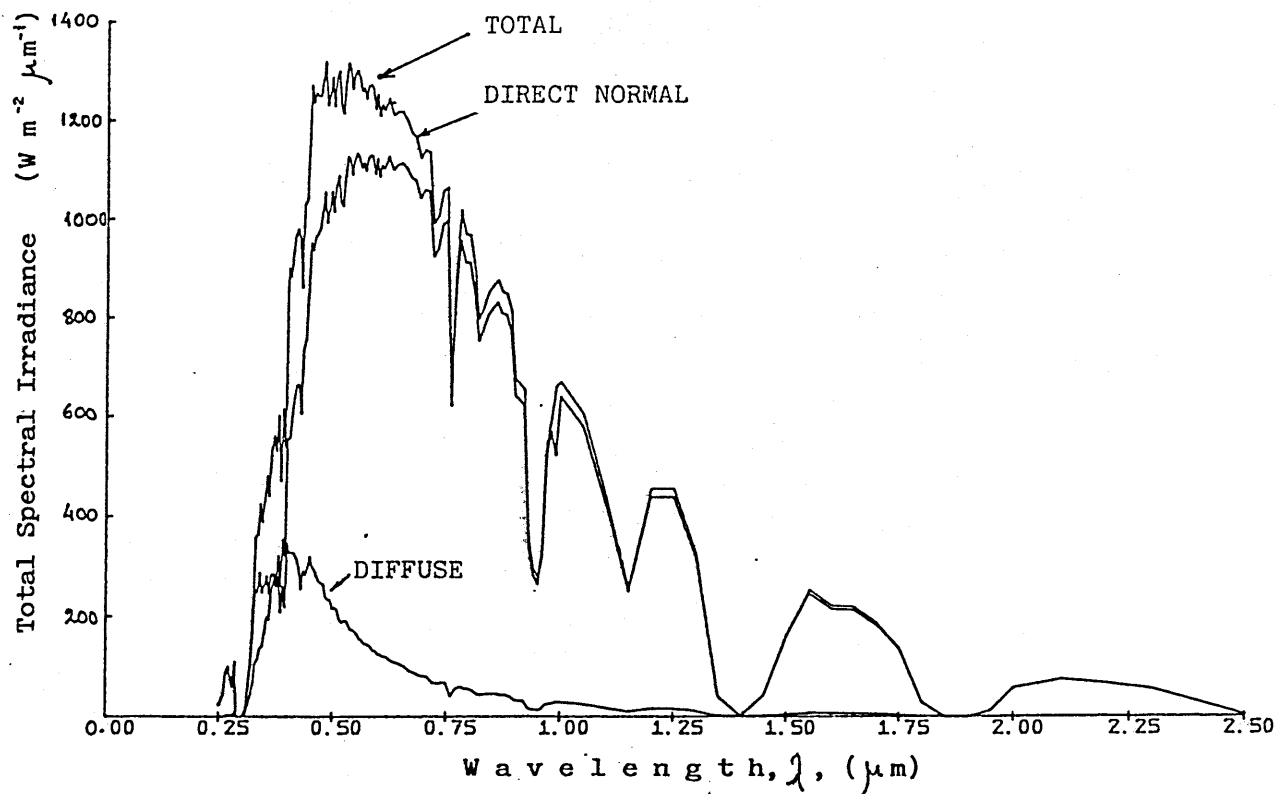


Figure 2.9.3 Magnitudes of total, direct, and diffuse radiation

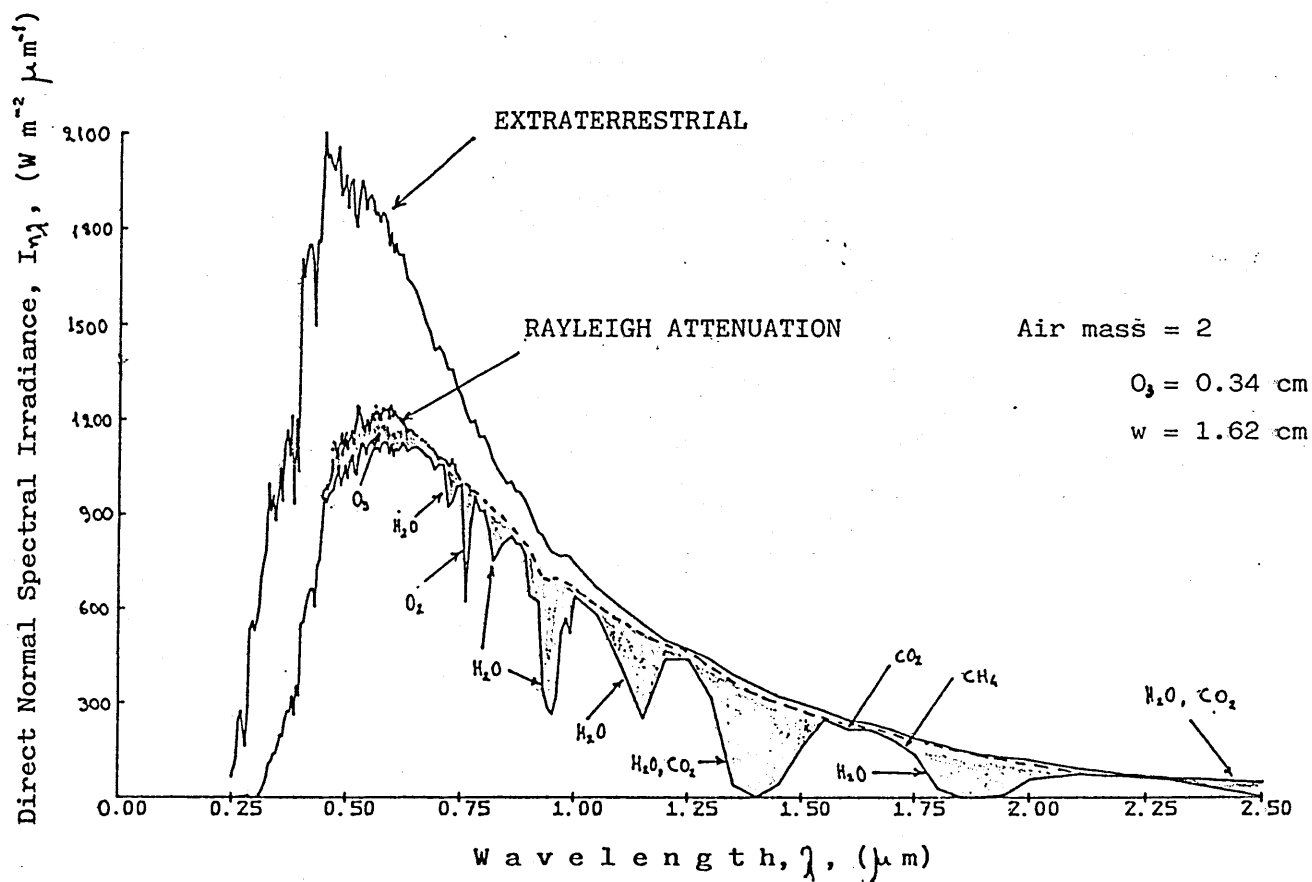


Figure 2.9.4 Identification of the various molecular absorbers.

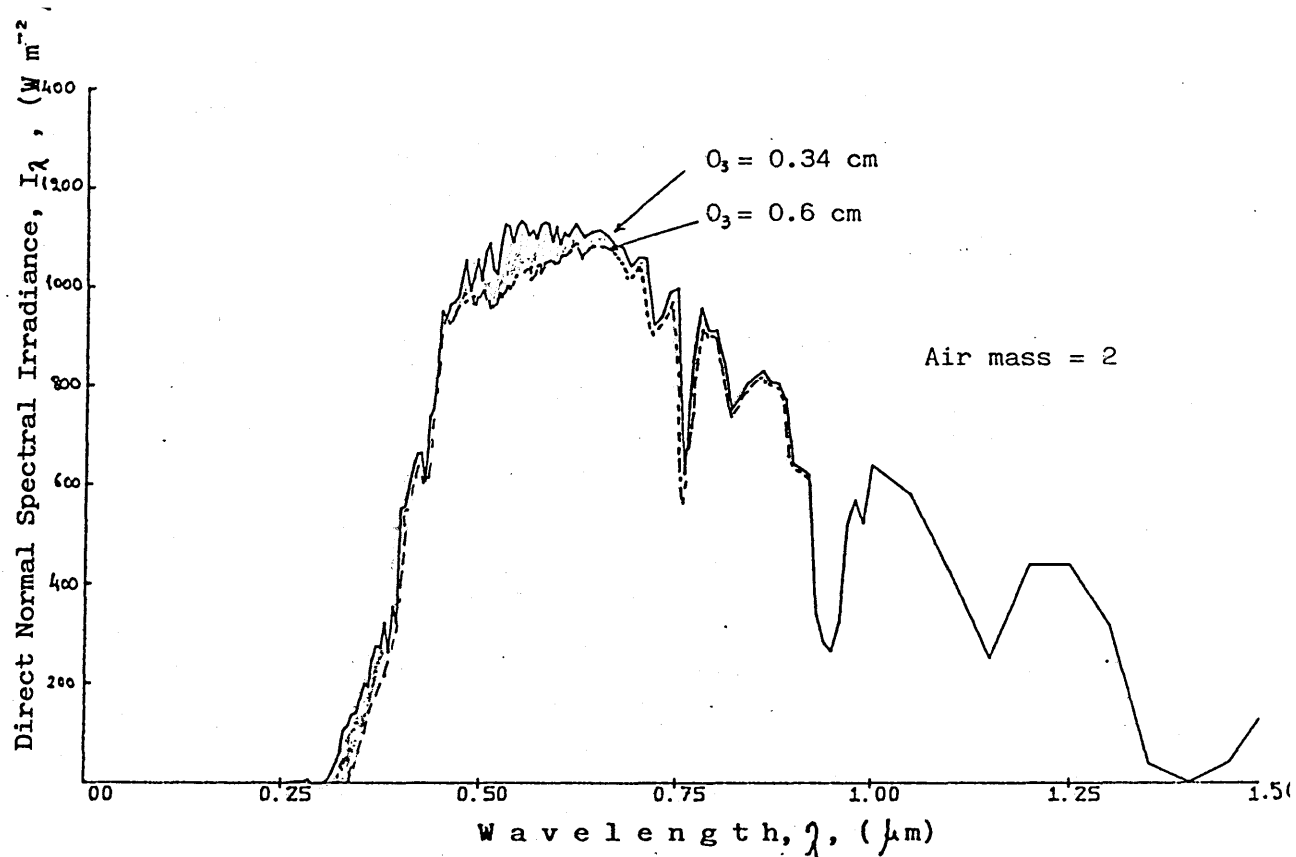


Figure 2.9.5 Spectral direct normal irradiance for different ozone concentrations.

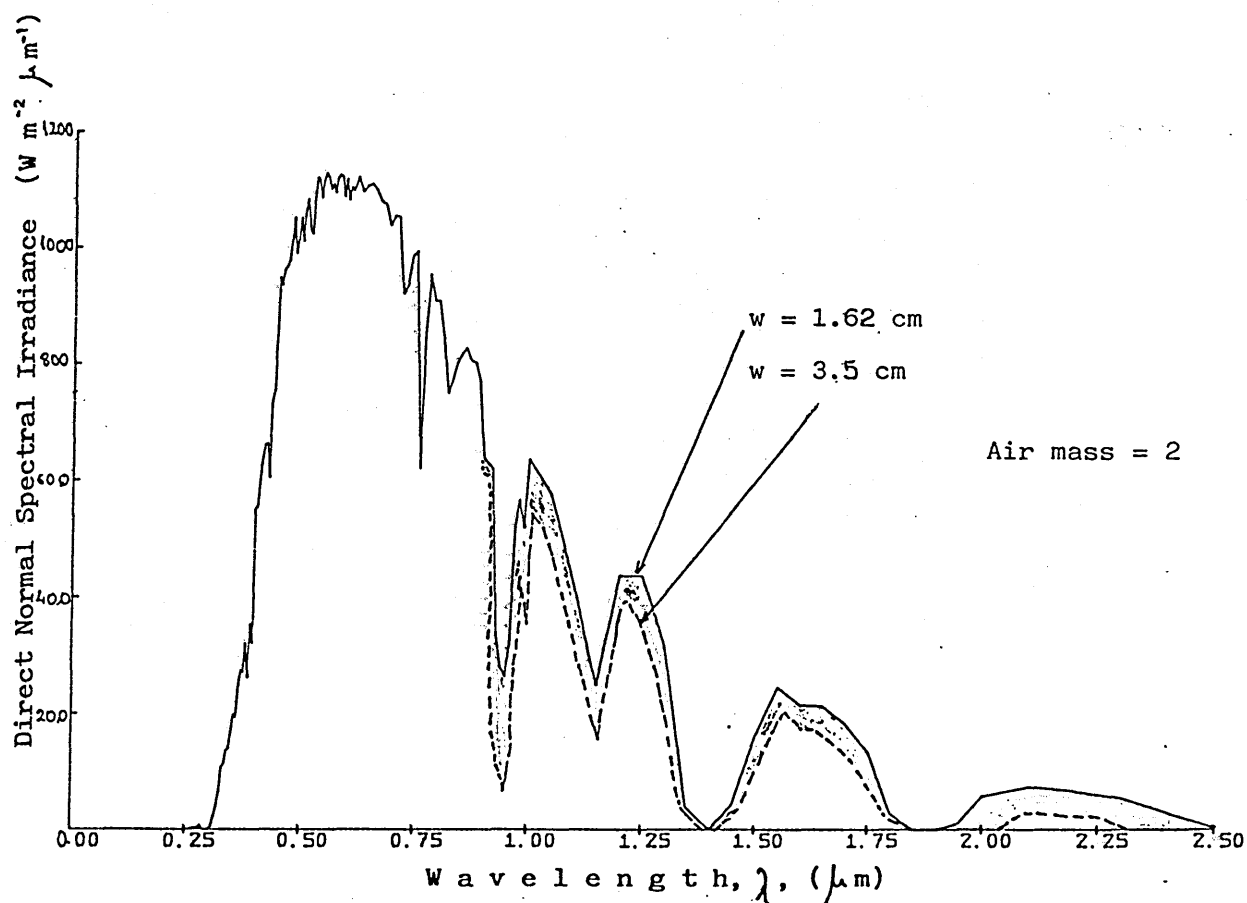


Figure 2.9.6 Spectral distribution of the direct normal component of sunlight for different amounts of precipitable water.

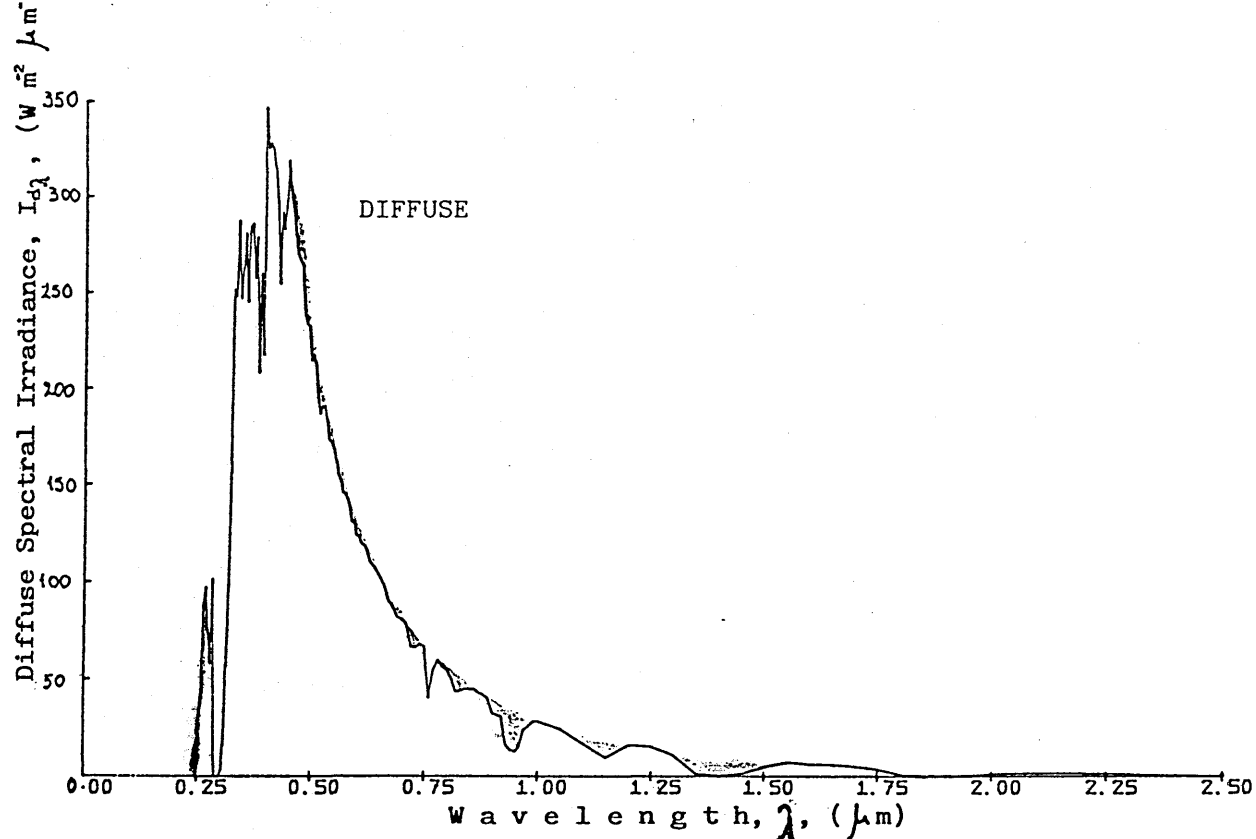


Figure 2.9.7 Diffuse spectral irradiance on a horizontal surface.
The shaded areas indicate increase from 0 to 0.344 cm
(NTP) and water vapor is increased from 0 to 1.62 cm

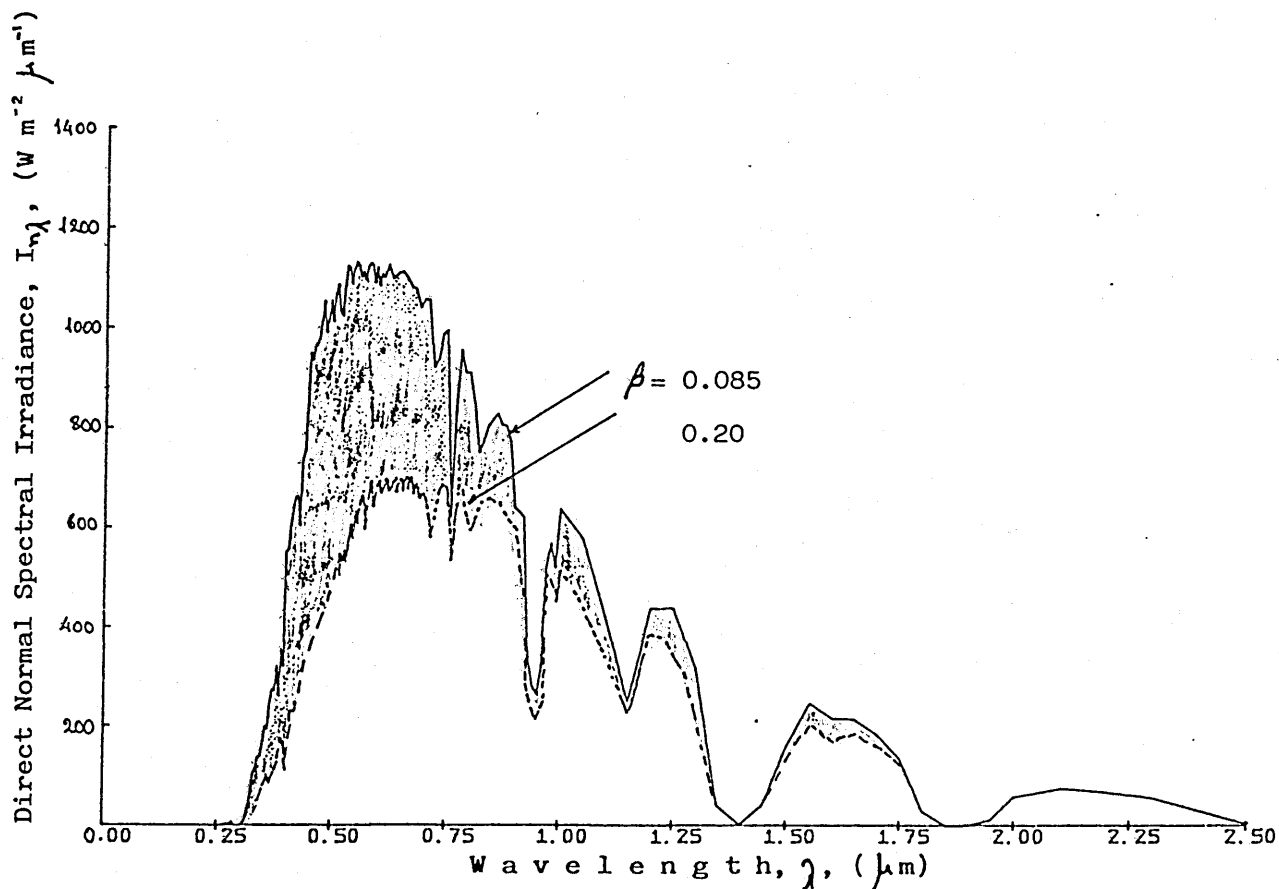


Figure 2.9.8 Direct normal spectral irradiance under different
aerosol amounts.

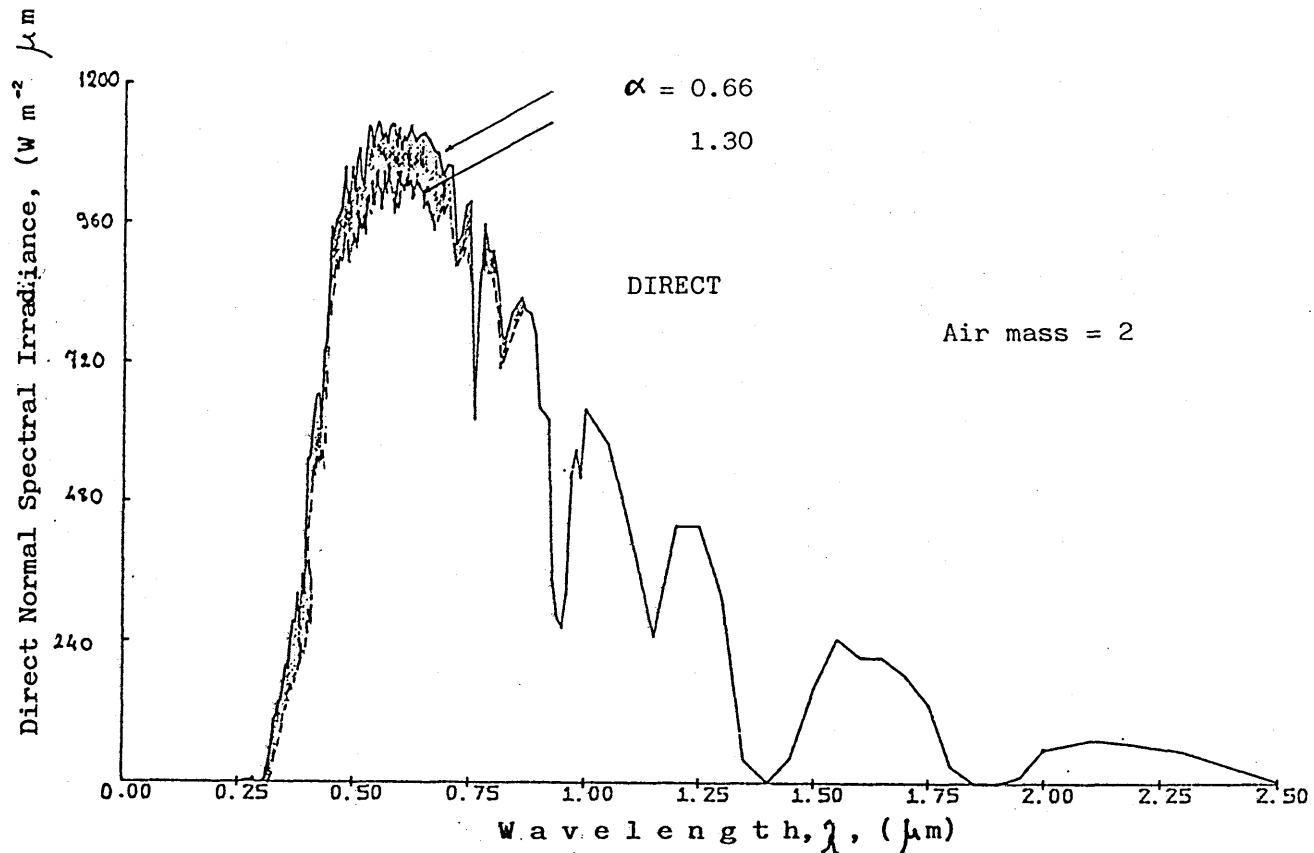


Figure 2.9.9 Direct normal spectral irradiance under varying values of α

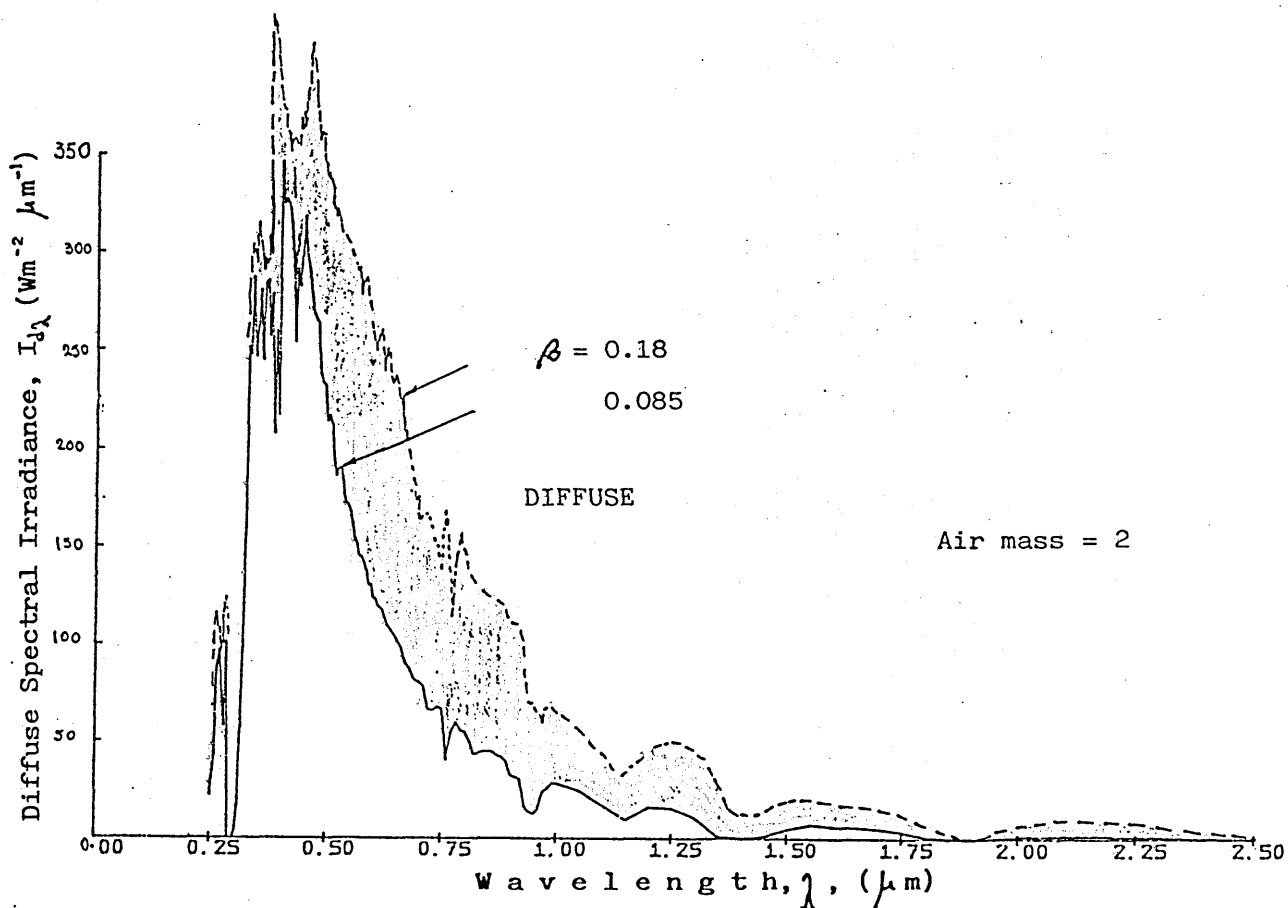


Figure 2.9.10 Diffuse spectral irradiance on a horizontal surface as a function of Angstrom's turbidity coefficient.

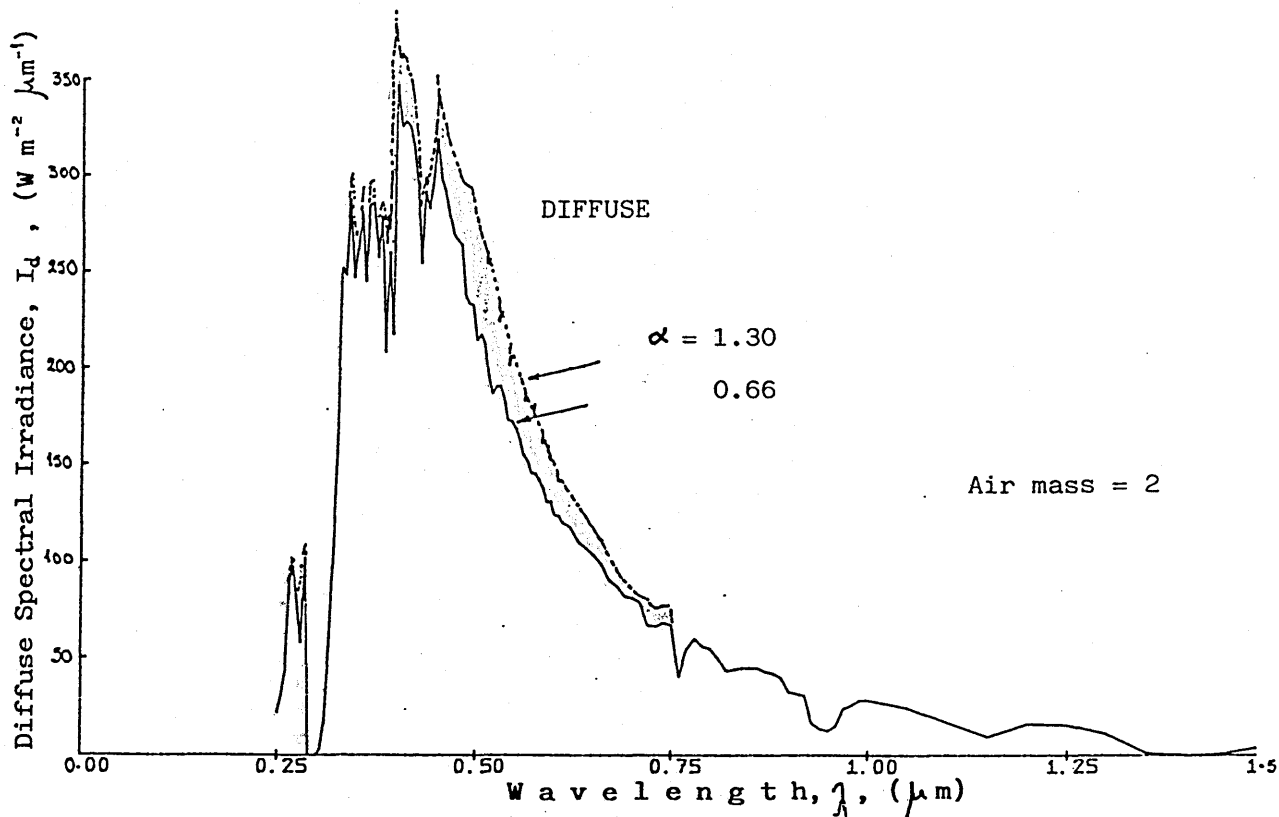


Figure 2.9.11 Diffuse spectral irradiance on a horizontal surface as a function α

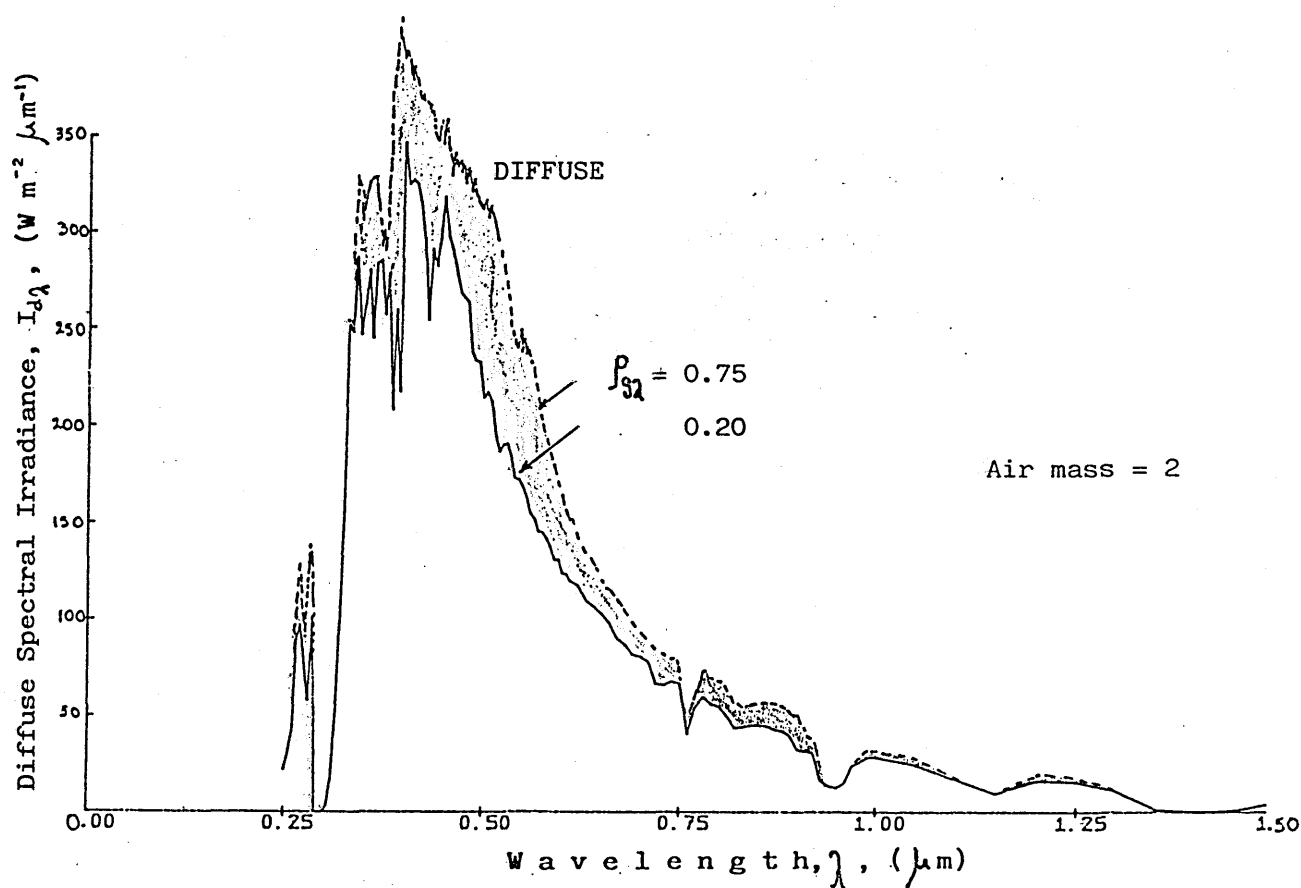


Figure 2.9.12 Diffuse spectral irradiance on a horizontal surface as a function of ρ_{92}

Chapter 3



OPTICS3.0 Introduction

An understanding of the radiation properties and characteristics of the various parts of a transwall module is essential for the analysis of the system. The materials used (glass, various dyes, water) have significant optical property variations with wavelength and in this chapter these variations are examined. The spectral dependance of their properties was measured and is recorded herein. Although incident solar radiation is taken to be unpolarized the transwall produces partial polarization as the radiation passes through the various materials and its treatment is also described in this chapter.

3.1 REFLECTION OF RADIATION3.1.1 Index of Refraction and Extinction Coefficient

The optical behaviour of a transparent substance can be characterized by two wavelength dependent physical properties, the index of refraction $n(\lambda)$ and the extinction coefficients $k(\lambda)$ which are respectively, the real and imaginary parts of its spectral complex refractive index.

$$\bar{n}(\lambda) = n(\lambda) - i k(\lambda) \quad (3.1.1)$$

The index of refraction, which determines the speed of light in the material, also determines the amount of light reflected from a single surface, while the extinction coefficient determines the amount of light absorbed in a substance in a single pass of radiation.

In the case of glass the variation of the refractive index with wavelength gives rise to a phenomenon termed dispersion. In general the refractive index decreases as the wavelength increases and the rate of decrease is greatest at the shorter wavelengths (30).

In the case of water the above statement applies with the difference that the spectral refractive index decreases rapidly in the region of $2\mu\text{m}$, see fig.3.1.1

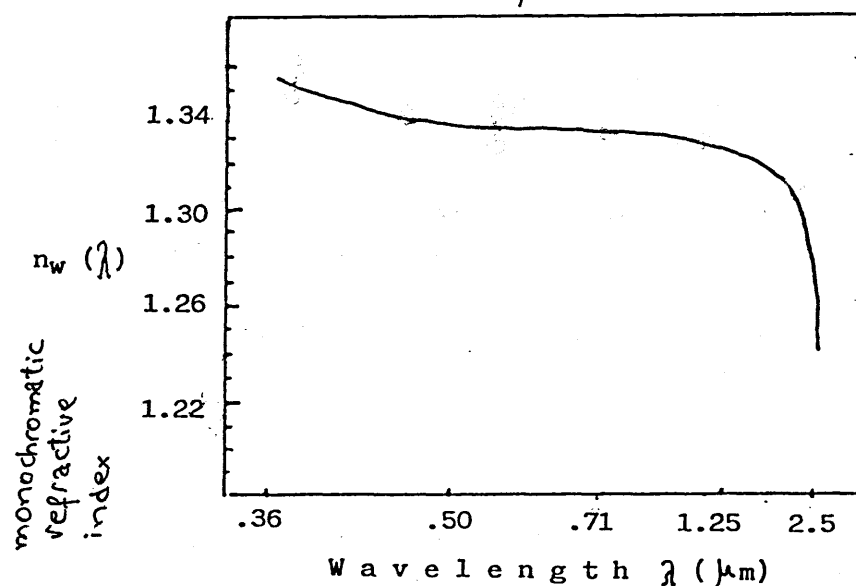


Fig. 3.1.1 shows the refractive index of water as a function of wavelength. (from Palmer (32)).

When a dye is used in the transwall the refractive index of the water dye solution is expected to be different to that of water. In fact, it has been found (45, 31) that the values of the refractive index, n , increase with concentration, but are not too different from that of $n \approx 1.33$ for pure water. In the present analysis the dye concentrations are very moderate (4 – 35ppm), so it is safe to assume that the refractive index of the dye solution remains the same as that of distilled water. This assumption is used everywhere in this thesis.

3.1.2 Fresnel's Law

The reflectance has two components corresponding to the two components of polarization resolved parallel and perpendicular to the plane of incidence.

The perpendicular (\perp) and parallel (\parallel) components, respectively, are given by the relations:

$$\rho_{\perp} = \left[\frac{\sin(\theta - \theta_r)}{\sin(\theta + \theta_r)} \right]^2 \quad (3.1.2a)$$

$$\rho_{\parallel} = \left[\frac{\tan(\theta - \theta_r)}{\tan(\theta + \theta_r)} \right]^2 \quad (3.1.2b)$$

(fig. 3.2.2.)

assuming smooth surfaces and that the incident radiation is unpolarized.

In a transwall module the following boundaries are possible for forward and backward directed rays:

- a) Air/glass boundary
- b) glass/water boundary
- c) water/glass boundary
- d) glass/air boundary

The reflectivity as a function of polarization and angle of incidence was investigated for boundaries (a) and (d).

These cases are summarized in figure 3.1.2

and (d).

The diagrams below correspond to $n_a = 1$ and $n_g = 1.51$.

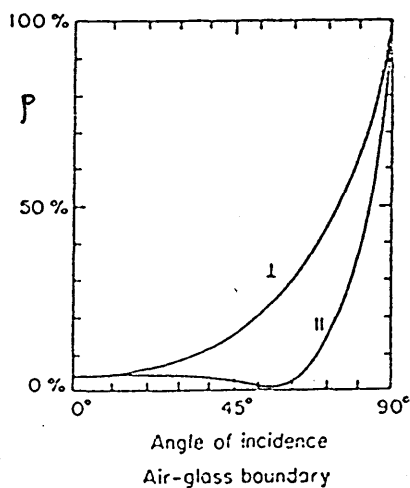
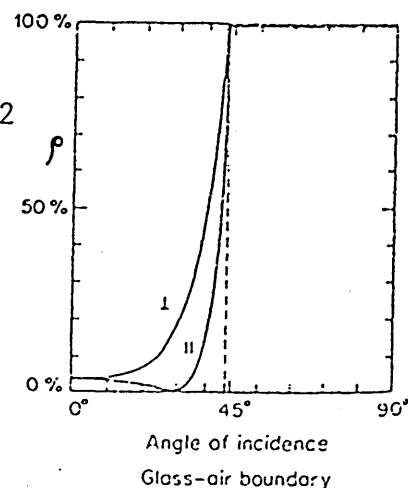


Figure 3.1.2



3.1.3 Reflection At Normal Incidence, R

Although the solar radiation never reaches zero angle of incidence for the vertical transwall, this concept is very useful when experiments are performed in laboratories or tests are carried out for inclined transwalls.

At normal incidence, there is no difference between the // and the \perp polarization of the incident beam, see figure 3.1.2a, hence

$$R = \rho_{\perp} = \rho_{//} = \left[\frac{n_2 - n_1}{n_2 + n_1} \right]^2 \quad (3.1.3a)$$

From Snell's law (3.1.2)

For air/glass interface $R = 0.041$ or 4.1%

The glass refractive index for wavelengths less than the cut off values can no longer be defined by a refraction value alone (33). It has to be expressed as a complex number, $n - ik$, see 3.1. This change in the character of the refractive index alters the expression defining the glass reflection. For radiation at normal incidence the latter is given by:

$$R = \frac{(n-1)^2 + k^2}{(n+1)^2 + k^2} \quad (3.1.3b)$$

Clearly, if k is large relative to n , then the value of R tends to one. In practice the reflection is found to have a wavelength dependence with maxima related through the above expression to changes in k , the extinction coefficient.

3.2 ABSORPTION OF RADIATION

Sometimes the terms absorption and extinction are used synonymously. This is wrong; extinction is the broader term which includes attenuation by both absorption and scattering (9).

$$\text{Extinction} = \text{Absorption} + \text{Scattering}$$

3.2.1 Laws of Attenuation

a) Bouguer-Lambert's law

The attenuation of radiation passing through a homogeneous, isotropic, semi-transparent medium, can be expressed by the Bouguer-Lambert Law which states: "The proportion of incident light absorbed by a medium is independent of its intensity, and that each successive unit layer of the medium absorbs an equal fraction of the light passing through it."

$$I_T(\lambda) = I_0(\lambda) \cdot e^{-\alpha_\lambda \cdot L} \quad (3.2.1a)$$

where $I_0(\lambda)$ is the intensity of the incident light, $I_T(\lambda)$ the intensity of the transmitted light, and α_λ is the monochromatic absorption coefficient.

b) Beer's Law

Beer's law is similar and applies to homogeneous absorbing materials. It is concerned with the variation in concentration of the absorbing component rather than variations in the thickness. Beer's Law states that the intensity of light at thickness L of a layer is:

$$I_T(\lambda) = I_0(\lambda) e^{-\beta_\lambda \cdot C \cdot L} \quad (3.2.1b)$$

where β_λ is the absorption coefficient for unit concentration

and C is the concentration. β_λ is called the molecular absorption coefficient when C is expressed in kilogram molecular weights and L is in meters.

Whenever a change in concentration of the absorbing component (dye, soluble salt etc.) of a homogeneous material causes a change in β_λ the material is said not to obey Beer's Law. Apparent deviations from Beer's Law are associated with the formation, or break up, of molecular aggregates and other modifications of the absorbing molecules and the solvent. A homogeneous material is characterized by the way α_λ and β_λ varies with wavelengths. To characterize heterogeneous (turbid) materials, the much more complicated theory of radiative transfer must be used (34).

When Beer's Law is stated with the common base 10 instead of the Napierian base e

$$I_\tau(\lambda) = I_o(\lambda) \cdot 10^{-\epsilon_\lambda \cdot C \cdot L} \quad (3.2.1c)$$

yields another quantity, introduced by Bunsen, that is often used to express the absorption characteristics of a material (34). ϵ_λ is called the molecular extinction coefficient when C is in gram molecular weights per unit volume ϵ_λ and β_λ are related according to the equation,

$$\epsilon_\lambda = \beta_\lambda \cdot \log_{10} e$$

3.2.2 Optical Density

Optical density A_λ is defined as the negative logarithm to base 10 of the transmittance.

$$A_\lambda = \log_{10} \frac{I_o}{I_\tau} = \log_{10} \frac{I_o}{I_\tau} = \epsilon_\lambda \cdot C \cdot L \quad (3.2)$$

in other words, the optical density of a given substance in a solution is directly proportional to the concentration

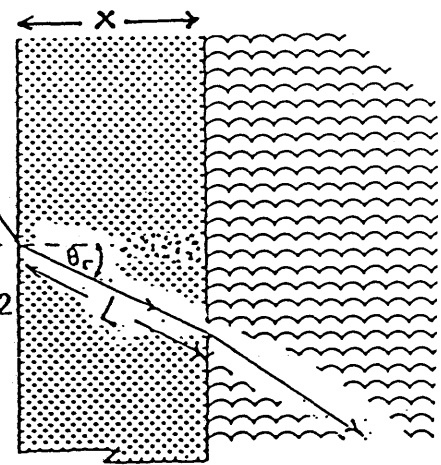
if L , the path length remains constant.

The path length is defined by figure 3.2.2 and the following.

$$L = \frac{x}{\cos \theta_r} \quad \text{or}$$

$$= \frac{x}{\left[1 - \left(\frac{\sin \theta}{\mu}\right)^2\right]^{1/2}} \quad \mu = \frac{n_a}{n_a}$$

Fig. 3.2.2

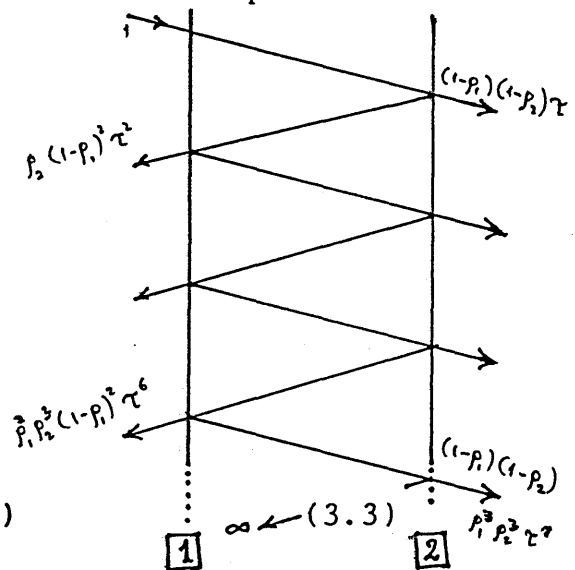


3.3 TRANSMITTANCE THROUGH AN ABSORBING MEDIUM - STOKES' EQUATIONS

Solar radiation frequently has to pass through a transparent medium with air on each side, such as a window glazing. Consider now the flow path of one radiation vector as it undergoes multiple reflections at each interface and between interface absorption as shown in figure 3.3.

The attenuation is given by 3.2.1a and the internal transmissivity,

$$\tau_g = 1 - \alpha = \frac{I_r(\lambda)}{I_o(\lambda)} = \exp(-k_\lambda L)$$



relates to the incidence angle at interface 1 and ξ is the parallel, //, or perpendicular, \perp , components corresponding to the incidence angle at interface 1.

$$\rho = \rho(\rho_\xi, \tau_a) = \rho_{1\xi} + \rho_{2\xi} \tau_a^2 (1 - \rho_{1\xi}^2) \left[1 + \rho_{1\xi} \rho_{2\xi} \tau_a^2 + \rho_{1\xi}^2 \rho_{2\xi}^2 \tau_a^4 + \dots \right]$$

$$\tau = \tau(\rho_\xi, \tau_a) = (1 - \rho_{1\xi})(1 - \rho_{2\xi}) \cdot \tau_a \left[1 + \rho_{1\xi} \rho_{2\xi} \tau_a^2 + \rho_{1\xi}^2 \rho_{2\xi}^2 \tau_a^4 + \dots \right]$$

The terms within the square brackets constitute an infinite summation series.

$$\rho(\rho_1, \tau_2) = \rho_{12} + \left[\rho_{23} (1 - \rho_{12})^2 \tau_2^2 / 1 - \rho_{12} \rho_{23} \tau_2^2 \right] \quad (3.3a)$$

$$\tau(\rho_1, \tau_2) = \tau_2 \left[(1 - \rho_{12}) (1 - \rho_{23}) / 1 - \rho_{12} \rho_{23} \tau_2^2 \right] \quad (3.3b)$$

It follows that the total absorption, α , as a function of (ρ_1, τ_2) is given by:

$$\alpha(\rho_1, \tau_2) = 1 - \rho(\rho_1, \tau_2) - \tau(\rho_1, \tau_2)$$

or $\alpha = (1 - \rho_{12}) \left[1 - \tau_2 - \tau_2^2 \rho_{23} + \tau_2 \rho_{23} \right] / (1 - \tau_2^2 \rho_{23} \rho_{12}) \quad (3.3c)$

The above expressions developed ^{here} are particularly useful when the one surface of the material has an antireflection coating.

For uncoated material $\rho_{12} = \rho_{23}$

The flux transmitted from one element to the next will be partly polarized even if the original beam was not. It is therefore necessary to process each component of polarisation separately before combining the overall value for the entire system. It is therefore incorrect to calculate an average for both components.

Table C.1⁺ shows this difference in the distribution of solar radiation for the transwall module used for various angles of incidence. Errors of up to 5 percent in the calculated total transmittance in the transwall can result from this improper averaging.

+

3.4 GLASS SPECTRAL TRANSMISSION

Glass like most transparent media transmits selectively; that is, transmittance is a function of wavelength of the incident radiation. 'Clear' glass has some slight colourisation stemming from impurities (Fe_2O_3) in the batch of raw materials.

Using a Beckmann spectrophotometer, see Appendix D, the transmittance of a 6 mm specimen of Pilkington glass is given in figures 3.4a and b. This type of glass is used as glazing in the solar test cell and to form the transwall modules.

From the figures it can be seen that glass transmits well in the visible spectrum, cutting off only that small portion of the UV $< 0.35 \mu\text{m}$ and $> 2.7 \mu\text{m}$ in the IR.

3.4.1 Glass Spectral Reflection

The intensity of the reflection from an air glass interface depends on the glass refractive index, the angle of incidence of the light, and the polarisation of the light. However, any spectral dependence of the reflection is solely associated with any change in the refractive index with wavelengths. (See 3.1.3).

For normal window or container glass, the change in the refractive index with wavelength is trivial (table C6).

3.4.2 Glass Composition

The soda-lime-silica composition of glass is of primary importance. It is the basis of most flat glass manufacture, albeit with secondary metal oxide additions for an improvement in the glass durability and melting performance.

Glass is composed of:

Na_2O 13 to 17%, CaO 5 to 10%, SiO_2 70 to 73%, by weight.

The remaining weight percentage is made up of various proportions of MgO , Al_2O_3 , Fe_2O_3 , K_2O and perhaps BaO (33).

3.4.3 Iron Oxide

Iron Oxide (Fe_2O_3) is the inevitable contaminant of the industrial sand used in window glass manufacture. Fe_2O_3 impurities up to 0.15% by weight may be accepted in the final glass, but a lower tolerance value would normally be preferable. Cost considerations dictate acceptance closer to the higher iron oxide limit.

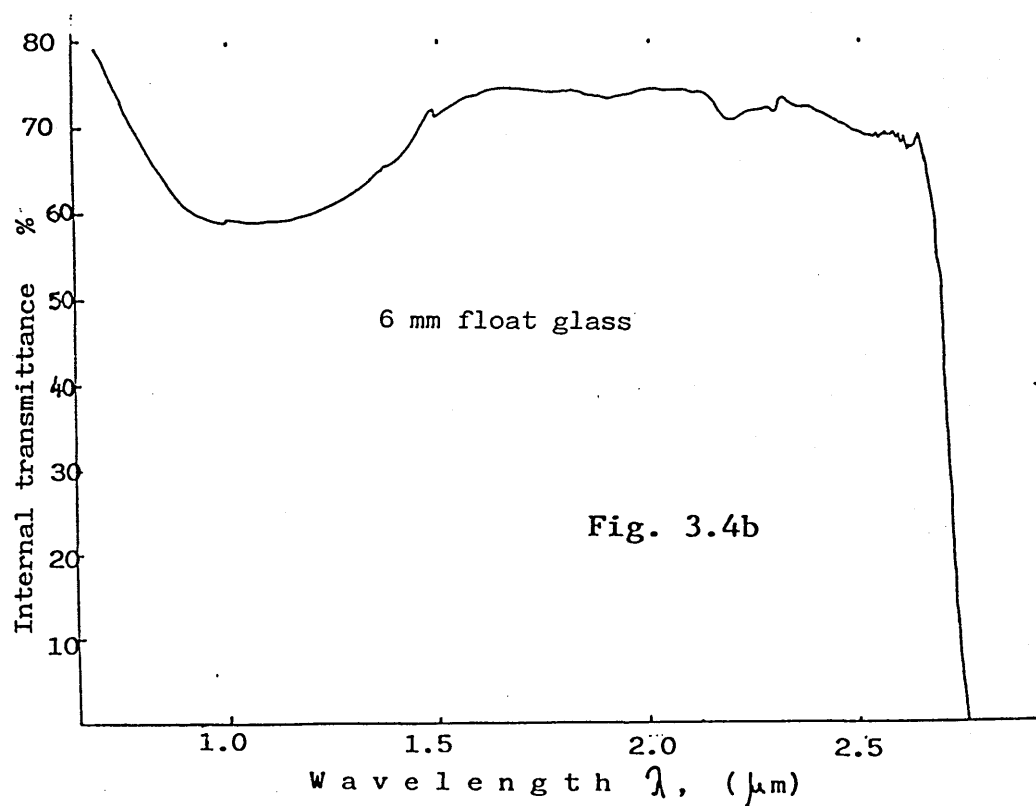
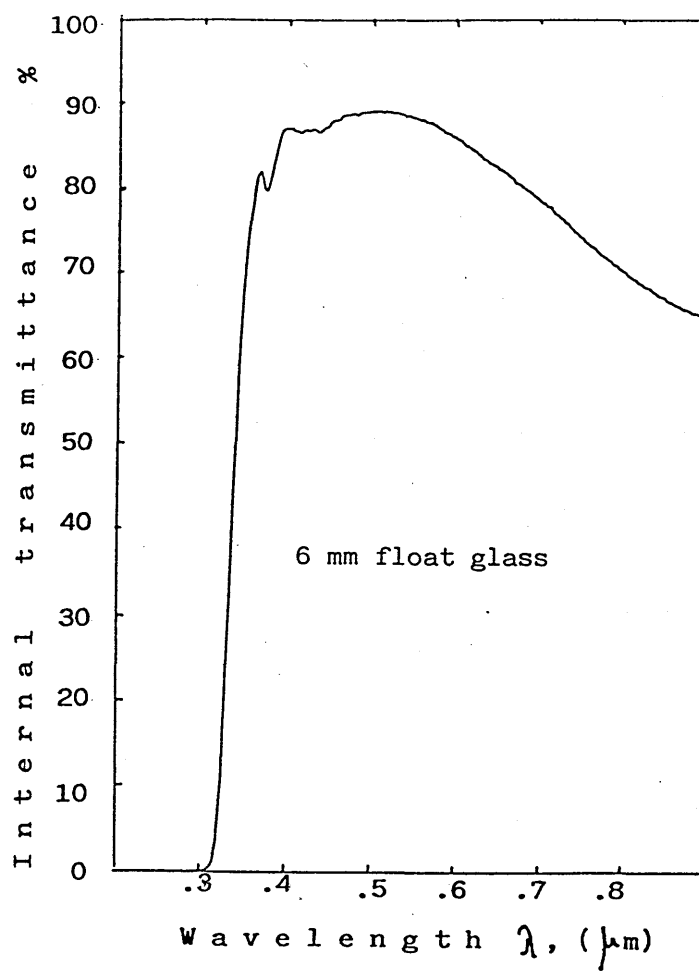
It was found by graphical[†] means that for the glass used, made by Pilkington Brothers Limited, the iron oxide content is $\sim 0.11\%$ by weight and this value was confirmed by (38) and its tolerance was given 0.108% min., 0.115% max.

Any effect associated with the iron oxide impurity of clear glass is not generally evident in normal viewing but is clearly evident from its green tinge when viewing along the glass edge.

3.4.4. Iron Oxide Optical Absorption in Soda-Lime-Silica Glass

Glass has minor absorption regions in the solar spectrum wavelengths, due primarily to iron impurities in the glass. Iron in soda lime silica glass is present as both ferrous (Fe^{2+}) and ferric (Fe^{3+}) ions, each ionic form having its particular absorption spectra (33). Iron oxide imparts a green colour to glass with the particular hue ranging from blue green to yellow green in accordance with the range of ferrous ferric ratios

Fig. 3.4a



Figures 3.4 a&b . Spectral transmission of float glass (6 mm). Reflection is not added.

from 0.5 to 0.3. The glass used has 75% ferrous and 25% ferric Fe_2O_3 content (38).

The absorption spectra of ferric iron are two weak absorption bands at .378 and .420 μm , and the absorption due to ferrous iron is the well-known single broad deep absorption band centred at 1.1 μm , (see graphs (3.4.4a,b)). The peaky characteristics of figure 3.4.4b is due to an increase in the instrument's sensitivity.

In addition to their visible absorption, both ferrous and ferric iron introduce strong UV absorption. The effect is to shift the glass optical cut-off to longer wavelengths, that is to values nearer the visible region.

3.5 GLASS SOLAR HEAT TRANSMISSION, $\tau_{sg\lambda}$

The solar heat transmission of glass is determined by combining the solar distribution[†] data $I_{n\lambda}$, with the glass spectral transmission values $\tau_{g\lambda}$ over a waveband.

$$\tau_{sg\lambda} = \sum_{\lambda_1}^{\lambda_1 + \Delta\lambda} I_{n\lambda} \cdot \tau_{g\lambda} \cdot \Delta\lambda \quad (3.5)$$

The total solar heat transmission of a glass includes a portion of solar heat absorbed by the glass which is re-radiated and convected to the^{room} interior. In the U.K. the fraction^{of this portion} is 0.31 for single glazing (33), and assumes still air conditions for the interior window glass surface but a wind velocity of 7 mph at the exterior surface.

Only a range of average values of the extinction coefficient of glass are usually quoted in the literature. This is mainly due to the complexity of glass composition, see 3.4.2, its high variability and uncertainty of the exact percentage proportions of its various constituents depending on the manufacturer, type of glass etc.

[†] spectral irradiance

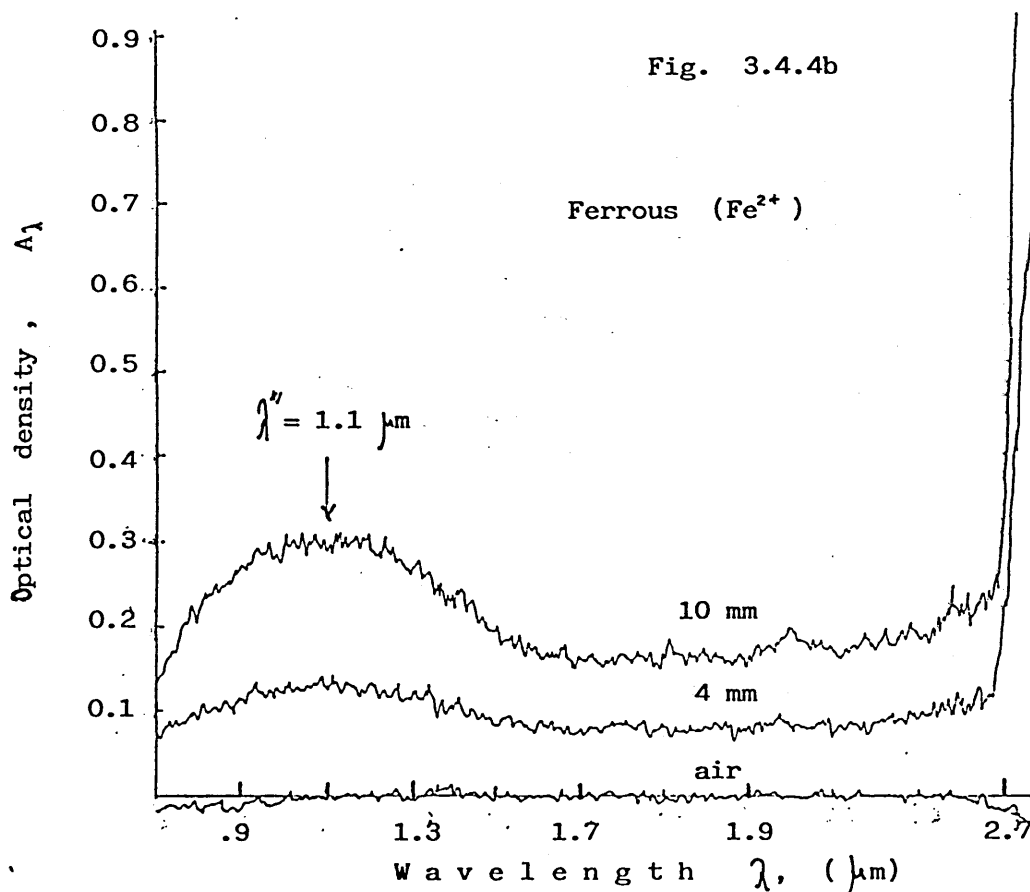
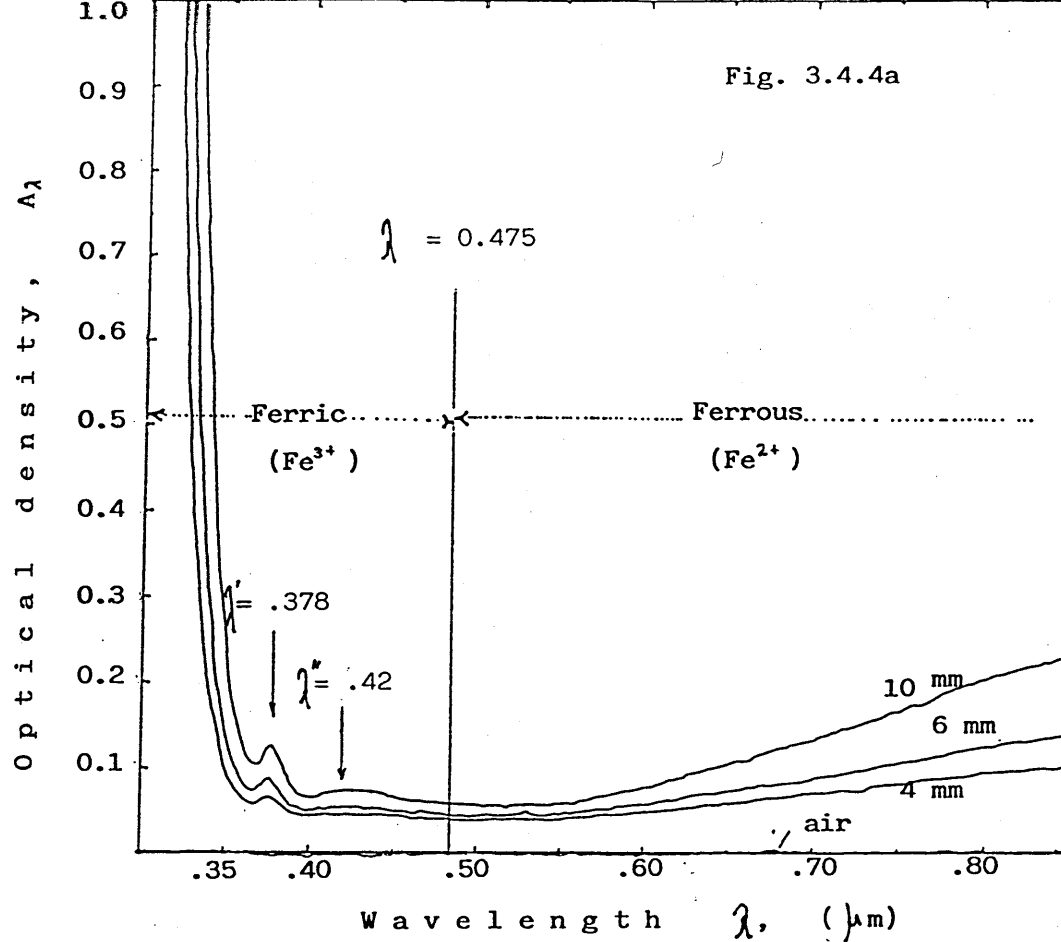


Figure 3.4.4a,b. The absorption regions and "peaks" of ferric and ferrous iron content in glass are identified. Reflection is not subtracted.

Paparsenos (3) using transmittance data for float glass obtained from Pilkington for two glass thicknesses solved a system of non-linear equations in order to produce values for the extinction coefficient of glass. His values were averaged over 8 and 12 wavebands and ^{are} used throughout in this thesis. This method though is uncertain because the convergence of the solution of the equations depends strongly on the first estimate, and the values obtained also depend on the glass thicknesses used.

Bamford (33) has found that the transmittance of a single glass plate varies appreciably even among plates made from the same lot of glass. The difference in surface structure will cause a further difference of $\pm 1\%$ and by another $\pm 1\%$ according to possible ferrous-ferric ratio variation between 0.3 and 0.5. Further variation is produced by dust, exposure to various chemical environments etc.

Thus for future analyses it is recommended to work in "transmittances" from direct measured data for a particular specimen and thickness of glass.

3.6 OPTICAL CONSTANTS OF WATER

Hale and Querry (39) have made a critical survey of the existing literature dealing with the optical properties of water at 25°C in the 0.2 to 200 μm wavelength region and have attempted to select a set of best values. Using even more up to date experimental data (32) for the region 0.7 to 2.1 μm their tables were slightly improved, see Appendix C. This 'improved' table was used to average numerically the values of $n(\lambda)$ and $k(\lambda)$ at 12 different wavelength bands. See table C.3

Water is relatively transparent in the visible and near infrared. These short wavelengths can penetrate many meters with little absorption, while the 'near' infrared is absorbed in few centimeters. Water is virtually opaque to the longer wavelengths.

3.6.1 The Choice of a Heat Transfer Storage Fluid For The Transwall Application

Choosing a heat-transfer storage fluid other than water is not cost effective, in fact there is little variance among a number of fluids tried by Burke et al.(41) as solar absorbers. They found that Dixylylethane (DXE) is the best solar absorber-storage fluid, but after preliminary thermal cycling tests, Therminol 66 was judged to have best combination of thermal stability, availability and modest cost.

The cost of the solvents for a transwall system is prohibitively high. A 0.6m x 1.2m x .157m module requires ~113 litres or 25 gallons of solvent. At 1979 prices Therminol 66 cost \$8 per gallon. This means a cost of \$200 for the solvent itself per transwall module!

3.7 ABSORPTION CHARACTERISTICS OF VARIOUS DYES

An ideal solar absorber should not only have large extinction coefficients for its absorption peaks, but more importantly it should have a non zero extinction coefficient at all high-intensity solar spectral wavelengths.

It has been found (41) that dark blue and purple coloured dyes are much more efficient solar absorbers than the orange ferrocene compounds or the yellow cobalt complex.

The selection, though, of a suitable colour of dye for transwall application depends strongly on the occupants preference so that psychological factors are likely to dominate the choice. For example, in Summer pale blue gives an illusion of cooling and in Winter rose suggests warmth and flatters skin tone. Conversely, green produces a sickly effect and is best avoided. If plants are to be grown in the transmitted light through transwalls then the wavebands essential for plant growth must be subject to minimum absorption. In effect this means that the transwall dye will be magenta in colour and this is described in more detail later.

The dyes used in the present study were water soluble and supplied by ICI, they were:

Name of dye	molecular weight	Colour	Characteristics
Lissamine Red B	526	pink-red	-it fades -it mixes easily
Lissamine Red 3GX (*)	526 (524) ^Δ	pink-red	-more awkward to mix than B -slight fade
Nylamine Red B 3B	526	pink-red	-substantial fade
Copper Chloride	170.5	light blue	-bad absorber -slightly toxic
Methyl Orange (*)	327.3	yellow	
Carbolan Rubine 2B (*)	721 (675) ^Δ	red - purple	-hard to mix -very slight fade if any
Acid Green B (*)	1015	green	

Table 3.7. * see p. 65

Basic dyes were avoided since they are not colour fast and they tend to plate the surface.

A preliminary screening test was made to determine the dye fastness after 2 months exposed to solar radiation from this test Lissamine Red B and Nylamine Red B 3B were rejected. With spectroscopy techniques it was found that copper chloride is not an adequate absorber and is also toxic. From table 3.7 the dyes marked by (*) were selected for further examination.

Recent recalculation from ICI (40) gives slightly different values for the molecular weights for Lissamine Red 3 GX and Carbolan Rubine (as free acid).

3.7.1 Beer's Law Check

As it was mentioned in 3.2.1b, a homogeneous material is said to obey Beer's law if the absorption coefficient remains constant with concentrations.

Beer's law was checked using Methyl Orange for 5 different strengths of solution, for the 2 spot values of λ extracted from figure 3.7.1. See table 3.7.1

W (ppm)	$\lambda = 0.400 \mu\text{m}$			$\lambda = 0.475 \mu\text{m}$		
	A_λ	k_λ (m^{-1})	% difference of k_λ	A_λ	k_λ (m^{-1})	% difference of k_λ
5	0.173	1.132×10^6	-0.9	0.297	1.944×10^6	6.6
10	0.349	1.142 "	0	0.557	1.823 "	0
20	0.677	1.108 "	-3.0	1.070	1.751 "	-3.9
30	1.005	1.096 "	-4.0	1.588	1.733 "	-4.9
40	1.445	1.182 "	3.5	uncertain		
50	1.673	1.076 "	-5.8			

Table 3.7.1

The "peaky" region in figure 3.7.1 for 40 and 50 ppm is not due to scattering effects but due to ^{the} machine's calibration. From the above it is safe to say that Beer's

law is obeyed for strengths of solutions relevant to transwall applications, ie. 5 to 50 ppm.

From table 3.7.1 it can also be seen that the accuracy in determining the extinction coefficient of a dye is in the order of 7%. This is primarily due to slight inaccuracy in weighing the dye before diluting it, also because of incomplete dilution of dye in water and finally because of scattering effects in the cells where the solution is tested and within the solution itself.

3.7.2 Results - Conclusions

Since the optical density of the water dye solution is the product of the fluid thickness and dye concentration, the desired value of 'absorptance', $A_{d-w}(x,c)$ for each fluid layer can be reached by varying either. A computing program was written taking into the account the attenuation of light as it passes through the glass. The evaluation of the dye as a solar energy absorber was made according to the relationship.

$$A_{d-w}(x,c) = \frac{\sum_{\lambda}^{\lambda+\Delta\lambda} \tau_{g\lambda} \cdot (1 - e^{-\epsilon_{\lambda} \cdot x \cdot c}) [I_d \cdot F_{d\lambda} + I_b \cdot F_{b\lambda}] \delta\lambda}{(I_d \cdot F_{d\Delta\lambda} + I_b \cdot F_{b\Delta\lambda})}$$

where $\tau_{g\lambda}$ = spectral transmission of glass, I_d = total diffuse radiation for air mass 2, I_b = total beam radiation for air mass 2. $F_{d\lambda}$ = spectral fraction of diffuse radiation, $F_{b\lambda}$ = spectral fraction of beam radiation.

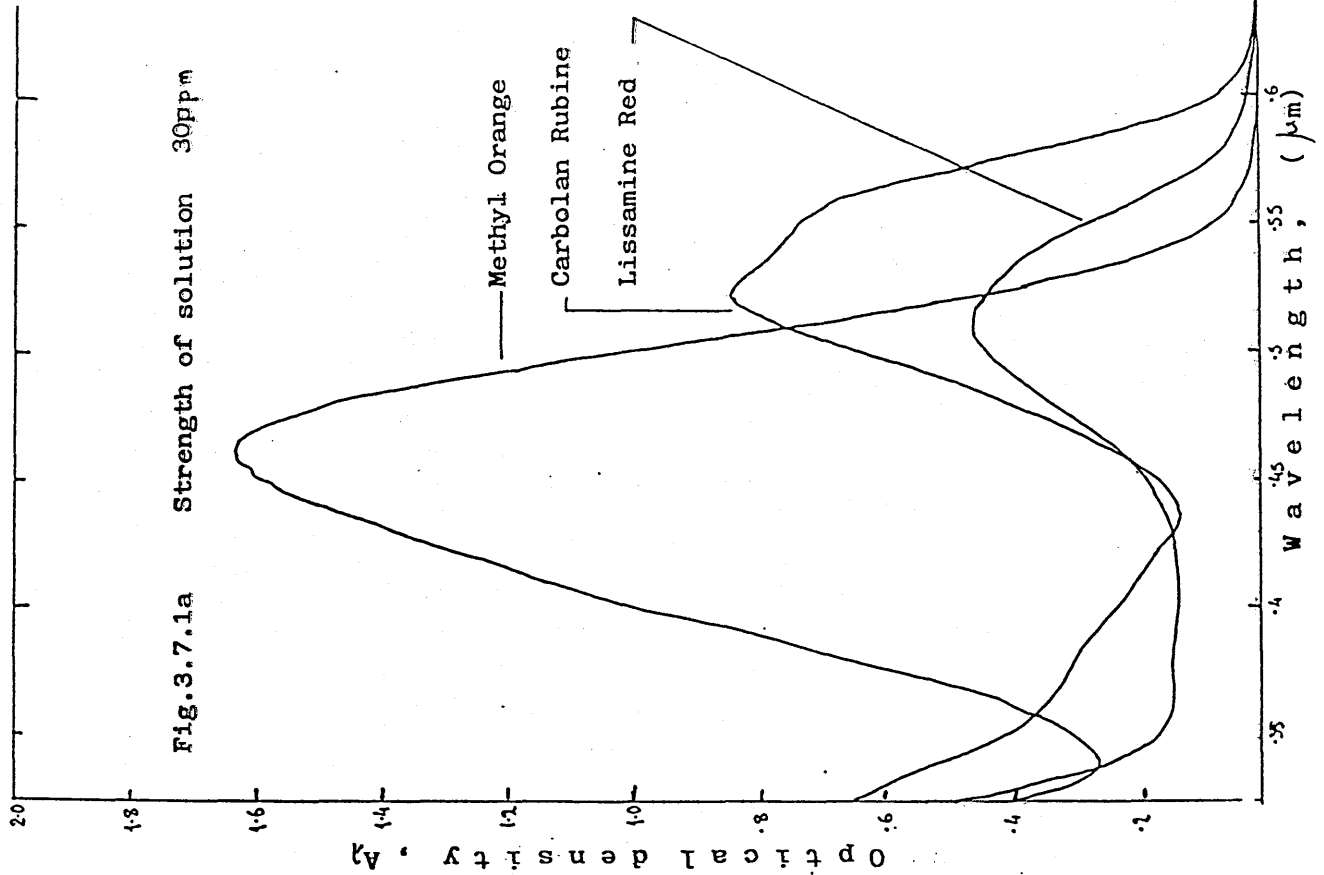
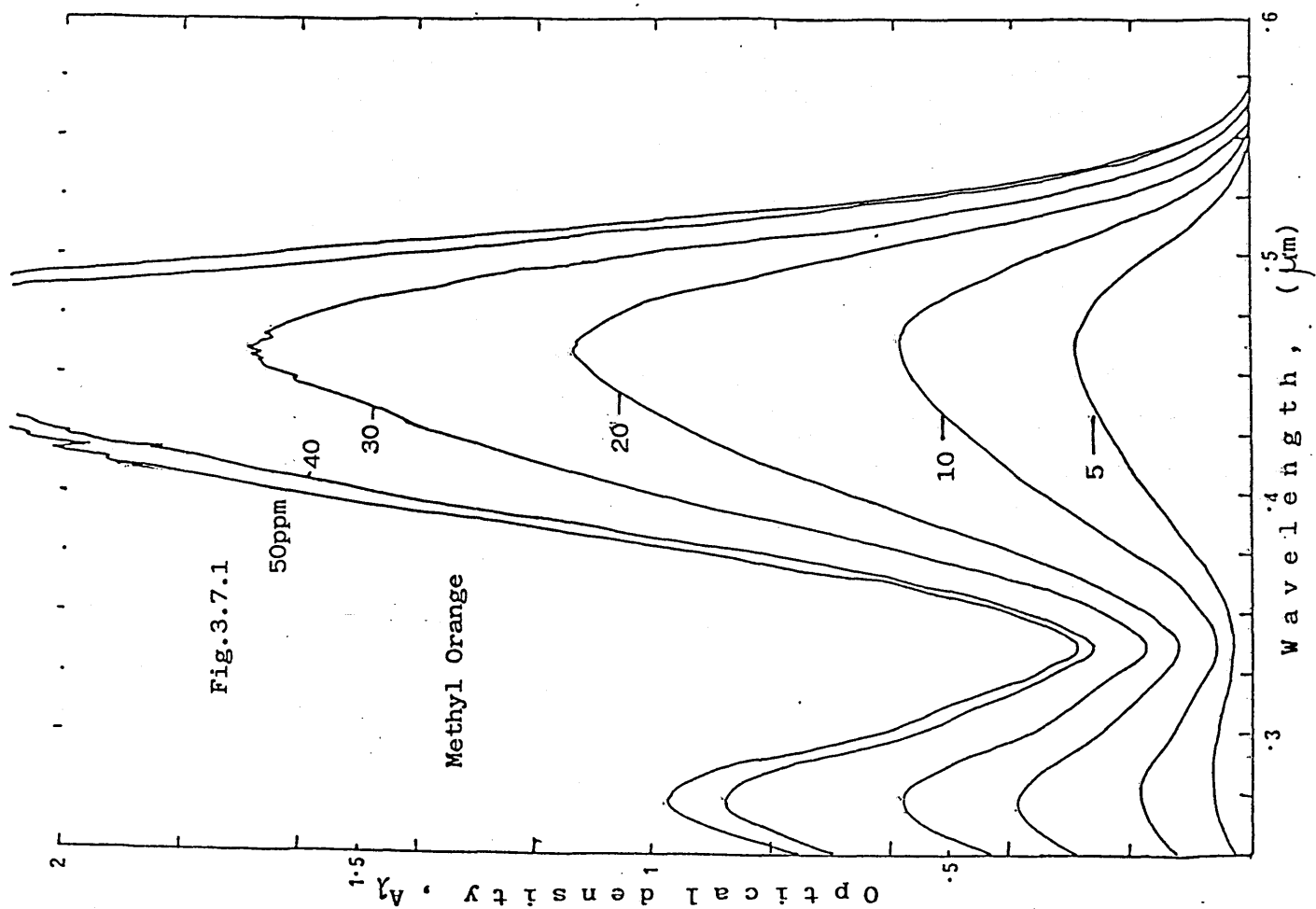
$A_{d-w}(x,c)$ is the fraction of the solar energy absorbed by the dye in a slab of thickness x and concentration C , averaged over the solar spectrum of air mass 2. ϵ_{λ} is the absorption coefficient of the water dye solution.

The optical absorption characteristics of various dyes over water was investigated for the case of the transwall. The solar absorption of the dyes of various concentrations in a fixed fluid layer were calculated. Among the dyes tested methyl orange is found to be a better absorber of solar radiation for moderate concentrations (<11 ppm) and acid green for concentrations >11 ppm, see figure 3.7.2a

The effect of various strengths of solutions for four dyes is shown in figure 3.7.2b & c.

3.7.3 Dye Selection for Glass-house Transwalls

It has been shown that the transwall system can reduce the energy costs of a horticultural glasshouse by 20 to 25%, ref. (29). For this purpose a dye must be chosen that transmits radiation in the wavebands necessary for plant growth. This requirement will apply of course to any situation in which plants are grown in the shade of transwalls e.g. conservatories. In the range where plants absorb best (widely separated bands in the violet and in the red), the monochromatic irradiance is reduced. In fact the most important wavebands for growth are: .39 to .47 μm (peaks at .425 to .46 μm) and .61 to .69 μm (peaks at .635 to .67 μm), though it must be added that plants have requirements in other wavelengths (42). Therefore a dye must be found which should absorb less in the above mentioned regions and absorb strongly in the "wasted" green and yellow regions of the spectrum mainly in the region of .47 to .505 μm .



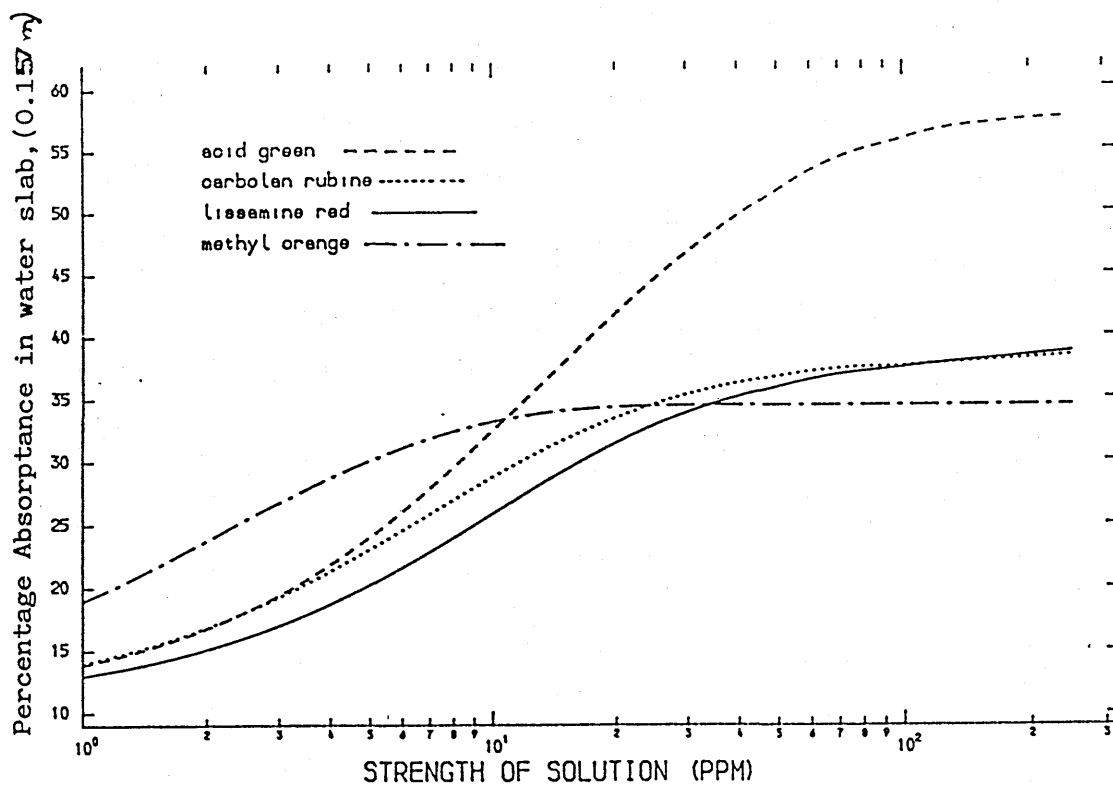


Figure 3.7.2a The effect of strength of solution (ppm) of different dyes on absorbance in a transwall.

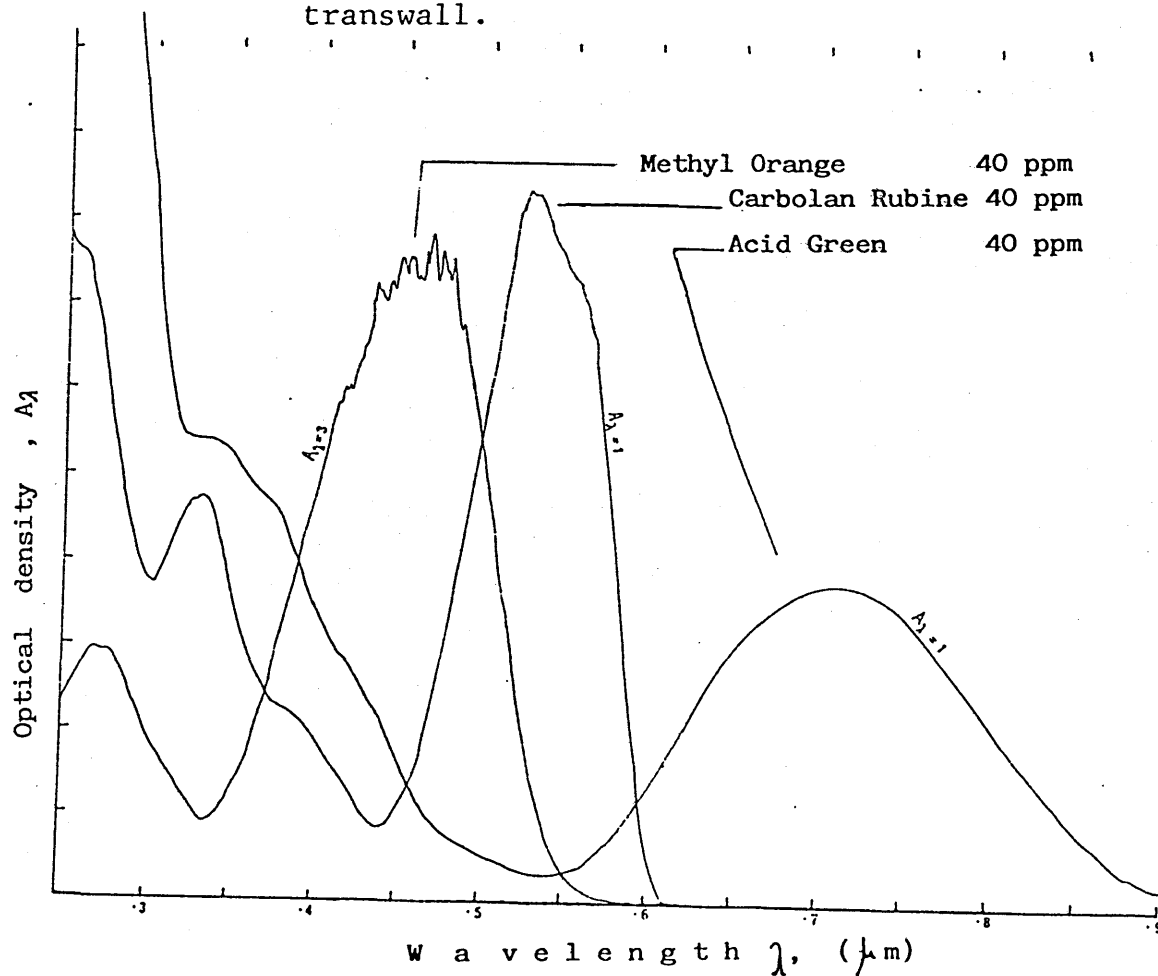


Figure 3.7.1b Absorption characteristics of dyes at the same strength of solution.

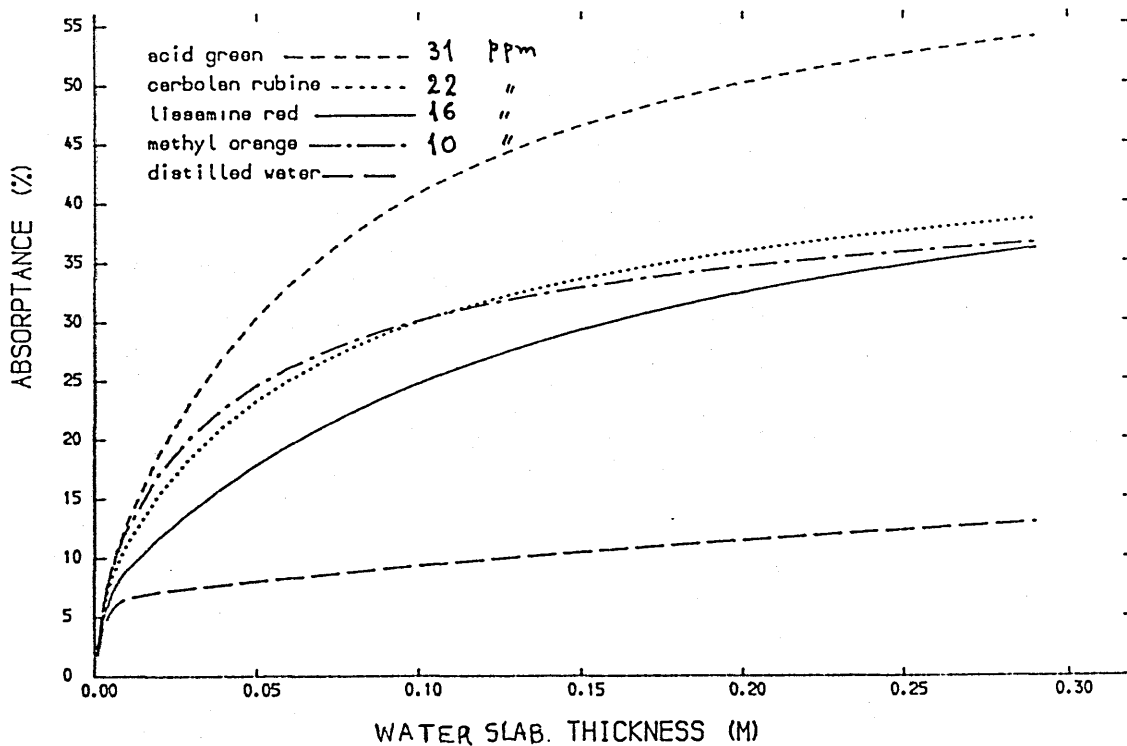


Figure 3.7.2b. Percentage absorbance versus water slab thickness in a transwall for four dyes.

Concentration is constant

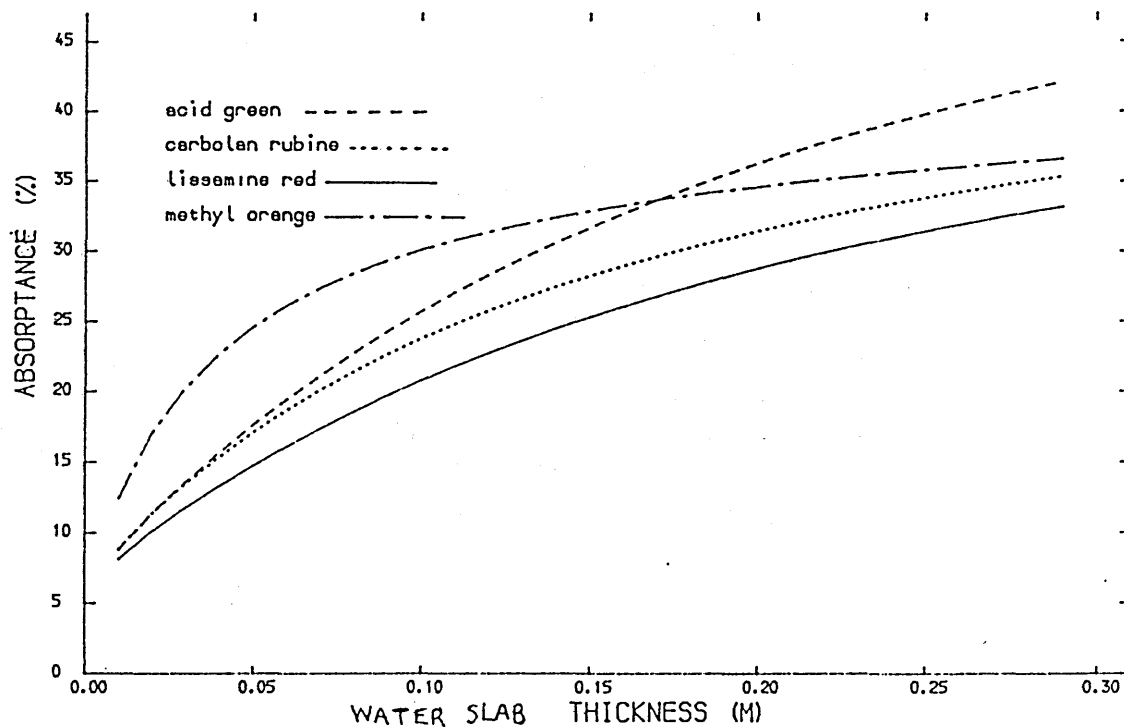


Figure 3.7.2c Strength of solution is constant (10 ppm)

It should be remembered that colour is characteristic of the eye and is in itself of no significance to plants.

From table 3.7.3 below it can be seen that the worst candidate for a dye in glasshouses, or in houses where there are plants, is methyl orange and the second worst is acid green as it was expected. Lissamine red and carbolan rubine seem to be the best for this duty. Carbolan rubine though, should be preferred because of its higher total absorptance, see figure 3.7.2c.

It was found that the addition of some Lissamine red in a carbolan rubine water mixture will be beneficial for plant growth since it will absorb less in the regions 0.39 to 0.43 μm and 0.61 to 0.63 μm . It is suggested a mixture of 4 rubine : 1 red by volume is ideal.

Table 3.7.3

Colour	Carbolan rubine	Methyl orange	Lissamine red	Acid green
Violet	10.8%	26.7%	11.0%	28.2%
Blue	16.2	25.4	22.7	15.7
Green	60.4	43.9	61.2	26.0
Yellow	7.5	0.0	2.4	8.6
Orange	1.5	0.0	0.07	14.7

Table 3.7.3 shows the percentage "absorptance" of four dyes in different colour regions in the spectrum.

Chapter 4

THE LUMPED SYSTEM APPROACH4.0 Introduction

The ultimate objective of the transwall programme is to develop and validate a computer program which will predict the performance of a transwall module using finite differences and effective conductivity to simulate the complex circulation patterns within the transwall. It is believed that this is the best compromise between Paparsenos' fundamental approach (3) with its excessive (mainframe) running time and, on the other hand, a single one-dimensional lumped system approach, i.e. the assumption of infinite thermal conductivity within the transwall.

It is recognised that the lumped system approach has several fundamental disadvantages. Clearly, it is at its best when there is vigorous circulation within the transwall when first receiving insolation. Conversely this approach should be least accurate when stratification and/or the absence of insolation inhibits water circulation. Further, this treatment cannot be used to predict the effects of varying the circulation to enhance performance, by additives or baffles (12) or to show the effect of replacing the normal glass walls with special solar glasses. It should also be recognised that in order to maintain the simplicity of this approach, its main advantage, the theory incorporates some substantial approximations. Despite these drawbacks the simplicity of the lumped system treatment is attractive and this chapter is devoted to comparing experimental temperatures with those predicted by this treatment.

15

In the first part of this chapter the lumped system equation for the incremental rise in the uniform temperature of the transwall is developed. Clearly, a key element in the equation is the radiation absorbed by the transwall. This in turn requires the development of a relatively simple one-dimensional treatment of reflected rays passing through a multi-slab system which involves the application of the basic equations. A much more elaborate two dimensional approach to the absorption of radiation, appropriate to a finite difference solution, is given in Chapter 5.

The diffuse radiation measured has to be incorporated into the lumped system temperature equation and the methodology of this is then considered. Associated with this is the way in which diffuse radiation reflected from the ground is taken into account and the measurements made to determine the reflectance.

The chapter now turns to the actual measurements associated with the transwalls' performance. The measurement of radiation by the Kipp and Zonen solarimeters is described together with an appraisal of the various correction factors. Details of the solar test cell are given followed by a description of the method by which temperatures are measured in, and on, the transwall. The variation of measured transwall temperatures with time are shown superimposed upon the predicted uniform temperature using the lumped system approach. The factors governing the accuracy of the lumped system analysis are considered and speculations made regarding the curious temperature distributions revealed within the transwall.

4.1 TREATMENT OF THE TRANSWALL

The accurate prediction of the temperature profiles within a transwall, and its associated heat transfer, is complex. Water absorbs strongly in the $+4\mu\text{m}$ region so that the first few millimeters of water adjacent to the front glass becomes heated and sets up a circulation pattern which is modified by thermal stratification. Varying absorption in the remaining fluid, and the back glass, adds to the circulation drive producing complex 3-D patterns. Heat transfer is thus dominated by convective phenomena which has the effect of producing a high effective conductivity, i.e. the internal heat transfer is the same as that of a static system with a high thermal conductivity.

A lumped system obviously requires that the temperature of the system is uniform, i.e. the glass, water, contents are at one temperature, T_w , and horizontal and vertical temperature gradients are ignored. The one dimensional nature of the system does not permit any variation of the heat transfer coefficients, transwall to surroundings, but the heat transfer on the glass side and the room side are allowed to differ from each other.

Letting

T_w = uniform mean temperature of the transwall

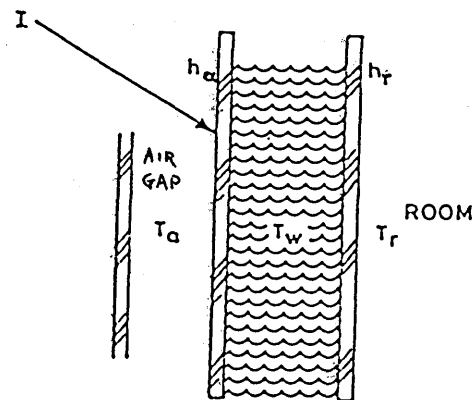
T_r = test cell temperature

$(I\alpha)$ = radiation absorbed/ m^2 wall

h_a, h_r = outer and inner surface overall heat transfer coefficients

mc = thermal capacity of the transwall per meter square

δt = elemental time change



see Test cell p.98,99

The air gap temperature T_a and the room temperature T_r are fairly similar and any difference is accounted for by the linear relation.

$$T_w - T_a = K \cdot (T_w - T_r) \quad (1)$$

where K is a constant[†] over the time integral 0 to t .

An energy balance gives

$$(I\alpha) - \left[h_a (T_w - T_a) + h_r (T_w - T_r) \right] = \frac{mc \cdot \delta T_w}{\delta t} \quad (2)$$

Assuming that the test cell temperatures remain constant over the time interval considered, then

$$\delta T_w = \delta (T_w - T_r) \quad (3)$$

Substitute (1) and (3) in (2)

$$(I\alpha) - \left[h_a \cdot K \cdot (T_w - T_r) + h_r (T_w - T_r) \right] = mc \cdot \frac{\delta (T_w - T_r)}{\delta t}$$

Rearranging and take to limit

$$\frac{d(T_w - T_r)}{(I\alpha) - (T_w - T_r) h} = \frac{dt}{mc}$$

$$\text{where } h = h_a \cdot K + h_r$$

integrate between time $t = 0, t = t$

$$\frac{1}{mc} \int_0^t dt = \int_{T_{w0}}^{T_{w1}} \frac{d(T_w - T_r)}{(I\alpha) - h(T_w - T_r)}$$

or

$$t = \frac{mc}{h} \cdot \ln \left[\frac{(I\alpha) - h \cdot (T_w - T_r)}{(I\alpha) - h \cdot (T_w - T_r)} \right]_{T_{w0}}^{T_{w1}}$$

[†] although K is assumed constant for simplicity it does in fact oscillate, see p.114

or

$$\frac{(I\alpha) - h \cdot (T_{w1} - T_r)}{(I\alpha) - h \cdot (T_{w0} - T_r)} = \exp \left[- \frac{h}{mc} \cdot t \right]$$

then

$$T_{w1} = T_r + \frac{(I\alpha)}{h} - \left[\frac{(I\alpha)}{h} - (T_{w0} - T_r) \right] \cdot \exp \left(- \frac{h}{mc} \cdot t \right) \quad (4.1a)$$

where T_{w0} and T_{w1} are the transwall temperatures before and after a time interval, t . It is usual to treat the system on a unit area basis, i.e. $(I\alpha)$ is per square meter frontal area. However, if the heat loss from the short sides is to be taken into account the equation can be modified by incorporating two areas A_1 and A_2 which represent respectively the area of the receiving face and the area of the receiving face plus part ($1/2$) of short sides⁺. mc is now the thermal capacity of the transwall.

The equation then becomes

$$T_{w1} = T_r + \frac{A_1(I\alpha)}{A_2 h} - \left[\frac{A_1(I\alpha)}{A_2 \cdot h} - (T_{w0} - T_r) \right] \cdot \exp \left(- \frac{h A_2}{mc \cdot A_1} \cdot t \right) \quad (4.1b)$$

4.2 THERMAL CAPACITY OF THE TRANSWALL MODULE, mc

The thermal capacity of the transwall module/ m^2 is the product of the transwall mass and its specific heat capacity. Neglecting the thermal capacity of the module frame, and the thermocouple support frame, the transwall module consists of three materials, namely glass, water, polystyrene (used as cover top). Their properties are

⁺ h changes to $h \cdot A_2 / A_1$

listed in table 4.2 below. The volume and hence the thermal mass, of the individual parts constituting a transwall module are:

Total volume of glass in transwall module = $1.879 \times 10^{-2} \text{ m}^3$

Total volume of polystyrene cover = $7.77 \times 10^{-3} \text{ m}^3$

Total volume of water in transwall module = $9.83 \times 10^{-2} \text{ m}^3$

$(mc)_{\text{glass}} = \text{density} \times \text{volume} \times \text{specific heat capacity} =$
 $= 3.54 \times 10^4 \text{ J/K}$

$(mc)_{\text{pol.}} = 2.02 \times 10^2 \text{ J/K}$

$(mc)_{\text{water}} = 4.10 \times 10^5 \text{ J/K}$ at 25°C

$(mc)_{\text{wall}} = (mc)_{\text{water}} + (mc)_{\text{glass}} + (mc)_{\text{pol.}}$
 $= 4.46 \times 10^5 \text{ J/K}$

TABLE 4.2

THERMAL PROPERTIES OF THE MATERIALS USED

Property	Thermal conductivity	Specific heat capacity	Density
Material	W/m·K	J/Kg·K	Kg/m ³
clear float glass	1.05 (#)	750 (¥)	2515 (#)
polystyrene (*)	0.048	1330	20
water (still)(¢)			
15°C	0.595	4186	999.0
20°C	0.603	4183	998.2
25°C	0.611	4181	997.1
30°C	0.618	4179	995.6
35°C	0.625	4178	994.0
40°C	0.632	4179	992.2

(#) Duffie and Beckman (4) , (*) Paparsenos (3)

(¥) Clarke (30) , (¢) Mayhew and Rogers therm. tables

4.3 ONE-DIMENSIONAL ABSORPTION OF RADIATION

In this section the equations developed in section 4.1 are applied to establish a one-dimensional algorithm for the absorption of radiation, ($I \propto$) of equation 4.1b, in the transwall. However, the system developed has a more general application.

4.3.1 1-D Ray Tracing Technique With Infinite Internal Reflections Between The Sub-systems

The transwall module can be considered as a transparent system made of 3 transparent elements with 4 interfaces, 1 to 4 (see Fig. 1). The history of one radiation vector as it undergoes multiple reflections at each interface and between the interfaces is as follows. Some portion of the radiation impinging on interface 1 is transmitted through to the adjacent transparent element with some fraction being subsequently retransmitted back across the common interface 2. If the interface reflectances are known then it is possible to process ^{the radiation within} the second element independently by treating the onward transmitted flux from element 1 as the initial incident flux on element 2. In this way, the process can continue for one forward pass through the multi-layered construction until all elements have been considered. The flux transmitted from one element to the next will be partly polarized even if the original beam was not. It is therefore necessary to process each component of polarisation separately before combining the overall value for the entire system. If the combining is done initially, errors

of up to 1.3 % may occur for angles of incidence up to 75° as shown in table C.1 (Appendix C). It should be noted that errors of 18 percent for greater angles of incidence in the calculated transmittance of a pane of glass can result from this improper averaging as indicated by Kreith and Kreider (5).

This is not the end of the process, however, since each element will reflect flux back to the element from which it initially received the shortwave energy. It is therefore possible to establish an algorithm to 'transmit' a single flux package from one transparent element to the other as calculation 'sweeps' are made in alternating directions until the flux quantities diminish in magnitude below some predetermined level. In this way the total absorption of each element can be determined as well as the total transmissivity of the combined system.

The equations for an infinite number of reflections in 3.3 are modified slightly in order to form the algorithm.

$$T_1 = \frac{\tau_g \cdot (1 - \rho_a) \cdot (1 - \rho_b)}{1 - \rho_a \cdot \rho_b \cdot \tau_g^2}$$

$$R_i = \rho_a + \frac{(1 - \rho_a)^2 \cdot \tau_g^2 \cdot \rho_b}{1 - \rho_a \cdot \rho_b \cdot \tau_g^2}$$

where i is the element number.

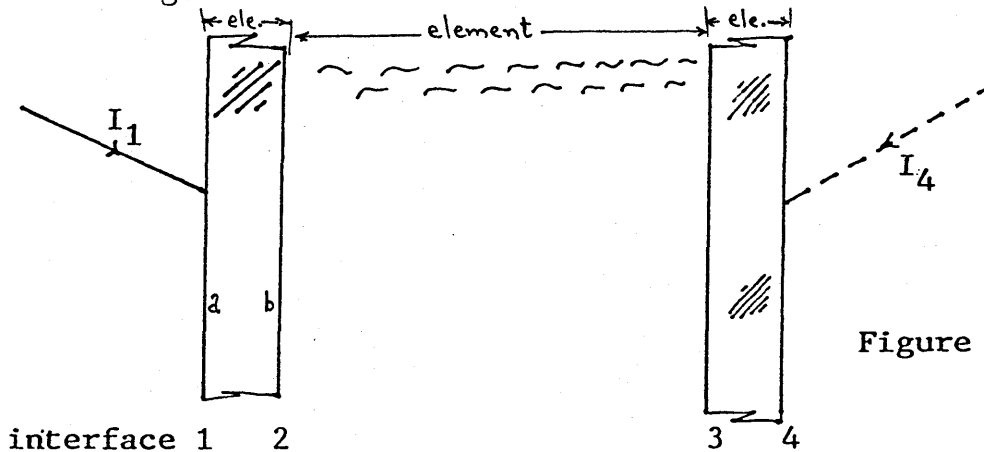
$$A_1 = (1 - \rho_a) \cdot \left[\frac{1 - \tau_g - \tau_g^2 \cdot \rho_b + \tau_g \cdot \rho_g}{1 - \rho_a \cdot \rho_b \cdot \tau_g^2} \right]$$

where ρ_a is the air/glass reflectivity

ρ_b is the glass/water reflectivity

τ_g is the glass transmissivity

τ_w is the water transmissivity
 T_1 is the transmittance of element 1
 R_i is the reflectance of element i
 A_1 is the absorptance of element 1
 I_1 is the radiation incident on interface 1, see figure below.



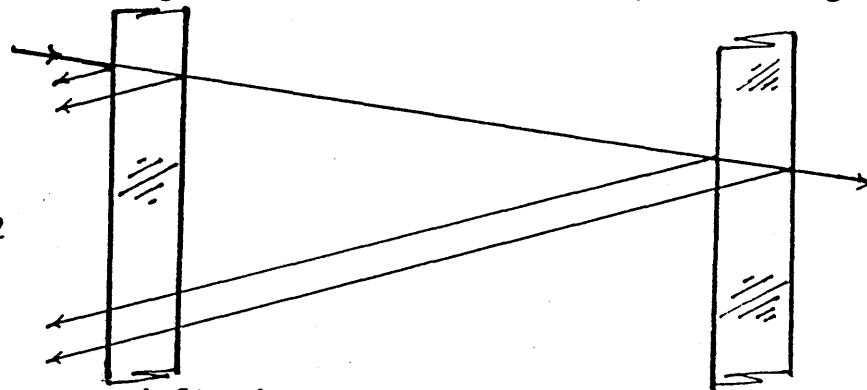
If shortwave radiation is simultaneously impinging on interface 4 (receiving internal reflections from surrounding surfaces i.e. room reflected radiation), then further absorption of the second beam I_4 will occur. The above expressions are then applied with $I_1 = I_4$ and the total absorption obtained by summing the component absorptions of each individual beam. The idea of backwards radiation and its treatment is discussed in the next chapter.⁺ In the lump system calculation the accuracy of the analyses does not justify the extra complication involved by treating the small amount of room radiation incident on the transwall using an infinite number of internal reflections. To account for the room radiation the simpler approach of one 'reflection per surface' technique was used.

⁺

4.3.2 A Closed Formula Example For The 1 - D Ray Tracing Technique

The development of a closed formula example of the 1-D ray tracing technique with an infinite number of internal reflections is presented for the calculation of the total reflectance, transmittance and absorptance of the system of figure 4.3.1. It is for one direction of the incoming radiation (i.e. radiation from the room is not treated in the same manner). These equations were used to compare numerically the difference in the infinite reflected ray tracing technique with the much more simpler approach of considering only one reflection of the primary ray as it passes through the different media, see figure 4.3.2.

Figure 4.3.2



The sub-systems are defined as

1 front glass, 2 water, 3 rear glass,

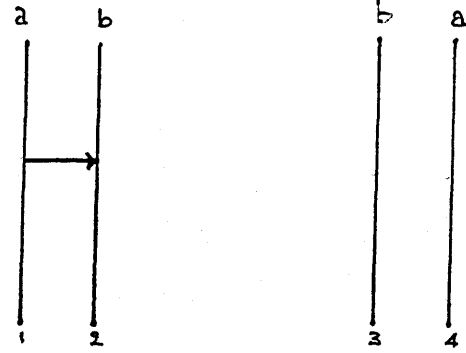
where R , T and A are the reflectance, transmittance and absorptance of the sub-systems. The forward direction is defined as the direction from the outside ambient air to water. The subscripts f and b denote the forward and backward direction. Below are presented the equations useful in obtaining the total reflectance and total transmittance of the system as well as the equations to calculate the individual absorptances.

Forward Direction, sub system 1, from interface 1 → 2 (p. 79)

$$R1 = \rho_a + \frac{\rho_b \cdot (1 - \rho_a)^2 \cdot \tau_g^2}{1 - \rho_a \cdot \rho_b \cdot \tau_g^2}$$

$$T1 = \frac{\tau_g \cdot (1 - \rho_a) \cdot (1 - \rho_b)}{1 - \rho_a \cdot \rho_b \cdot \tau_g^2}$$

$$A1 = (1 - \rho_a) \cdot \left[\frac{1 - \tau_g - \tau_g^2 \cdot \rho_b + \tau_g \cdot \rho_b}{1 - \rho_a \rho_b \tau_g^2} \right]$$

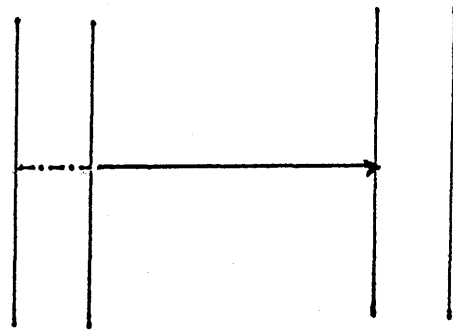


Forward direction, sub system 2, from interface 2 → 3

$$R2 = T1 \cdot \left\{ \rho_b + \frac{\rho_b \cdot (1 - \rho_b)^2 \cdot \tau_w^2}{1 - \rho_b^2 \tau_w^2} \right\}$$

$$T2 = T1 \cdot \left\{ \frac{(1 - \rho_b)^2 \cdot \tau_w}{1 - \rho_b^2 \tau_w^2} \right\}$$

$$A2 = T1 \cdot \left\{ (1 - \rho_b) \cdot \left[\frac{1 - \tau_w - \tau_w^2 \cdot \rho_b + \tau_w \rho_b}{1 - \rho_b^2 \tau_w^2} \right] \right\}$$

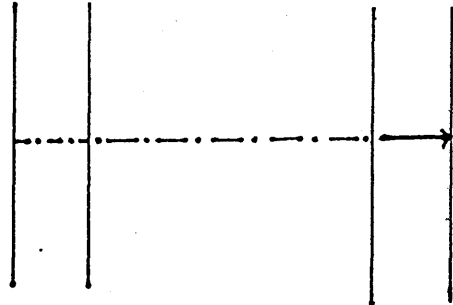


Forward direction, sub system 3, from interface 3 → 4

$$R3 = T2 \cdot \left\{ \rho_b + \left[\frac{\rho_a \cdot (1 - \rho_b)^2 \cdot \tau_g^2}{1 - \rho_a \cdot \rho_b \cdot \tau_g^2} \right] \right\}$$

$$T3 = T2 \cdot T1$$

$$A3 = T2 \cdot \left\{ (1 - \rho_b) \cdot \left[\frac{1 - \tau_g - \tau_g^2 \rho_a + \tau_g \rho_a}{1 - \rho_a \rho_b \tau_g^2} \right] \right\}$$

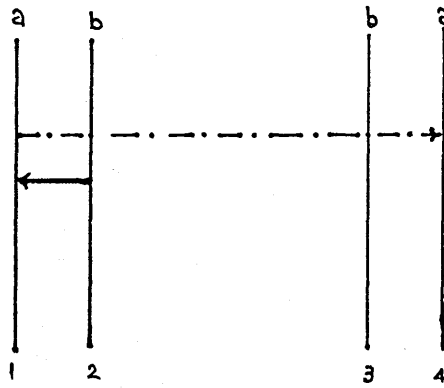


Backward direction, sub system 1, from interface 2 \rightarrow 1

$$R1_b = R2 \cdot \frac{R3}{T2}$$

$$T1_b = R2 \cdot T1$$

$$A1_b = R2 \cdot \frac{A3}{T2}$$

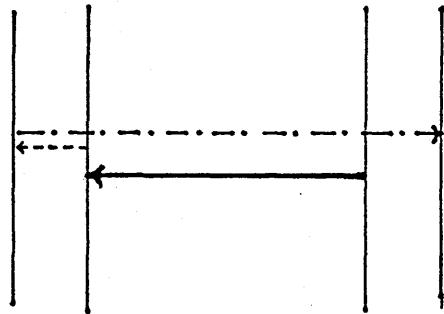


Backward direction, sub system 2, from interface 3 \rightarrow 2

$$R2_b = R3 \cdot \frac{R2}{T1}$$

$$T2_b = R3 \cdot \frac{T2}{T1}$$

$$A2_b = R3 \cdot \frac{A2}{T1}$$

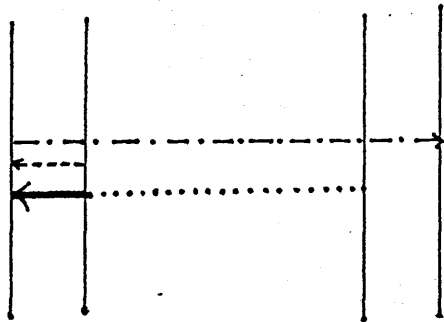


Backward direction, sub system 1, from interface 2 \rightarrow 1

$$R1'_b = T2_b \cdot \frac{R3}{T2}$$

$$T1'_b = T2_b \cdot T1$$

$$A1'_b = T2_b \cdot \frac{A3}{T2}$$

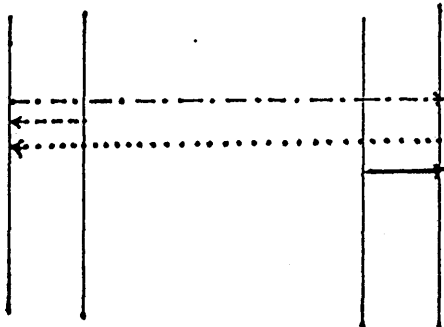


Forward direction, sub system 3, from interface 3 \rightarrow 4

$$R3_f = R2_b \cdot \frac{R3}{T2}$$

$$T3_f = R2_b \cdot T1$$

$$A3_f = R2_b \cdot \frac{A3}{T2}$$

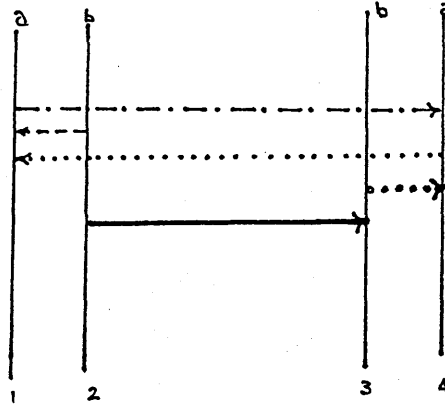


Forward direction, sub system 2, from interface 2 \rightarrow 3

$$R2_f = R1_b \cdot \frac{R2}{T1}$$

$$T2_f = R1_b \cdot \frac{T2}{T1}$$

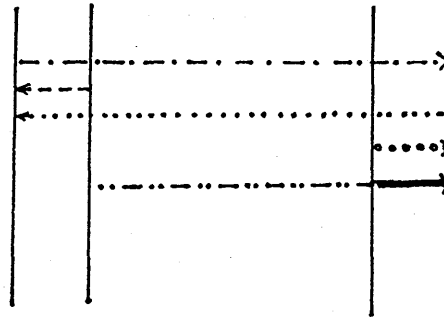
$$A2_f = R1_b \cdot \frac{T2}{T1}$$



Forward direction, sub system 3, from interface 3 \rightarrow 4

$$T3'_f = T2_f \cdot T1$$

$$A3'_f = T2_f \cdot \frac{A3}{T2}$$



Hence

$$\text{Total reflectance} = R1 + T1_b + T1'_b$$

$$\text{Total transmittance} = T3 + T3_f + T3'_f$$

$$\text{Total front glass absorptance} = A1 + A1_b + A2'_b$$

$$\text{Total water absorptance} = A2 + A2_b + A2_f$$

$$\text{Total rear glass absorptance} = A3 + A3_f + A3'_f$$

4.3.3 Comparison of the Infinite Reflections With The Simple One Reflection Technique - Numerical Example

Assuming the same conditions as in the example of Appendix F $\rho_a = 0.066$ and $\rho_b = 0.005$, and considering for simplicity an overall extinction coefficient for glass and water the following transmittances were obtained $\tau_g = 0.685$, $\tau_w = 0.59$, (incident radiation = 100). Using the above information for the rays shown in figure 4.3.2, and the equations developed above for an infinite number of internal reflections, the two methods were compared. The results and the percentage error in adopting the simpler approach are shown in table 4.3.3 below.

TABLE 4.3.3

	total reflectance	total transmit.	front gl. a b s o r p t a n c e	water a b s o r p t a n c e	rear glass a b s o r p t a n c e	amount of energy considered A + T + R
simple	7.363	23.910	29.586	26.651	12.304	99.814
inf. (∞)	7.391	23.690	29.828	26.600	12.192	99.701
%	+0.38	-0.93	+0.81	-0.19	-0.92	100.000

From the above table it can be seen that the errors involved are less than 1%, so this method ^{need} be used only when great accuracy is required.

4.4 DIFFUSE RADIATION FROM THE SKY

The contribution of diffuse radiation to the fractional energy in the various wavebands has been considered in Chapters 2 and 3, and it is now necessary to consider how to incorporate the diffuse radiation measured by the solarimeters into the $(I\alpha)$ term of the lumped system. The performance of an optical system depends on the relative magnitude of the intensity in all directions of the incoming diffuse radiation. The distribution of this incident diffuse radiation depends in turn on the distribution of the sky diffuse radiation intensity

over the sky dome. This distribution is not uniform and varies with the sky conditions. The intensity of sky diffuse radiation can be mapped by a radiometer scanning the sky dome, though it can take several minutes during which time the sky conditions may change substantially. The distribution of sky diffuse radiation is uneven for clear skies with a strong dependence on the zenith position of the sun. Maximum intensities occur near the sun and, to a lesser extent, near to the horizon. The former is called circumsolar radiation and is caused by strong forward scattering of the aerosol particles the extent of which depends on the atmospheric turbidity and the zenith angle of the sun. The latter is called horizon brightening and results from the scattering by a larger air mass viewed by an observer in that direction. Various models have been developed to determine the diffuse radiation falling on a surface given the diffuse radiation on the horizontal. The only model considered here is the isotropic.

4.4.1 Isotropic Model

This is the most common model used and assumes the diffuse radiation is uniform over the sky dome. The radiation falling on an inclined surface I_i can be related to that measured by the solar test cell solarimeter, I_{sd} , by the well known configuration factor

$$I_i = \frac{I_{sd} (1 + \cos \gamma)}{2}$$

Results of numerical simulations presented by Dave

(51), and Iqbal (6), showed that the isotropic distribution model for the sky radiation systematically underestimates the diffuse energy contribution to the sun facing planes.

It is recognised that anisotropic models such as Klucher's⁽⁴⁸⁾ and Hay's⁽⁶⁰⁾ for diffuse radiation can give more accurate values but the adoption of these models requires a reassessment of the effective angle of incidence for diffuse radiation. In order to use the values given by Brandemuehl and Beckman (43) it was decided to use the widely adopted isotropic model.

4.4.2 Ground* — Reflected Diffuse Radiation On An Inclined Surface

The diffuse radiation striking the transwall does not all come directly from the sky dome. Some is reflected from the ground and its treatment is now considered.

Consider a plane inclined at an angle γ from the horizontal.

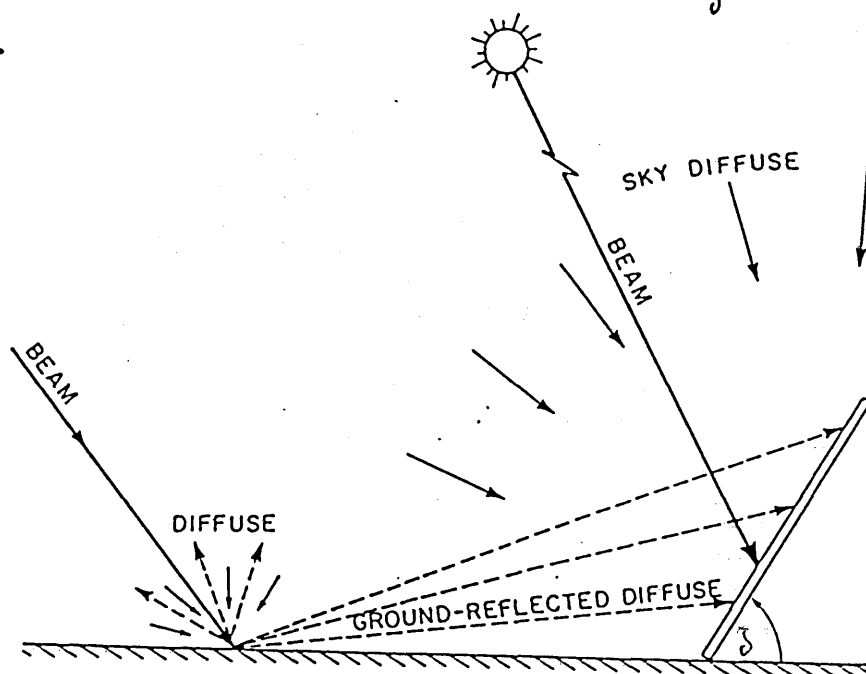


Figure 4.4.2 Radiation falling on an inclined surface

(*) The word "ground" here means a composite of all earth's surface that the inclined plane "sees".

The radiation arriving on the ground is composed of both beam and diffuse components. Depending on the earth's cover, the albedos for beam and diffuse radiation ρ_b and ρ_d respectively may not be identical. The radiation reflected by the ground cover into an inclined plane can be written as follows:

$$I_{dg} = (I_b \cdot \rho_b + I_d \cdot \rho_d) \cdot \frac{1}{2} \cdot (1 - \cos \theta)$$

There is uncertainty though over the spectrum of the diffuse radiation from the ground and this matter requires proper investigation.

4.4.3 Ground Reflectance

Under clear and cloudless skies global radiation is composed primarily of direct radiation. When the ground is covered with a layer of water, or with plants having glossy leaves, the reflection of such radiation is usually anisotropic. Iqbal (6) found that there is very little difference between the isotropic and the anisotropic ground reflected radiation. Anisotropy of the ground reflected radiation is large when the sun is near the horizon. Paltridge et al. (49) present curves relating reflectance and solar altitude for different surfaces, and from these curves the following equation was developed for the ground reflectance

$$\rho_{bgr} = \rho_{gr} + (1 - \rho_s) \cdot \exp[-0.1 \cdot (90 - \alpha)]$$

where α is the altitude angle in degrees and ρ_{gr} the surface reflectivity.

The above expression covers all common ground covers and the surface reflectivity, ρ_{gr} , is obtained from

standard tables such as the one provided by Iqbal (6).

The reflectance also varies with wavelength. Except for ice, snow and water all surfaces exhibit low values for ρ in the visible wavelengths and a rapid increase for wavelengths beyond $0.7 \mu\text{m}$. Because of the lack of information in the literature concerning this variation of reflectance, and because other uncertainties involved in measuring and modelling diffuse radiation, the dependence of ρ with wavelength was ignored in the analyses of the lumped system thermal modelling, and in the 2-D absorption modelling of the transwall.

The surface immediately outside the test cell at MERA, see photograph 1, is weathered asphalt with white stones. Half square meter areas were picked at random and the number and the size of stones were measured. The reflectivity of weathered asphalt is 0.18 and of white marble is 0.56 from Iqbal (6). This sampling gave an average ground reflectance, ρ_s , of 0.2 which is a fairly typical value for general ground conditions.

The ground reflectance was also confirmed by measurement. It was measured by two back to back silicon cells mounted in a horizontal position 1 meter above the ground. The cell facing the sky measures the global incident solar radiation and the one facing the ground the reflected energy (reflectance is the ratio of the reflected to the incident energy). Average values of such measurements were taken under overcast conditions so the measured ground reflectance corresponds to diffuse reflectance, ρ_d . Very good agreement was achieved by the direct measurement method and the "area sample" method.

Note $\rho_{\text{ground}} = \rho_{\text{diffuse}}$

4.4.4 Transmission of Diffuse Radiation

In order to calculate the attenuation of radiation it is essential to know the path length. This in turn requires the slab thickness and incidence angle. The latter is generally known for beam radiation, but obviously diffuse radiation poses a problem. If isotropic diffuse radiation is assumed then it is possible, if tedious, to sum the radiation over all angles. The presentation of the results can be simplified by defining an equivalent angle for beam radiation that gives the same transmittance as for diffuse radiation.

Brandemuehl and Beckman (43) presented their results in graphical form for the effective beam radiation incidence angle, ψ , versus the slope of the plane for diffuse radiation from the sky and from the ground. Two best fit equations for each case were also available. For a vertical surface as in the case of the transwall under investigation.

$$(\psi)_{\text{ground}} = 60^\circ, \text{ and } (\psi)_{\text{sky}} = 59^\circ$$

From Brandemuehl's plot it was noted that the variation of the sky diffuse effective angle of incidence with the inclination of the receiving surface is very small, namely 59.5° to 57° , and this confirms the rule that "for sky diffuse radiation the incidence angle is 58° irrespective of the surface slope".

For ground diffuse, ψ , they suggest

$$(\psi)_{\text{ground}} = 90^\circ - 0.5788\beta + 0.002693 \beta^2$$

where β is the collector slope in degrees.

The angles of $(\psi)_{\text{ground}} = 60^\circ$ and $(\psi)_{\text{sky}} = 59^\circ$ compare

very well with that suggested by Hottel and Woertz (46) for hemispherical isotropic diffuse radiation, 58° , and with Paparsenos' (3) for isotropic sky diffuse radiation and with two different models of anisotropic diffuse radiation, 60° to 63° . Clarke (30) though suggests a much lower incidence angle, 51° , for anisotropic sky conditions. In the present analysis a compromise of the above available values was made and a value of 62° seemed to be more appropriate for the test conditions at M.E.R.A. This value was further confirmed by the findings of Seah (44).

4.5 MEASUREMENT OF SOLAR RADIATION

The direct and diffuse components of the irradiance in the plane of the collector aperture are required. Global solar radiation on a horizontal plane was measured using a Kipp and Zonen CM5 solarimeter placed on the right top corner of the test cell. Global solar radiation incident on a vertical parallel plane behind the glazing was determined by a Kipp and Zonen CM3 solarimeter positioned directly above the transwall module, while the diffuse solar radiation falling on the horizontal surface was measured by a Kipp and Zonen CM5 shade ring solarimeter mounted on the left top corner of the test cell, see photograph 2(p.96). The three solarimeters were connected to a programable logger, a Solatron Orion System, normally programed to take measurements every 30 seconds and set to print the standard deviation and average radiation over every 15 minute period. The measured global, I_{gl} , and diffuse, I_d , solar radiation on a

horizontal surface, gave the direct solar radiation from the following relation:

$$I_b = (I_{gl} - I_d) / \sin \alpha$$

where the solar altitude angle α is obtained as described in Appendix A. The solarimeters were calibrated at the Met. Office, Bracknell recently.

4.5.1 Solarimeter Corrections

i) Cosine effect

The solarimeters are required to be corrected for the angular dependence of absorptance of their sensing elements. This is the well known "cosine effect" and a correction is required for incidence angles greater than 65° . The cosine effect varies with the ratio of direct radiation to diffuse radiation, and this effect is more pronounced when this ratio is high. McGregor (50) examined in detail the cosine behaviour in Kipp and Zonen CM5 solarimeters and from his curves the following relation was developed

Sensitivity of global solarimeter, SG, is

$$SG = 1.0019 - 5.35 \times 10^{-4} \cdot \theta$$

where θ is the angle of incidence in degrees.

Another correction that was applied to both solarimeters (global and diffuse) is a temperature correction i.e. (-0.15% in sensitivity/ $^\circ\text{C}$ from 10°C). Therefore the true radiation will be:

$$I_{\text{true}} = \frac{I_{\text{measured}} \times \text{Calibration in W/m}^2}{[1 - 0.0015 \cdot (T - 10)]}$$

(ii) Shade Ring Correction

The measurement of diffuse sky radiation was accomplished by means of a Kipp and Zonen CM5 solarimeter fitted with a shading ring to shield the receiver from the direct solar beam. The ring, which cast a shadow of projected width somewhat larger than the solarimeter sensor in order to cover the dome, is mounted on a polar axis so as to obscure the entire diurnal path of the sun. Adjustments are necessary every few days to allow for changing solar declinations. The shade ring used has the form of an adjustable circular metal strip 50 mm width of radius 177.5 mm.

The shade ring obscures not only the sun but also an area of the sky too large to be ignored, so the measured values must be corrected to compensate for the sky radiation cut off by the ring. The fraction, X , blocked by the ring is given by the Drummond semi-empirical equation(6):

$$X = \frac{2b_r}{\pi r_r} \cos \delta \cdot \left[\left(\frac{\pi \cdot a}{180} \right) \cdot \sin \phi \cdot \sin \delta + \cos \phi \cdot \cos \delta \cdot \sin a \right]$$

where b_r and r_r are the width and radius of the shade ring, and δ , a , and ϕ are the solar declination, azimuth at sunrise and latitude respectively.

The above equation is only a geometric correction. For isotropic sky conditions the correction factor, CF , to be applied is

$$CF = \frac{1}{1-X}$$

The correction factor for the shade ring used for the latitude of Glasgow is shown in figure 4.5.1 as it varies with time of the year.

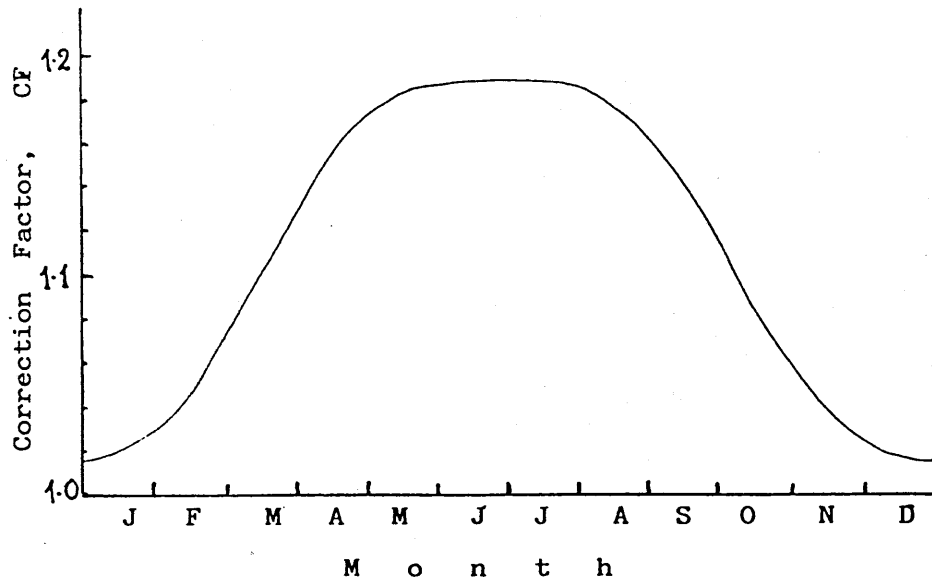


Figure 4.5.1 Correction factors for the shade ring used to account for shading of the detector from diffuse radiation.[†]

A maximum CF, of 1.184–1.187 occurs in the period 16 May to 20 August, and a minimum CF of 1.018 – 1.015 for the 4 December to 5 January.

Le Baron et al. (52) studied the effects of the reflectance of the inner surface of the shade ring and found that the Drummond equation slightly (~5 percent) underestimates the loss of scattered irradiance for a black matt inner surface.

As it was stated earlier Drummond's equation assumes that the diffuse radiation received is uniform over the sky dome. However, even with overcast skies this assumption is incorrect and Drummond recommended an additional correction to account for the anisotropic sky, so that the final correction factors are:

$$CF' = CF + 0.07 \quad (\text{cloudless sky})$$

$$CF' = CF + 0.03 \quad (\text{overcast sky})$$

$$CF' = CF + 0.04 \quad (\text{partly cloudy sky})$$

[†] Author's values

This total correction was investigated at M.E.R.A. for the shade ring described above against the simple isotropic correction factor, CF, and it was found that an additional correction of about 5% was required for clear skies and no additional correction for overcast and partly cloudy skies. My disagreement in adopting an additional correction factor for anisotropic sky radiation for overcast and partly cloudy skies is due mainly to the fact the Drummond carried out his investigations with an Eppley shade ring of different dimensions and at a different site. The above findings were also confirmed by Schüepp (53) who also realised that an additional correction of 6 to 9% was required for clear skies and no additional correction for overcast skies.

McWilliam's (54) tests using Kipp and Zonen instruments in Eire suggested an anisotropic correction, CF'', given by

$$CF'' = 1.1578 - 0.1548 \left(\frac{I_d}{I_{gl}} \right)^3 - 1.43 \times 10^{-4} \delta$$

where I_d = diffuse radiation uncorrected for anisotropic sky but geometrically for isotropic sky

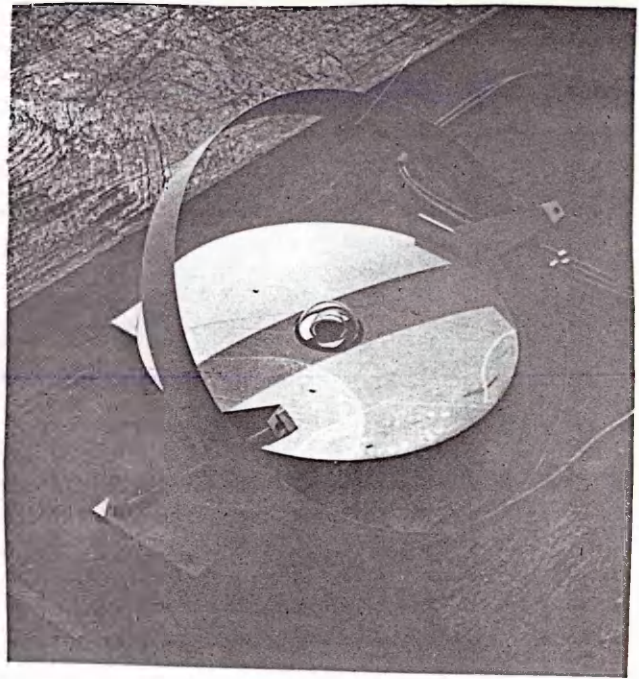
I_{gl} = global radiation on horizontal

δ = declination in degrees

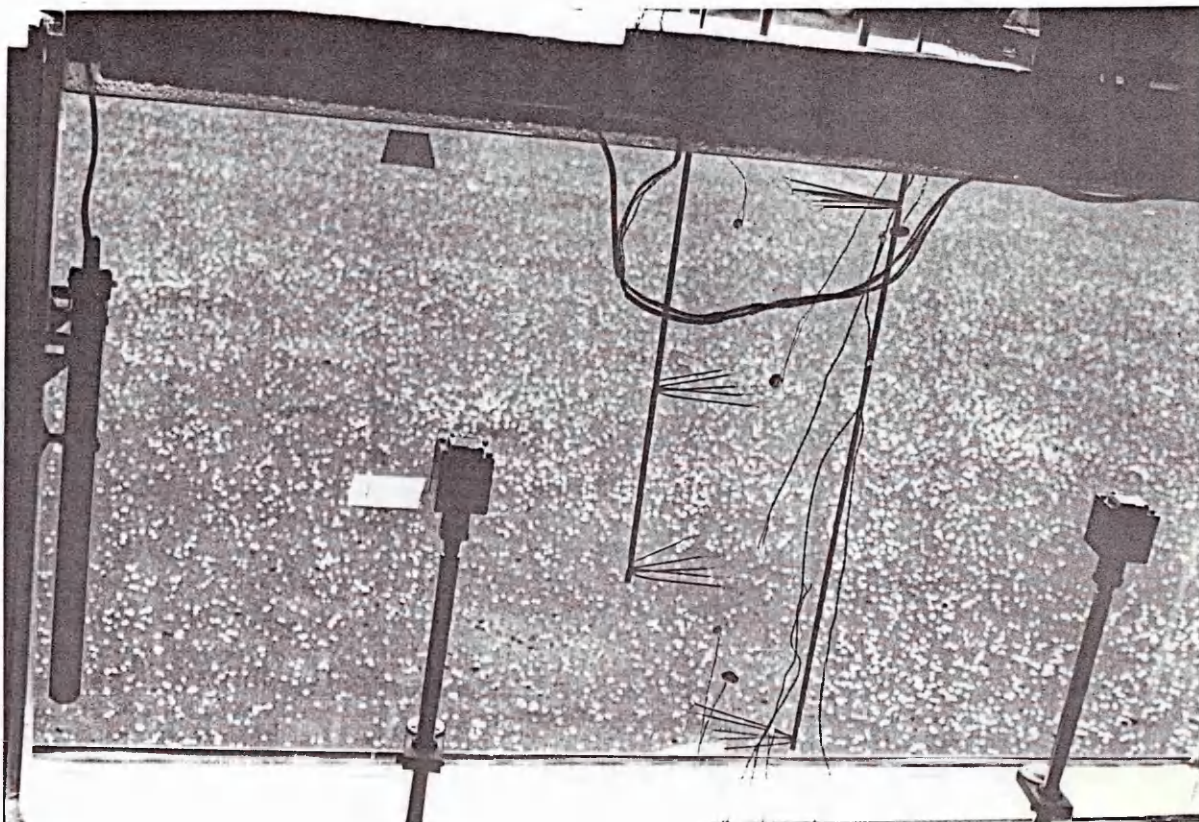
Applicable for altitude angles greater than 10°C.

The corrected diffuse radiation (anisotropic) = $CF'' \cdot I_d$

The results of McWilliam's work showed that diffuse radiation, geometrically corrected for isotropic sky conditions, showed an underestimate of 6% on average, though 1/6th of all results showed an underestimation of more than 15%.



- Photograph 1 Typical ground surface outside test cell.
- Photograph 2 Shade ring solarimeter. Measures diffuse radiation.
- Photograph 3 Thermocouple water temperature measuring system.
R.S. silicon cell components.



From the above, it seems very difficult to develop a single accurate unified treatment of this subject. In the analyses presented in this thesis, the widely accepted Drummond's equation was used with only an extra correction for clear skies.

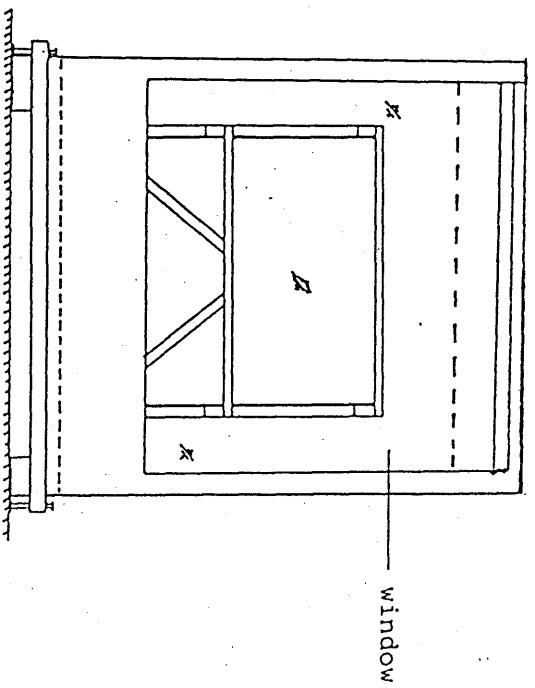
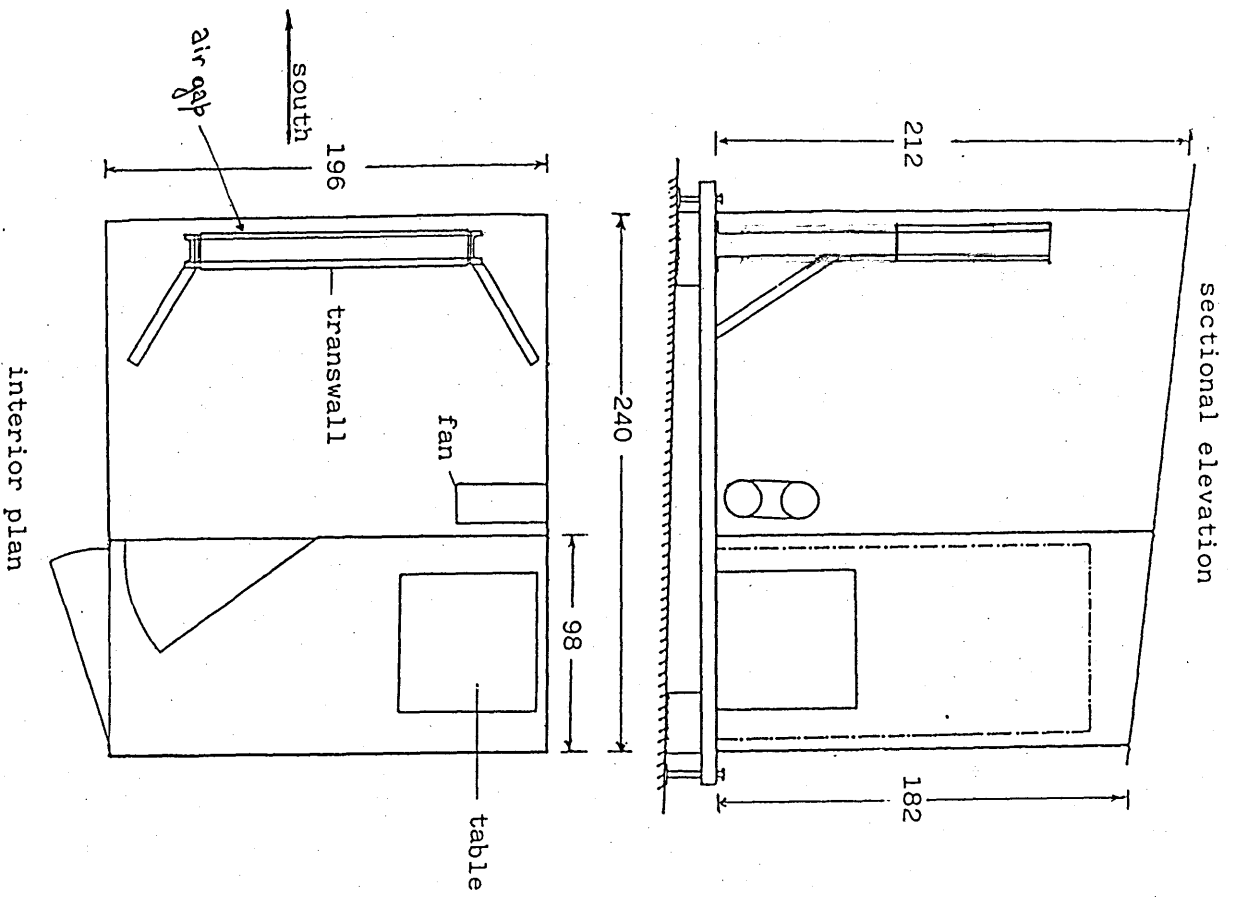
(iii) Tilt Effect

Solarimeters are calibrated in a horizontal upward direction, and when mounted in an inclined or downward direction they may show a small change in response. This change occurs mainly because of a change in the heat transfer pattern inside and outside the hemispherical glass dome. McGregor (50) found that for a Kipp and Zonen CM3 and CM5 instruments there is a reduction of only 2% in sensitivity when the solarimeter is rotated to the vertical. This correction was applied for the vertical solarimeter above the transwall module.

4.6 DESCRIPTION OF THE TEST CELL

The test cell is shown in photographs 4&5, and figure 4.6. The glazed area, 1.62 m x 1.75 m of 6 mm glass, faces due south as a typical passive solar system in the northern hemisphere requires. During the night or the non-operating hours the glazing area is covered entirely with an insulating cover made of three sections, for convenience, of 50 mm thick expanded polystyrene block faced with Dural sheet for protection.

The external walls, roof and floor are constructed

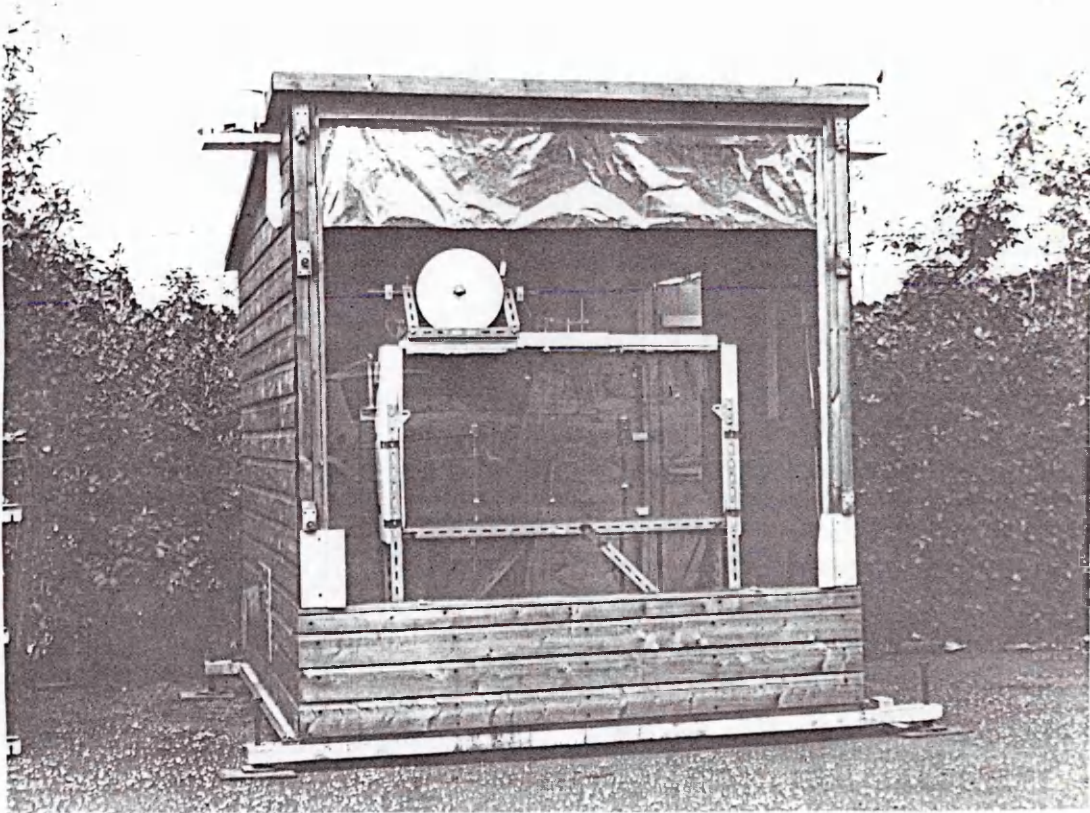


scale 1/34

- (i) Dimensions shown are interior
- (ii) All dimensions are in mm.
- (iii) Window, 162 x 175 mm, single glazed, 6 mm clear float glass.

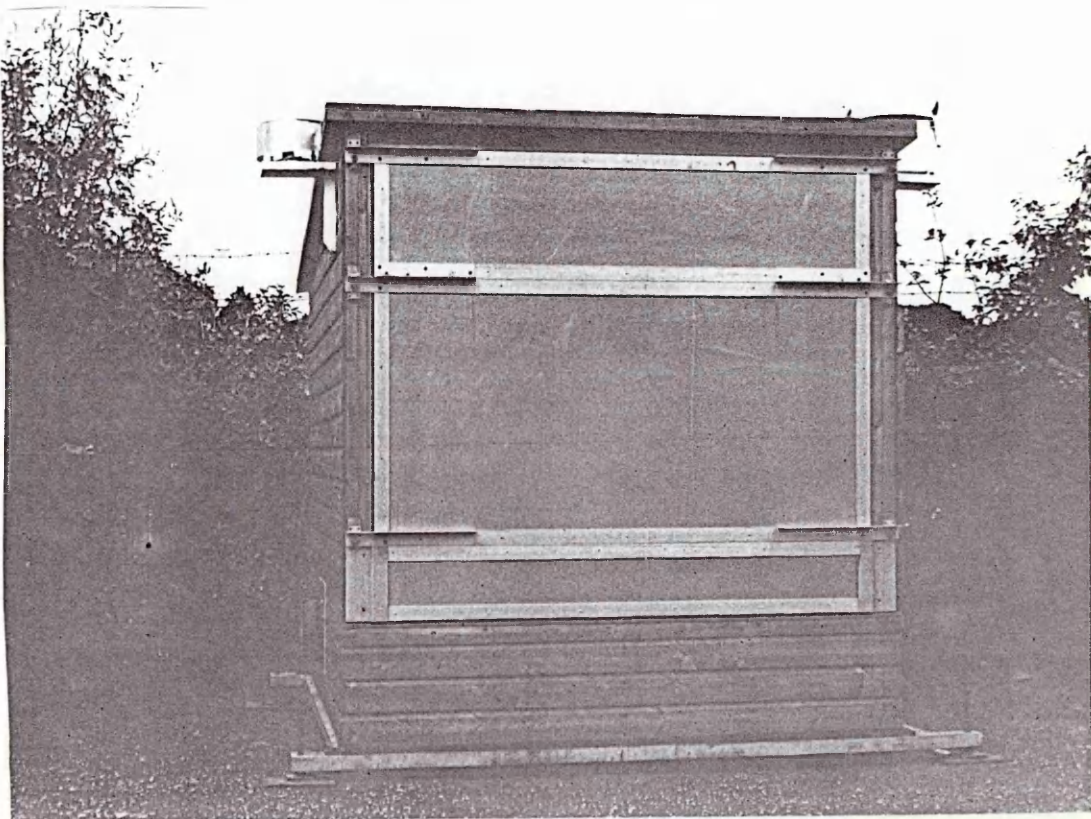
Figure 4.6

solar test cell at M.E.R.A.



Photograph 4 The test cell at M.E.R.A. without the covers.

Photograph 5 The test cell at M.E.R.A. with the covers on.



from 100 x 12 mm tongued- and -grooved planking treated with preservatives which gives a medium brown appearance. The interior walls are not lined but they have proved to be relatively wind tight. The roof is covered by standard bitumen sheeting and the interior wall is formed from 15 mm chipboard. The whole test cell is bolted onto a welded steel framework of 100 x 50 mm channel iron with 75 mm x 37 mm channel cross members pitched at 600 mm. The whole framework can be levelled by four large jacking screws at each corner. The framework which carries the transwall, or transwalls, is made from Handy angle so arranged that the transwall load is taken through to the steel framework. 7

The test cell is unequally divided by the interior wall to give access to the logger without disturbing conditions within the test compartment. If left to its own devices the test cell air temperature can reach 40 °C, and by day is usually higher than the transwall temperature. In order to achieve some degree of (crude) control over the temperature a 7½ inch Vent-Axia fan was installed in the west wall. It was thought useful to be able to minimise, or enhance, vertical temperature gradients in the test room so a swivelling duct is fitted to the fan which allows the cool air to be directed either to the top, or to the bottom, of the test compartment. This is used in conjunction with sliding vents, top and bottom, to the logger compartment.

Since the transwall mass to test compartment volume is at present much larger than in a practical building situation no attempt has been made to model the test cell/transwall system as a whole. Only the performance

of the transwall itself is considered. Future work may require that the system as a whole be considered, probably with a much smaller transwall, and this would require the complete reappraisal of the test cell, its instrumentation and the installation of a much more elaborate temperature control system.

Test Cell Location

From maps obtained from the Department of Geography of the University of Glasgow the precise geographical position of the test cell was determined:

Longitude 4.3° West

Latitude 55.9° North

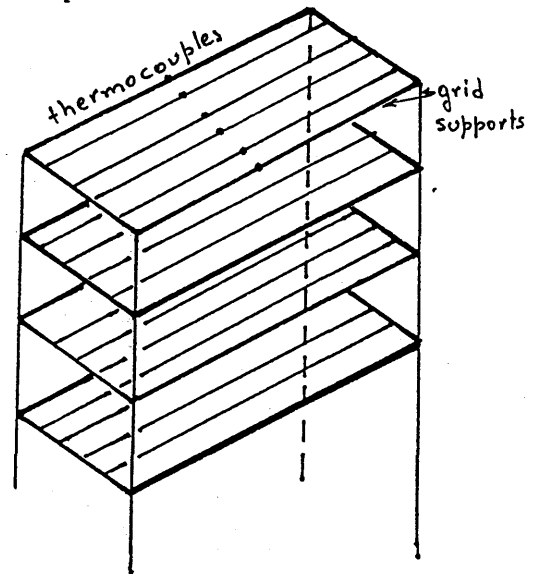
4.7 TEMPERATURE MEASUREMENT

In all 40 Chromel-Alumel thermocouples of 1.5 mm o.d. were used to measure the temperatures of ambient air, the temperatures of water volumes, the temperatures of the transwall surfaces and the temperatures of the test cell interior. Three thermocouples are 1.5 mm o.d. stainless steel sheathed and the remainder are made from 0.3 mm PTFE insulated cable. The beads are formed by an electrical discharge thermocouple welder. Chromel-Alumel thermocouples were chosen for the test cell environment in order to match those used in the transwall. The thermocouples were connected to a data logger and print outs were usually collected every fifteen minutes. Twenty thermocouples monitored the water temperature and another twenty the various surfaces and air volumes. The accuracy of the temperature measurements was $\pm 0.1^{\circ}\text{C}$.

4.7.1 Temperature of Water

The temperatures of the water in the transwall was measured by four planes of five thermocouple 'fingers' as shown in figure 4.7.1a. The reason this system was adopted is given hereunder.

It is important that the temperature sensors interfere as little as possible with the phenomena within the transwall. This effectively rules out the more stable resistance thermometers in favour of thermocouples. A series of grids in which thermocouples are stretched between supports was also ruled out because although it can minimise interference with the flow patterns it is difficult to make with the thermocouples all at the same tension. Experience with these grids indicates that if one thermocouple breaks then all thermocouples in the grid have to be replaced, and wires are prone to droop out of line in the course of time.



In the system adopted fingers of stainless steel hyperdermic tubing 1.75 mm o.d. x 1.25 mm i.d. support PTFE insulated Chromel-Alumel thermocouples to within 20 mm of the tip. Chromel-Alumel was chosen in preference to the more stable Copper-Constantan because it is mechanically stiffer and so the free length at the tip is less likely to move. The thermocouple wires pass up the 4.5 mm o.d. vertical tubes which can be raised, lowered, and rotated by clamps on the top of the transwall, see figure 4.7.1b.

The transwall will operate only over a limited range of temperatures, 15 - 35°C, and so calibration, or more accurately matching, was limited to these temperature levels. A large Dewar flask in a well insulated box was placed on its side and the two of the five 'fingers' arranged so that the ten thermocouple leads were interlaced in a horizontal line to overcome any slight vertical temperature gradient. The thermocouples were connected by individual thermocouple connectors to cold junctions sitting in two carefully prepared ice baths. The cold junctions consist of pairs of 10 mm x .5 m glass tubes down which runs each thermocouple wire together with a 1.5 mm insulated copper wire. The wires are loosely twisted at the ends and submerged in about 30 mm of mercury to give good electrical and thermal contact. Melted paraffin wax is poured down each tube to seal in the mercury. The copper leads were joined to a heavy duty thermocouple switch connected across a high precision DVM. The Dewar flask was sealed and, after being left to settle for three days, the emfs were recorded. One of the set of five fingers was arbitrarily selected as a reference and moved to the second set of five and so on. Thus the thermocouples were compared against each other. The thermocouple emfs all agreed to within $\pm 1 \mu\text{V}$ ($\pm 0.025^\circ\text{C}$), except for thermocouple numbers 6 and 7 which consistently registered 2 μV above the others. It was noticed that moving the thermocouples about could produce differences of 2 μV (0.05°C) but since the accuracy required is no greater than $\pm 0.1^\circ\text{C}$ this was considered satisfactory.

The distance between internal glass surfaces is 156 mm, and the horizontal distances of the thermocouples from the south transwall glass are as follows.

Code number	Vertical positions from bottom glass (mm)	Horizontal distances from south glass (mm)
1	A = 542	5
2		40
3		80
4		118
5		148
6	B = 383	10
7		33
8		85
9		122
10		152
11	C = 224	15
12		35
13		80
14		110
15		150
16	D = 58	5
17		28
18		77
19		116
20		150

4.7.2 Temperatures of Transwall Surfaces and Test Cell Space

The position of the thermocouples with their code numbers are indicated as shown in figures 4.7.2a & b. The thermocouples attached to the glass window surface and transwall glass surfaces were held by silicon adhesive. Where necessary thermocouples were shielded from solar

radiation by small shields made from fine aluminised Melinex. Tests by Paparsenos (3) showed that thermocouples immersed in water would not show any significant temperature error (in relation to $\pm 0.1^{\circ}\text{C}$ required accuracy) due to solar radiation provided the water thickness was greater than 2 mm.

The position of the thermocouples and code numbers are listed below:

Code no.	41	room temperature near transwall lower (stand)
	42	room temperature near transwall middle (stand)
	43	room temperature near transwall upper (stand)
	46	equipment room temperature east
	47	equipment room temperature west
Code no.	21	inside window upper
	24	inside window lower
	22	transwall glass inner S-side (38 cm from bottom)
	23	transwall glass inner N-side (25.5 cm from bottom)
	25	thermocouple (probe) between window and tank
	26	room temperature central
	44	room temperature east
	45	room temperature west
	27	ambient temperature North (shaded)
	31	transwall glass outer S-side upper
	32	transwall glass outer S-side lower
	33	transwall glass outer N-side upper
	34	transwall glass outer N-side middle/upper
	35	transwall glass outer N-side middle/lower
	36	transwall glass outer N-side lower

4.8 COMPUTING PROGRAM OPERATION

A computing program was constructed to predict the temperature variation of the lumped system using as input experimental readings from actual runs. The program has the following features.

- 1) Using the equations listed in Appendix A, it calculates the position of the sun for a given day of year and local time.
- 2) The output in mV of the two horizontal solarimeters (global and diffuse) are incorporated and the program then, after making the necessary corrections, calculates the beam and diffuse radiation in Watts per meter², incident on the system.
- 3) The equation 4.1b was used to predict the temperature rise in the transwall, after a given period of time. Because $(I\alpha)$ varies with time, the time was divided into intervals of 15 minutes and $(I\alpha)$ was taken as constant over that period.
- 4) Only an initial average wall temperature was necessary and then the prediction became 'initial' and so on until the analysis ceased to operate. The heat transfer coefficients of the transwall module and the surroundings (stream of air between wall and air gap/and room interior) were extracted from table G.1, Appendix G and assumed to be unchanged during the run.

5) Other variable inputs were the ambient temperature, an average room temperature and the air gap temperature obtained from thermocouples 27, 42 and 25 respectively.

4.9 WATER TEMPERATURE MEASUREMENT

The non uniformity of the measured temperature distribution of water in the transwall is demonstrated in figures 4.9a and 4.9b. The following observations were made:

- 1) The largest vertical temperature difference observed was 2.7°C .
- 2) The largest horizontal temperature difference observed was 0.6°C for the upper (1-5) thermocouples.
- 3) When the water in the transwall is heated it sets up circulation patterns. The "seagull" pattern of the horizontal temperature distribution figure 4.9a, suggests the circulation system shown below.

The same pattern was observed by Paparsenos (3) with an entirely different thermocouple system. He used fewer thermocouples, and at the time, it was put down to thermocouple inconsistency. However, these latest tests were made with matched thermocouples and the development of the pattern can be clearly seen. The answer probably lies in a complex flow pattern in the transwall noting that only a slow circulation of fluid is liable to have a profound effect on the effective conductivity of the fluid and consequently the temperature distribution. The creeping of the water up, or down, the glass walls will produce boundary layers of varying thickness and

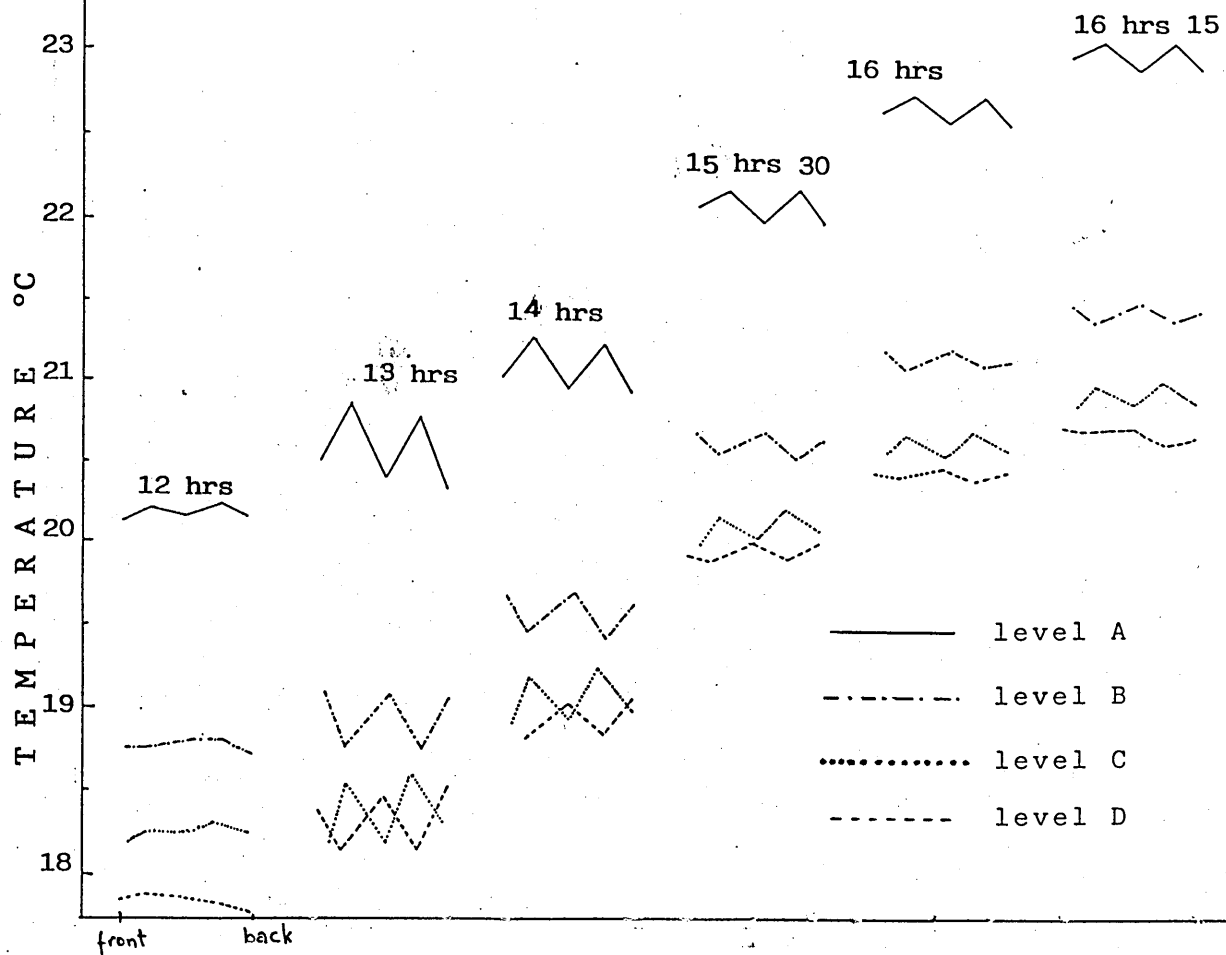


Figure 4.9a. Horizontal water temperature variation with time. 20th of June.

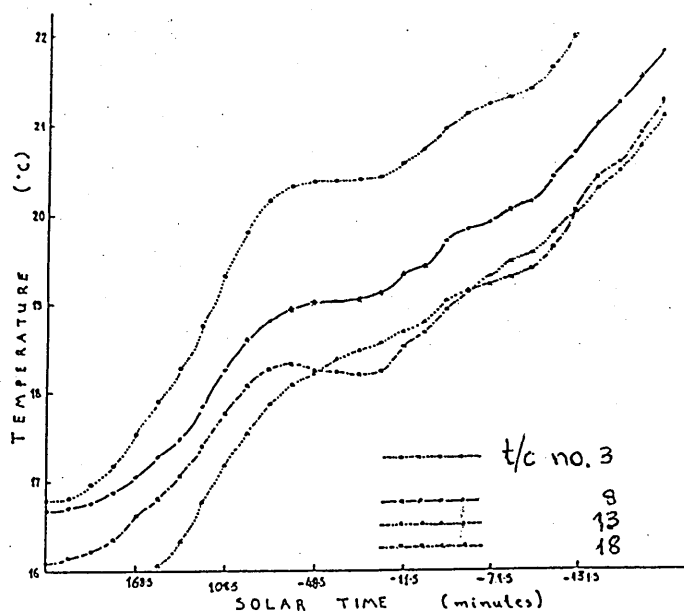
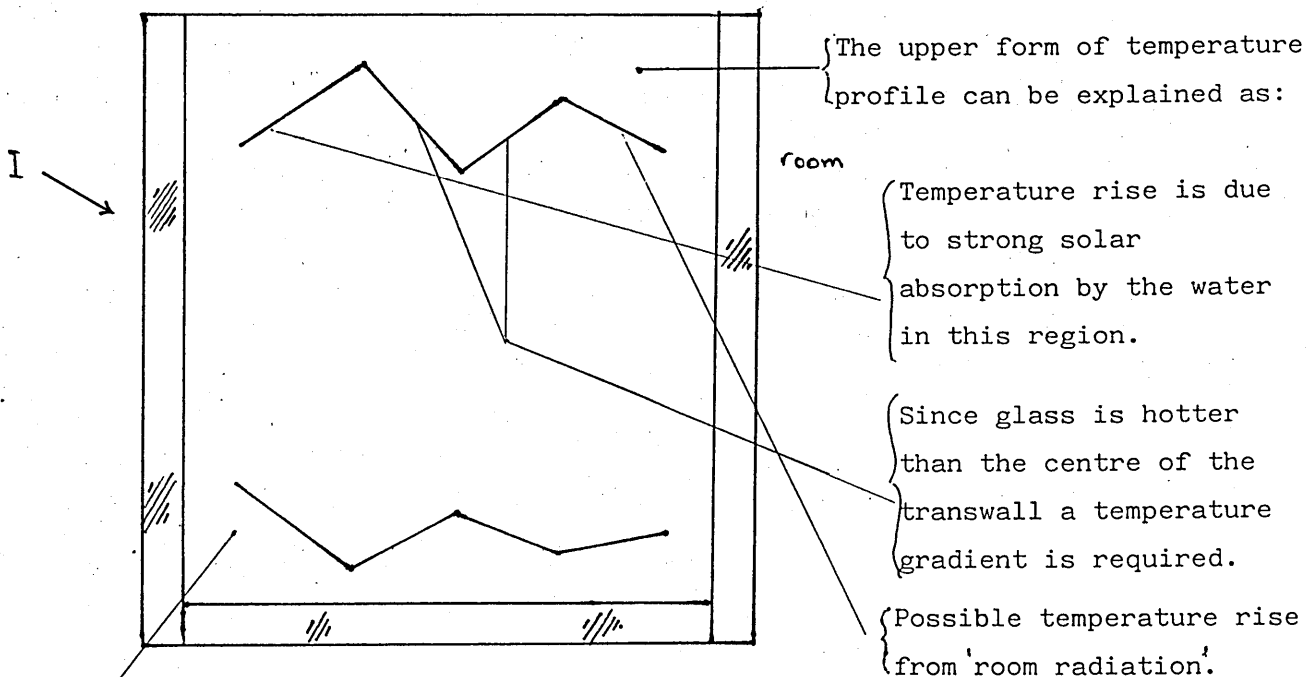


Figure 4.9b Vertical water temperature stratification. 20th of June.

stratification effects add to the complexity since the diagram shows that the stratification gradient is far from linear in form. The circulation patterns require further experimental investigation possibly by placing more thermocouples within the transwall to investigate the temperature distribution more closely. The use of possible flow visualisation techniques are difficult to implement since dye streaks, or particles, tend to absorb radiation and give false indications of what is happening. Also circulation velocities are very low and the dye streak is liable to disperse. The pattern of the horizontal temperature distribution, figure 4.9a, showed a remarkable constancy over a long period of time with "seagull" patterns all being the mirror image of the one immediately above and below. The 'peaks' of this figure represent the measured horizontal temperatures which are jointed between one another by straight lines.



When the pattern inverts the phenomenon cannot be explained.

4.10 LUMPED SYSTEM RESULTS

a) Temperature Rise Prediction - Insolation is Present

On the basis of the experimental results obtained on the 20th June, see figures 4.9a & b, curve 3[†] of figure 4.10a is the most likely to be correct. For this case a K value of 1.5 and the experimental values of heat transfer 11.8 and 7.5 W/m²K, from Appendix G were used. This gives an 18% overprediction error in the ^{transwall} temperature rise over a period of 7 hours. Overprediction is to be expected in this situation since the room temperature is higher than that of the transwall. This can be explained as follows. The actual heat transfer from the surroundings to the transwall involves the product of the surface heat transfer coefficient and the temperature difference room to transwall surface. The lumped system approach uses an average temperature which is uniform throughout the transwall and dominated by the water. Thus, fundamentally the lumped system cannot cater for the higher glass surface temperatures which are inevitable in this case. These arise from the absorption of radiation particularly in the transwall glass facing the window, and from the fact that heat transfer from the surroundings is inwards to the cooler transwall centre and obviously the temperature gradients are such that the glass temperatures are higher. This effect can be seen from figure 4.10b where there is a marked correlation between the window side mean transwall glass surface temperature and the absorption of radiation in the transwall. The room temperature reacts more slowly due to thermal damping

[†] The 4 curves predicting the mean transwall temperature with time using different combinations of K and heat transfer coefficients are summarised on p.113

but both are up to 2°C higher than the measured mean transwall temperature. The effect of higher glass surface temperatures on the heat transfer varies, and it will overpredict the heat transfer from 10 to 60%. It is worth noting that this problem of the higher glass temperatures will not arise with a plastic film type of transwall since the absorption and thermal capacity of the plastic film is very small.

The sensitivity of the predicted temperature rise to the surface heat transfer coefficients can be seen from curves 1 and 4 of figure 4.10a, below.

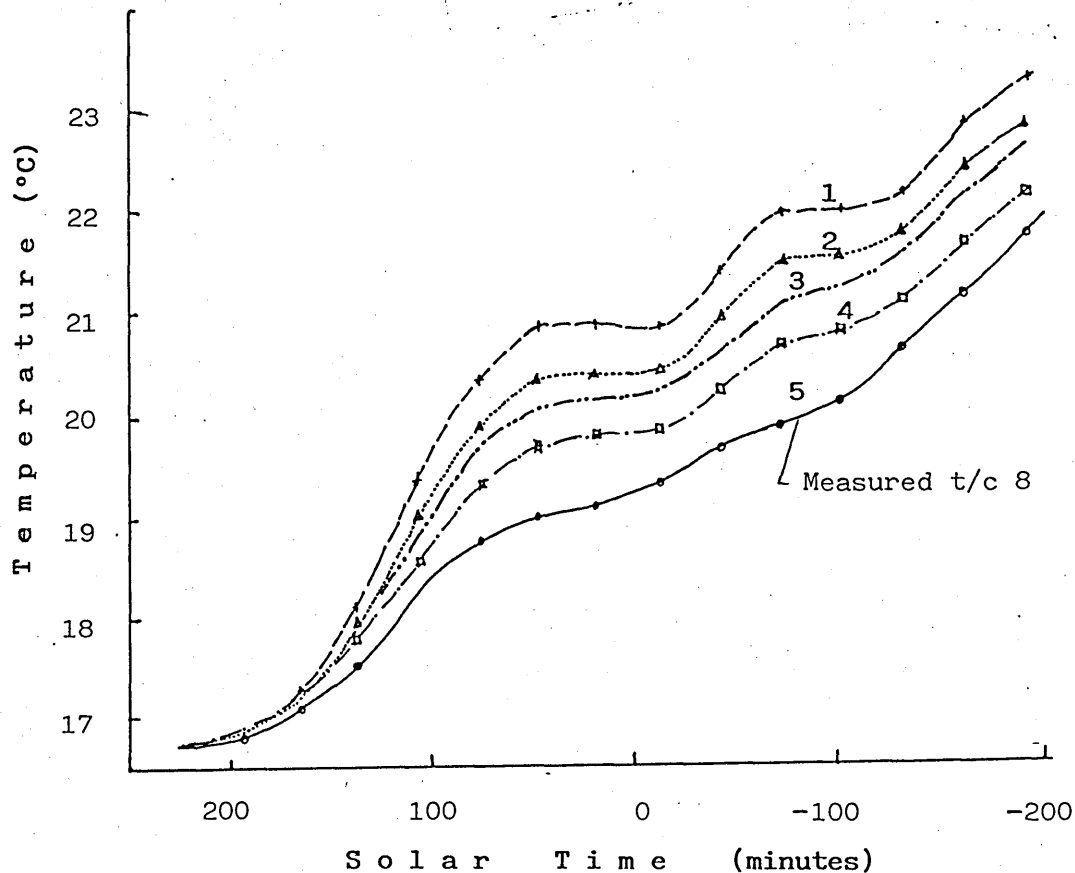


Figure 4.10a Measured versus predicted temperature rise.
curve codes p.113

Curve 1 uses the heat transfer values for the 'warm' situation i.e. when the transwall is from 24 to 28°C , and has values of 18.4 and $12.4 \text{ W/m}^2\text{K}$ for the outer

and inner transwall glasses respectively. If these values are used the error in temperature prediction rises to 30%. The curve 4 has the lowest heat transfer coefficients of $7.5 \text{ W/m}^2\text{K}$ for both glass surfaces and these are obtained from the theory of laminar flow over a flat vertical plate (5). In this case the final temperature is within 8% of the measured values. However, the heat transfer coefficient in the transwall/window air gap is too low for credibility. Clearly as proposed in Chapter 6 more work is required to establish the actual heat transfer coefficients to better than 10%.

Associated with uncertainty in the heat transfer coefficients is the ratio, K , of the temperature difference transwall/room to transwall/air gap. Recalling that the overall heat transfer coefficient, associated with one side, is

$$h = K h_a + h_r$$

where h_a is the air gap/glass surface heat transfer coefficient and h_r is the corresponding one for the room side/glass surface of the transwall. Often the difference between the room and the air gap mean temperatures is neglected and consequently K is unity. However, measurements show, for this run, that the mean value of K is 1.48 with a first standard deviation of 0.25. The variation of K with time is shown in figure 4.10b. The value chosen for K has a substantial effect on the accuracy as it can be seen from the curves 1, 2, 3, 4 of figure 4.10a.

curve 3	$K = 1.5$	$h_a = 11.8$	and	$h_r = 7.5 \text{ W/m}^2\text{K}$
curve 4	$K = 1.0$	"	"	(superimposed)
curve 1	$K = 1.5$	$h_a = 18.4$	and	$h_r = 12.4 \text{ W/m}^2\text{K}$
curve 2	$K = 1.0$	"	"	"

In order to preserve the simplicity of the lumped system approach K is taken as one value, but clearly from figure 4.9b K is far from uniform.

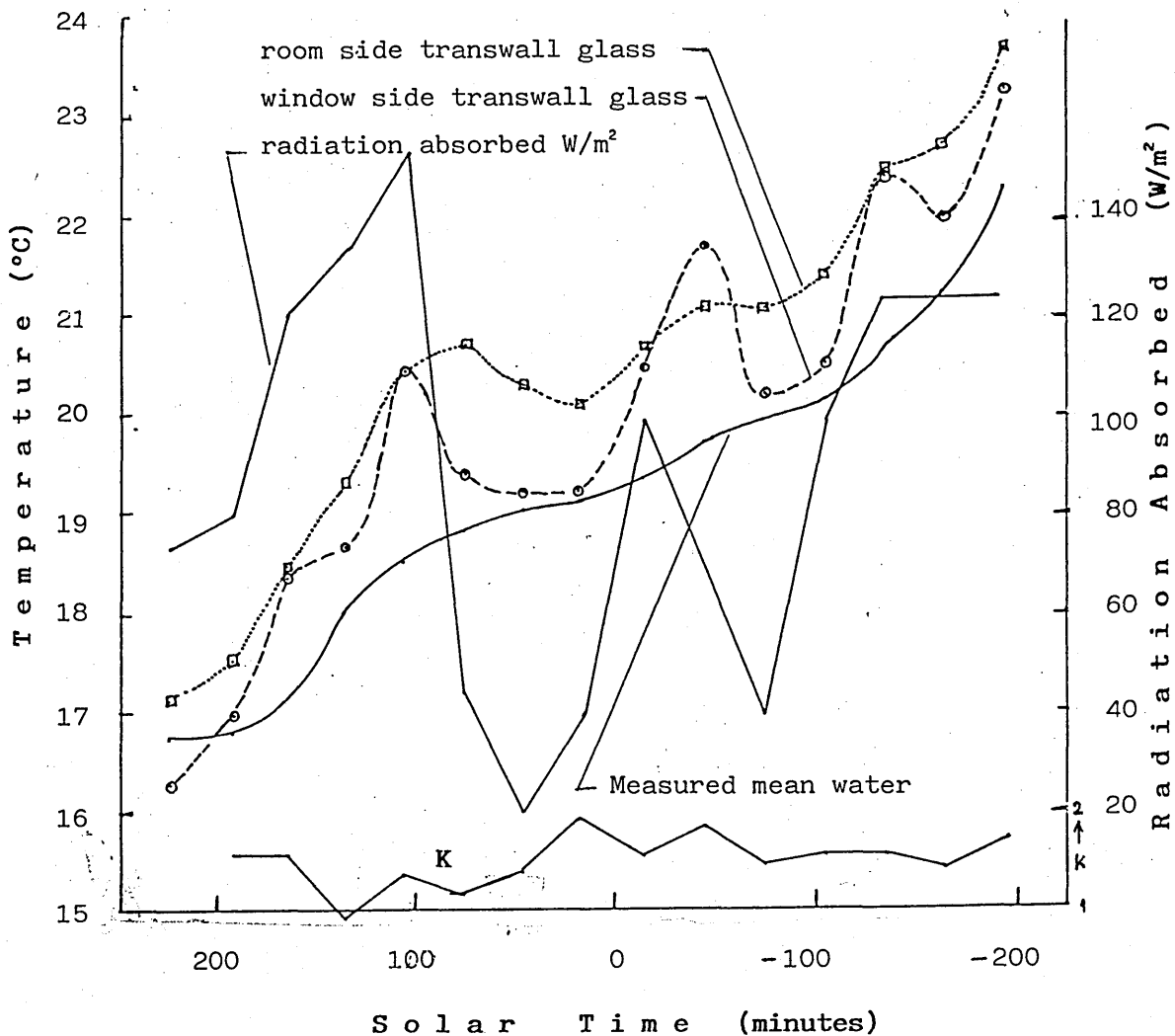


Figure 4.10b Measured transwall temperatures on 20th June and predicted radiation absorbed versus solar time.

b) Temperature Fall Prediction Insolation is Absent

When the cooling curve of the transwall during a night run, 23 - 24th August is considered, figure 4.10c, it is seen that the predicted cooling curve from the lumped system equation 4.1b with $(I\alpha = 0)$, is closer to the measured temperature than when insolation is present, figure 4.10a. In fact the predicted temperature fall over 14

hours is only 8% below the measured value. Various factors can account for the improved accuracy in the absence of insolation. The value of the temperature ratio, K , is more uniform at 1.11 with a first standard deviation reduced to 0.04. But more significantly the glass/water temperature difference is less in the absence of insolation, so that the actual temperature difference controlling the heat transfer, room to glass surface, is closer to the assumed difference room to 'lump' temperature.

The water circulation in the transwall which maintains the effective rather than the true (static) thermal conductivity is probably less during the night run, and this might be expected to produce a greater divergence between the predicted and the measured values. However, it is believed that the reduction in the glass/water temperature difference more than compensates for this.

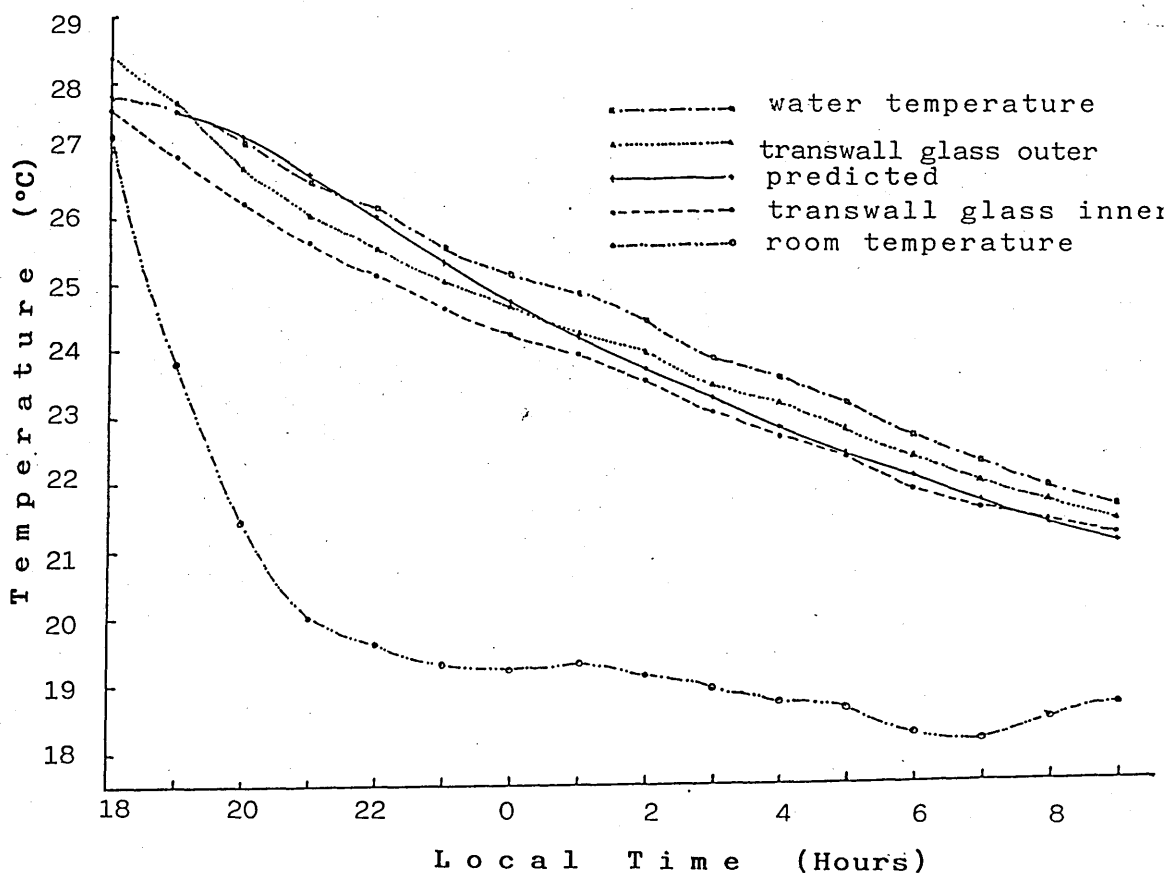


Figure 4.10c Temperature fall in the transwall
predicted versus measured temperatures

Conclusion

It is suggested that the lumped system approach in predicting ^{the accuracy of} the temperature rise in a transwall, and thus its performance, is probably about 18%. If solar insolation is absent then the lumped system approach can predict the temperature fall to within 8%. However, a method of analysis for a solar system which is accurate only in the absence of solar radiation cannot be considered practical.

If the transwall uses thick glass walls the lumped system cannot account for the difference in glass and water temperatures. This system is also vulnerable to accurate pre-knowledge of the temperature difference ratio K . The situation can be improved by treating the glass and water as different lumped systems or alternatively by working with 'adjusted' heat transfer coefficients which relate to room-centre transwall temperature differences. Both these approaches add to the complexity and destroy the simplicity of the ^{lumped} system. It is believed that the finite difference approach has more to offer in accuracy and flexibility with some admitted degree of complexity.

2-D ANALYSIS OF THE RADIATION ABSORBED IN A TRANSWALL MODULE5.0 Introduction

This chapter is devoted to a two-dimensional computer analysis of the energy absorbed in the transwall module. The program developed is intended to form part of a larger program which will model the phenomena within the transwall using finite difference methods, and consequently the absorption of radiation is required for the individual slabs (typically 5 x 7) into which the transwall volume is divided.

The two-dimensional nature of the analysis requires that for beam radiation each slab volume is multiplied by two factors, a shade factor and an acceptance factor. The former will have a range of values from zero through to unity depending on if, say, the top cover completely, partially or fails to shade the slab; the latter will have a range from unity through to zero depending on whether radiation reflected from the bottom is fully received, partially received, or not received by the slab volume under consideration. This approach requires that the location of the three-dimensional limiting rays within the transwall is defined. In order to account for refraction within the transwall a concept of 'effective' altitude and azimuth angles is developed to establish ray location, and this forms the first part of this chapter. The rays defined, the chapter then goes on to consider the methodology of the shading and acceptance factors. All rays have their own shade and acceptance factors apart from the very weak ones where conveniently one general shade or acceptance factor is used.

The absorption of diffuse radiation by individual slabs is associated with individual slab view factors and their treatment is described.

Clearly if a system of infinite reflections were to be considered in this two-dimensional field then the proliferation of shading, acceptance and view factors for each ray will be enormous. This problem is overcome by an approximation which considers only one reflection at each surface.

The program requires the division of the solar spectrum into wavebands each with its own properties, i.e. extinction coefficient, fractional energy level, etc. This makes a large demand on the available RAM of a nominal 64K micro and if a large number of slabs are chosen then the number of wavebands has to be reduced. In order to speed up the computer running time, and to reduce the demand on the RAM, a single waveband approach has been developed for a reduced accuracy analysis which is covered in this chapter and in appendix E.

The shortwave radiation reflected from the room into the transwall (backwards radiation) and the reverberations of the incident radiation between the transwall and the window are also considered. The level of backwards radiation was established by a correlation derived by experimental means.

The methodology of ray tracing, shading, acceptance view factors now established equations are then developed for the absorption of radiation in each slab. The predictions of the computer program were validated with experiment and good agreement was achieved between theory

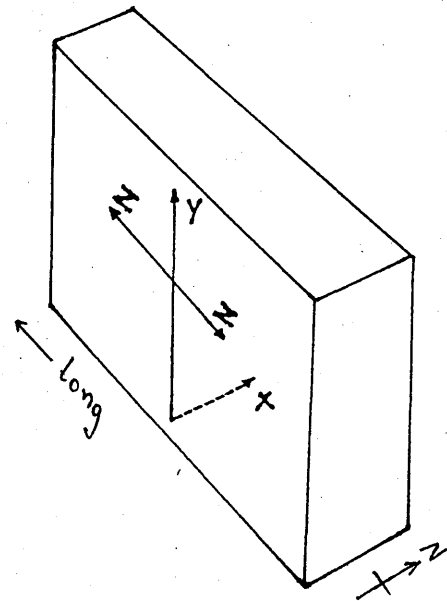
and experiment. The computer program was then used to identify and quantify various factors relevant to the absorption of radiation, namely, the effect of varying the number of wavebands, the effect of one general spectrum rather than different ones for beam and diffuse radiation depending on the air mass and type of cloud cover, the effect of different dyes and high absorbing glass was also considered.

5.1 TREATMENT OF ABSORPTION IN A 2-D TRANSWALL

The following basic features were considered.

Accepting that shading occurs it is necessary to calculate the absorption in the various volumes into which the transwall is divided. This approach is essential if a finite difference solution is to be employed to find the temperature distribution within the transwall. As a subset of this approach is the methodology of incorporating multiple reflections.

The transwall in this case is considered to be long and the method is strictly two-dimensional, at least in the sense that absorption is taken to vary in the x - y plane but is uniform in the z direction. However, it should be noted that the 3-D nature of the beam radiation must be taken into account.



In all this work the transwall is taken to face due south since this is the situation of the module in the test cell. In order to apply the equations to other orientations it is only necessary to incorporate the wall azimuth angle, $\pm a_w$, with the solar azimuth, a , term, ie replace $\cos a$ with $\cos(a-a_w)$.

Shade/acceptance factors for Beam Radiation within the Transwall

Consider beam radiation striking the transwall as shown in figure 5.1 below. The vectors representing the beam will be fore-shortened ie. inclined into and

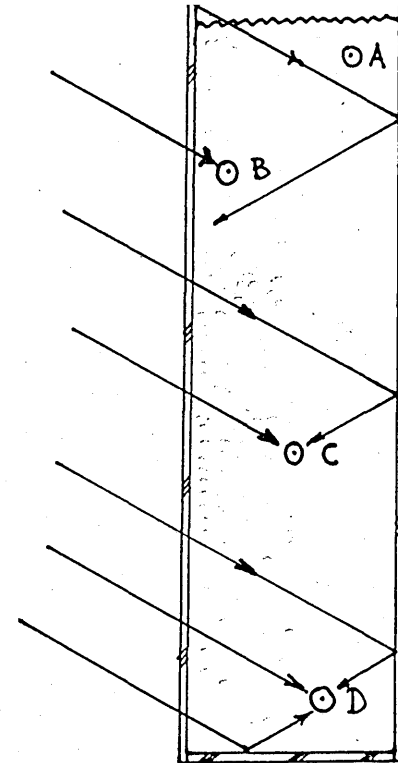
out of the plane of the paper. If one reflection is considered at the glass/air interface then,

Point A will receive no beam radiation.

Point B will receive direct radiation but no reflected radiation.

Point C will receive both direct and reflected radiation.

Point D will receive both direct and reflected radiation from the back and in addition radiation reflected from the base.



Thus each volume of the transwall has to be associated with its own shading and acceptance factors. The latter is taken to mean a factor which controls the acceptance of reflected radiation. If multiple reflections are assumed then the shading and acceptance factors become increasingly complicated. Note that because of the downward component of the beam vectors the radiation, and absorption, will increase towards the base. A major weakness of the one dimensional approach is that it will not show this effect.

Diffuse Radiation

Certain assumptions are necessary for the treatment of diffuse radiation.

- (1) Sky radiation is isotropic.
- (2) Diffuse radiation is treated as having an effective angle of incidence $\psi = 62^\circ$ in order to calculate the internal transmission. The angle of 62° is

supported by Beckman and Brandemuehl (43) and also by measurements undertaken as part of a final year undergraduate project (44). It is worth noting that anisotropic models of sky radiation, such as Klucher or Hay, give different angles.

- (3) No shadow factors are involved but view factors are. The view factors to be considered are not only for the sky but also for the diffuse radiation reflected off the bottom of the transwall.

5.2 Refractive Altitude and Azimuth Angles

When calculating shadow factors it is essential to find where the limiting beam vector strikes the horizontal and vertical planes of the various slabs. This is most easily done using the altitude, α , and solar azimuth, a , angles.

Consider ray \vec{lm} . It is required to find the distances $x = kl$ and $y = lm$ figure 5.2. From the triangles kmn , klm it is seen that:

$$x = \frac{L \cdot \tan \alpha}{\cos a}$$

or

$$x = \frac{L \cdot \sin \alpha}{\cos \alpha \cdot \cos a} = \frac{L \cdot \sin \alpha}{\cos \theta}$$

equally $y = \frac{L}{\cos \alpha \cdot \cos a} = \frac{L}{\cos \theta}$

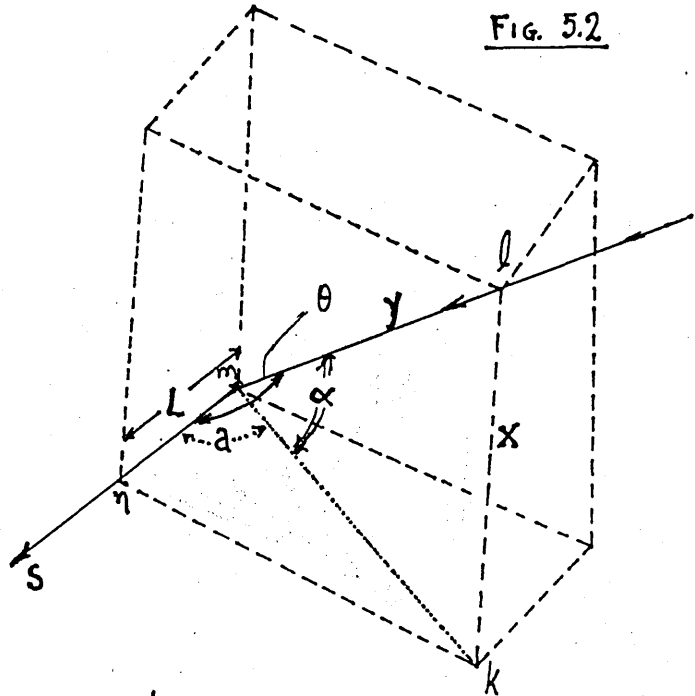


Fig. 5.2

Unfortunately in a transwall the incident ray is refracted as it passes through the different media, so the altitude and solar azimuth angles calculated in air do not apply.

It is necessary, therefore, to calculate 'effective' altitude and azimuth angles for each material of different refractive index.

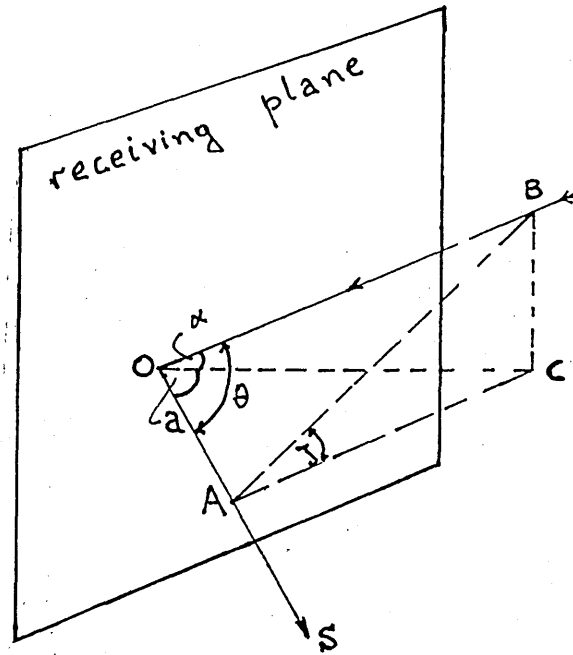
Consider the incident beam BO striking a south facing receiving plane. OS is the normal to the plane, and triangle ABC, is parallel to the receiving plane.

OA is of unit length.

θ_r = refractive angle.

α_r = altitude of refracted ray.

a_r = solar azimuth " " .



The angle of inclination of the incident plane, γ , will be the same as the angle of inclination, γ , of the refracted plane since the incident and refracted rays lie in the same plane.

the angle γ is given by triangle ABC

$$\gamma = \tan^{-1} \left(\frac{\sin \alpha}{\cos \theta \cdot \tan a} \right) = \tan^{-1} \left(\frac{\tan \alpha}{\sin a} \right) \quad (5.2.1)$$

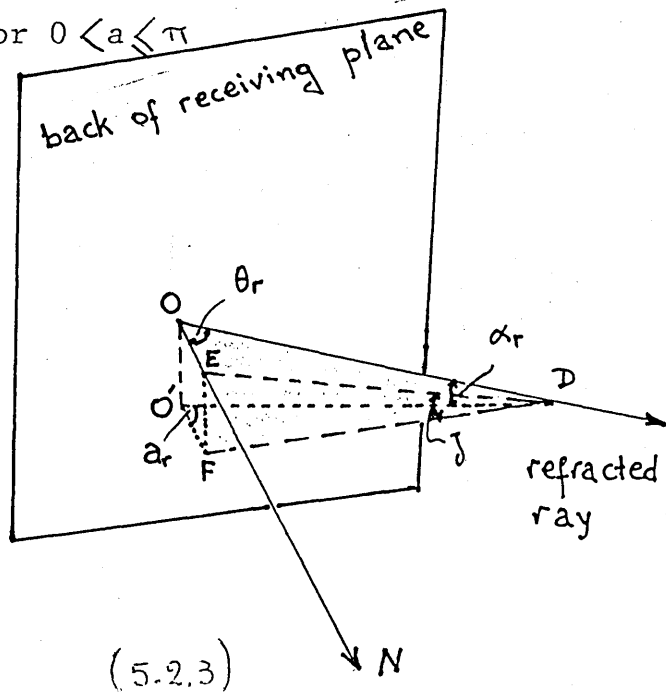
if $a = 0$ then $\gamma = 90^\circ$, for $0 < a \leq \pi$

The refracted solar azimuth, a_r , is given by triangle O'FD

$$a_r = \tan^{-1} (\tan \theta_r \cos \gamma) \quad (5.2.2)$$

and the refracted altitude angle, α_r , is given from triangle O'D.

$$\begin{aligned} \alpha_r &= \sin^{-1} \left(\frac{\tan \theta_r \cdot \sin \gamma}{1/\cos \theta_r} \right) \\ &= \sin^{-1} (\sin \theta_r \cdot \sin \gamma) \end{aligned} \quad (5.2.3)$$



When the ray passes from glass to water it will be bent again, but it will still be in the same incident plane inclined at the same angle γ to the horizontal.

From (5.2.2 & 5.2.3) $\cos\theta = \cos\alpha_r \cdot \cos\alpha_r$ (5.2.4)

In particular for the exterior glazing and front transwall glass the refractive solar azimuth and altitudes are:

$$\alpha_{r1} = \tan^{-1} (\tan\theta_{ag} \cdot \cos\gamma)$$

$$\alpha_{r1} = \sin^{-1} (\sin\theta_{ag} \cdot \sin\gamma)$$

and for the water slabs

$$\alpha_{r2} = \tan^{-1} (\tan\theta_{gw} \cdot \cos\gamma)$$

$$\alpha_{r2} = \sin^{-1} (\sin\theta_{gw} \cdot \sin\gamma)$$

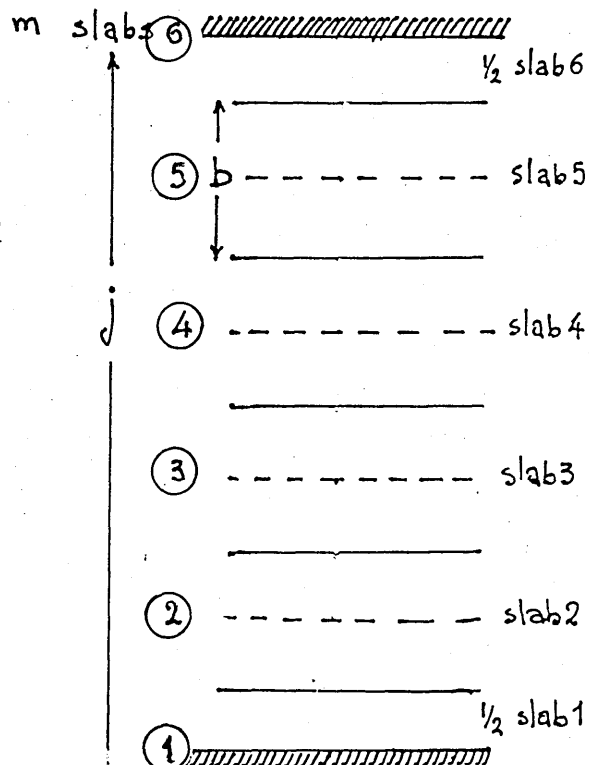
5.3 Slab Divisions

The overriding factor in the way slab volumes are chosen is that they are compatible with a finite difference analysis.

a) Vertical slabs (*)

Absorption variation in a vertical direction should not be too great and 5 slabs should usually suffice. A half slab top and bottom will be required for the finite difference solution so that a temperature node is at the centre of a slab.

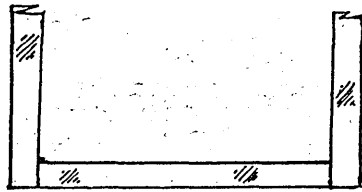
slab height: $b = \frac{1}{m}$



(*) 'Vertical slabs' are defined as the horizontal divisions in the vertical direction. The opposite will apply for the 'horizontal slabs'.

b) Horizontal slabs

There are substantial advantages to be gained in keeping the outer and inner half slabs homogeneous i.e. not mixing water and glass in the same slab. By so doing there are no internal reflections within the half slab, and the ultimate finite difference solution is far less cumbersome. Since the glass thickness will be 10 mm irrespective of the transwall width (6 mm would be too weak, 12 to 15 mm too expensive) then this requirement fixes the outer half slab width as 1 cm leading to 2 cm for an internal slab.

Thus, in any optimisation program the overall (nominal) width of the transwall should be in multiples of 2 cm.  ←Overall width→

The current transwall is 18 cm (nominal) overall giving 9 slabs (8 full slabs and 2 half slabs), and if a 12 cm width were chosen then 6 slabs is the most convenient value.

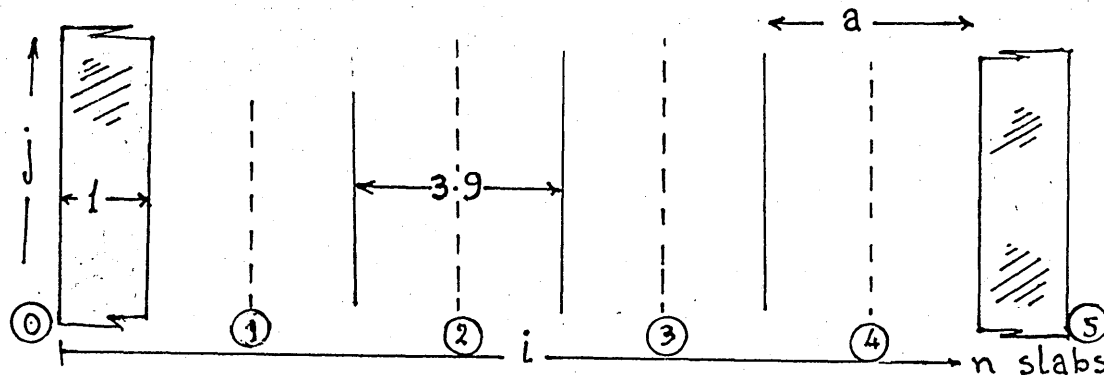
However, if for any reason it is desired to reduce the number of horizontal slabs for the current 18 cm transwall, say for speed of computation or insufficient computer memory, then two alternatives present themselves.

(i) If, say, five horizontal slabs are required, and if these are to be of equal width, then the half slabs at start and finish will be non-homogeneous and their absorption will have to be recalculated. This involves the addition of fairly complex extra terms and this choice should not be undertaken lightly. Appendix H, demonstrates this complication.

(ii) The easier alternative is to abandon a uniform slab width for glass and water. The first and last

slabs will now be part slabs, rather than half slabs, and the water thickness will be divided into equal slab widths. This approach will give accurate values for absorption though care will be required if this approach is to be incorporated into the (future) Finite Difference Effective Conductivity program.

e.g. for 4 water slabs $a = \frac{15.7}{4} = 3.93 \text{ cm}$



slab numbers 1 to 4 inclusive are water slabs only, 0 and 5 are glass only.

In the above i and j represent the individual slabs and n & m the total number of slabs in the horizontal and vertical directions respectively.

5.4 FACTORS AFFECTING THE ABSORPTION OF A TRANSWALL

It is necessary to analyse the following factors for the accurate prediction of the energy absorbed by the transwall under investigation.

5.4.1 Reverberations of Incident Radiation Between the Transwall and the Window.

The radiation striking the transwall will be increased by progressively decreasing multiple reflections between the glazing and the transwall. Since the planes of the window and transwall are parallel, then the incidence

angles, glazing and transwall, will be the same and consequently the reflectance, window and transwall, will be the same for beam radiation. Equally for an effective angle of incidence the reflectances, window and transwall, for diffuse radiation will be the same.

Let ρ_b and ρ_d be the reflectances of beam and diffuse radiation, respectively.

Radiation received by transwall reflected from window, R_f is:

$$\begin{aligned}
 R_f &= (I_b \sum \rho_b^2 + \rho_b^4 + \rho_b^6 + \dots) + \\
 &\quad (I_d \sum \rho_d^2 + \rho_d^4 + \rho_d^6 + \dots) \\
 &= \frac{I_b \rho_b^2}{1 - \rho_b^2} + \frac{I_d \rho_d^2}{1 - \rho_d^2}
 \end{aligned}$$

where I_b and I_d is the amount of radiation passing through the window.

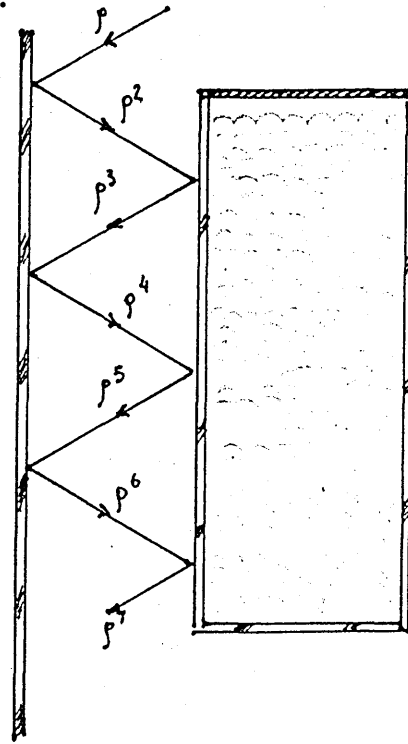


fig. 5.4.1

Thus it is only necessary to increase the beam and diffuse radiation striking the transwall glass by this amount. It is worth noting that beam radiation will still have directional properties. Since ρ rarely exceeds 10% the effect of these reflections is limited.

In addition to the reverberations of the incident radiation between the transwall and the window "backwards" radiation will also be involved i.e. radiation emerging from the transwall which originates from internal reflections within the transwall and from short wave radiation reflected from the room, see 5.11. These additional sources of radiation are reflections of reflections and can safely be ignored.

The idea of "backward" reverberations was used only for determining more accurately the absorptance of the window glass.. In this case the radiation received by glazing reflected from the transwall, R_b is:

$$R_b = \left\{ I_b \sum_{\infty} \rho_b + \rho_b^3 + \rho_b^5 + \dots \right\} + \left\{ I_d \sum_{\infty} \rho_d + \rho_d^3 + \rho_d^5 + \dots \right\}$$

$$= \frac{I_b \rho_b}{1 - \rho_b^2} + \frac{I_d \rho_d}{1 - \rho_d^2}$$

5.4.2 Number of Reflections

Ideally the two-dimensional approach should consider an infinite number of internal reflections. However, this would mean a large number of shade and acceptance factors for each volumetric slab of the transwall and a consequent massive expenditure in computing time.

The most cost effective solution is to consider only the stronger reflected rays. For a given strength of incident ray these will be from interfaces where the respective refractive indices have the greatest difference. The diagram in Appendix F shows the quantities of the reflected rays in a transwall module. In this analysis the following definition was applied for the number of rays considered, see figure 5.4.2.

"From every possible surface one reflection is allowed through the different media before leaving the system."

5.4.3 Shadow Factors, SF

Shadow factors are considered only for beam radiation and they follow the same pattern:

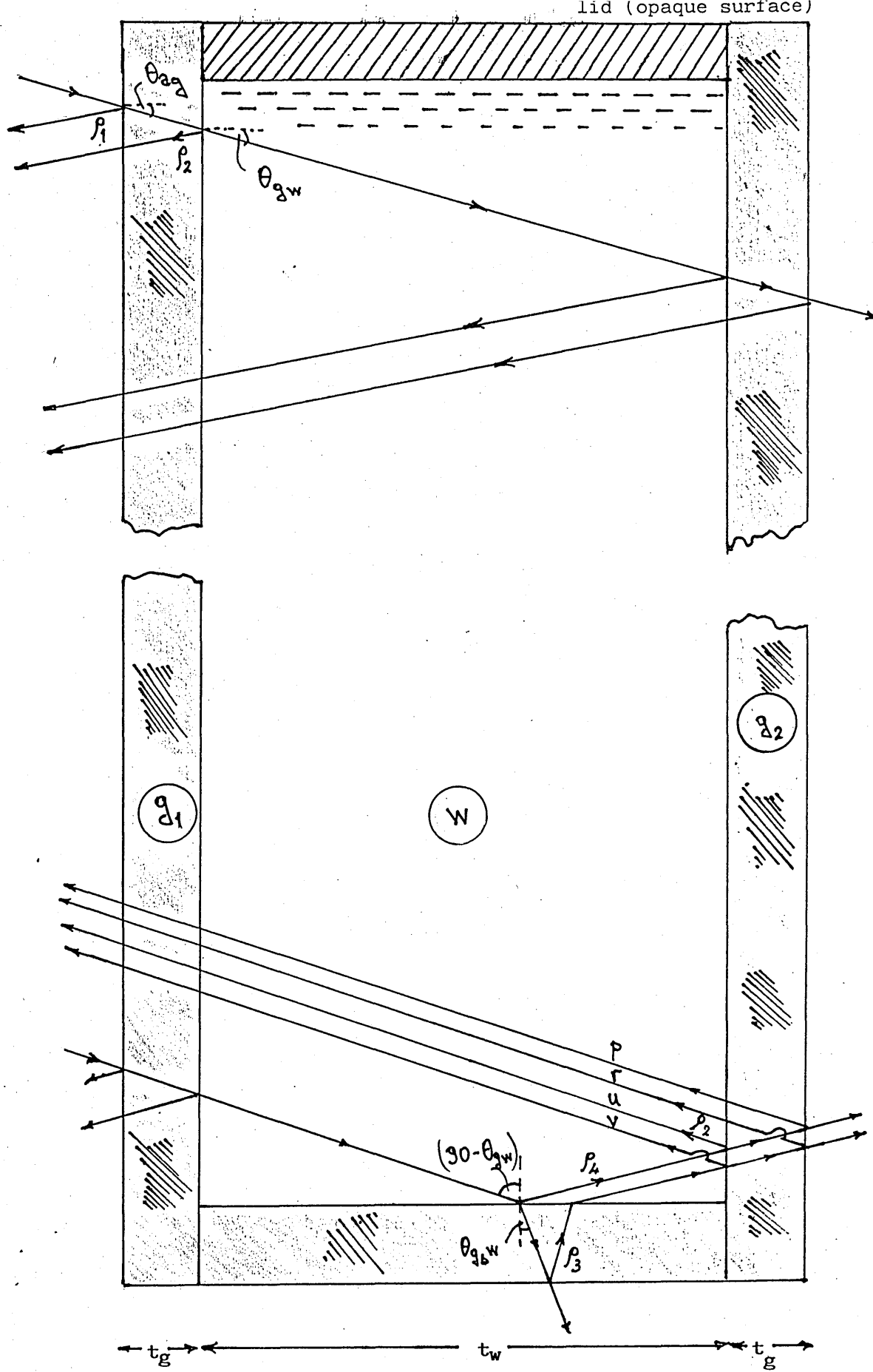


Figure 5.4.2

Section through a transwall with the type of reflected rays considered in the present analysis.

$SF(j) = 0$ if the slab does not receive any reflected radiation (slab is completely above the limiting ray).

$SF(j) = 1$ if all the slab receives reflected radiation (slab is completely below the limiting ray).

$SF(j) = 0 \rightarrow 1$ if part of the slab receives reflected radiation.

An example of how the shadow factors for rays c and d, figure 5.4.3 are determined follows:

Let the displacement of beam through the window glass be, DX.

$$\therefore DX = t_{gz} \cdot \frac{\tan \alpha_{r1}}{\cos \alpha_{r1}}$$

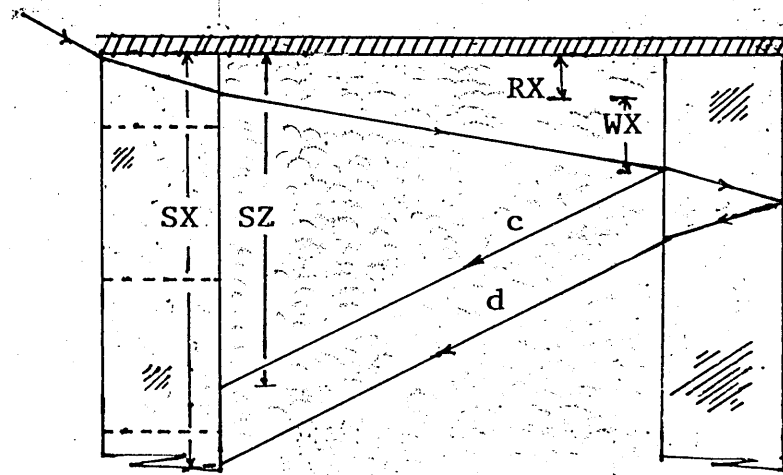


Figure 5.4.3

Multiplane

The displacement of ^{the} beam through the transwall glass, RX, and water, WX, are given by:

$$RX = t_g \frac{\tan \alpha_{r1}}{\cos \alpha_{r1}}, \quad WX = t_w \frac{\tan \alpha_{r2}}{\cos \alpha_{r2}}$$

α_{r1} , α_{r2} , a_{r1} , and a_{r2} are given in 5.2. Hence shadow factor for outer glass slab j, for ray c, is given as follows:

$$SZ = RX + 2 \cdot WX + DX \quad \text{and for ray d, } SX = 3 \cdot RX + 2 \cdot WX + DX$$

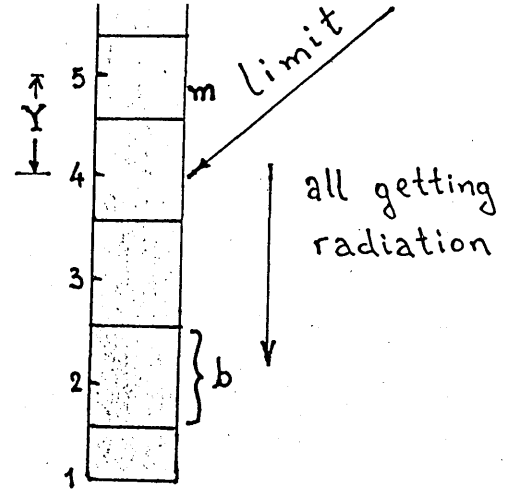
Let $Y_c = SZ - b/2$

and $Y = SX - b/2$

Slabs getting full reflected radiation } $= (m - 1) - \text{INT}(Y_c/b)$

Slabs number getting part radiation } $= m - \text{INT}(Y_c/b)$

Shadow factor of slab hit by boundary ray } $= \frac{b - (Y_c - \text{INT}(Y_c/b) \cdot b)}{b}$



Therefore

$$(SF_1)_c = 1 - Y_c/b + \text{INT}(Y_c/b)$$

similarly for ray d, i.e. $(SF_1)_d = 1 - Y_d/b + \text{INT}(Y_d/b)$

Similar treatments were adopted for the shadow factors concerning the absorption of various water slabs and the rear glass slabs, the former will be functions of both i and j i.e. $SF(i, j)$.

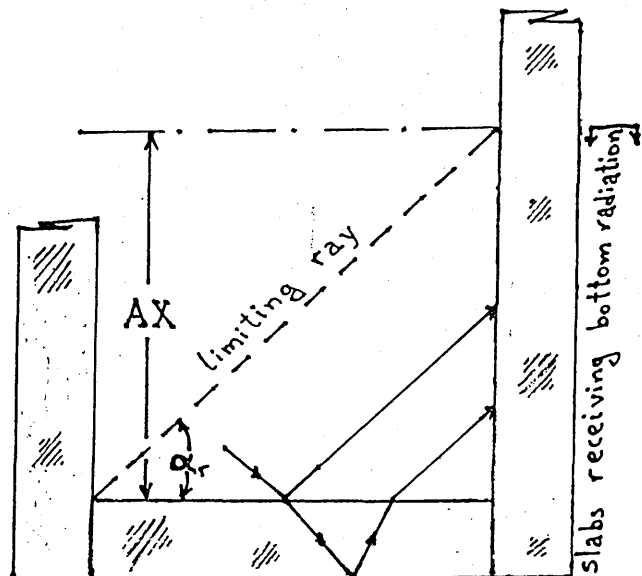
5.4.4 Acceptance Factors, AF

Some water and inner glass slabs will not receive reflected beam radiation. For example, consider the case of the inner transwall glass, figure 5.4.4.

If the limiting height for the inner glass to receive radiation reflected from base be AX , then

$$AX = t_w \frac{\tan \alpha_r}{\cos 2\alpha_r}$$

An acceptance factor is defined, $AF(j)$, so that for slabs completely above the limiting ray (height AX)



$AF(j) = 0$ (for slab numbers higher than 2),

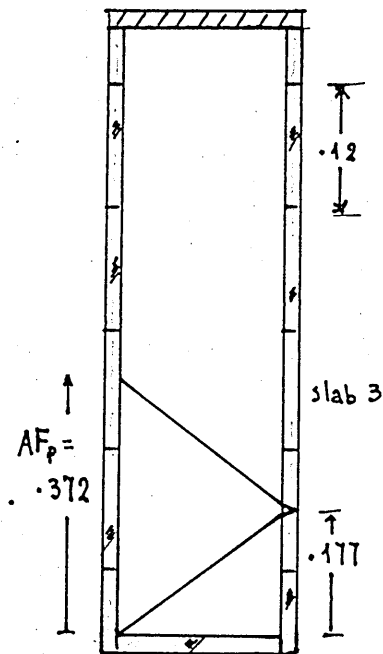
$AF(j) = 1$ for slabs completely below.

For the slab which intercepts the limiting ray

$$AF(J) = \frac{AX - \left\{ b/2 + b \cdot \text{INT} \left(\frac{AX - b/2}{b} \right) \right\}}{b}$$

It was found that the maximum height to which the limiting ray was reflected from the bottom and accepted by the rear glass is 0.177 m, (i.e. in the middle of slab 2).

Taking into the account the slight vertical displacement of this limiting ray through the rear glass and allowing it to be reflected from the rear glass-air interface and then to be "accepted" by front glass, the maximum height reached by this ray was found to be 0.372 m (i.e. slightly above the middle of slab 3).



Because rays, p,r,u,v, figure 5.4.2 are very weak the complication of individual acceptance factors is not justified by the accuracy of the whole analysis of the transwall system. The maximum acceptance factor, AF_p , was chosen to cover all four rays.

5.4.5 Reflection of Radiation in Bottom Glass

Irrespective of where a ray strikes the tank bottom the path lengths will be the same in water, see figure 5.4.5a

$$\begin{aligned} \text{Water transmission path} \quad a_1 + a_2 &= \frac{x}{\cos \alpha_{r2}} + \frac{\frac{t_w - D}{\cos \alpha_{r2}} - x}{\cos \alpha_{r2}} \\ &= \frac{t_w - D}{\cos \alpha_{r2} \cdot \cos \alpha_{r2}} = \frac{t_w - D}{\cos \theta_{gw}} = \text{constant} = L_{wb} \end{aligned}$$

Figure 5.4.5a

Section through an inclined to axes transwall.

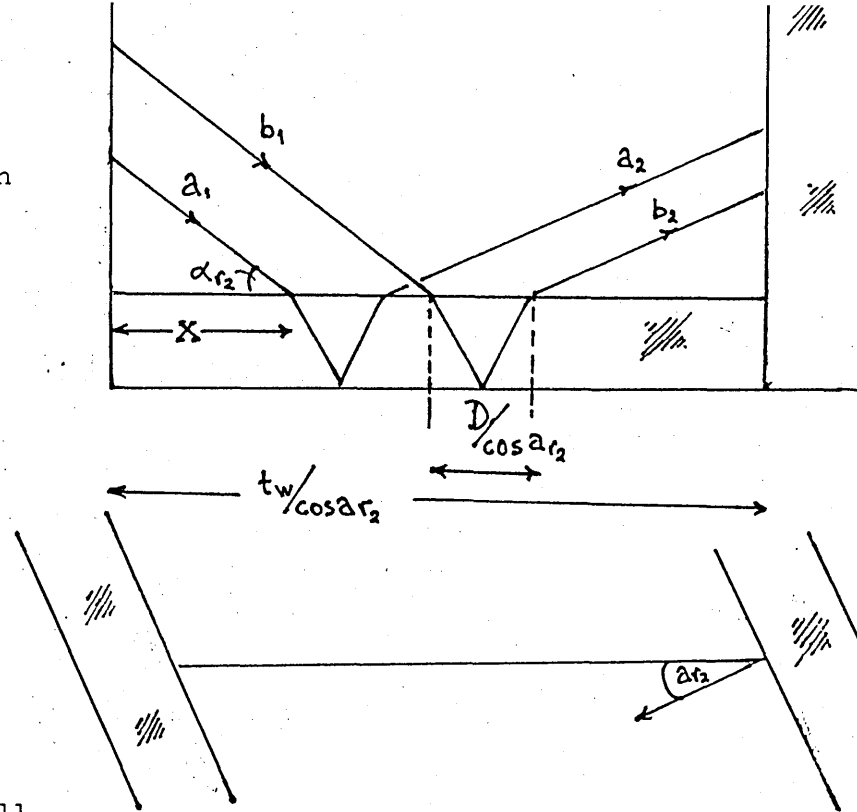


Figure 5.4.5b

Plane of a ray inclined to the axis of a transwall.

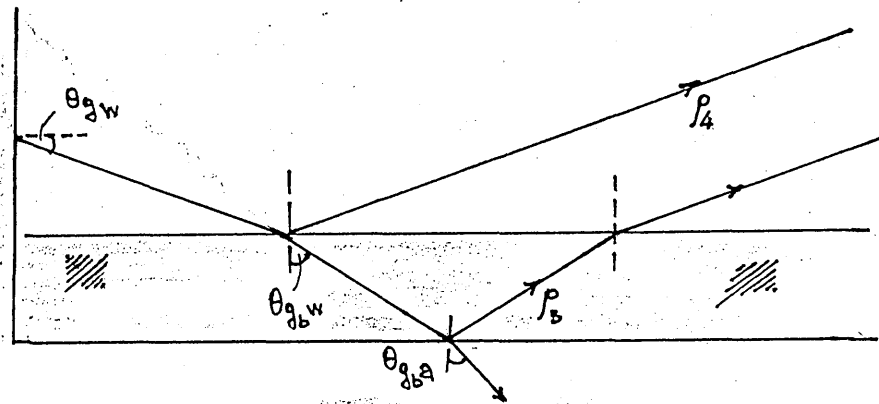
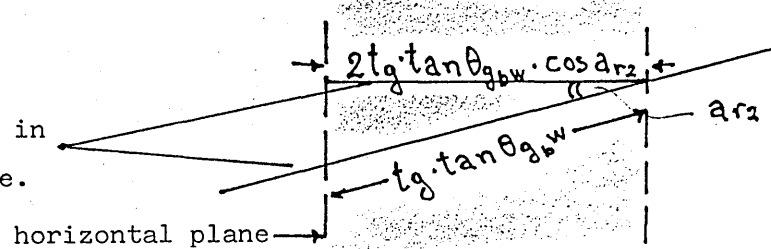


Figure 5.4.5c

Figure 5.4.5d

Both rays are in the same plane.



Let $\theta_{g_{bw}}$ and $\theta_{g_{ba}}$ be the refractive angles of bottom glass-water and air interface respectively, then from Snell's Law:

$$\begin{aligned}\theta_{g_{bw}} &= \sin^{-1} \left[\sin(90 - \theta_{gw}) \frac{n_w}{n_g} \right] \\ &= \sin^{-1} \left(\cos \theta_{gw} \frac{n_w}{n_g} \right)\end{aligned}$$

and

$$\theta_{g_b a} = \sin^{-1} \cdot (\cos \theta_{g_w} \cdot n_w)$$

The horizontal displacement D of the ray through the transwall bottom glass can be defined from

$$D = 2 \cdot t_g \cdot \cos \alpha_{r2} \cdot \tan \theta_{g_b w}$$

It was also found that for angles of incidence 61.3° ,

$$\rho_3 = 1.$$

5.5 BEAM RADIATION ABSORBED BY THE TRANSWALL

The necessary tools for the development of the absorptance equations of the individual layers of the transwall have been analysed. The absorptance equations follow.

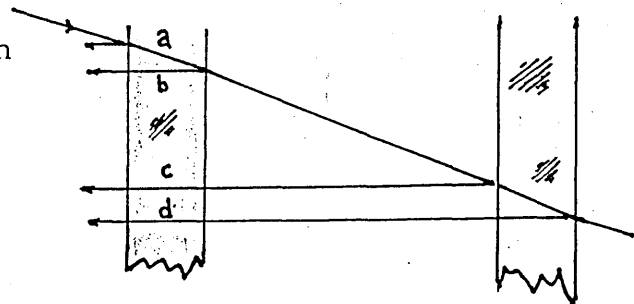
The beam radiation that enters the outer transwall glass is:

$$I_b = (I_b)_{g_2} \cdot \cos \theta \cdot (1 - \rho_i)$$

where $(I_b)_{g_2}$ is the radiation transmitted through the window glass after infinite internal reflections.

5.5.1 Beam Radiation Absorbed in Outer Transwall Glass, α_{g_1}

Considering the rays shown in figure 5.5.1



The perpendicular component of beam radiation absorbed in outer glass, $(\alpha_{g1})_1$, is

$$\begin{aligned}
 (\alpha_{g1})_1 = & \circ I_b (1 - \tau_{g1}) + \\
 & \circ I_b \cdot \tau_{g1} \rho_2 \cdot (1 - \tau_{g1}) + \\
 & \circ I_b (SF_1(j))_c \cdot \tau_{g1} (1 - \rho_2) \cdot \tau_w \rho_2 \cdot \tau_w \cdot (1 - \tau_{g1}) + \\
 & \circ I_b (SF_1(j))_d \cdot \tau_{g1} (1 - \rho_2) \cdot \tau_w (1 - \rho_2) \cdot \tau_{g2} \rho_1 \cdot \tau_{g2} \cdot \tau_w (1 - \tau_{g1})
 \end{aligned}$$

including the rays reflected by the bottom glass and rearranging

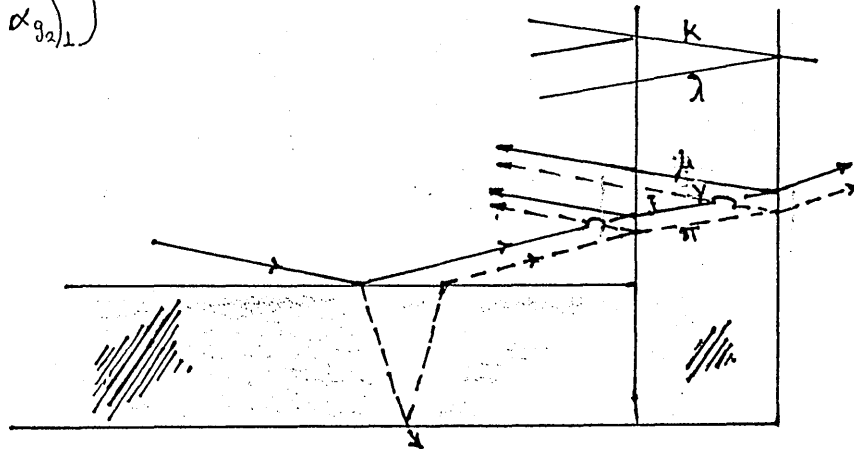
$$\begin{aligned}
 (\alpha_{g1})_1 = & \circ I_b (1 - \tau_{g1}) \cdot \left\{ 1 + \tau_{g1} \rho_2 + \tau_{g1} (1 - \rho_2) \cdot \tau_w \cdot \left\{ (SF_1(j))_c \cdot \rho_2 \cdot \tau_w + \right. \right. \\
 & (SF_2(j))_d \cdot (1 - \rho_2) \cdot \tau_w \cdot \tau_{g2}^2 \cdot \rho_1 + AF_2(j) \cdot \left[\rho_2 + \right. \\
 & \left. \left. (1 - \rho_2) \cdot \rho_1 \cdot \tau_{g2}^2 \right] \cdot \left[\tau_w \rho_4 + (1 - \rho_4) \cdot \tau_{wb} \cdot \tau_{g2}^2 \cdot \rho_3 \right] \right\} \left. \right\}
 \end{aligned}$$

where $(SF_1(j))_c$ and $(SF_2(j))_d$ are the shadow factors for the rays c and d, and $AF_2(j)$ is the acceptance factor of the outer glass for the bottom reflected rays.

5.5.2 Beam Radiation Absorbed in Inner Transwall Glass, α_{g2}

The perpendicular component of beam radiation absorbed in inner glass, $(\alpha_{g2})_1$ } = rays (k + l + m + n + o + p)

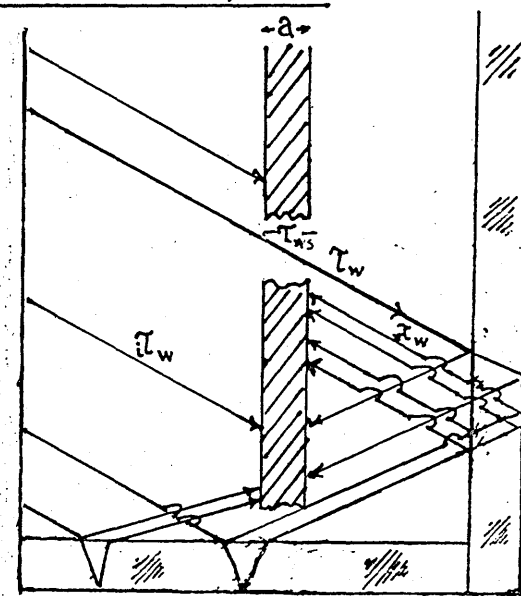
Fig. 5.5.2



$$\begin{aligned}
 (\alpha_{g2})_1 = & \circ I_b \cdot \tau_{g1} (1 - \rho_2)^2 (1 - \tau_{g2}) \cdot \left\{ SF_2(j) \cdot \tau_w + AF_1(j) \right. \\
 & \left. \left[\tau_w \rho_4 + \tau_{wb} \cdot (1 - \rho_4) \cdot \tau_{g2}^2 \cdot \rho_3 \right] \right\}
 \end{aligned}$$

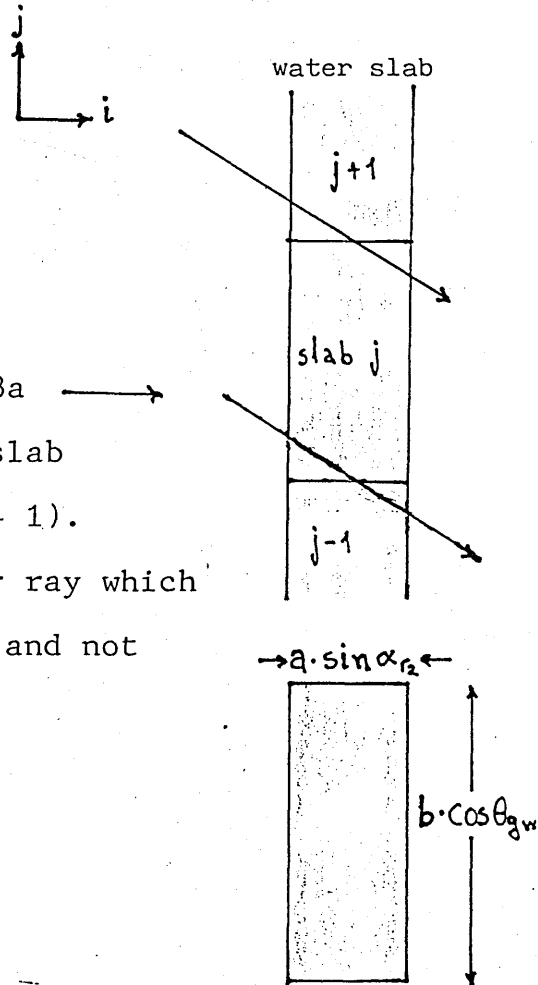
5.5.3 Beam Radiation Absorbed in Water Slabs, α_w

In general a water slab will absorb beam radiation directly, and from reflection off the bottom and the inner glass surfaces, as shown in figure 5.5.3.



a) Horizontal Slab Surfaces

It is assumed that radiation only enters the vertical walls of the slabs and not the horizontal surfaces. In fig.5.5.3a the upper ray will be counted to slab $(j + 1)$ and not part to j and $(j + 1)$. This will be balanced by the lower ray which will be credited solely to slab j and not partly to $(j-1)$.



b) Path Lengths

The following path lengths and hence the corresponding transmittances need to be defined:

Path length through water slab, $L_{ws} = \frac{a}{\cos \theta_{gw}}$

$$\text{Water path length of incident beam, } iL_w = \frac{a(i-1)}{\cos\theta_{gw}} .$$

$$\text{Water path length of reflected ray, } rL_w = \frac{a(n-i-1)}{\cos\theta_{gw}} .$$

$$\text{Water path length through base, } iL_{wb} = \frac{a(i-1)-D}{\cos\theta_{gw}} .$$

where a is the slab width and the corresponding transmittances are: τ_{ws} , τ_w , τ_w , τ_{wb} , ρ_{i-4} defined in figure 5.4.2. The beam radiation absorbed by a water slab is given by

$$\begin{aligned} (\alpha_w) = & I_b \cdot (1 - \tau_{ws}) \cdot \tau_{g1} (1 - \rho_2) \cdot \left\{ SF_3(i, j) \cdot \tau_w + \right. \\ & \tau_w \cdot \tau_w \left[SF_4(i, j) \cdot \rho_2 + SF_5(i, j) \cdot (1 - \rho_2) \cdot \tau_{g2}^2 \rho_1 \right] + \\ & AF(i, j) \cdot (\rho_4 \cdot \tau_w + (1 - \rho_4) \cdot \tau_{wb} \cdot \tau_{g3}^2 \rho_3) + \\ & \left. \tau_w \cdot AF'(i, j) \cdot (\rho_2 + \rho_1 \cdot (1 - \rho_2) \cdot \tau_{g2}^2) \cdot (\rho_4 \cdot \tau_w + \right. \\ & \left. (1 - \rho_4) \cdot \tau_{g3}^2 \rho_3 \cdot \tau_{wb}) \right\} \end{aligned}$$

5.6 DIFFUSE RADIATION ABSORBED BY THE TRANSWALL

A problem arises in summing diffuse radiation over the waveband intervals because reflected radiation is composed of part beam and part diffuse. This can be overcome by fixing a ratio between beam and diffuse radiation.

$$IR_\lambda = \frac{I_{mb} \cdot F_{b\lambda}}{I_{md} \cdot F_{d\lambda}}$$

where I_{mb} is the measured diffuse radiation

I_{md} is the measured beam radiation (m^2 normal)

$F_{b\lambda}$ is the fractional diffuse in waveband $\left(\sum_{\lambda} F_{d\lambda} = 1 \right)$

$F_{d\lambda}$ is the fractional beam radiation in waveband $\left(\sum_{\lambda} F_{b\lambda} = 1 \right)$

5.6.1 Effective Sky Dome Angle

The transwall will not see a complete quarter sphere of the sky dome because of the shading of the roof. The maximum effective sky dome angle χ measures 101° for the transwall under test. The effect on the view factor is

$$\frac{1 + \cos 101}{2} = 0.404$$

Fig. 5.10.1

instead of 0.5.

Assuming that the window is long in relation to length l_1 , the effective sky dome angle χ_1 for a slab on the outer transwall will be given by:

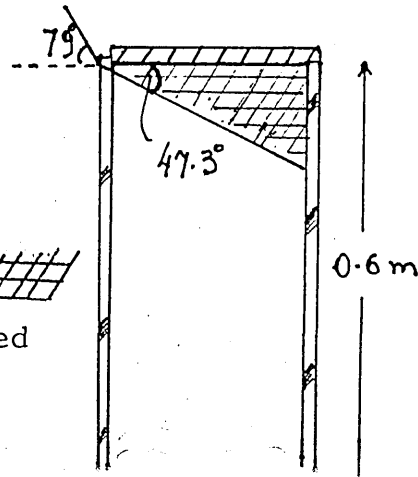
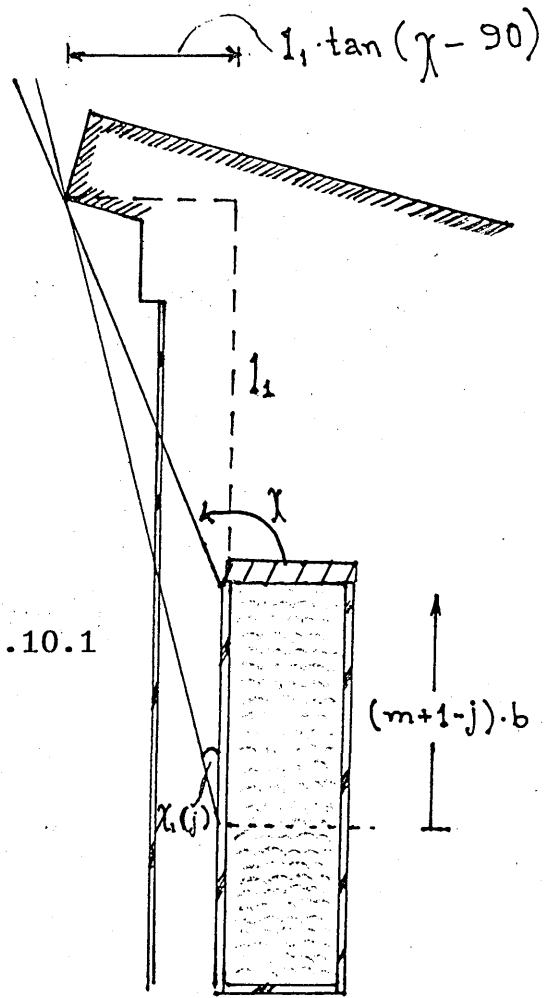
$$\chi_1(j) = \tan^{-1} \left\{ \frac{l_1 \tan(\chi - 90)}{[1 - DJ + b \cdot (m+1-j)]} \right\}$$

where DJ is analogous to DX, see 5.4.3 (the vertical displacement in window glass for an effective diffuse angle ψ)

From the above it is seen that the maximum angle of incidence in the vertical plane will be $(180-101) = 79^\circ$ due to the roof overhang and this will be refracted to give an effective sky angle χ_3 .

For $\theta = 79^\circ$ the corresponding refractive angle is 47.3° .

Thus only the cross hatched volume would have a substantially restricted view factor (i.e. relative to 101°)



Consider a ray from the element shown in figure 5.6.1b. The limiting ray will graze the roof corner and pass through the centre of the element. The following dimensions are known a, l_1, c, d , f has to be calculated.

From geometry:

$$v = 90 - w, \quad \alpha = 90 - y$$

$$\sin x = \frac{\cos v}{n_g}$$

$$\sin y = \frac{\cos v}{n_w}$$

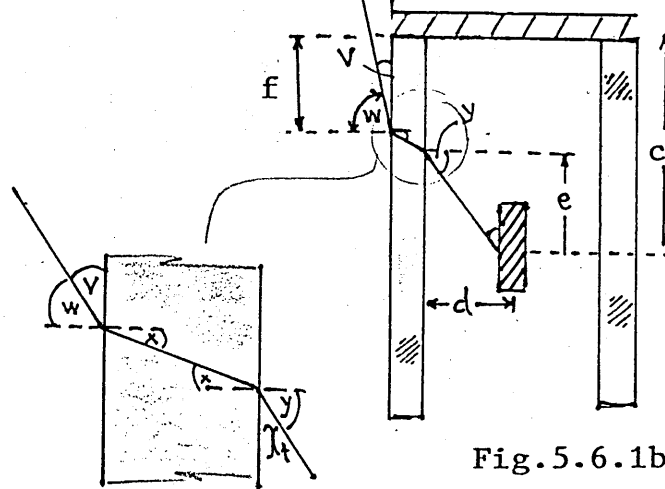


Fig.5.6.1b

$$\text{now } \tan v = \frac{a}{l_1 + f} = \frac{a}{l_1 + (c - t_g \cdot \tan x - d \cdot \tan y)} \quad (5.6.1a)$$

$$\tan v = \frac{a}{l_1 + c - t_g \cdot \tan \left[\sin^{-1} \left(\frac{\cos v}{n_g} \right) \right] - d \cdot \tan \left[\sin^{-1} \left(\frac{\cos v}{n_w} \right) \right]}$$

It is necessary now to solve for v so that the true sky angle $\chi_t, \chi_t = v + 90$ can be found.

The trial and error solution will be too time consuming for the program since it is required for each element, and so an approximate solution is necessary using a value of χ_2 defined by: (see fig. 5.6.1c)

$$= \tan^{-1} \left(\frac{a}{l_1 + c} \right) \quad (5.6.1b)$$

The other possibility would have been to use a more general approach to cover all three surfaces i.e. front and rear glass and water slabs, using an element in the middle of the transwall as shown in figure 5.6.1c.

In this case

$$\chi_a = \tan^{-1} (d/c) \quad (5.6.1c)$$

These approximations and their effects were investigated.

Using $a = 0.17$, $l_1 = 0.88$, $t_g = 0.01$ equations 5.6.1a,b&c were compared, for three different settings of c and d .

See table 5.6.1.

Fig. 5.6.1c

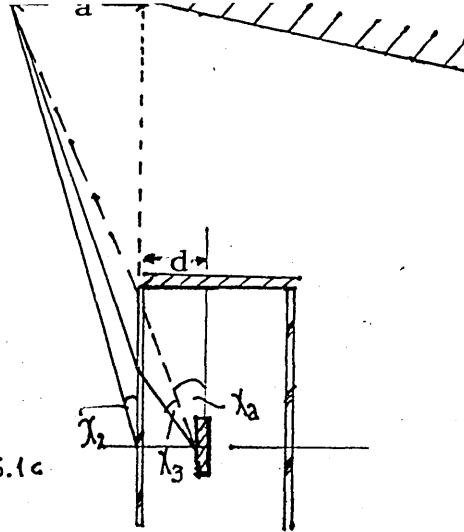


TABLE 5.6.1

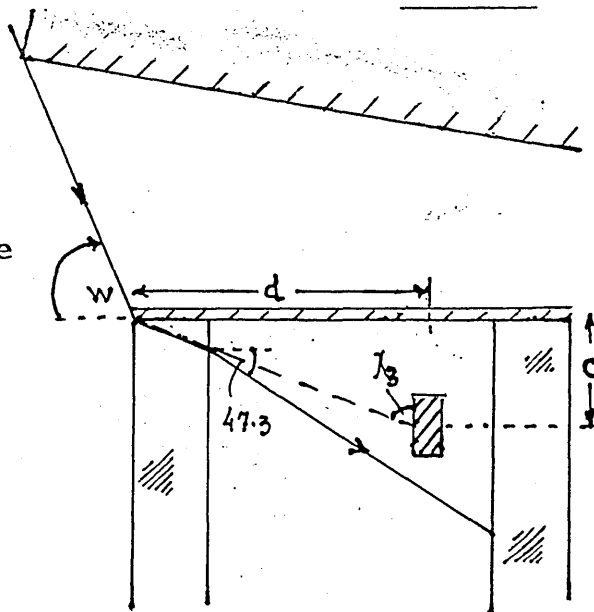
c	d	χ_t	χ_a	χ_2	$\frac{1+\cos\chi_t}{2}$	$\frac{1}{2}(1+\cos\chi_2)$	$\frac{1}{2}(1+\cos\chi_2)$	% diff. $\chi_t - \chi_a$	% diff. $\chi_t - \chi_2$
0.3	0.07	90+8.7	90+13.1	90+8.2	0.424	.387	.429	8.7	1.2
0.3	0.16	90+9.7	90+28.1	90+8.2	0.416	.264	.429	36.5	3.0
0.5	0.10	90+7.7	90+11.3	90+7.0	0.433	.402	.439	7.2	1.0

The table above suggests that the approximate angle, χ_a , is adequate for the front transwall glass and water slabs in the middle, but it does produce substantial error for the rear glass and water slabs (particularly those in the upper half of the transwall).

The first approximation of using simply $\chi_2 = \tan^{-1}\left(\frac{a}{1+c}\right)$ is reasonably accurate over the whole transwall outside of the hatched volume.

The problem of the hatched volume

The limiting ray has a refracted angle of 47.3° for the particular geometry of the transwall, and its position in the solar test cell.



The term $t_g \tan \cdot \left\{ \sin^{-1} \left(\frac{\cos v}{n_g} \right) \right\}$ is small in relation to the other terms in equation 5.6.1a and hence can be neglected (In fact it contributes less than 1% to the value of the angle v)

$$\text{Hence } (90 - \chi_3) = \tan^{-1} \left(\frac{c}{d} \right)$$

$$\sin w = n_w \sin(90 - \chi_3)$$

$$\text{sky dome angle } (v + 90) = (180 - w)$$

$$\chi_3 = 180 - \sin^{-1} \left[n_w \sin(\tan^{-1} c/d) \right]$$

this will apply to those slabs with their centres above the limiting angle of 47.3° .

5.6.2 Diffuse Radiation Absorbed in Outer Glass, α'_{g1}

For the rays shown in figure 5.5.1 the following equation was developed for diffuse radiation absorbed in the outer glass. All the symbols used below have the usual meanings and the dashed terms represent diffuse radiation.

$$\begin{aligned} \alpha'_{g1} = & \circ I_d \cdot (1 - \tau'_{g1}) \left\{ VF_1 \cdot \left\{ 1 + \tau'_{g1} \rho'_2 + \tau'_{g1} \cdot (1 - \rho'_2) \cdot \tau'_w \cdot \right. \right. \\ & \left. \left[\rho'_2 + (1 - \rho'_2) \cdot \tau'^2_{g2} \cdot \rho'_1 \right] \right\} + \tau'_{g1} \cdot (1 - \rho'_2) \cdot \tau'_w \cdot VF_{b1}(j) \cdot \\ & \left. \left(\rho'_2 + (1 - \rho'_2) \cdot \rho'_1 \cdot \tau'^2_{g2} \right) \left[\tau'_w \rho'_4 + (1 - \rho'_4) \tau'_{wb} \cdot \tau'^2_{g3} \cdot \rho'_3 \right] \right\} \end{aligned}$$

VF_1 , and VF_{b1} are the view factors for the outer glass and rear and front transwall glass respectively, see 5.6.3 and 5.6.4 and $\circ I_d$ is the diffuse radiation that enters the outer transwall glass.

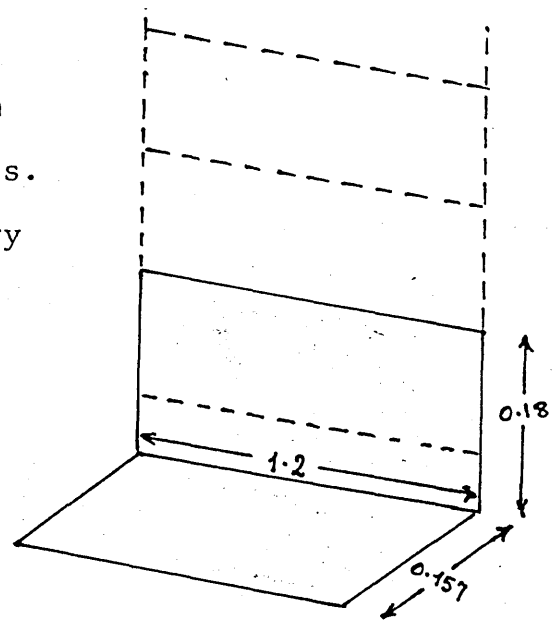
5.6.3. Diffuse Radiation Absorbed in Inner Glass, α_{g2}

View Factors

a) Normally for diffuse radiation reflected from ground onto a vertical wall, the ground is (relatively) infinite

and the view factor is 0.5.

In the case of the transwall bottom to back wall the view factor is less. It is necessary to make an arbitrary assumption to simplify calculation, that only the lower 2 slabs of the inner transwall glass receive reflected diffuse radiation off the base. This assumption is consistent with the acceptance factor used for beam radiation 5.4.4.



The values in figure 2.6.3a give a view factor $VF_b = 0.297$ from Ozişik (8).

b) The adoption of χ_2 means that one sky dome view factor, $\frac{1}{2}(1 + \cos \chi_2)$ will apply to all elements on one row, i.e. with a common value provided they are outside the hatched volume.

The view factor for the inner glass will be

$$VF_2(j) = 0.5 \left\{ 1 + \cos \left[\chi_2(j) + 90 \right] + (1 + IR_g) \cdot \rho_g \right\}$$

and $VF_{b2} = VF_1(j)$, and ρ_g is the ground reflectivity

$$\alpha'_{g_2} = I_d \cdot \tau'_{g_1} \cdot (1 - \rho'_2)^2 \cdot (1 - \tau'_{g_2}) \cdot (1 + \tau'_{g_2} \cdot \rho'_1) \left\{ \tau'_w \cdot VF_2(j) + VF_{b2}(j) \left[\rho'_4 \cdot \tau'_w + \tau'_{wb} \cdot (1 - \rho'_4) \cdot \rho'_3 \cdot \tau'^2_{g_b} \right] \right\}$$

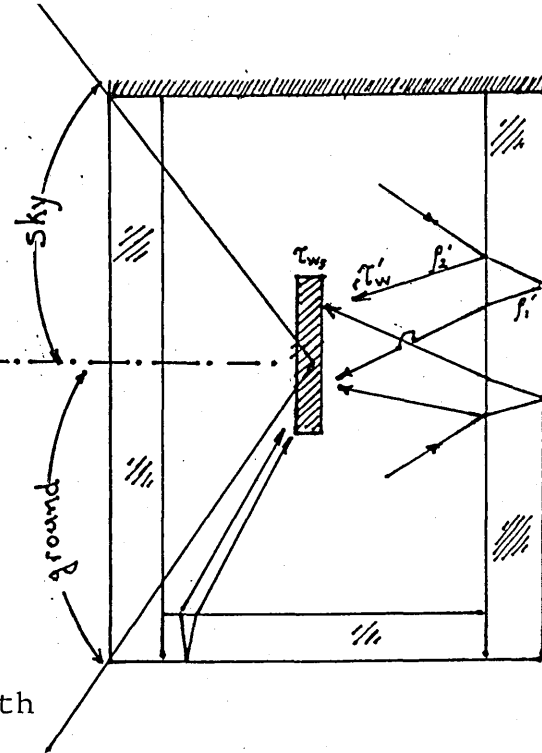
where $VF_{b2}(j) = 0.5 \left\{ 1 + \cos \left[\chi'(j) + 90 \right] \right\} \cdot VF_b$ & $\chi'(j) = \chi_1 \left[\text{INT} \left(\frac{j}{2} \right) \right]$

5.6.4 Diffuse Radiation Absorbed in Water Slabs, α'_w .

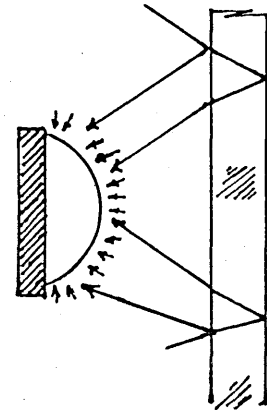
A view factor is used for diffuse radiation striking the "front" of the slab from the sky and from the ground.

The diffuse radiation reflected from the inner transwall

glass is an order of magnitude less than from the front and a simplifying assumption of unit view factor can be taken with distances calculated to the slab centre. If this assumption is not made then the accurate alternative is to integrate over the surface noting that both the water and glass path lengths vary and consequently the strength of the rays striking the slab will also vary. The computational complexity is considered unjustified for the small gain in accuracy.



The diffuse radiation from the sky (but not the ground) reflected off the bottom glass is assumed to be partially absorbed within the lower two water slabs to be consistent with the assumption of the inner glass.



The perpendicular component of diffuse radiation absorbed in water slab (i,j) is:

$$(\alpha_w^i) = {}_0I_d (1 - \tau_{wb}^i) \cdot \tau_{gi}^i \cdot (1 - \rho_2') \left\{ VF_w \cdot \left\{ \tau_w^i + \tau_w^i \cdot \tau_w^i (\rho_2' + (1 - \rho_2') \cdot \tau_{gi}^{i2} \cdot \rho_1') \right\} + VF_{bw} \cdot \left\{ \rho_4' \cdot \tau_w^i + (1 - \rho_4') \cdot \tau_{wb}^i \cdot \tau_{gb}^{i2} \cdot \rho_3' + \tau_w^i \cdot (\rho_2' + \rho_1' \cdot (1 - \rho_2') \cdot \tau_{gi}^{i2}) \cdot \left[\rho_4' \tau_w^i + (1 - \rho_4') \cdot \tau_{gb}^{i2} \cdot \rho_3' \tau_{wb}^i \right] \right\} \right\}$$

where VF_w and VF_{bw} are the view factors of slabs receiving sky and ^{ground} diffuse radiation, and only sky diffuse radiation respectively.

5.7 SINGLE WAVEBAND ANALYSIS

The aim of the analyses of the present chapter were to produce an analytical package for the transwall which would run on a micro. However, when it became clear that the capacity of most nominal 64k micros would be exceeded it was decided to modify the program to give a choice of a single waveband thus avoiding the 8 and 12 waveband cycles for each volume. Correlations relating average extinction coefficient values and path lengths had to be developed for both water and glass substances, see Appendix E.

The equations developed for the absorption of radiation by the various slabs were also modified in order to consider the passage of the rays through water as 'one'. This is demonstrated in the example below.

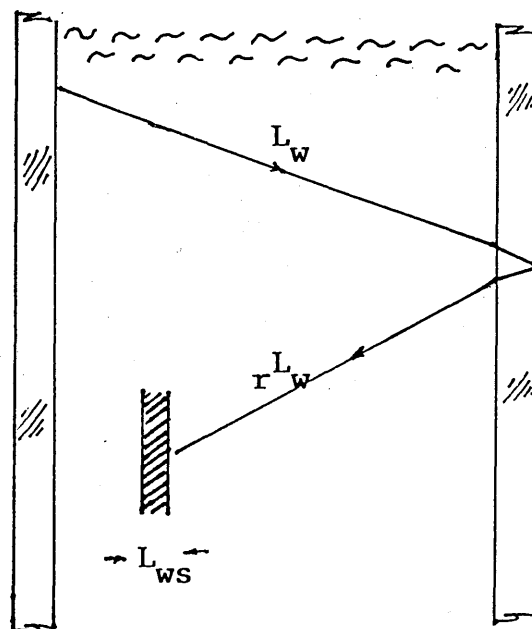
Consider the ray passage shown in figure 5.7.

Instead of considering three separate transmittances namely τ_{ws} , τ_w , τ_r , the ray through the water is considered as 'one'. In this case an overall path length is defined as:

$$L_r = L_w + rL_w + L_{ws}$$

hence

$$\tau_r = \exp(K_w \cdot L_r)$$



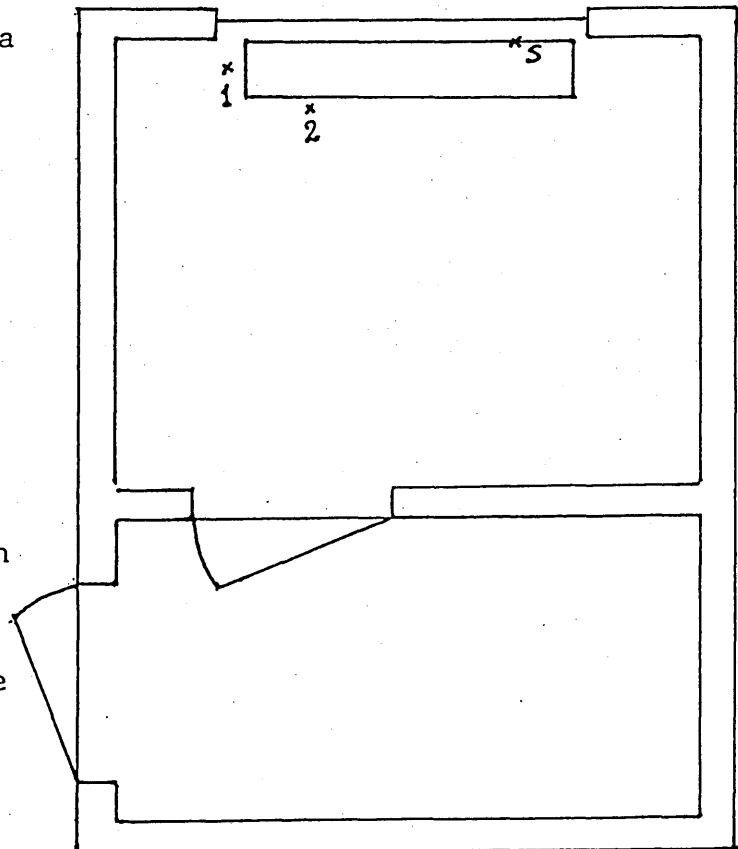
5.8 TREATMENT OF BACKWARDS RADIATION FROM ROOM

Allowing that the spectrum of room reflected radiation consists of short wavelengths then one solution is simply to treat the room reflected radiation as diffuse, and then add it to the diffuse radiation reflected from the inner transwall glass/air interface. This has the advantages of apparent simplicity and the fact that the energy distribution with wavelength will be much the same for both diffuse radiation fluxes.

The shortwave radiation reflected from the room falling on the rear transwall glass is likely to vary with the sun's position. Measurements were undertaken to quantify the dependance and the results were used to obtain a variable factor with which the back radiation should be multiplied.

5.8.1 Room Radiation Measurment

Data was obtained on a fairly sunny day. The radiation after passing through the glass was measured by one of the R.S.component silicon cells at position 1, see section 5.9. Another one of the triple silicon cell detectors was at position 2 to measure the back radiation from the room and the radiation



transmitted through the transwall. The radiation through the glass was checked against the vertical solarimeter, S, and good agreement was achieved.

It is reasonable to assume that, for a given position of the sun, the reflected radiation is a straight fraction of the energy entering the window less what is absorbed in the transwall and measurements of radiation were made to validate this assumption. The quantity ρ_r is defined as

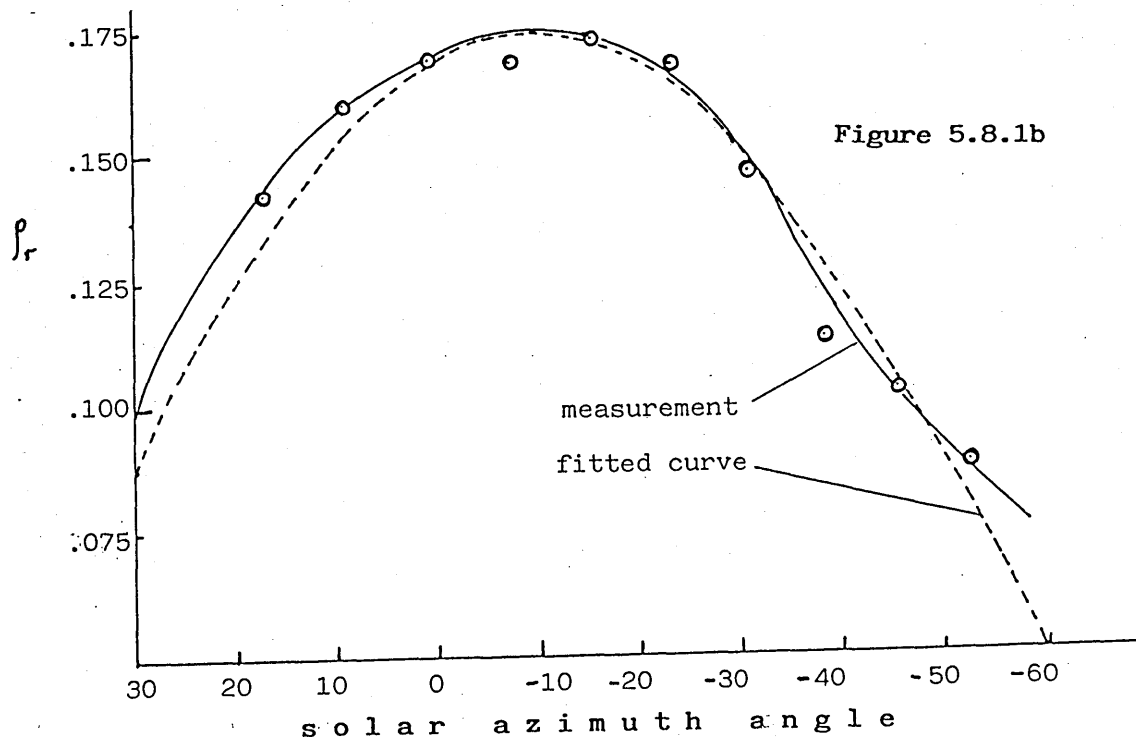
ρ_r = 'reflectance' of room obtained by measurement

$$\frac{\text{diffuse radiation falling on plane of room at rear transwall glass}}{\text{radiation entering room} - \text{radiation absorbed in transwall}}$$

ρ_r is shown plotted against the solar azimuth angle in figure 5.8.1b. Also shown is the fitted curve given by

$$\rho_r = 0.175 \cos[1.5(a + 10)]$$

where a is the solar azimuth (+am, -pm) in degrees.



This curve is asymmetric because of the asymmetric interior of the solar test cell and equipment.

Clearly in the computer program it is necessary to evaluate the denominator for the expression defining ρ_r , namely the radiation entering the room and the radiation absorbed in the transwall. The former is easily calculated but not an accurate value for the latter without a complete iteration. The room radiation, however, is small, circa 5% of the incident radiation on the front of the transwall and so an approximation is used in which the absorption is calculated as a single ray in a one dimensional system.

$$Q_A = A_{tw} \left\{ I_b \tau_{wgb} \cos \theta \cdot c_b \cdot (1 - \rho_1) + \frac{1}{2} \cdot I_d \cdot \tau_{wgd} (1 - \rho_1) \cdot c_d \right\}$$

where Q_A = radiation absorbed

A_{tw} = transwall area

I_b = beam radiation

I_d = diffuse radiation

τ_{wgb} = transmittance window glass beam/diffuse

τ_{wgd} = reflectance glass beam/diffuse

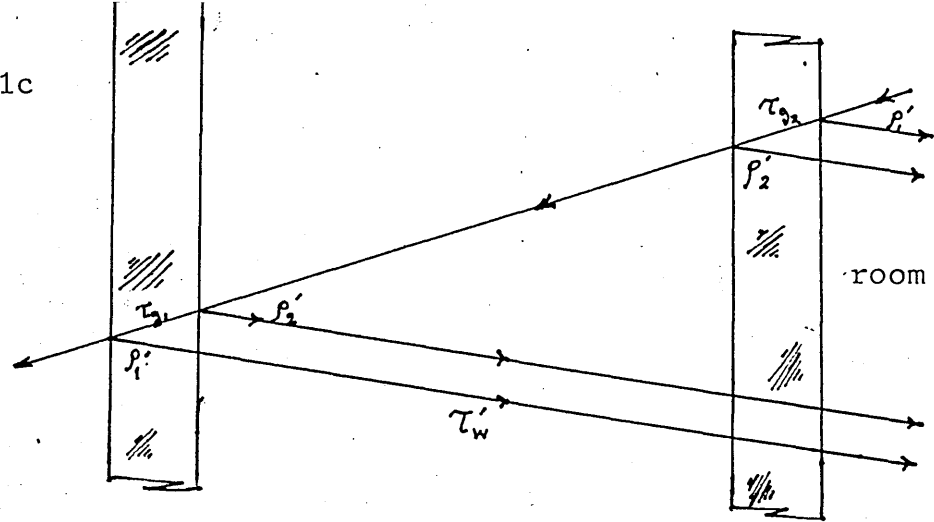
$$C_b = 1 - \exp \left\{ - (k_{g1} \cdot L_g + k_{g2} \cdot L_g + k_w \cdot L_w) \right\}$$

$$C_d = 1 - \exp \left\{ - (k_{g1} \cdot dL_g + k_{g2} \cdot dL_g + k_w \cdot dL_w) \right\}$$

When the room radiation is taken into account the following equations for room radiation absorption 5.8.1a-5.8.1b are added to equations, 5.6.2 - 5.6.5. In the analysis of the backward radiation from the room, the view factors are taken as unity and the reflections from the bottom glass are ignored since the extra complication is not justified by this second order effect. The rays considered are shown in figure 5.8.1c.

Figure 5.8.1c

Front Glass



$$(\alpha_{g1})_r = (1 - \tau'_g) \cdot \tau'_w \cdot \tau'_{g2} (1 - \rho'_1) \cdot (1 - \rho'_2)^2 \cdot (1 + \tau'_{g1} \rho'_1) \cdot \rho_r \cdot I_r$$

Rear Glass

$$(\alpha_{g2})_r = (1 - \tau'_{g2}) \cdot (1 - \rho'_1) \cdot \left\{ 1 + \tau'_{g2} \left[\rho'_2 + (1 - \rho'_2) \tau'^2_w \rho'_2 + \tau'^2_w \cdot (1 - \rho'_2)^2 \cdot \tau'_{g1} \cdot \rho'_1 \right] \right\} \cdot \rho_r \cdot I_r$$

Water Slabs

$$(\alpha_w)_r = (1 - \rho'_1) (1 - \rho'_2) \tau'_{g2} \cdot \left[\tau'_w - \tau'_k + \rho'_2 \cdot (\tau'_m - \tau'_1) + (1 - \rho'_2) \tau'^2_{g1} \cdot \rho'^2_1 \cdot (\tau'_m - \tau'_1) \right] \cdot \rho_r \cdot I_r$$

where

$$\begin{aligned} \tau'_k &= \exp \left\{ -k_w \left[l_w + (n - i) \right] / \cos \theta_{gw} \right\} \\ \tau'_1 &= \exp \left\{ -k_w (l_w + ia) / \cos \theta_{gw} \right\} \\ \tau'_m &= \exp \left\{ -k_w \left[l_w + (i - 1) \cdot a \right] / \cos \theta_{gw} \right\} \end{aligned}$$

are the different transmittances considered and I_r is defined as:

I_r = radiation entering room - radiation absorbed in transwall

The computer program for the absorption of radiation was validated by measuring the ratio of the normal incident radiation on the transwall to the normal radiation transmitted. These measurements were undertaken with R.S. component silicon cells (ref. no. 307-137) which had been calibrated against the Kipp and Zonen solarimeters. The calibration was carried out with 0.22Ω resistors connected across the silicon cells and the output, the voltage across the resistors, recorded as mV on the Orion logger. The calibration constant was linear up to an angle of incidence of 45° and thereafter a cosine correction is normally applied up to the limiting angle of 75° incidence. The silicon cells form part of 2 matched radiation detectors. Each has three cells permanently fixed to 3 faces of a 4 cm cube mounted on a levelling stand.

One cell was located parallel to the window and the other immediately behind the transwall opposite the centre of slab 3 in a 5 vertical slab division. The external beam and diffuse radiation were recorded from the global and shade ring Kipp and Zonen (CM5) solarimeters. The radiation striking the transwall was measured by another Kipp and Zonen (CM3) solarimeter orientated vertically and used as a check on the silicon cell by the window. The transwall was filled with distilled water. The measured transmittance is taken as the ratio of the radiation incident on the cell behind the transwall to the radiation incident on the cell immediately behind the window.

The program was run using 6 wavebands from $0.35\mu\text{m}$ to $1.1\mu\text{m}$. Longer wavelengths were discarded because the silicon cell has a cut off at $1.1\mu\text{m}$.

over a range of solar angles and it is concluded that the program has been validated.

TABLE 5.9

time from solar noon (min)	altitude °	azimuth °	incidence °	beam (Wm^{-2})	diffuse (Wm^{-2})	percentage transmittance program	percentage transmittance measured
+63	23.6	17.0	28.8	789	91	52.9	52.6
+ 3	24.9	0.8	24.9	822	74	53.5	53.8
57	23.8	15.4	28.1	820	59	53.6	54.6
117	20.5	31.0	36.6	788	55	52.9	53.6
177	15.3	45.6	47.5	671	48	51.4	51.9

5.10

MODEL SIMULATION RESULTS

The analyses and equations developed in this chapter and used to construct a computing program, now validated, was run to investigate the parameters governing the absorption of radiation in a transwall. The time taken per run is about 25 minutes on a Commodore 64 micro.

The RAM was found to be inadequate for the size and complications of the calculations. This was the reason for reducing the number of horizontal water slabs from 9, as it was originally suggested, to 5 using an 8 waveband spectrum. When the 12 waveband spectrum was employed a further reduction to 3 horizontal water slabs was necessary. Therefore, it is strongly recommended that the future running of this program is done on a larger capacity micro especially when it is going to be a subroutine of the finite difference method for predicting the temperature distribution within the system. Another, probably better, alternative is to convert it to a Fortran to run on the mainframe computer.

The computing program was run to investigate the following:

- a) the total radiation absorbed in water varying the number of water slabs
- b) accounting for the backward radiation coming from the interior of the test cell
- c) the effect of having two different spectra for beam and diffuse radiation
- d) the effect of replacing the rear transwall glass with an Antisun glass
- e) the enhancement of absorption using a dye such as Lissamine red
- f) the effect of different air masses for the absorption of beam radiation in the transwall
- g) the effect of different clearness indices for the absorption of diffuse radiation in the transwall
- h) the effect of wavelength dependant refractive indices for water and glass
- i) the effect of using 12, 8, and single wavebands

The following input conditions were used:

$I_{m(diffuse)} = 208.1 \text{ W m}^{-2}$ $I_{m(global)} = 519.8 \text{ W m}^{-2}$ $\gamma = 62^\circ$
day no. = 69 time = 12 noon

The absorptions quoted are in Watts/metre length/module.

- a) First of all the effect of the number of horizontal water slabs was investigated for the above input conditions for 8 wavebands, 5 vertical slabs, diffuse radiation having the same spectrum as beam, and no room radiation.

Table 5.10a shows this effect for varying the number of water slabs from 1 to 5.

TABLE 10a

The No. of water (horizontal) slabs	Total radiation absorbed in water (in Watts)
1	68.710
2	68.601
3	68.585
4	68.584
5	68.609

Therefore if just the radiation absorbed in the transwall water slabs is needed, say for a lumped system approach, then one water slab can be safely used saving a lot of computing time.

b) The computing program provides us with a choice to take into account the backward radiation coming from the interior of the test cell. As explained in 5.7 for simplicity this is only going to alter the diffuse radiation absorbed by the transwall volumes. The above mentioned input conditions were used with the only change that room radiation is included. The results are summarized in table 5.10b.

TABLE 5.10b

		RR	NR	Percentage increase in	
		Diffuse radiation absorbed (in Watts)		Diffuse	Total
front glass		21.02	19.35	8.0	2.1
water slab no.	1	15.60	15.47	0.8	0.2
	2	1.36	1.22	10.0	2.9
	3	1.04	0.89	14.2	4.8
	4	1.03	0.83	19.0	6.8
	5	2.94	0.76	74.1	46.7
rear glass		10.70	6.56	38.7	13.4

RR = account is taken for the 'room radiation'

NR = no room radiation

These results are by no means absolute because the percentage increase depends on the amount of radiation falling on the transwall and on the number of rays considered for the backward radiation.

The method adopted here for including the backward radiation falling on a transwall, shows that it is essential that it be taken into account for the accurate determination of the radiation absorbed by the rear glass and last water slab.

c) The program was run to determine the effect on the absorption of the various transwall slabs of having two different spectra for beam and diffuse radiation. The spectrum of diffuse radiation used was for a clearness index greater than 0.7 (i.e. very clear skies), for 8 wavebands ref.(3).

TABLE 5.10c

		Diffuse radiation absorbed (in Watts)		% change in	
		one spectrum	two spectra	D i f f u s e	T o t a l *
front glass		21.02	18.25	15.2	3.6
water slabs	1	15.60	8.75	78.2	13.9
	2	1.36	1.01	34.1	7.9
	3	1.04	0.84	24.1	7.0
	4	1.03	0.89	15.2	5.0
	5	2.94	5.45	46.0	34.9
rear glass		10.70	14.31	25.3	10.4

* Total radiation is beam plus diffuse radiation.

From the above table it can be seen that even for clear skies, where the diffuse radiation spectrum differs less when it is compared with the direct radiation spectrum, there is a considerable change in the amount of radiation absorbed by a transwall.

d & e) As it was mentioned in Chapters 1 and 3 there are several ways of enhancing the absorptance of a transwall. Table 10d,e below shows the various absorptances for 3 cases: A is an ordinary transwall, B it uses Antisun glass for its rear transwall glass and C 20 ppm of Lissamine red 3GX dye is mixed with water.

TABLE 5.10d,e

T o t a l R a d i a t i o n A b s o r b e d (in Watts)			
	A(ordinary)	B(Antisun)	C(dye)
front glass	76.87	74.51	75.46
water slab no.	1	49.22	49.04
	2	4.39	4.19
	3	2.88	2.67
	4	2.71	2.43
	5	7.18	3.94
	66.38		62.26
			87.35
			31.48
			22.58
			17.69
			19.09
			178.18
rear glass	34.59	140.20	23.33

From the above it can be seen that when Antisun glass replaces the rear ordinary transwall glass there is an increase of 75.3 % in the absorption of the rear glass and a decrease of 6.6 % in radiation absorbed by water, but when 20 ppm of Lissamine red dye is used there is an increase of 65 % in water and a decrease of 48.2 % in rear glass absorption.

The slight reduction of the radiation absorbed in the front glass and water slabs for the Antisun case, is because in the above calculations the radiation coming from the room was considered, thus when Antisun glass forms the rear transwall glass it allows less radiation through the transwall hence the above reduction.

f) The effect of choosing different spectra for beam radiation for three different air masses was investigated. Table 5.10f below^{shows} the absorption of radiation in the transwall for air masses 1,2, and 4, for 8 wavebands while the angle of incidence was kept constant at 30°. For the location of the test cell in Glasgow it was found that the smallest possible zenith angle is 32.4°, occurring on June 22nd at 12hr 19sec local time, giving a minimum air mass of 1.18.

TABLE 5.10f

Air mass		1	2	4
Surface		B e a m R a d i a t i o n A b s o r b e d		
front glass		57.12	58.62	61.03
water slab no.	1	39.72	40.47	45.47
	2	3.17	3.37	3.56
	3	1.89	2.04	2.18
	4	1.67	1.81	1.94
	5	1.60	1.73	1.84
rear glass		20.04	20.28	19.68

It can be seen from table 5.10f that the radiation absorbed by the transwall when spectra corresponding to air masses 1 and 4 are used and compared with air mass 2 spectrum the percentage difference is not great. As it was stated earlier, 5.2.8, for most engineering calculations the air mass 2 spectrum can be safely employed.

g) The effect on the absorption of diffuse radiation of the transwall by increasing the number of wavebands

from 8 to 12 was investigated. Also the effect on the absorption using different clearness indices for the diffuse radiation was investigated for 3 water slabs.

TABLE 5.10g

Surface	Percentage difference in diffuse relative to 12 wavebands	Number of wavebands				
		12	8	8	8	8
		Clearness index				
		$k_T > .7$ $.5 < k_T < .7$ $.25 < k_T < .5$ $k_T < .25$				
Glazing	+9.3	5.80	6.34	5.96	5.82	5.82
Front glass	-3.1	19.83	19.21	19.00	19.69	20.08
Slab 1	water	+26.8	5.08	6.44	11.48	13.23
Slab 2		-6.4	1.72	1.61	1.48	1.55
Slab 3		-2.9	4.81	4.67	4.58	4.00
Rear glass	+10.6	18.49	16.52	12.42	11.61	11.23

The best agreement in absorption between the 12 waveband diffuse spectrum and the 8 wavebands spectra for different clearness indices from table 5.10g was the one corresponding to $k_T > .7$. That was expected since the 12 waveband spectrum it is for cloudless atmosphere, see chapter 2.

h) The effect of wavelength dependant refractive indices for water and glass on the absorption of the transwall was investigated. The refractive indices were split into 8 and 12 wavebands. Hardly any difference ($\sim 1\%$) in the results was observed. Therefore the extra complication and computing running time was not justified with the slight improved accuracy achieved by splitting the refractive indices into wavebands.

i) Finally the effect of increasing the number of wavebands from 1 to 8 and then to 12 was investigated. The results for beam and total radiation absorbed by the transwall for the three above mentioned cases are shown in table 5.10i. The percentage difference in the absorption by increasing the number of wavebands from 8 to 12 is also shown.

TABLE 5.10i

waveband no.	Beam radiation absorbed			Total radiation absorbed		
	12	8	%	12	8	%
surface						
glazing	14.45	13.19	- 8.7	20.25	19.58	-3.3
front glass	62.42	58.86	- 7.2	83.25	78.06	- 6.2
slab 1	22.77	26.67	+17.1	27.85	33.93	+18.9
slab 2	4.00	3.80	- 5.0	5.72	5.41	- 5.4
slab 3	3.44	3.23	+ 6.1	8.26	7.90	- 4.3
rear glass	24.89	25.88	+4.0	42.39	43.39	+2.3

TABLE 5.10i

waveband no.	Beam radiation absorbed			Total radiation absorbed		
	8	single	%	8	single	%
s u r f a c e						
glazing	13.19	14.44	+8.6	19.56	20.63	+5.5
front glass	58.62	76.02	+29.7	76.87	103.32	+34.4
slab 1	40.47	43.48	+7.4	49.23	62.39	+26.7
slab 2	3.37	4.43	+31.4	4.39	6.98	+59.0
slab 3	2.04	2.81	-	2.88	4.61	+60.1
slab 4	1.82	2.08	+14.3	2.71	3.63	+33.9
slab 5	1.73	1.66	- 4.0	7.18	5.48	-23.7
rear glass	20.28	30.37	-	34.59	45.14	+30.5

From tables 5.10i it can be seen that increasing the number of water slabs the absorption in water falls.

The single waveband analysis overpredicts the amount of radiation absorbed by the transwall with worse agreement in diffuse radiation absorbed. These results suggest that the single waveband analysis is incapable of giving accurate absorption values without undue complexity, and the *raison d'être* for the single waveband is the avoidance of complexity.

Chapter 6

CONCLUSIONS AND FUTURE WORK

Achievements

The following are the major achievements described in this thesis.

- 1) The transwall system has been reviewed and its advantages and design criteria given.
- 2) A 'Glasgow atmosphere' has been developed which, for the usual test conditions of clear skies, gives the irradiance levels in the various wavebands for varying air masses.
- 3) The absorption/extinction coefficients for various dyes and transwall materials have been measured.
- 4) The accuracy of the lumped system approach has been investigated and its application critically examined. It is concluded that it can predict the temperature rise with an error of about 20%[†] for a glass transwall, and with an error probably substantially lower for the plastic film transwall.
- 5) A computing program for the two-dimensional absorption of radiation in the transwall has been written and validated. This is the first major step in a programme to analyse the performance of a transwall using the finite difference method believed necessary as a result of the analysis using the lumped system.

Future Work

In order to calculate the absorption of radiation in the transwall, whether by the lumped system or by finite differences, it is necessary to know the various absorption coefficients of the absorbing media as a function[†] subject to the assumptions made

of wavelength or, in practice, of wavebands. Unless new dyes are used the absorption coefficients already measured should suffice. Probably Lissamine Red 3GX will be used as the 'test' dye.

The accurate determination of the irradiance levels associated with each waveband is a crucial factor in the absorption of energy in the transwall. The fractional irradiance in each waveband, in this thesis, is tied only to clear sky radiation, since it was thought to be the logical start into the problems of the solar energy on partly cloudy and cloudy skies. Although only one class of sky conditions for the fractional energy is presented in Appendix I, the whole concept is much more complicated than that and a proper investigation might become necessary. The depletion of the direct beam by the clouds depends on the type of clouds, their thickness, and the number of layers.

There are a number of authors among them Liu and Jordan (55), Hollands (56), Carroll (57), Collares-Pereira and Rabl (58) who have developed models and correlations for the theoretical determination of direct, diffuse and directional intensity of diffuse radiation, using sunshine and total cloud cover data. A more powerful model suggested in future work should require data on the type and optical properties of clouds, cloud amount, thickness, position, and the number of layers for the appropriate location.

The experimental work requires improvements. The radiation reflected about the test cell needs to be quantified better and a system to log the output from six silicon cells has already been installed, see

photograph 3 . The fitting of the experimental data collected from measurements of the temperature of an even larger number of points inside the transwall module of the test cell would allow the calculation of the effective conductivity for this particular transwall module. The single values for the four different test cell conditions of the heat transfer coefficients, see Appendix C, are too uncertain for accurate work. The variable nature of the heat transfer suggests, that 'heat transfer meters' should be used and logged. What sort, or design, of meter is unclear at present but an instrument might be developed in which the temperature change of a small disc heated under computer control could be related to the heat transfer coefficients. In evaluating heat transfer coefficients it would be useful to have knowledge of the air velocities in the vicinity of the transwall module and this could be achieved by modified vane type anemometers reading down to 0.05 m/s. These velocities could be used in a heat loss correlation obtained by allowing the transwall to cool and calculating the energy released. The insulation around the 'non operational' surfaces of the module has already been improved, see photograph I.1 in Introduction.

The lumped system approach could usefully be tested with the plastic membrane type transwall. This would not suffer from raised glass temperatures and is probably accurate enough, certainly for a glasshouse application where the temperature ratio K is more likely to be close to unity. Another approach to treating a glass transwall would be to produce a correlation which would link the elevated glass temperature to the glass properties,

dimensions, external heat transfer, and ultimately to the lumped water temperature. Alternatively a method might be to create three 'lumps' rather than one in order to vary the temperatures of the glasses and the water. However, this would require knowledge of the heat transfer between the glasses and the water which, in effect, is a return to the problems of quantifying the effective conductivity.

A computing program to evaluate the temperature distribution and circulation patterns within, and the heat transfer without, the transwall, should be constructed and then be incorporated with the current two dimensional program. The construction and linking should be straightforward with only one major problem: to quantify an effective conductivity in two -dimensions. Correlations do exist for the effective conductivity of a fluid flow between hot and cold vertical infinite plate.

Kutaleladze (59) suggests the following correlation for the effective conductivity, K_e , of the above case.

$$K_e = 0.18 K_w (N_{Gr_L} \cdot N_{Pr})^{\frac{1}{4}}$$

where

$$N_{Gr} = \frac{g \cdot \beta \cdot L^3 \cdot \Delta T}{\nu^2} \quad N_{Pr} = \frac{\mu \cdot C_p}{K_w}$$

K_w = water
conductivity

which for water around 20 - 35°C reduces to

$$K_e = 67.0 \cdot K_w \cdot L^{\frac{3}{4}} \cdot \Delta T^{\frac{1}{4}}$$

where L is the gap between the plates and ΔT is the temperature difference between the plates.

From the above description it can be seen that the fluid flow between the hot and cold plates is not truly the transwall situation and it has been found that Kutaleladze's

correlation gives temperature profiles somewhat steeper than experiment. This correlation could be the broad basis for another applicable to a closed cell. Some preliminary work has been done on a heat transfer rig to develop such a correlation. A less satisfactory, and time consuming, alternative is to write the program first, then develop a correlation to fit the measured temperature distribution in transwalls of varying aspect ratio. Again some preliminary work has been done, but it is unable as yet to mimic the curious 'winged' temperature profile which exists in practice. In searching for an effective conductivity correlation some knowledge of the flow patterns in the transwall would be most useful. Unfortunately velocities are very low, a few mm per minute, and in the full size modules are liable to disperse so that the accurate tracing of a point, or dye front, is very difficult. Furthermore, unless care is taken in the choice of a dye the absorption of radiation can distort the results. The use of neutral buoyant particles is, in some ways, a better solution but the density of the water changes as it heats and thus would lead to a short time shot only.

In the longer term after the transwall performance is modelled, then the 'pay off' can begin when the model is incorporated into a sophisticated building services modelling program. The considerable potential of the transwall, in all its variation, can then be promoted.

Appendices

SOLAR GEOMETRY AND TIME

The geometric aspects that influence the solar energy incident on a collecting surface are considered. Trigonometric equations of solar geometry and time are presented.

A.1. Sun-Earth Distance r

The earth revolves around the sun in an elliptical orbit with the sun at one of the foci. Fig. A.1.

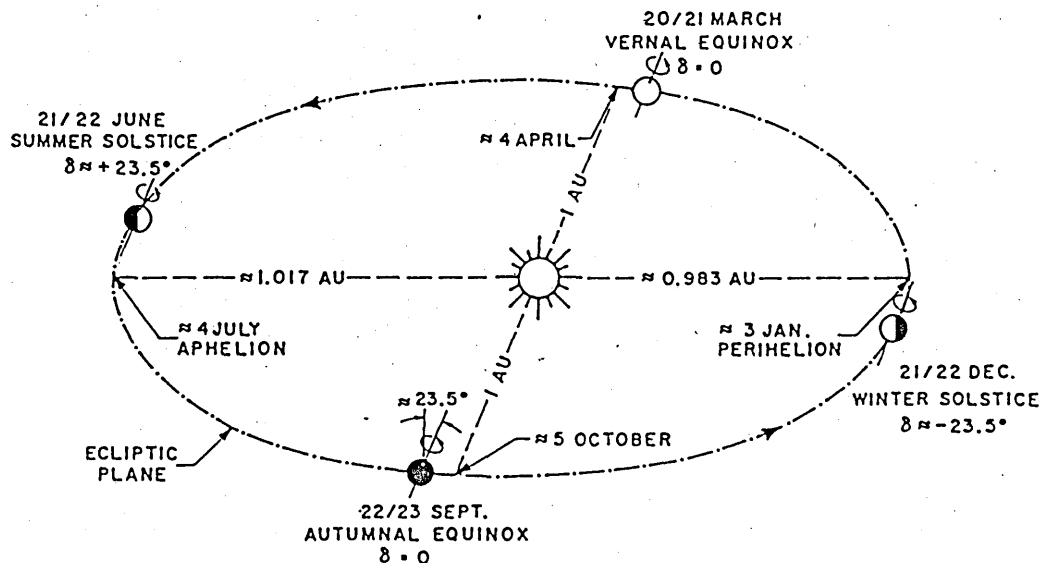


Figure A.1 Motion of the earth around the sun.

A.2. Variation of Extraterrestrial Radiation

Variation of the earth sun distance however, does lead to variation of extraterrestrial radiation flux, in the range of $\pm 3.5\%$ and occasionally greater changes occur as when a large sunspot crosses the solar disc. See figure A.2.

The dependence of extraterrestrial radiation on time of the year is indicated by:

$$I_{0n} = I_{sc} E_o \quad (I_{sc} = 1367 \text{ Wm}^{-2}) \quad (A.2)$$

The amount of solar radiation reaching the earth is inversely proportional to the square of its distance from the sun; an accurate value of the sun-earth distance is, therefore, important. The mean sun-earth distance r_o is called one astronomical unit.

$$1 \text{ A U.} = 1.496 \times 10^{11} \text{ m}$$

Spencer(2) developed the following expression for the eccentricity correction factor of the earth's orbit, E_o .

$$E_o = (r_o / r)^2 = 1.000110 + 0.034221 \cos I + 0.001280 \sin I + 0.000719 \cos 2I + 0.000077 \sin 2I \quad (A.2a)^*$$

Γ , is called the day angle in radians. It is represented by:

$$\Gamma = 2\pi(d_n - 1)/365 \quad (\text{A.2b})$$

where d_n is the day number of the year, ranging from 1 on 1 January to 365 on 31 December.

A.3. Solar Declination, δ

Solar declination is the angular position of the sun at the noon with respect to the plane of the equator. It is zero at the vernal and autumnal equinoxes (literally equal nights) and has a value of $+23.45^\circ$ at the summer solstice and -23.45° at the winter solstice, see figure A.1. δ can be +ve or -ve in the N or S hemisphere. Spencer(2) presented the following expression for δ in degrees:

$$\delta = (0.006918 - 0.399912\cos\Gamma + 0.070257\sin\Gamma - 0.006758\cos 2\Gamma + 0.000907\sin 2\Gamma - 0.002697\cos 3\Gamma + 0.00148\sin 3\Gamma) \cdot (180/\pi) \quad (\text{A.3})^*$$

Error is $1^\circ 42'$ max compared to Cooper's equation.

A.4. Solar Time Equation of Time, E_t

All angles are based on solar time, with solar noon as the time the sun crosses the meridian of the observer. Solar time generally does not coincide with local time. The two main reasons for this variance are:

- (1) the earth sweeps out unequal areas on the ecliptic plane as it revolves around the sun, and
- (2) the earth's axis is tilted with respect to the ecliptic plane.

The correction is called the equation of time and again from Spencer (2), the following series gives the equation of time (in minutes).

$$E_t = (0.000075 + 0.001868\cos\Gamma - 0.032077\sin\Gamma - 0.014615\cos 2\Gamma - 0.04089\sin 2\Gamma) \cdot (229.18) \quad (\text{A.4a})^*$$

Solar time = G.M.T. + E_t

$$T_s = \text{local standard time} + 4 \cdot (L_s - L_e) + E_t \quad (\text{A.4b})$$

where L_s is the standard meridian of the local time zone, and

L_e is the longitude of the location in question in degrees West.

A.5 Position of the Sun Relative to Inclined Surfaces

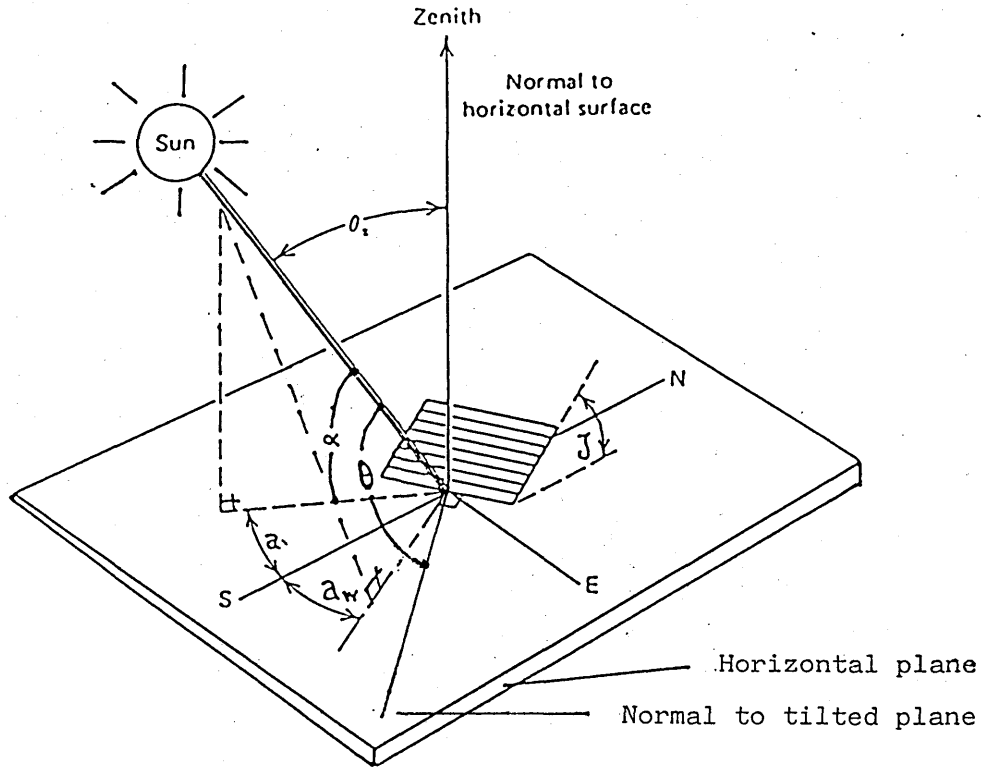


Figure A5 Position of Sun Relative to an Inclined Plane

The incidence angle, θ , is defined as the angle between the normal to a surface and a line collinear with the sun's rays.

For a surface tilted at an angle γ to the horizontal and having azimuth angle a_w , figure A5, the angle of incidence is given by:

$$\begin{aligned} \cos\theta = & (\sin\phi \cdot \cos\gamma - \cos\phi \cdot \sin\gamma \cos a_w) \cdot \sin\delta \\ & + (\cos\phi \cdot \cos\gamma + \sin\phi \cdot \sin\gamma \cos a_w) \cos\delta \cdot \cos w \\ & + \cos\delta \cdot \sin\gamma \cdot \sin a_w \sin w \end{aligned} \quad (\text{A5.a})$$

where ϕ is the geographic latitude, in degrees, north positive and w is the hour angle, noon zero and morning positive.

a) Horizontal Surfaces

i.e. $\gamma = 0^\circ$, then equation (A.5a) becomes:

$$\cos\theta = \sin\phi \cdot \sin\delta + \cos\phi \cdot \cos\delta \cdot \cos\omega \quad (\text{A.5b})$$

Equation A.5b can be solved for the sunrise hour angle ω_s . At sunrise, $\theta = 90^\circ$, therefore equation A.5b results in:

$$\cos\omega_s = -\sin\phi \cdot \sin\delta / \cos\phi \cdot \cos\delta$$

$$\text{or} \quad \omega_s = \cos^{-1}(-\tan\phi \cdot \tan\delta) \quad (\text{A.5c})$$

And also the azimuth angle of the sun at sunrise is

$$\gamma_s = \cos^{-1}(-\sin\delta / \cos\phi) \quad (\text{A.5c'})$$

b) Vertical Surfaces

i.e. $\beta = 90^\circ$ then equation (A.5a) becomes:

$$\cos\theta = -\cos\phi \cdot \cos\alpha_w \sin\delta + \sin\phi \cdot \cos\alpha_w \cos\delta \cdot \cos\omega + \cos\delta \cdot \sin\alpha_w \sin\omega$$

(A.5d)

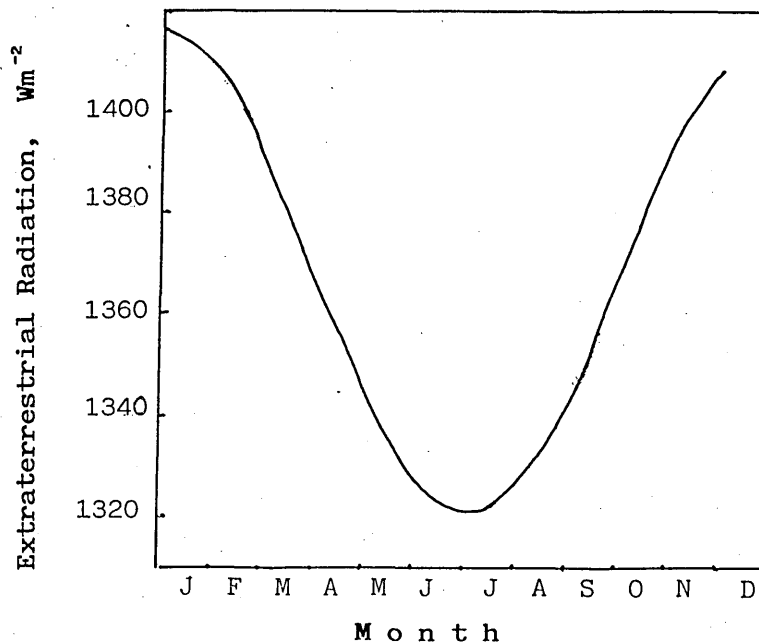


Figure A.2. The variation of extraterrestrial solar radiation with the time of the year.

(*) Spencer's equations (A.2a, A.3, A.4a) were chosen for greater accuracy since all calculations were done by computer. Simpler expressions do exist (see Duffie and Beckman (4)).

SOLAR RADIATION TABLES

The solar constant and its spectrum are defined as in table B.1,(6).

From this table (4th column) it can be easily verified that 99% of solar energy is in the wavelength range $0.25 - 4.0 \mu\text{m}$. At the end of the same column, the irradiance totals 1367 Wm^{-2} , and this is the currently accepted value of the solar constant i.e. $I_{sc} = 1367 \text{ Wm}^{-2}$ (6).

The solar constant is the total energy of all wavelength received from the sun on unit area exposed normally to the sun's rays in unit time at the mean sun-earth distance in the absence of the earth's atmosphere.

The spectral distribution of solar radiation received at the surface of the earth, is subject to wide variation because of the following factors:

1. Variations in the sun itself.
2. Variations in the sun-earth distance.
3. Differences in atmospheric scattering
 - a) by air molecules, b) by water vapour, c) by aerosols.
4. Differences in atmospheric absorption by O_2 , O_3 , H_2O , CO_2 .

The results of a typical clear sky atmosphere, for the latitude of Glasgow, at air mass 2, are presented in table B.5.

The attenuation coefficients of uniformly ^{mixed} gases, water vapour and ozone are presented in tables B.2, B.3 and B.4 respectively. They are all from Leckner(21).

The ozone coefficients are listed for wavelengths longer than $0.29 \mu\text{m}$ because practically all radiation at shorter wavelengths is absorbed by the ozone layer.

Virtually all radiation is absorbed at $> 4.0 \mu\text{m}$. Furthermore, only 1% of extraterrestrial solar irradiance is contained in wavelengths greater than $4.0 \mu\text{m}$; consequently, these tables are limited to this wavelength.

(#) A separate computing program was written to summarize the solar irradiance in the wavelength range $0-\lambda$ (Fig. B5, columns 3,5,7). The program is a special form of Simpson's rule and since the function of the curve is not known the inputs were values of the function (i.e. the solar spectral irradiance of specified intervals (wavelengths)).

EXTRATERRESTRIAL SOLAR SPECTRAL IRRADIANCE AT MEAN SUN EARTH DISTANCE

λ	$I_{0\lambda}$	$\Sigma I_{0\lambda}$	$P_{0-\lambda}$	λ	$I_{0\lambda}$	$\Sigma I_{0\lambda}$	$P_{0-\lambda}$	λ	$I_{0\lambda}$	$\Sigma I_{0\lambda}$	$P_{0-\lambda}$	λ	$I_{0\lambda}$	$\Sigma I_{0\lambda}$	$P_{0-\lambda}$
0.250	64.56	2.51	0.18	0.475	2016.25	247.45	18.10	0.790	1142.50	756.23	55.32	1.900	136.01	1273.42	93.16
0.255	122.50	2.84	0.21	0.480	2055.00	257.62	18.85	0.800	1144.70	767.69	56.16	1.950	126.00	1280.08	93.64
0.260	91.25	3.47	0.25	0.485	1901.26	267.64	19.58	0.810	1113.00	779.02	56.99	2.000	118.50	1286.30	94.10
0.265	253.75	4.29	0.31	0.490	1920.00	276.98	20.26	0.820	1070.00	789.93	57.79	2.100	93.00	1296.72	94.86
0.270	275.00	5.70	0.42	0.495	1965.00	286.59	20.97	0.830	1041.00	800.50	58.56	2.200	74.75	1305.00	95.47
0.275	212.50	6.87	0.50	0.500	1862.52	296.37	21.68	0.840	1019.99	810.77	59.31	2.300	63.25	1312.05	95.98
0.280	162.50	7.86	0.57	0.505	1943.75	305.80	22.37	0.850	994.00	820.96	60.06	2.400	56.50	1317.96	96.41
0.285	286.25	9.12	0.67	0.510	1952.50	315.50	23.08	0.860	1002.00	830.85	60.78	2.500	48.25	1323.16	96.80
0.290	535.00	10.97	0.80	0.515	1835.01	325.05	23.78	0.870	972.00	840.61	61.49	2.600	42.00	1327.66	97.12
0.295	560.00	13.91	1.02	0.520	1802.49	333.79	24.42	0.880	966.00	850.39	62.21	2.700	36.50	1331.57	97.41
0.300	527.50	16.54	1.21	0.525	1894.99	343.33	25.12	0.890	945.00	859.94	62.91	2.800	32.00	1334.98	97.66
0.305	557.50	19.26	1.41	0.530	1947.49	352.67	25.80	0.900	913.00	869.26	63.59	2.900	28.00	1337.97	97.88
0.310	602.51	22.13	1.62	0.535	1926.24	362.34	26.51	0.910	876.00	878.16	64.24	3.000	24.75	1340.60	98.07
0.315	705.00	25.51	1.87	0.540	1857.50	371.87	27.20	0.920	841.00	886.81	64.87	3.100	21.75	1342.99	98.24
0.320	747.50	29.09	2.13	0.545	1895.01	381.22	27.89	0.930	830.00	895.10	65.48	3.200	19.75	1344.99	98.39
0.325	782.50	32.70	2.39	0.550	1902.50	390.72	28.58	0.940	801.00	903.27	66.08	3.300	17.25	1346.84	98.53
0.330	997.50	37.51	2.74	0.555	1885.00	400.17	29.27	0.950	778.00	911.18	66.66	3.400	15.75	1348.48	98.65
0.335	906.25	42.34	3.10	0.560	1840.02	409.42	29.95	0.960	771.00	918.90	67.22	3.500	14.00	1349.96	98.76
0.340	960.00	46.79	3.42	0.565	1850.00	418.71	30.63	0.970	764.00	926.58	67.78	3.600	12.75	1351.30	98.85
0.345	877.50	51.45	3.76	0.570	1817.50	427.94	31.31	0.980	769.00	934.21	68.34	3.700	11.50	1352.51	98.94
0.350	955.00	55.89	4.09	0.575	1848.76	437.11	31.98	0.990	762.00	941.88	68.90	3.800	10.50	1353.60	99.02
0.355	1044.99	61.08	4.47	0.580	1840.00	446.22	32.64	1.000	743.99	949.41	69.45	3.900	9.50	1354.59	99.09
0.360	940.00	65.72	4.81	0.585	1817.50	455.44	33.32	1.050	665.98	984.76	72.04	4.000	8.50	1355.49	99.16
0.365	1125.01	71.01	5.20	0.590	1742.49	464.21	33.96	1.100	606.04	1016.27	74.35	4.100	7.75	1356.31	99.22
0.370	1165.00	76.92	5.63	0.595	1785.00	473.16	34.61	1.150	551.04	1045.16	76.46	4.200	7.00	1357.05	99.27
0.375	1081.25	82.15	6.01	0.600	1720.00	481.98	35.26	1.200	497.99	1071.43	78.38	4.300	6.50	1357.72	99.32
0.380	1210.00	88.32	6.46	0.605	1751.25	490.71	35.90	1.250	469.99	1095.66	80.15	4.400	6.00	1358.33	99.37
0.385	931.25	93.11	6.81	0.610	1715.00	499.35	36.53	1.300	436.99	1117.96	81.78	4.500	5.50	1358.89	99.41
0.390	1200.00	98.30	7.19	0.620	1715.00	516.51	37.79	1.350	389.03	1138.51	83.29	4.600	5.00	1359.40	99.45
0.395	1033.74	103.61	7.58	0.630	1637.50	533.22	39.01	1.400	354.03	1156.97	84.64	4.700	4.50	1359.86	99.48
0.400	1702.49	109.81	8.03	0.640	1622.50	549.73	40.22	1.450	318.99	1173.91	85.88	4.800	4.00	1360.29	99.51
0.405	1643.75	118.40	8.66	0.650	1597.50	565.79	41.39	1.500	296.99	1189.28	87.00	4.900	3.75	1360.69	99.54
0.410	1710.00	126.68	9.27	0.660	1555.00	581.10	42.51	1.550	273.99	1203.52	88.04	5.000	3.47	1361.04	99.57
0.415	1747.50	135.37	9.90	0.670	1505.00	596.65	43.65	1.600	247.02	1216.48	88.99	6.000	1.75	1363.50	99.75
0.420	1747.50	143.98	10.53	0.680	1472.50	611.50	44.73	1.650	234.02	1228.52	89.87	7.000	0.95	1364.79	99.84
0.425	1692.51	152.69	11.17	0.690	1415.02	625.86	45.78	1.700	215.00	1239.74	90.69	8.000	0.55	1365.52	99.89
0.430	1492.50	160.74	11.76	0.700	1427.50	640.28	46.84	1.750	187.00	1249.69	91.42	9.000	0.35	1365.96	99.93
0.435	1761.25	168.74	12.34	0.710	1402.50	654.28	47.86	1.800	170.00	1258.55	92.07	10.000	0.20	1366.24	99.95
0.440	1755.02	177.59	12.99	0.720	1355.00	668.10	48.87	1.850	149.01	1266.42	92.64	25.000	0.12	1366.97	100.00
0.445	1922.49	187.02	13.68	0.730	1355.00	681.84	49.88	(*) see next page for explanation.							
0.450	2099.99	196.86	14.40	0.740	1300.00	695.28	50.86								
0.455	2017.51	207.15	15.15	0.750	1272.52	708.17	51.81								
0.460	2032.49	217.29	15.90	0.760	1222.50	720.62	52.72								
0.465	2000.00	227.59	16.65	0.770	1187.50	732.70	53.60								
0.470	1979.99	237.50	17.37	0.780	1195.00	744.52	54.47								

TABLE B.1
Adapted from Frolich and Wehrli (35)

(*) see next page for explanation.

TABLE B.1

Adapted from Frolich and Wehrli (35)

(λ) is the wavelength (μm), I_{λ} the solar spectral irradiance averaged over small bandwidth centred at λ ($\text{Wm}^{-2}\mu\text{m}^{-1}$), $\sum_c^{\lambda} I_{\lambda}$ the integrated solar irradiance in the wavelength range $0-\lambda$ (Wm^{-2}), and percentage of solar constant associated with wavelengths shorter than λ .

TABLE B.2

SPECTRAL ABSORPTION COEFFICIENTS OF UNIFORMLY MIXED GASES

λ (μm)	k_{λ}	λ (μm)	k_{λ}	λ (μm)	k_{λ}
0.76	0.300E + 01	1.75	0.100E - 04	2.80	0.150E + 03
0.77	0.210E + 00	1.80	0.100E - 04	2.90	0.130E + 00
		1.85	0.145E - 03	3.00	0.950E - 02
1.25	0.730E - 02	1.90	0.710E - 02	3.10	0.100E - 02
1.30	0.400E - 03	1.95	0.200E + 01	3.20	0.800E + 00
1.35	0.110E - 03	2.00	0.300E + 01	3.30	0.190E + 01
1.40	0.100E - 04	2.10	0.240E + 00	3.40	0.130E + 01
1.45	0.640E - 01	2.20	0.380E - 03	3.50	0.750E - 01
1.50	0.630E - 03	2.30	0.110E - 02	3.60	0.100E - 01
1.55	0.100E - 01	2.40	0.170E - 03	3.70	0.195E - 02
1.60	0.640E - 01	2.50	0.140E - 03	3.80	0.400E - 02
1.65	0.145E - 02	2.60	0.660E - 03	3.90	0.290E + 00
1.70	0.100E - 04	2.70	0.100E + 03	4.00	0.250E - 01

TABLE B.3

SPECTRAL ABSORPTION COEFFICIENTS OF WATER VAPOUR

λ (μm)	$k_{\text{wa}\lambda}$ (cm^{-1})	λ (μm)	$k_{\text{wa}\lambda}$ (cm^{-1})	λ (μm)	$k_{\text{wa}\lambda}$ (cm^{-1})
0.69	0.160E - 01	0.93	0.270E + 02	1.85	0.220E + 04
0.70	0.240E - 01	0.94	0.380E + 02	1.90	0.140E + 04
0.71	0.125E - 01	0.95	0.410E + 02	1.95	0.160E + 03
0.72	0.100E + 01	0.96	0.260E + 02	2.00	0.290E + 01
0.73	0.870E + 00	0.97	0.310E + 01	2.10	0.220E + 00
0.74	0.610E - 01	0.98	0.148E + 01	2.20	0.330E + 00
0.75	0.100E - 02	0.99	0.125E + 00	2.30	0.590E + 00
0.76	0.100E - 04	1.00	0.250E - 02	2.40	0.203E + 02
0.77	0.100E - 04	1.05	0.100E - 04	2.50	0.310E + 03
0.78	0.600E - 03	1.10	0.320E + 01	2.60	0.150E + 05
0.79	0.175E - 01	1.15	0.230E + 02	2.70	0.220E + 05
0.80	0.360E - 01	1.20	0.160E - 01	2.80	0.800E + 04
0.81	0.330E + 00	1.25	0.180E - 03	2.90	0.650E + 03
0.82	0.153E + 01	1.30	0.290E + 01	3.00	0.240E + 03
0.83	0.660E + 00	1.35	0.200E + 03	3.10	0.230E + 03
0.84	0.155E + 00	1.40	0.110E + 04	3.20	0.100E + 03
0.85	0.300E - 02	1.45	0.150E + 03	3.30	0.120E + 03
0.86	0.100E - 04	1.50	0.150E + 02	3.40	0.195E + 02
0.87	0.100E - 04	1.55	0.170E - 02	3.50	0.360E + 01
0.88	0.260E - 02	1.60	0.100E - 04	3.60	0.310E + 01
0.89	0.630E - 01	1.65	0.100E - 01	3.70	0.250E + 01
0.90	0.210E + 01	1.70	0.510E + 00	3.80	0.140E + 01
0.91	0.160E + 01	1.75	0.400E + 01	3.90	0.170E + 00
0.92	0.125E + 01	1.80	0.130E + 03	4.00	0.450E - 02

(+)

is the mean
effective height of
ozone layer for
Glasgow

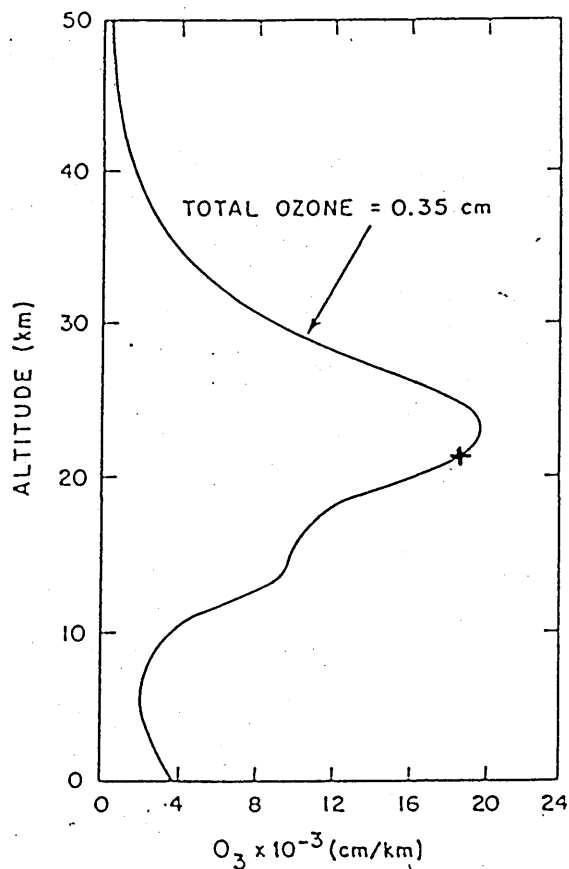


Figure B. 1 Variation of ozone concentration with
geographic altitude. Adapted from Iqbal (6)

Table B.4. SPECTRAL ABSORPTION COEFFICIENT FOR OZONE

$\lambda (\mu\text{m})$	$k_{o_3} (\text{cm}^{-1})$	$\lambda (\mu\text{m})$	$k_{o_3} (\text{cm}^{-1})$	$\lambda (\mu\text{m})$	$k_{o_3} (\text{cm}^{-1})$
0.290	38.000	0.485	0.017	0.595	0.120
0.295	20.000	0.490	0.021	0.600	0.125
0.300	10.000	0.495	0.025	0.605	0.130
0.305	4.800	0.500	0.030	0.610	0.120
0.310	2.700	0.505	0.035	0.620	0.105
0.315	1.350	0.510	0.040	0.630	0.090
0.320	0.800	0.515	0.045	0.640	0.079
0.325	0.380	0.520	0.048	0.650	0.067
0.330	0.160	0.525	0.057	0.660	0.057
0.335	0.075	0.530	0.063	0.670	0.048
0.340	0.040	0.535	0.070	0.680	0.036
0.345	0.019	0.540	0.075	0.690	0.028
0.350	0.007	0.545	0.080	0.700	0.023
0.355	0.000	0.550	0.085	0.710	0.018
0.445	0.003	0.555	0.095	0.720	0.014
0.450	0.003	0.560	0.103	0.730	0.011
0.455	0.004	0.565	0.110	0.740	0.010
0.460	0.006	0.570	0.120	0.750	0.009
0.465	0.008	0.575	0.122	0.760	0.007
0.470	0.009	0.580	0.120	0.770	0.004
0.475	0.012	0.585	0.118	0.780	0.000
0.480	0.014	0.590	0.115	0.790	0.000

TABLE B.3

	Direct		Diffuse		Total	Global on horizontal
λ (μm)	I_{λ} ($\text{Wm}^{-2}/\mu\text{m}$)	$\sum_0^{\lambda} I_{\lambda}$ (Wm^{-2})	$I_{d\lambda}$ ($\text{Wm}^{-2}/\mu\text{m}$)	$\sum_0^{\lambda} I_{d\lambda}$ (Wm^{-2})	$I_{T\lambda} = I_{\lambda} + I_{d\lambda}$ ($\text{Wm}^{-2}/\mu\text{m}$)	$\sum_0^{\lambda} I_{\lambda}$ (*) (Wm^{-2})
0.250	0.20	0.001	21.50	0.164	21.70	
0.255	0.43	0.001	31.36	0.233	31.79	
0.260	0.84	0.005	42.49	0.317	43.43	0.319
0.265	2.44	0.010	89.02	0.536	91.46	0.541
0.270	3.60	0.028	97.11	1.143	100.71	1.157
0.275	3.68	0.040	75.33	1.430	79.01	1.450
0.280	3.65	0.064	57.66	1.903	61.31	1.935
0.285	8.13	0.084	101.36	2.168	109.49	2.210
0.290	0.00	0.124	0.00	2.675	0	2.737
0.295	0.00	0.124	0.00	2.675	0	2.737
0.300	0.03	0.124	0.09	2.675	0.12	2.737
0.305	1.27	0.126	3.41	2.681	4.68	2.744
0.310	6.77	0.144	16.63	2.726	23.40	2.798
0.315	23.09	0.194	56.71	2.848	79.80	2.945
0.320	40.78	0.377	98.25	3.295	139.03	3.483
0.325	64.42	0.551	156.23	3.719	220.65	3.994
0.330	107.09	1.050	251.46	4.919	358.55	5.443
0.335	114.73	1.417	247.52	5.751	362.25	6.458
0.340	137.46	2.216	286.86	7.434	424.32	8.540
0.345	139.80	2.677	246.38	8.289	386.18	9.625
0.350	167.20	3.649	261.50	9.957	428.70	11.778
0.355	199.22	4.258	280.22	10.860	479.44	12.985
0.360	193.18	5.568	244.62	12.668	437.80	15.447
0.365	248.04	6.302	284.01	13.549	532.05	16.694
0.370	274.33	7.991	285.22	15.445	559.55	19.433
0.375	270.81	8.890	256.67	16.350	527.48	20.790
0.380	321.13	10.780	278.47	18.100	599.60	23.470
0.385	260.96	11.740	207.78	18.910	468.74	24.770
0.390	353.92	13.630	259.59	20.380	613.51	27.180
0.395	319.91	14.750	216.83	21.170	536.74	28.530

(*) See next page for explanation.

0.400	551.30	17.25	346.32	22.83	897.62	31.44
0.405	555.51	19.09	324.33	23.95	879.84	33.48
0.410	601.68	22.85	327.36	26.12	929.04	37.52
0.415	638.73	24.91	324.66	27.20	963.39	39.64
0.420	662.13	29.19	315.16	29.35	977.29	43.92
0.425	663.50	31.39	296.41	30.37	959.91	46.04
0.430	604.24	35.69	253.90	32.28	858.14	50.09
0.435	735.14	37.91	291.14	33.19	1026.28	52.11
0.440	754.04	42.82	282.00	35.11	1036.04	56.48
0.445	847.24	45.48	299.53	36.08	1146.77	58.78
0.450	949.89	51.28	318.29	38.11	1268.18	63.70
0.455	934.81	54.40	297.31	39.13	1232.12	66.28
0.460	962.86	60.65	291.06	41.11	1253.92	71.37
0.465	967.59	63.85	278.43	42.06	1246.02	73.92
0.470	977.88	70.30	268.33	43.90	1246.21	78.98
0.475	1014.19	73.61	265.62	44.78	1279.81	81.52
0.480	1052.37	80.53	263.52	46.55	1315.89	86.74
0.485	989.74	84.01	237.21	47.39	1226.95	89.31
0.490	1014.48	90.62	232.95	48.96	1247.43	94.18
0.495	1052.98	94.05	231.96	49.74	1284.94	96.67
0.500	1010.77	100.97	213.81	51.25	1224.58	101.64
0.505	1067.52	104.42	217.09	51.97	1248.61	104.08
0.510	1084.49	111.54	212.26	53.41	1296.75	109.07
0.515	1030.14	115.05	194.25	54.09	1224.39	111.50
0.520	1023.50	121.88	186.19	55.37	1209.69	116.18
0.525	1083.31	125.37	190.13	56.10	1273.44	118.55
0.530	1122.56	132.63	190.35	57.26	1312.91	123.44
0.535	1118.20	136.35	183.34	57.89	1301.91	125.92
0.540	1086.92	143.72	172.51	59.09	1259.43	130.80
0.545	1117.23	147.37	171.79	59.67	1289.02	133.20

(*) λ is the wavelength (μm), I_{λ} , and $I_{d\lambda}$ the beam and diffuse spectral intensities averaged over small bandwidth centred at λ ($\text{Wm}^{-2}\mu\text{m}^{-1}$), $\sum_{\lambda}^{\lambda_0} I_{\lambda}$, $\sum_{\lambda}^{\lambda_0} I_{d\lambda}$, and $\sum_{\lambda}^{\lambda_0} I_{\lambda}$ the integrated solar irradiances in the wavelength range $0-\lambda$ (Wm^{-2}) for beam, diffuse, and global on horizontal, respectively, and I_{η} is the sum of the beam and diffuse intensities.

0.550	1129.62	154.81	168.42	60.80	1298.04	138.05
0.555	1122.87	158.56	162.36	61.36	1285.23	140.47
0.560	1100.73	165.96	154.51	62.42	1255.24	145.24
0.565	1111.74	169.63	151.64	62.94	1263.38	147.58
0.570	1094.55	176.99	145.12	63.93	1239.67	152.25
0.575	1121.52	180.66	144.76	64.42	1266.28	154.56
0.580	1127.10	188.12	141.77	65.38	1268.87	159.24
0.585	1123.84	191.85	137.85	65.84	1261.69	161.57
0.590	1088.08	199.25	130.22	66.75	1218.30	166.17
0.595	1119.15	202.93	130.67	67.19	1249.82	168.44
0.600	1082.49	210.29	123.38	68.04	1205.87	172.97
0.605	1106.06	213.92	123.13	68.46	1229.19	175.19
0.610	1097.98	221.25	119.59	69.27	1217.57	179.66
0.620	1123.59	232.30	117.26	70.48	1240.85	186.39
0.630	1096.93	239.75	109.87	71.00	1206.80	190.87
0.640	1107.43	243.20	106.61	71.48	1214.04	192.84
0.650	1110.96	250.57	102.96	72.18	1213.92	197.21
0.660	1099.62	265.28	98.23	73.54	1197.85	205.54
0.670	1080.81	272.51	90.14	74.16	1170.95	210.14
0.680	1075.53	286.83	86.99	75.36	1162.52	218.49
0.690	1038.34	293.85	81.54	75.92	1119.88	222.55
0.700	1055.89	307.67	80.57	77.00	1136.46	230.54
0.710	1053.66	314.69	78.22	77.53	1131.88	234.56
0.720	920.10	328.20	66.51	78.54	986.81	242.32
0.730	936.30	334.36	65.96	78.98	1002.26	245.84
0.740	986.04	346.98	67.75	79.86	1053.79	253.01
0.750	993.57	353.55	66.65	80.31	1060.22	256.73
0.760	619.36	365.48	40.22	81.11	659.58	263.50
0.770	850.78	370.38	54.44	81.43	905.22	266.25
0.780	954.29	382.02	59.84	82.17	1014.13	272.80
0.790	908.36	388.20	55.77	82.55	964.13	276.27
0.800	908.30	400.25	54.64	83.30	962.94	283.02
0.810	846.27	406.06	49.91	83.64	896.18	286.28

0.820	749.43	416.95	43.36	84.29	792.79	292.37
0.830	774.23	422.03	43.97	84.58	818.20	295.18
0.840	802.85	431.61	44.77	85.17	847.62	300.55
0.850	816.34	437.79	44.73	85.47	861.07	303.92
0.860	827.63	448.67	44.59	86.06	872.22	309.95
0.87	805.59	454.09	42.69	86.35	848.28	312.94
0.88	801.73	464.77	41.80	86.92	843.53	318.84
0.89	769.87	469.98	39.52	87.19	809.39	321.71
0.90	639.03	479.69	32.31	87.69	671.34	327.10
0.91	630.46	483.93	31.40	87.91	661.86	329.41
0.92	619.01	492.26	30.39	88.32	649.40	333.98
0.93	337	495.26	16.35	88.48	354.10	335.72
0.94	281.04	499.53	13.42	88.68	294.46	338.08
0.95	263.56	501.31	12.42	88.77	275.98	339.06
0.96	320.89	505.05	14.92	88.94	335.81	341.08
0.97	521.78	508.00	23.95	89.07	545.73	342.60
0.98	566.99	515.10	25.71	89.40	592.70	346.46
0.99	629.16	519.12	28.18	89.58	657.34	348.62
1.00	637.01	527.50	28.19	89.96	665.20	353.18
1.05	576.81	530.00	24.15	90.30	600.96	355.30
1.10	422.54	548.25	16.82	91.00	439.36	365.13
1.15	248.64	569.01	9.45	91.64	258.09	375.69
1.20	436.90	580.61	15.93	92.06	452.83	381.79
1.25	436.66	609.61	15.33	93.11	451.99	397.31
1.30	315.58	622.00	10.68	93.54	326.26	403.97
1.35	38.96	637.90	1.28	94.10	40.24	412.69
1.40	1.18	638.51	0.04	94.12	1.22	413.04
1.45	42.17	639.36	1.30	94.15	43.47	413.44
1.50	159.03	642.98	4.76	94.25	163.79	415.21
1.55	245.51	655.20	7.17	94.60	252.68	421.55
1.60	214.57	662.83	6.14	94.83	220.71	425.58
1.65	212.52	677.04	5.90	95.23	218.42	433.08
1.70	182.26	683.56	4.94	95.41	187.20	436.52
1.75	133.57	694.78	3.54	95.72	137.11	442.47
1.80	27.80	697.04	0.72	95.79	28.56	443.87
1.85	0.04	698.28	0.00	95.82	0.04	444.60
1.90	0.21	698.28	0.01	95.82	0.22	444.60

2.00	57.36	700.16	1.42	95.86	58.78	445.31
2.1	74.03	706.80	1.73	96.02	75.76	448.73
2.2	65.60	710.00	1.47	96.09	67.07	451.09
2.3	54.20	713.23	1.18	96.15	55.38	452.07
2.4	28.48	715.76	0.60	96.21	29.08	453.50
2.5	2.79	718.32	0.06	96.27	2.85	455.02
2.6	0.00	718.34	0.00	96.27	0.00	455.07
2.7	0.00	718.34	0.00	96.27	0.00	455.07
2.8	0.00	718.34	0.00	96.27	0.00	455.07
2.9	0.37	718.36	0.01	96.28	0.38	455.08
3.0	2.05	718.51	0.04	96.28	2.09	455.12
3.1	1.93	718.81	0.03	96.28	1.96	455.26
3.2	3.40	719.03	0.06	96.29	3.46	455.35
3.3	2.23	719.37	0.04	96.29	2.27	455.56
3.4	1.31	719.45	0.02	96.30	1.33	455.62
3.5	5.39	720.05	0.09	96.30	5.48	455.78
3.6	9.66	720.80	0.15	96.31	9.81	456.04
3.7	9.01	722.09	0.14	96.33	9.15	456.69
3.8	8.66	722.72	0.13	96.34	9.79	456.99
3.9	7.74	723.87	0.12	96.35	7.86	457.57
4.0	7.91	724.40	0.12	96.36	8.03	457.83
4.1	7.45	725.42	0.11	96.38	7.56	458.36
4.2	6.74	725.93	0.10	96.38	6.84	458.61
4.3	6.26	726.81	0.09	96.40	6.35	459.06
4.4	5.78	727.17	0.08	96.40	5.86	459.28
4.5	5.30	727.92	0.07	96.41	5.37	459.65
4.6	4.83	728.26	0.07	96.42	4.90	459.82
4.7	4.35	728.89	0.06	96.43	4.41	460.14
4.8	3.86	729.16	0.05	96.43	3.91	460.28
4.9	3.63	729.66	0.05	96.44	3.68	460.54
5.0	3.36	729.90	0.04	96.44	3.40	460.66
6.0	1.70	731.50	0.02	96.46	1.72	461.31
7.0	0.93	731.75	0.01	96.46	0.94	461.50
8.0	0.54	731.90	0.01	96.46	0.55	461.67
9.0	0.34	732.20	0.00	96.47	0.34	461.82
10.0	0.20	732.60	0.00	96.47	0.20	461.82
25.0	0.12	734.69	0.00	96.47	0.12	463.06

OPTICAL CONSTANTS OF WATER, DYES AND GLASS

C.1 Percentage error when improper averaging of polarization is used

TABLE C.1

Angle of incidence	30°	45°	60°	75°
Total transmittance	—	0.3	1.2	4.3
Total reflectance	0.2	0.9	1.4	0.9
Total absorptance	—	—	0.2	0.6
Absorptance front glass	—	—	—	0.3
Absorptance water dye	—	—	—	0.5
Absorptance rear glass	—	—	0.3	1.3

C.2 Optical constants of water at 25 °C

 k_w = absorption coefficient n_w = refractive index

TABLE C.2

λ (μm)	$k_w(\lambda)$ (m^{-1})	$n_w(\lambda)$	λ (μm)	$k_w(\lambda)$ (m^{-1})	$n_w(\lambda)$
0.250	3.35×10^2	1.362	0.800	1.25×10^{-1}	1.330
0.275	2.35	1.354	0.825	1.80	1.330
0.300	1.60	1.349	0.850	2.79	1.330
0.325	1.08	1.346	0.875	3.71	1.329
0.350	6.50×10^{-3}	1.343	0.900	4.86	1.329
0.375	3.50	1.341	0.925	9.65	1.329
0.400	1.86	1.339	0.950	2.67	1.328
0.425	1.30	1.338	0.975	3.74	1.328
0.450	1.02	1.337	1.00	3.10	1.327
0.475	9.35×10^{-4}	1.336	1.05	1.40	1.327
0.500	1.00×10^{-3}	1.335	1.10	1.68	1.326
0.525	1.32	1.334	1.15	8.87	1.326
0.550	1.96	1.333	1.20	10.94	1.325
0.575	3.60	1.332	1.30	13.80	1.324
0.600	1.09×10^{-2}	1.332	1.40	138	1.322
0.625	1.39	1.331	1.50	230	1.320
0.650	1.64	1.331	1.60	90	1.318
0.675	2.23	1.331	1.70	77	1.315
0.700	3.57×10^{-2}	1.331	1.80	125	1.312
0.725	7.38	1.331	1.90	870	1.310
0.750	1.62×10^{-1}	1.331	2.00	1100	1.306
0.775	1.48	1.330	2.10	455	1.302

 ∞

C.3 Average optical properties of water and clear float glass

TABLE C.3

wavelength band (μm)	w a t e r		g l a s s	
	$k_w(\lambda), (m^{-1})$	$n_w(\lambda)$	$k_g(\lambda), (m^{-1})$	$n_g(\lambda)$
0.250 - 0.350	1.81×10^{-2}	1.351	550.00	1.511
0.350 - 0.390	4.30×10^{-3}	1.344	24.02	1.514
0.390 - 0.455	1.43×10^{-3}	1.338	11.13	1.515
0.455 - 0.499	9.66×10^{-4}	1.336	8.65	1.517
0.499 - 0.575	1.95×10^{-3}	1.334	7.33	1.512
0.575 - 0.595	7.00×10^{-3}	1.333	9.17	1.517
0.595 - 0.620	1.15×10^{-2}	1.332	11.82	1.513
0.620 - 0.770	6.86×10^{-1}	1.331	23.34	1.511
0.77 - 0.9	2.65×10^{-1}	1.330	47.76	1.514
0.9 - 1.2	4.16	1.327	54.92	1.512
1.2 - 2.1	311	1.315	55.24	1.511
2.1 - 25	∞	1.342	250	1.510

C.4 Optical density of various dyes

From the experimental graphs 3.7.1b and D.2, values of the optical density were extracted over a $0.025 \mu\text{m}$ interval for four different dyes. These results are listed in table C.4 below.

TABLE C.4

λ (μm)	O P T I C A L S P E C T R A L D E N S I T Y				(*)
	A.G.	C.R.	M.O.	L.R.	
0.250	0.767	0.354	0.124	0.568	
0.275	0.859	0.257	0.175	0.421	
0.300	0.690	0.180	0.123	0.596	
0.325	0.449	0.238	0.070	0.346	
0.350	0.426	0.165	0.073	0.127	
0.375	0.369	0.113	0.190	0.113	
0.400	0.275	0.089	0.341	0.120	
0.425	0.210	0.053	0.470	0.124	
0.450	0.135	0.061	0.568	0.169	
0.475	0.070	0.162	0.551	0.287	
0.500	0.046	0.305	0.347	0.423	
0.525	0.030	0.409	0.110	0.430	
0.550	0.026	0.363	0.000	0.281	
0.575	0.048	0.183	0.000	0.084	
0.600	0.099	0.001	0.000	0.014	
0.625	0.172	0.000	0.000	0.000	
0.650	0.235	"	"	"	
0.675	0.271	"	"	"	
0.700	0.291	"	"	"	
0.725	0.289	"	"	"	

C.5 Calculation of average absorption coefficient for a waveband

The radiation transmitted over a waveband $d\lambda$ is given by

$$I_\lambda = I_\lambda \cdot d\lambda \cdot \exp(-kCL)$$

where I_λ is the spectral irradiance, k is the absorption coefficient of the dye/water solution, C is the concentration, L the path length. However, it is impractical to integrate under the spikey intensity-wavelength curve and it becomes necessary to use numerical integration to produce "mean effective" absorption coefficients for each of the wavebands. The mean absorption coefficient is defined by the relation

$$\lambda_1 \cdot F_{\lambda_1} \cdot \exp(-K_m C x) = \sum_{\lambda_1 - \lambda_2} f_\lambda \exp(-k C x)$$

where F = fraction of energy in waveband $\lambda_1 - \lambda_2$
 f = fraction of energy in waveband $\pm \frac{1}{2} \lambda$ at $\lambda \mu\text{m}$
 K_m = mean absorption coefficient
 C = concentration
 x = path length

In practice the product $K_\lambda C x$ is obtained as a fraction from the absorption curves generated by the spectrophotometer and x is taken simply as the cell thickness. The fraction of energy, as detailed in section 3.7, is a function of air mass and, of course, the nature of the radiation, viz beam or diffuse. Since beam radiation dominates the transwall absorption, and observing the rule "when in doubt use air mass two", the fractional energy, f_λ , is appropriate to beam radiation, a.m. 2, and its waveband is unity, a half micron on each side of the designated wavelength.

It should be noted, though, that a straight arithmetic average of the product, $K_\lambda C x$, will yield a mean absorption coefficient that is accurate enough for most purposes. For example, for Lissamine red 3GX over the fairly wide waveband 0.4-0.6 μm the arithmetic average for K_m is $0.332 \times 10^6 \text{ m}^{-1}$ while the more accurate method gives $0.315 \times 10^6 \text{ m}^{-1}$, a difference of only 5%. Note further that since the water/dye solution is measured relative to water the absorption coefficient k_m is described as 'dye over water', i.e. the absorption coefficient of water alone for the same waveband has to be added to k_m to give the absorption coefficient of the solution.

(*) A.G., C.R., M.O., L.R. in table C.4 correspond to Acid Green at 31 ppm, Carbolan Rubine at 22 ppm, Methyl Orange at 10 ppm, and Lissamine Red at 40 ppm respectively.

T A B L E C.6

wavelength band (μm)	refraction index of water	extinction coefficient of water (m^{-1})	extinction coefficient of Lissamine Red (Kg of water/ mole dye x m)	refractive index of clear float glass	extinction coefficient of clear float glass (m^{-1})	extinction coefficient of antisu glass (m^{-1})	fractional average solar radiation air mass = 2	clearness index $0.25 < K_T < 0.50$ (light overcast)
0.30 - 0.35	1.346	4.43×10^{-2}	0	1.511	540.4	146.5	0.006	0.069
0.35 - 0.4	1.341	1.77×10^{-2}	0.176×10^6	1.514	20.6	153.7	0.022	0.098
0.40 - 0.60	1.335	1.48×10^{-2}	0.315×10^6	1.514	8.9	125.3	0.279	0.333
0.60 - 0.75	1.331	3.89×10^{-1}	0.010×10^6	1.511	21.8	108.4	0.215	0.162
0.75 - 0.90	1.329	2.58×10^0	0	1.512	44.5	125.4	0.142	0.104
0.90 - 1.20	1.326	7.11×10^1	0	1.511	55.2	157.9	0.146	0.113
1.20 - 2.10	1.315	7.11×10^3	0	1.513	33.4	101.6	0.150	0.094
2.10 - 4.10	1.332	2.00×10^6	0	1.510	224.79	2000.0	0.040	0.027

C.6 Average properties of the various substances and fraction of solar radiation used in the analyses of Chapter 5.

The average optical properties of water, clear float glass, Antisun glass, and the fractional average solar radiation (beam for clear sky conditions at air mass 2 and diffuse for light overcast conditions with clearness index $0.25 < K_T < 0.50$) were extracted from Paparsenos (3).

(*) Pilkington Antisun Grey 41/60.

APPENDIX D

EXPERIMENTS IN DETERMINING THE SPECTRAL ABSORPTION

COEFFICIENTS OF DYES

Optical absorption data on various dye solutions were recorded on a Beckman spectrophotometer at ambient temperature in the visible and near infrared portions of the spectrum. The type of spectrophotometer used is a two-beam two-detector instrument in which light from the monochromator is divided by a beamsplitter and passes simultaneously through the sample and the reference and is incident on two photodetectors, figure D.1.

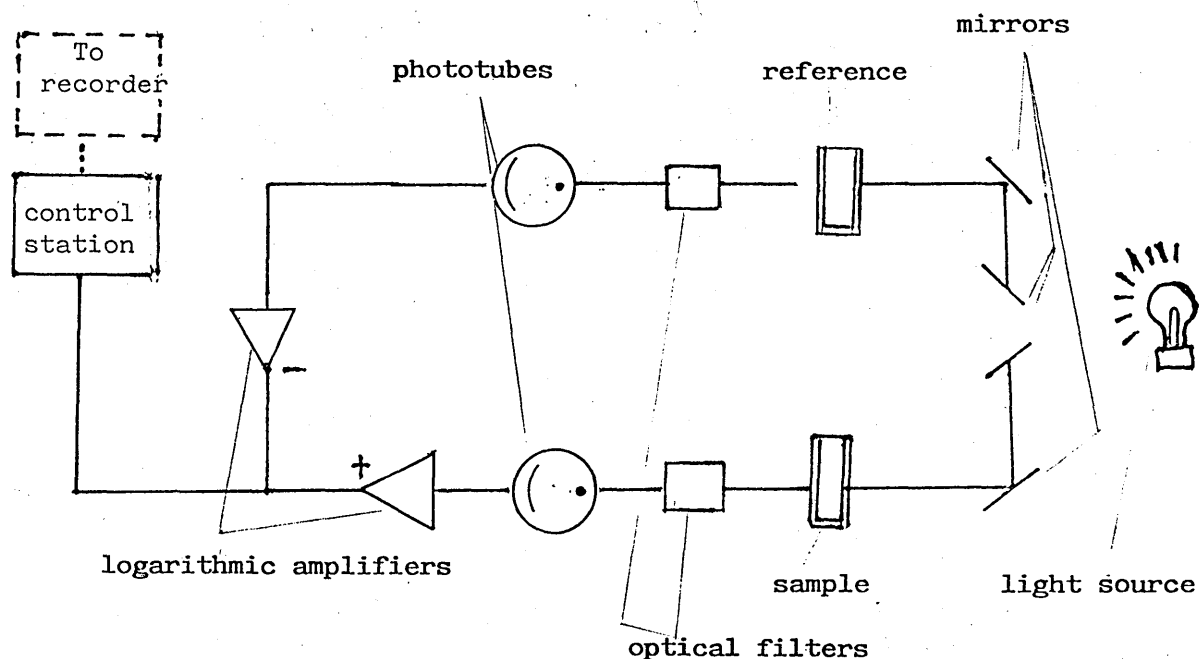


Figure D.1 Schematic diagram of the spectrophotometer used.

The currents from these phototubes are amplified in logarithmic amplifiers and the difference in the amplified signal is then taken and is proportional to the concentration of the sample. The use of logarithmic amplifiers allows one to achieve a signal which is proportional in a linear fashion to the concentration of the material being analysed in the sample. From the above it can be seen that the quantity measured on a readout device is the spectral optical density of a substance, see 3.2.2.

Two identical cells of layer thickness 1 cm were used in a double-beam absorption measurement. A_1 is measured directly since

interface relations common to both sample and reference cells are equivalent and essentially cancel each other. The reference cell contained distilled water and the test cell dye dissolved in distilled water. Therefore the quantity of A represents the energy attenuation of an optical beam by the dye alone because all spectra were obtained in a double beam mode with the solvent placed in the reference cell.

Typical data is shown in figure 3.7.1c for 3 different dyes of 40 ppm strength of solution, and in figure 3.7.1a for 30 ppm.

The spectral molecular absorption coefficient were calculated from (eq. 3.2.1b), where C is in kilogram molecular weights per unit volume.

$$\text{i.e.} \quad C = \frac{W \cdot \rho_w}{M} \quad (D.1)$$

where W is the strength of the solution (kg dye/kg water)

M is the molecular weight of the particular dye

ρ_w is the density of water at 20°C (998.2 kg/m³)

The output of the spectrophotometer used was compared against curves supplied by ICI. Such comparison is shown in figure D.2 for Lissamine Red 3GX. The solid line represents the ICI curve for a 1 cm thick cell with a solution of 48 ppm. The (+) represents the results obtained by the Beckman spectrophotometer. The lower values obtained by the 'Beckman' is probably due to ageing of the dye used (4+ years old), and if due allowance is made for this the values agree well.

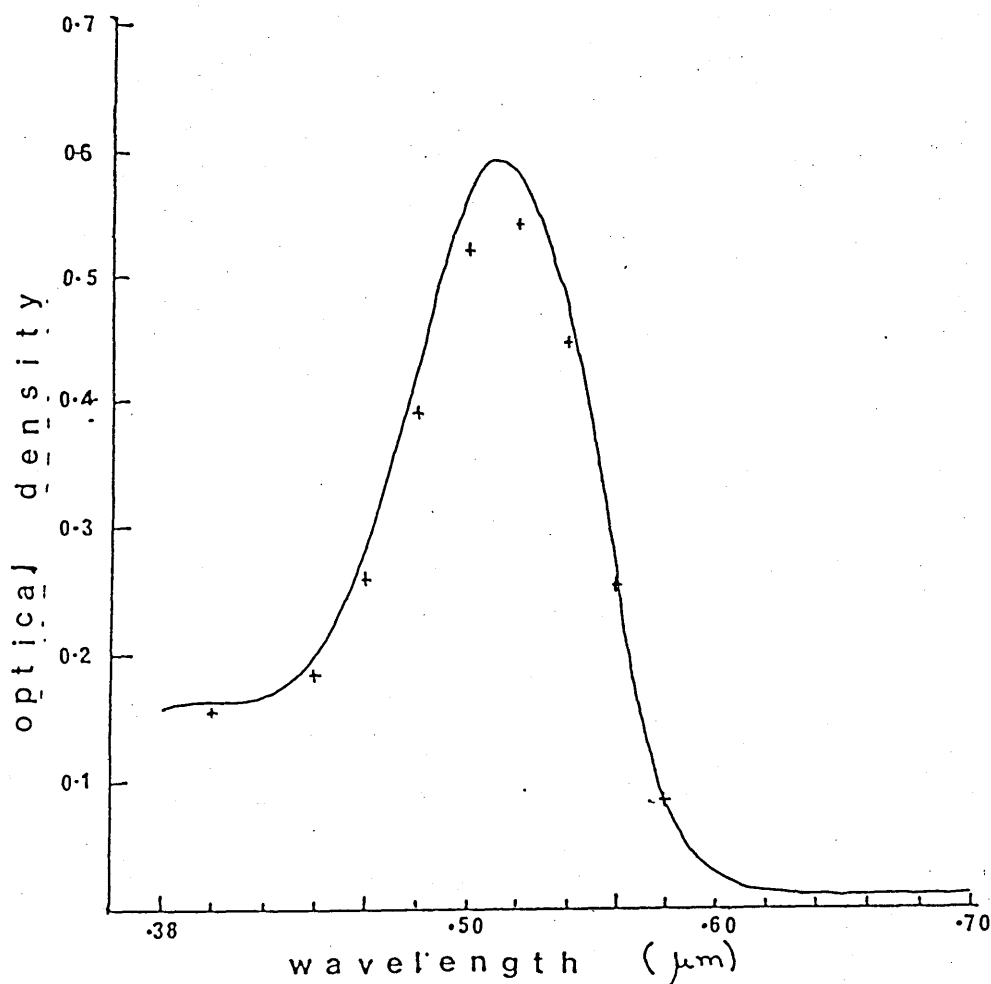


Figure D.2 Comparison of Values of the Spectrophotometer used Against ICI's for Lissamine red 3GX at 48ppm.

APPENDIX E

AVERAGE OPTICAL CONSTANTS FOR WATER AND GLASS

For the single waveband analysis, Chapter 5, average values for the refractive indexes and extinction coefficients of glass and water are needed.

E.1 Refractive Indexes

Because the values of the refractive indexes listed in table C.3 depend on the type of spectrum used an arithmetic average is incorrect.

The following equation was used to average the values of n and

$$\bar{n} = \frac{I_b \sum F_{bi} n_i + I_d \sum F_{di} n_i}{I_b + I_d} \quad (E.1)$$

where n_i is the value of the refractive index of the material, for a waveband i , and $\sum_{i=1}^m F_{bi} = 1$, $\sum_{i=1}^m F_{di} = 1$.

E.2 Extinction/Absorption Coefficients

The extinction coefficient of glass, k_g , and absorption coefficient of water, k_w , depend strongly on the path length as well as the type of spectrum.

When averaging for the extinction coefficient the path length, L is not separable. Summing equation (3.3) over the spectrum, for both beam and diffuse radiation.

$$\bar{k} = (1/\bar{L}) \cdot \log_e \left\{ \frac{I_b \sum F_{bi} \exp(-k_i L_i) + I_d \sum F_{di} \exp(-k_i L_i)}{(I_b + I_d)} \right\} \quad (E.2)$$

In the present analysis $\bar{L}_g = \frac{\bar{x}/2}{\cos 19.3}$ and $\bar{L}_w = \frac{\bar{x}/2}{\cos 22.1}$

were chosen as typical for the case of the transwall module under investigation. The refractive angles 19.3 and 22.1 correspond for an angle of incidence of 30°.

$$\bar{x} = \frac{0.006 + 2 \times 0.01}{3} = 8.7 \text{ mm}$$

where 0.006 is the thickness of glazing of the glass of the tank, and $t_w = 0.157 \text{ m}$. Further t_w and \bar{x} should be halved for an average extinction coefficient.

For appropriate path lengths the average extinction coefficients of glass and water were found. Using these results correlations were developed figure E.1 and E.2, but in the case of glass a single value for the average extinction coefficients can be safely employed. The above analysis gives $\bar{k}_g = 36.6 \text{ m}^{-1}$ and $\bar{k}_g = 38.6 \text{ m}^{-1}$ for 8 and 12 wavebands respectively.

For water the following correlations are suggested.

$$\bar{k}_w = 4.603 + 0.21 / I_w \quad (\text{m}^{-1}) \quad (\text{E.3})$$

using 8 wavebands

$$\text{and} \quad \bar{k}_w = 0.703 \cdot L_w^{-0.69} \quad (\text{m}^{-1}) \quad (\text{E.4})$$

using 12 wavebands

Equation E.3 should be preferred because of its better correlation coefficient.

*
The terms I_b and I_d are the total amounts of beam and diffuse radiation in W/m^2 for air mass 2. Were extracted from table B.5, Appendix B, and were used above for 'weight' averaging.

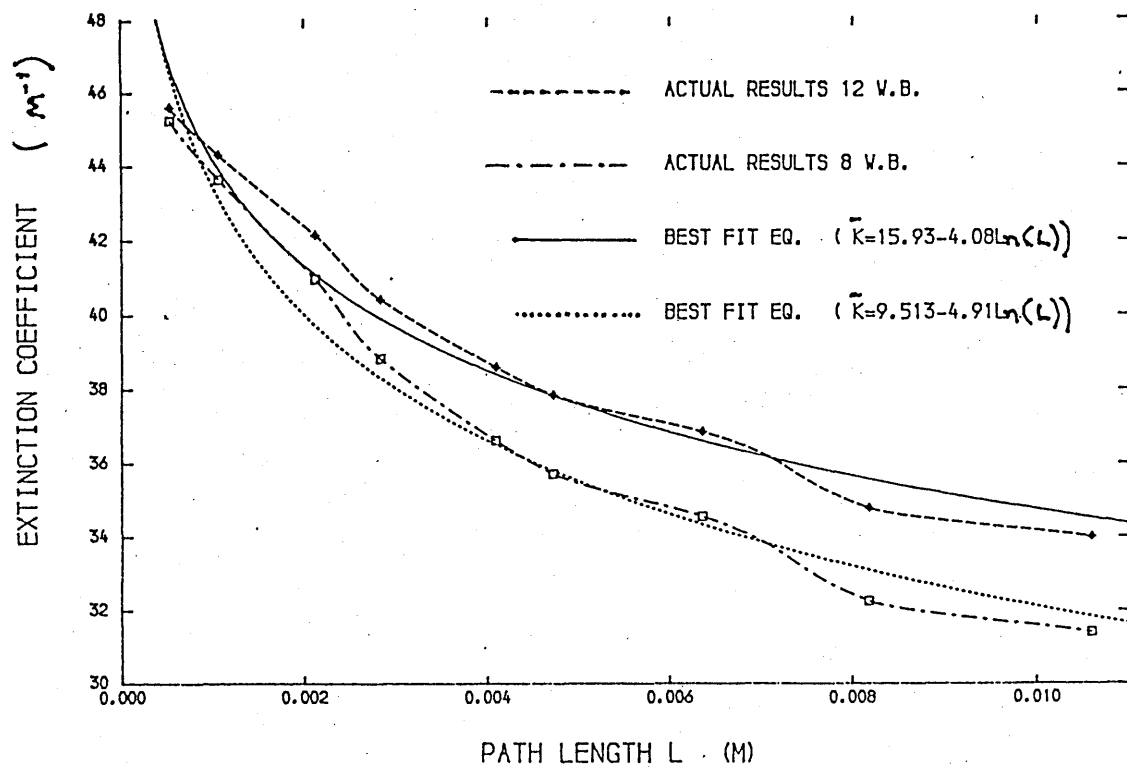


Figure E.1 Average Extinction Coefficient of Glass - Path Length.

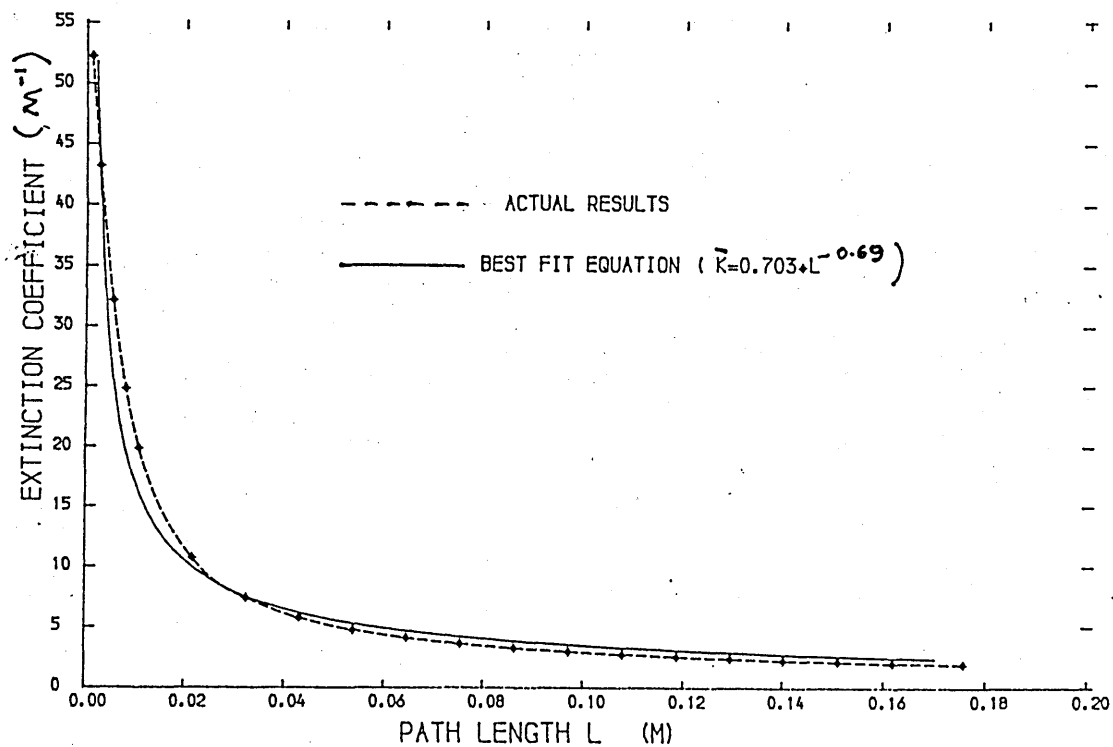


Figure E.2 Average Extinction Coefficient of Water - Path Length.

STRENGTH OF REFLECTED RAYS IN A TRANSWALL MODULE

The respective strengths of reflected rays are shown in fig. F.1
It is for a 10 mm glass transwall module. The following assumptions
were made:

Time: mid August, 1½ hrs from solar noon, (chosen to
average 10-4pm collection time).

Altitude: $\alpha = 44.6^\circ$

Solar azimuth: $\alpha = 32.8^\circ$

Angle of incidence: $\theta = 53.2^\circ$

These give a reflectance at air/glass interface = 0.066

and reflectance at glass/water interface = 0.005

Eight wavebands were used and the figure of 100 refers to the strength
of a beam after passing through 6 mm glass.

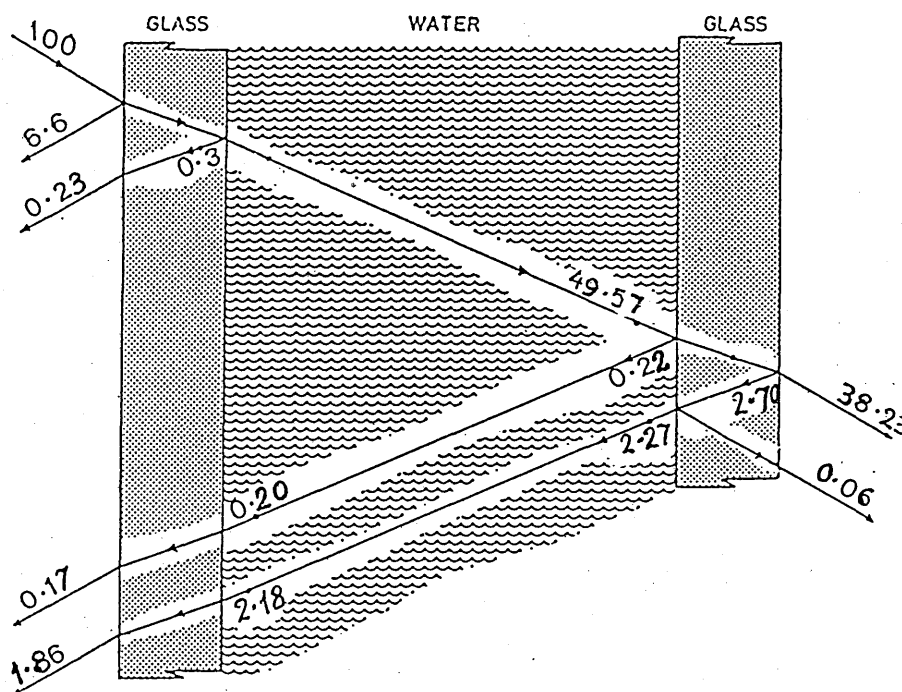


Figure F.1 Strength of reflected rays

Fig. F.1 above, clearly shows that the ray reflected from the back
glass/air interface is stronger than the ray reflected from the first
glass/water interface, 0.6% versus 0.2%.

MEASUREMENT OF HEAT TRANSFER COEFFICIENTG.1 Description of Heat Transfer Rig

In order to have some measure, even approximate, of the heat transfer coefficients from the transwall to the surroundings apparatus designed for another project was used. This consists basically of two copper sheets (25.4 cm x 20.6 cm) embedded in which^{is} a heating cable and the rear sides are insulated with polystyrene. The front surface consists of a 3 mm glass sheet stuck on to the copper in order that the long wavelength emittance will be similar to that of the transwall. The arrangement is shown in figure G.1. Three type K thermocouples are fitted, one immediately under the glass, one on the rear of the copper sheet (as a check), and one in the convective air stream immediately in front of the glass.

The principle of operation is when steady state is achieved the energy dissipation of the heating cable is equal to the heat transfer from the glass, making due allowance for various corrections. The heating cable is supplied from a heavy duty battery bank and the power consumption measured by standards quality voltmeter and ammeter.

G.2 Sample Calculation

A sample calculation for determining the combined (radiative and convective) heat transfer coefficient for the transwall module using a heat transfer rig is demonstrated below.

When the rig temperatures have stabilised and are close to the transwall glass temperature the following readings are necessary to calculate the heat transfer coefficient.

Heating element	Power (W)	Temperature †(air film) °C	Temperature (front plate) °C
voltage current			
8.06V 0.75A	6.06	21.2	27.5

$$\text{Power dissipated in the plate} = 6.06 \left(\frac{92.9}{92.9 + 19} \right) = 5.03 \text{ W}$$

The term in the bracket is a correction and accounts for the energy dissipation due to the heating cable. i.e. 92.9 cm is the length of

† just outside boundary layer

the heating cable in the plate and (92.9 + 19) cm is the length of the heating cable as leads to the terminals.

These 5.03 Watts are due to both radiation and convection.

$$h_a = \frac{\text{Power dissipated in the plate}}{(\text{Area of plate}) \times (\text{Temperature difference between front plate \& air film temperature})}$$

$$= \frac{5.03}{0.0518 \times (27.5 - 21.2)} = 15.4 \text{ W/m}^2 \text{ K}$$

The rig was placed directly above the transwall module and it was facing out when the heat transfer (h_a) was measured and it was facing towards the interior when (h_r) was under investigation. For every case the experiment was performed for the following combinations:

warm	transwall	(24 - 28 °C)	no fan [†]
warm	tranwall	(24 - 25 °C)	with the fan on
cool	transwall	(17 - 19 °C)	no fan
cool	transwall	(16 - 18 °C)	with the fan on

Table G.1 below, shows the experimental results of the combined heat transfer coefficients. (*)

TABLE G.1

	h_a (W/m ² K)	h_r (W/m ² K)
warm/no fan	18.4	12.4
warm/with fan	13.7	8.9
cool/no fan	11.8	7.5
cool/with fan	7.4	8.4

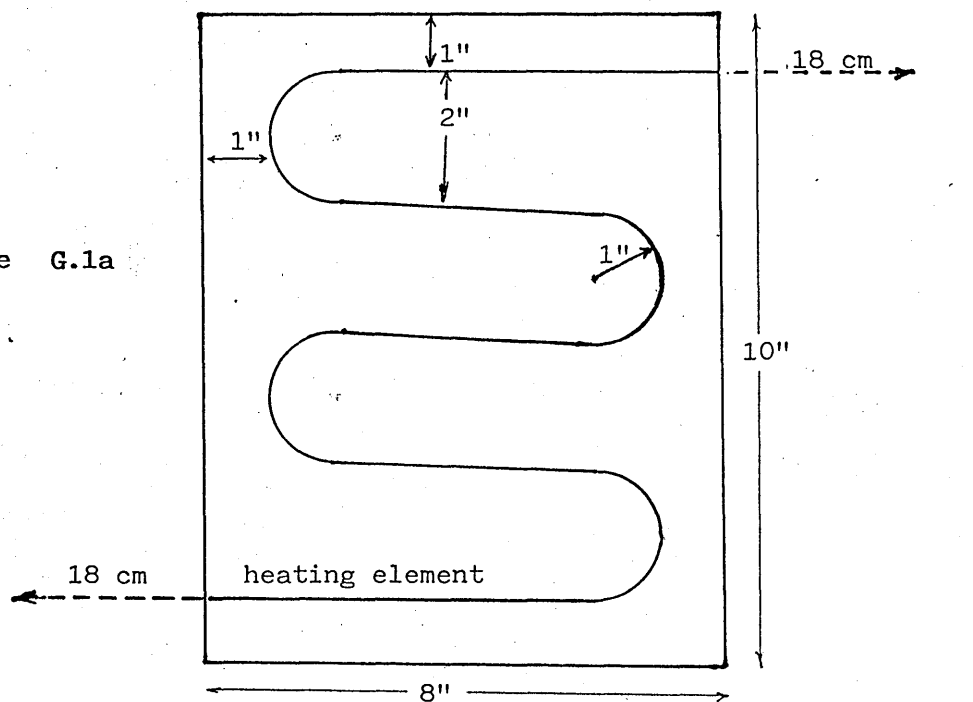
The smoke traces showed that the fan is pushing the air down over the transwall surface. This accounts for the decrease of the heat transfer coefficients of the above table when the fan is on.

(*)

Both convective and radiative

[†] test cell fan p. 93, 100

Figure G.1a



Heating element

copper plate $\frac{1}{8}$ thick

make: Sodern

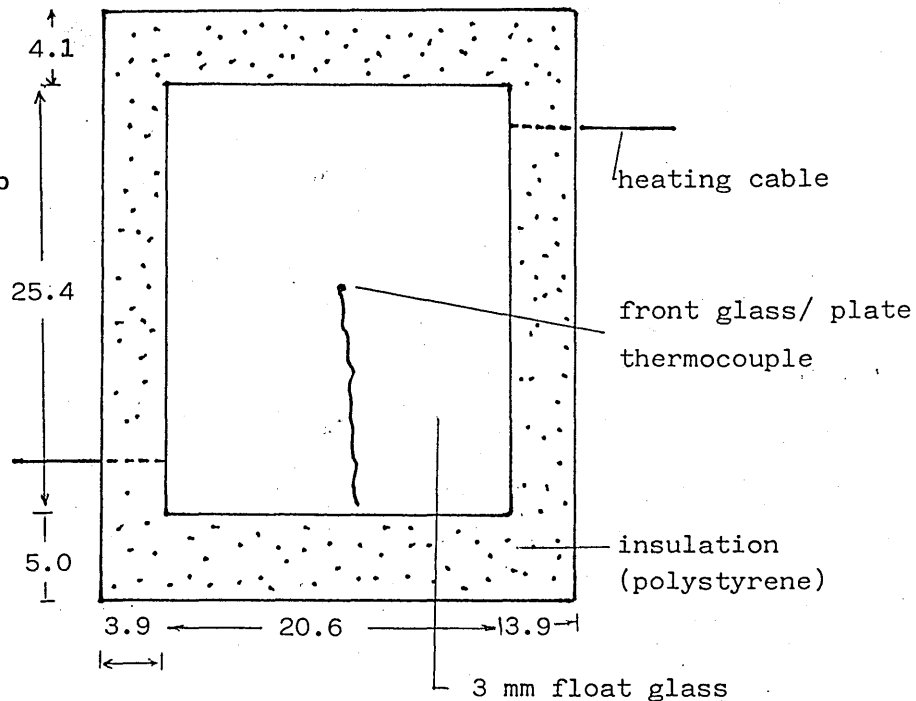
type: Thermocoax

dia. 1.2 mm, Nickel Chrome $\frac{80}{20}$

Length of cable in the plate = $4 \times 18 \text{ cm} + 2 \times 5 \text{ cm} + 3 \times 4 \text{ cm}$

= 36.57" or 0.929 m

Figure G.1b



all distances in cm.

Figure G.1 a&b. Grooved copper plate and heating cable.

NON-HOMOGENEOUS HALF SLAB METHOD

Figure H.1 below shows a transwall section with non-homogeneous half end slabs. For convenience only 3 water slabs are shown. The "extra terms" developed are for the outer transwall glass for the perpendicular or the parallel component of beam radiation.

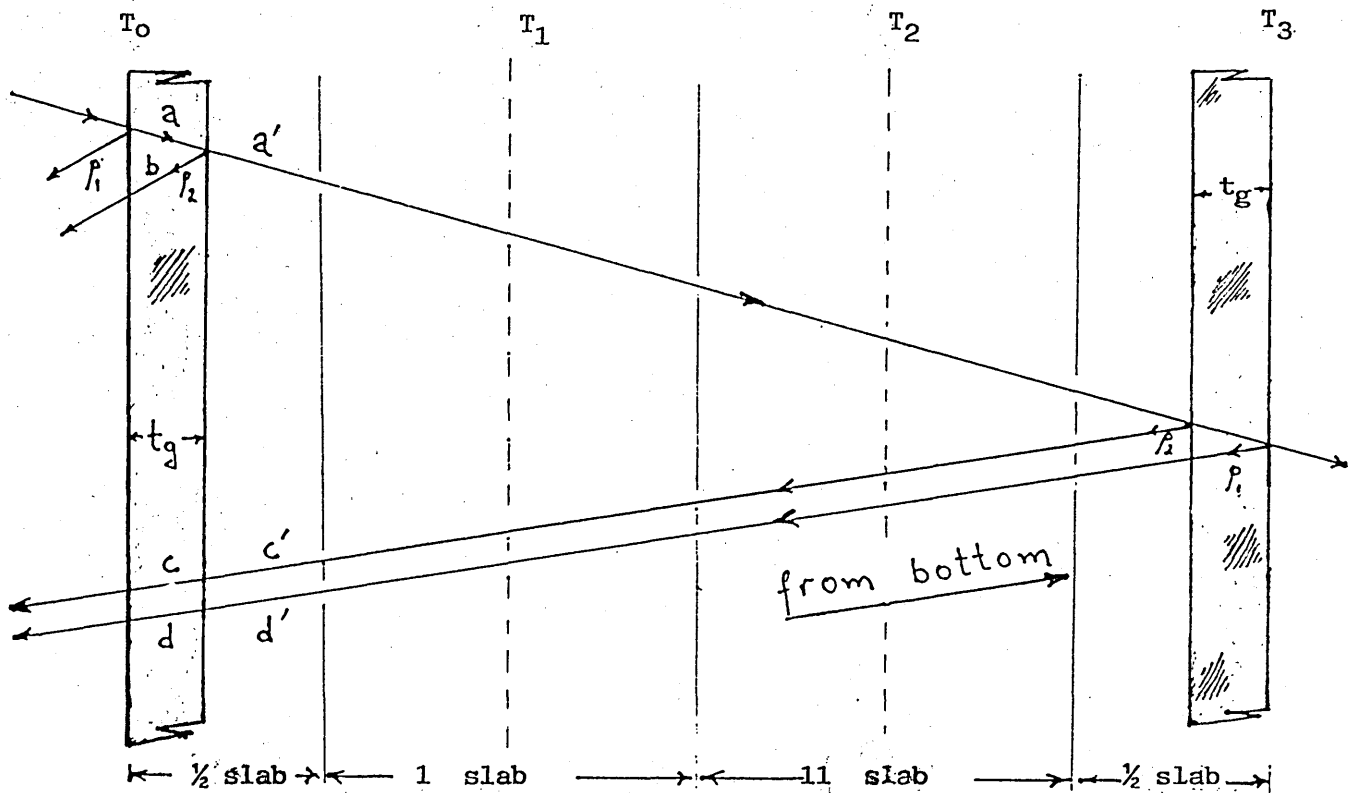


FIGURE H.1

A new path length accounting for the first (and last) half water slab was introduced, namely

$$L_{wx} = \frac{(a/2 - t_g)}{\cos \theta_{jw}}$$

corresponding to a transmittance τ_{wx}

Equation 5.9.1a will have additional terms added. However, it is easier to follow if start is made on unreduced equation 5.9.1a which comprises four blocks, viz. 1,2,3,4.

$$\text{1st block (ray a, a')} = {}_0I_b(1-\rho_2) \cdot \tau_{g1} \cdot (1-\tau_{wx})$$

2nd block (ray b) will not be affected by the introduction of water into the half slab.

$$\text{3rd block (ray c, c')} = (SF_1(j))_c \cdot {}_0I_b \cdot \tau_{g1}(1-\rho_2) \cdot \tau_w \cdot \rho_2 \cdot (\tau_w - \tau_{wx}) \cdot (1-\tau_{wx})$$

$$\text{4th block (ray d, d')} = (SF_1(j))_d \cdot {}_0I_b \cdot \tau_{g1}(1-\rho_2) \cdot \tau_w(1-\rho_2) \cdot \tau_{g2} \cdot \rho_1 \cdot \tau_{g2}(\tau_w - \tau_{wx}) \cdot (1-\tau_{wx})$$

The extra terms can be reduced to

$$\begin{aligned} (ET_b)_{g1} = & {}_0I_b(1-\rho_2) \cdot (1-\tau_{wx}) \cdot \tau_{g1} \left\{ 1 + (SF_1(j))_c \cdot \tau_w \rho_2 \cdot (\tau_w - \tau_{wx}) \right. \\ & \left. + (SF_1(j))_d \cdot \tau_w(1-\rho_2) \cdot \tau_{g2}^2 \cdot \rho_1 \cdot (\tau_w - \tau_{wx}) \right\} \end{aligned}$$

When the rays reflected from the base of the transwall are included the above expression becomes more complex.

Similar 'extra terms' can be found and added to the equations for the absorption in the water slabs and the rear glass. It is also important to note that the shade and acceptance factors will change slightly due to a wider slab and different refractive angles θ_{ag} and θ_{gw} .

The extra terms for diffuse radiation will be more complex because these also incorporate separately the diffuse radiation coming from the room interior, i.e. two extra term blocks will be required.

APPENDIX I

AIR MASS CONSIDERATION FOR THE LATITUDE OF GLASGOW — FRACTION OF

ENERGY FOR DIFFUSE RADIATION IN BRITAIN

The amount of attenuation by absorption and scattering depends exponentially on the optical path, that is, on the air mass, see 2.5. For 55.9° latitude, at Glasgow, the 12,30 hr elevation of June 11 is $57^\circ 11'$ corresponding to air mass 1.19, and at December 10, it is $12^\circ 20'$ corresponding to air mass 4.68. In figure I.1 the air mass is shown as a function of the time of day for different months of the year (for latitude 59.9°) using an average day for each month as recommended by Klein (1), see table I.1.

A passive solar house for the climate and location of Glasgow is said to be "receptive" for the intervals of time listed in table I.1. For these intervals of time a typical value for monthly average air mass has been worked out. The time intervals shown are somewhat arbitrary but are loosely based on radiation levels.

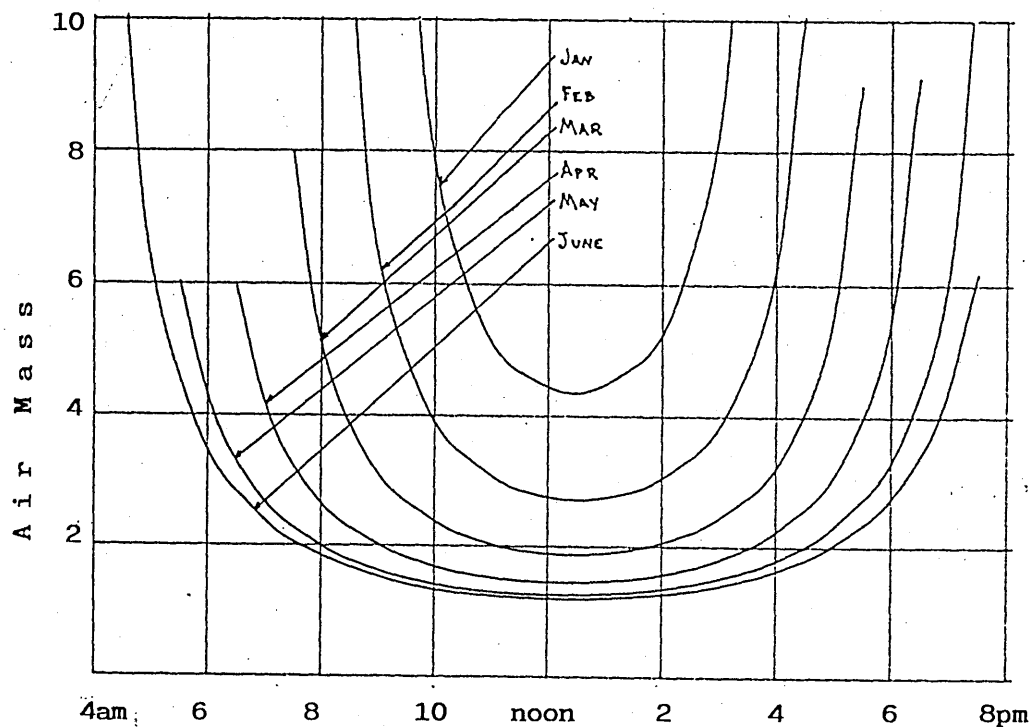


Figure I.1. Air mass as a function of time of day for different days of the year.

Month	d_n for ith day of month	Date	d_n day of year *	Time interval	Average air mass	Characteristic Solar constant declination	$I_{on} (Wm^{-2})$ #	Eccentricity E_o
For the average day of the month at Glasgow								
January	i	17	17	9.30-13.30	6.4	-20.8	1413.4	1.034
February	31 + i	16	47	8.30-14.30	4.4	-12.4	1401.0	1.025
March	59 + i	16	75	7.30-16.30	3.1	-1.8	1381.3	1.010
April	90 + i	15	105	7.30-17.30	2.1	9.7	1357.3	0.993
May	120 + i	15	135	7.00-18.30	1.9	18.8	1336.5	0.978
June	151 + i	11	162	7.00-18.30	1.7	23.1	1324.6	0.969
July	181 + i	17	198	7.00-18.30	1.7	21.3	1322.3	0.967
August	212 + i	16	228	7.00-17.30	1.9	13.8	1332.5	0.975
September	243 + i	15	258	7.00-16.30	2.4	3.2	1351.7	0.989
October	273 + i	15	288	8.30-16.30	4.0	-8.4	1375.4	1.006
November	304 + i	14	318	9.00-14.30	4.7	-18.2	1397.6	1.022
December	334 + i	10	334	9.30-13.30	6.2	-21.6	1406.6	1.029

T A B L E I.1

(*) Recommended average day for each month (from Klein (1)). The average day is that day which has the extraterrestrial radiation closest to the average for the month.

(#) Using $I_{sc} = 1366.8 \text{ W/m}^2$, see table B.1.

The daily extraterrestrial radiation on a horizontal surface is given by:

$$H_o = \frac{24}{\pi} \cdot I_{sc} \cdot E_o \cdot \sin \phi \cdot \sin \delta \cdot \left[(\pi/180) \cdot \omega_s - \tan \omega_s \right]$$

where ω_s is the sunrise hour angle in degrees, from equation (A.5c) and E_o is the eccentricity correction factor from equation (A.2a)

In many engineering calculations, the monthly average extraterrestrial daily radiation on a horizontal surface, \bar{H}_o , is often required. It is possible to determine the particular day (that is, a particular declination) which has irradiation equal to the monthly average hourly irradiation. Defining such a particular declination as a characteristic declination, δ_c , see table I.2, we may now write \bar{H}_o as follows:

$$\bar{H}_o = H_o|_{\delta = \delta_c}$$

Hence the monthly average clearness indices for the two locations can be found.

Liu and Jordan (55) have shown that solar climate at a particular location can be characterized by the clearness index \bar{K}_T

$$\bar{K}_T = \frac{\bar{H}}{\bar{H}_o} \quad \text{is the ratio of}$$

daily global radiation on a horizontal surface
extraterrestrial daily insolation on a horizontal surface

The parameter K_T , which is an indicator of the daily clearness was found for two different locations in Britain, at Aldergrove and Easthamstead (in N. Ireland and London respectively), \bar{H} was extracted from table I.3 and these values correspond with the average radiation falling at 11.30 every month.

Paparsenos (3) adopting Hull's method worked out the fraction of diffuse solar radiation at 8 different wavelength bands over the total solar spectrum for 4 regions of clearness index, see table I.2.

TABLE I.2

Weather type	Clearness index, K_T
clear sky	> 0.70
haze	$0.50 - 0.70$
light overcast	$0.25 - 0.50$
heavy overcast	< 0.25

TABLE I.3							
Month	Date (*)	Day number, d _n	Distribution of daily average irradiation on a horizontal surface (MJ/m ²)	(#)	Extraterrestrial daily insolation on a horizontal surface, H _o	Clearness index K _T	
			E'hamst'd				
			Aldergrove			Aldergrove	E'hamst'd
Jan	17	17	1.73	2.23	6.43	0.27	0.27
Feb	14	45	4.14	4.47	12.19	0.34	0.32
Mar	15	74	7.83	8.36	20.42	0.38	0.38
Apr	15	105	13.05	11.95	29.93	0.44	0.38
May	15	135	15.61	15.88	37.66	0.41	0.41
Jun	10	161	18.85	18.80	41.30	0.46	0.45
Jul	18	199	15.74	16.93	39.54	0.40	0.42
Aug	18	230	12.92	14.04	33.04	0.39	0.41
Sep	18	261	9.53	10.51	24.17	0.39	0.41
Oct	19	292	4.98	6.13	15.04	0.33	0.36
Nov	18	322	2.61	3.29	8.08	0.32	0.33
Dec	13	347	1.40	1.91	5.90	0.24	0.24

(*) Recommended by Iqbal (6)

(#) Extracted from Met. 0.912, "Solar Radiation Data for the United Kingdom 1951-1975."

The results in table I.3 above suggest that for Britain when monthly average calculations are performed a single spectrum for the fraction of diffuse radiation can be safely used since the K_T range is 0.24 - 0.46. The fraction of energy for K_T 0.25 - 0.50 is listed in table C.6, Appendix C. The above results also suggest an average value of the clearness index of 0.39 for both sites for a 10 month period from February to November with a standard deviation of only 0.05.

References

REFERENCES

- (1) Klein S.A., "Calculation of Monthly Average Insolation on Tilted Surfaces." Solar Energy, 19 p. 325, (1977)
- (2) Spencer J.W., "Fourier Series Representation of the Position of the Sun." Search 2(5) p. 172, (1971)
- (3) Paparsenos G. "The Analysis of the Transwall Passive Solar System." Ph.D. thesis in Mechanical Engineering Department, Glasgow University. (1983)
- (4) Duffie J.A. and Beckman W.A. "Solar Engineering of Thermal Processes." John Wiley and Sons, New York, (1980)
- (5) Kreith F. and Kreider J.F. "Principles of Solar Engineering." Hemisphere Publishing Corporation and McGraw Hill Book Company, New York, (1978)
- (6) Iqbal M. "An Introduction to Solar Radiation." Academic Press, London, (1983)
- (7) Dickinson W.C. and Cheremisinoff P.N. Solar Energy Technology Handbook Parts A and B, Dekker, New York, (1980)
- (8) Ozisik M.N. "Radiative Transfer and Interaction with Conduction and Convection." J. Wiley and Sons, London, (1973)
- (9) Meyer-Arendt J.R. "Introduction to Classical and Modern Optics." Prentice-Hall, New Jersey, (1972)
- (10) Robinson N. "Solar Radiation." American Elsevier, New York, (1966)

- (11) Hull J.R., McClelland J.F., Hodges L., Huang J.L., Fuchs R., Block D.A. "Effect of Design Parameter Changes on the Thermal Performance of a Transwall Passive Solar Heating System." Proc. 5th National Passive Solar Conference, Amherst, MA, Oct. 22-26, I.S.E.S. New York, pp.394-398. (1980)
- (12) Fuchs R. and J.F. McClelland "Passive Solar Heating of Buildings Using a Transwall Structure." Solar Energy, 23, pp.123-128. (1979)
- (13) Hull J.R., McClelland J.F., Hodges L., Fuchs R., Block D.A. "Solar Heating Performance Results for a Transwall Test Prototype System." Proc. 1980 Annual Meeting, I.S.E.S., Phoenix, Arizona, I.S.E.S., New York. (1980)
- (14) Mercer R., McClelland J., Hodges L., Szydlowski R. "Recent Developments in the Transwall System." Proc. 6th National Passive Solar Conf. Portland, Oregon, I.S.E.S., New York. (1981)
- (15) McClelland J.M. and Fuchs R. "A Preliminary Study of Passive Solar Heating Performance and Visual Clarity for a Transwall Structure." Proc. 3rd National Passive Solar Conference, San Jose, California. I.S.E.S., New York. (1979)
- (16) McClelland J.F., Mercer R.W., Hodges L., Szydlowski R.F., Sildes P.H., Struss R.G., Hull J.R., Block D.A. "Transwall - A Modular Visually Transmitting Thermal Storage Wall - Status Report" Solar World Forum, Vol. 3., Brighton, Pergamon Press, Oxford. (1981)
- (17), (18) McClelland J.F. "Transwall Research." AMES Laboratory USDOE, Iowa State University. Internal reports W-7405.Eng. 82 and WPAS BD-01 (1982)

- (19) Sodha M.S., Bansal N.K., Sant Ram "Periodic Analysis of a Transwall, A Passive Heating Concept." Applied Energy 14 pp. 33-48. (1983)
- (20) Boer K.W. "The Solar Spectrum at Typical Clear Weather Days." Solar Energy Vol. 19(5) p. 525-538 (1977)
- (21) Lechner B., "The Spectral Distribution of Solar Radiation at the Earth's Surface - Elements of a Model." Solar Energy (20(2) pp. 143-150. (1978)
- (22) Plant J.A. "The Climate of Glasgow." Meteorological Office, Climatological Services (Met. 0.3) Climatological memorandum no. 60.
- (23) Peterson J.T. and Flowers E.C. "Interactions between Air Pollution and Solar Radiation." Solar Energy, Vol. 19, p. 23-32. (1977)
- (24) Kasten F. "A New Table and Approximate Formula for Relative Optical Air Mass." Arch. Meteorol. Geophys. Bioklimatol Ser. B. 14, pp. 206-223. (1966)
- (25) Gotz F.W.P. et al. "The Vertical Distribution of Ozone in the Atmosphere." Meteor. z vol. 51, pp. 416-445 (1934)
- (26) Unsworth M.H. and Monteith J.L. "Aerosol and Solar Radiation in Britain." Quart., J.R. Met. Soc. 98 pp. 778-797. (1972)
- (27) Moon P. "Proposed Standard Solar Radiation Curves for Engineering Use." J. Franklin Inst. 230, pp. 583-617. (1940)

- (28) Brine D.T. and Iqbal M. "Diffuse and Global Solar Spectral Irradiance Under Cloudless Skies." Solar Energy 30(5), pp. 447-453. (1983)
- (29) Nisbet S.K. and Kwan C.M. "The Application of the Transwall to Horticultural Glasshouses." Paper provisionally accepted by Solar Energy
- (30) Clarke J.A. "Energy Simulation in Building Design." Adams Hilgen Ltd., Bristol. (1984)
- (31) Usmanov Y.U. et al. "On the Optical Characteristics of the Solar Pond." Geliotekhnika 7 No. 3, pp. 78-81. (1976)
- (32) Palmer K.F., Williams D. "Optical Properties of Water in the near Infrared." Journal of the Optical Society of America, 64(8), pp. 1107-1110. (1974)
- (33) Bamford C.R. "Colour Generation and Control in Glass." Glass Science and Technology 2, Elsevier, Amsterdam. (1977)
- (34) Woodlife T.J. "SPSE Handbook of Photographic Science and Engineering." J. Wiley and Sons, New York. (1973)
- (35) Frohlich C. and Brusa R.W. "Solar Radiation and its Variation in Time." Solar Physics 74, pp. 209-45. (1981)
- (36) Solar Radiation Data for the U.K. 1951-1975, Met. O 912, Meteorological Office, Bracknell. (1977)
- (37) Tickner K. Private Communication, ICI, Organics Division, Manchester. (1984)
- (38) Linsley G.F., Solar Energy Advisory Service, Pilkington Brothers Limited, St. Helens. Private Communication (1985)

- (39) Hale G.M. and Querry M.R. "Optical Constants of Water in the 200 nm to 200 μ m Wavelength Region." Applied Optics, Vol. 12, No. 3. (1973)
- (40) Doma F. Private Communication, ICI, Organics Division, Manchester. (1986)
- (41) Burke A.R., Hudgens C.R., Wittenberg L.J., "Chemical and Optical Studies of Heat Transfer fluids Containing Solar Energy Absorbers." American Institute of Chemical Engineers, Annual Meeting, 86th, Houston, Texas. (April 1979)
- (42) Canham A.E. "Artificial Light in Horticulture." Centrex Publishing Co., Eindhoven. (1966)
- (43) Brandemuehl M.J. and Beckman W.A., "Transmissions of Diffuse Radiation Through CPC and Flat Plate Collector Glazings." Solar Energy, 24, 511-513. (1980)
- (44) Seah C.H. "Radiation in the West of Scotland." Undergraduate project, Department of Mechanical Engineering, University of Glasgow, Glasgow. (1986)
- (45) Rajvanshi A.K. "Effect of Various Dyes on Solar Distillation." Solar Energy Vol. 27 pp. 51-65. (1981)
- (46) Hottel C. and Woertz B.B. "The performance of the Flat-Plane-Solar-Heat Collectors." Transactions of the American Society of Mechanical Engineers, 64, p. 91. (1942)
- (47) Temps R.C. and Coulson K.L. "Solar Radiation Incident Upon Slopes of Different Orientations." Solar Energy 19(12), pp. 179-184. (1977)
- (48) Klucher T.M. "Evaluation of Models to Predict Insolation on Tilted Surfaces." Solar Energy 23(2), pp. 111-114. (1979)

- (49) Paltridge G.W. and Platt C.M.R. "Radiative Processes in Meteorology and Climatology" American Elsevier, (1976)
- (50) McGregor J. "The Implications for Calibration and Field Use of Non-ideal Cosine Behaviour in Kipp and Zonen CM-5 Pyranometers" Solar Radiation Data-Series F, Vol. 2, D. Reidel, Lancaster. (1985)
- (51) Dave J.V. "Validity of the Isotropic-distribution Approximation in Solar Energy Estimations", Solar Energy Vol. 19, pp. 331-333. (1977)
- (52) Le Baron B.A., Peterson W.A., Dirmhirn I. "Correction for Diffuse Irradiance Measured With Shadow Bands." Solar Energy Vol. 25, pp. 1-13. (1980)
- (53) Schuepp W. "Enregistrement Séparé des Composantes du Rayonnement Solaire." Bull. Serv. Météorol. Congo Belge 8, pp. 11-20 (as cited by reference 6). (1952)
- (54) McWilliams S. "Investigation of the Accuracy of Shading Ring Corrections Applied in the Measurement of Diffuse Solar Radiation." Commission of the European Communities, Energy Report EUR 8910 EN, Luxembourg. (1984)
- (55) Jordan R.C. and Liu B.Y.H. "The Interrelationship and Characteristic Distribution of Direct, Diffuse and Total Solar Radiation." Solar Energy 4, pp. 1-19. (1960)
- (56) Hollands K.G.T. "A Derivation of the Diffuse Fraction's Dependence on the Clearness Index." Solar Energy Vol. 35 pp. 131-136. (1985)
- (57) Carroll J.J. "Global Transmissivity and Diffuse Fraction of Solar Radiation for Clear and Cloudy Skies as Measured and as Predicted by Bulk Transmissivity Models." Solar Energy Vol. 35 No. 2, pp. 105-118. (1985)

- (58) Collares Pereira M. and Rabl A. "The Average Distribution of Solar Radiation-Correlations Between Diffuse and Hemispherical and Between Daily and Hourly Insolation Values." Solar Energy Vol. 22, pp. 155-164. (1979)
- (59) Kutateladze S. and Borishanskii V. "A Concise Encyclopedia of Heat Transfer." Pergamon Press, Oxford. (1966)
- (60) Hay J.E. "Study of Shortwave Radiation on Non-Horizontal Surfaces." Rep. 79-12, Downsview, Ontario, Atmospheric Environmental Service. (1979)
- (61) Drummond A.J. "On the Measurement of Sky Radiation." Arch. Meteorol. Geophys. Bioklim B9, 124-148. (1956)

